UNIVERSITY OF SOUTHAMPTON

FACULTY OF MEDICINE

Academic Unit: Human Development and Health

The Effect of Substrate Topography on Skeletal Stem Cell Behaviour

by

Shona Jane Waddell

Thesis for the degree of Doctorate of Philosophy

OCTOBER 2018

Supervised by Professor Richard OC Oreffo

Dr Maria Carmen de Andrés González

Dedication

This thesis is dedicated to my mother, June Waddell.

You were here to see me start, but not to finish. I kept my promise. This is only the beginning.

UNIVERSITY OF SOUTHAMPTON

ABSTRACT

FACULTY OF MEDICINE

Discipline: Biological Sciences

Thesis for the degree of Doctor of Philosophy

THE EFFECT OF SUBSTRATE TOPOGRAPHY ON SKELETAL STEM CELL BEHAVIOUR

Shona Jane Waddell

Advances in modern medicine have led to a welcome increase in life expectancy. Unfortunately, this is associated with an increase in diseases of the elderly including osteoporosis and osteoarthritis. Current treatment is met with mixed success and invasive joint replacements have limited lifespan. New strategies for treatment of degenerative bone disease are urgently needed.

Skeletal tissue has a remarkable capacity to regenerate and this has been ascribed to the skeletal stem cell (SSC) which can differentiate towards osteogenic, chondrogenic and adipogenic lineages. Given the ability of SSCs to differentiate into osteoblasts, SSCs have been studied for their potential to treat complications of degenerative bone disease. In order to use SSCs in the clinic, an osteogenic population must be selected from the total SSC population. One approach to do this has harnessed the potential of surface topographical cues to drive cell fate and function and enhance osteogenic differentiation of SSCs.

This thesis details the potential for SSCs to differentiate into osteoblasts and the potential to employ topographical cues to enhance or modulate this process. A range of topographical cues have been examined for SSC fate and function on different substrates including a near square arrangement of nanopits, cell-bioimprinted surface, and a biomimetic approach - nacre and prism surfaces. The near square nanopit surface was found to not induce osteogenic differentiation. Bioimprinted surface material was found to have a moderate effect of SSC behaviour and topography of these surfaces had a limited effect on SSC behaviour. Nacre surface topography alone were observed to modulate expression of osteogenic markers as well as upregulation of metabolomic profile to a level similar to chemically induced osteogenic differentiation, however a small data set was studied for these experiments. The prism surface was thought to possibly maintain SSC phenotype, as metabolomic activity decreased when cultured on these surfaces. To conclude, nacre topographical surfaces showed promising results to enhance osteogenic differentiation however this must be studied further, in an *in vivo* model in order to fully understand its potential for a topographical surface in treatment of degenerative bone disease.

Table of Contents

Table of Figures

Table of Tables

Declaration of Authorship

I, ...[please print name]

declare that this thesis and the work presented in it are my own and has been generated by me as the result of my own original research.

[title of thesis] .....

.....

I confirm that:

1. This work was done wholly or mainly while in candidature for a research degree at this University;
2. Where any part of this thesis has previously been submitted for a degree or any other qualification at this University or any other institution, this has been clearly stated;
3. Where I have consulted the published work of others, this is always clearly attributed;
4. Where I have quoted from the work of others, the source is always given. With the exception of such quotations, this thesis is entirely my own work;
5. I have acknowledged all main sources of help;
6. Where the thesis is based on work done by myself jointly with others, I have made clear exactly what was done by others and what I have contributed myself;
7. [Delete as appropriate] None of this work has been published before submission [or] Parts of this work have been published as: [please list references below]:

Signed: .....

Date: .....

Acknowledgements

I would like to gratefully acknowledge the support of supervisors Prof. Richard Oreffo and Maria “May” Carmen de Andrés González. First to Richard for allowing this PhD to be possible in the first place! With his support, and professional network, we enjoyed many successful collaborations which were essential to the progression of this PhD. On top of this, Richard oversaw my experiments, provided guidance towards experiments which would need to done, taught about the scientific progress and generally made sure everything went smoothly! May was most definitely a huge help in the lab. She trained me, discussed my data in detail, kept check on my progress and was my go to person for any problems.

I am very fortunate to have a supportive family who enabled me to be in a position where I can undertake such levels of higher education. My family helped me move down to Southampton, set up my life here (including much furniture from my sister Kirsty) and learn to live independently. Although they were far away, my Dad, Mum and Kirsty (and even nephew Lewis!) were always on call. I always looked forward to my trips home while I was studying. I have good memories of the sleeper bus to Glasgow – a money saving God send so I could go home lots of times with my stipend!

Unfortunately, while I was studying, my Mum passed away from cancer and never saw me finish. I will always be so thankful for everything she has ever done for me. All the care and encouragement turned me into the person I am today. She would be very proud to see me finish and achieve this – in fact it was my last promise! I was very lucky to have supervisors who really understood what I was going though and allowed me to have the time off I needed. I will be forever grateful. An extra special thanks goes to May and Julia Wells, who helped my lab work continue while I was away home. This meant countless media changes and lysate preparations and it means more to me now than I realised at the time.

My PhD had two very successful collaborations with Prof Matt Dalby at University of Glasgow and Prof Tim Woodfield at University of Otago. I was also very lucky to visit their labs, maybe not so interesting to go to my home town of Glasgow, but definitely interesting to visit New Zealand! While meeting colleagues including Isha Mutreja and Monica Tsimbouri, I learned how other labs work, how they focussed their research as well as education on new concepts and ideas.

During my time at Southampton I made many friends in Bone & Joint research group. The collective lunchtime stress outlet was a key part to my success! Support in the lab goes out

the Julia Wells (already mentioned☺), Stef and Kate – always available when there was problems. All my fellow PhD students and the post docs were very good to talk to about issues and the atmosphere in the group was so friendly!

I had many long chats with my good friend Tsiloon Li. He was very supportive of life as a scientist, having already finished, and was a key part to the nights out! As well, my friend Emma Budd, who I eventually published with, I learned a lot from. I have some very good memories of us at the Science tent at Glastonbury and one day we will go back there. A notable mention to all the friends and lab members who joined for beers after work, including David Gibbs, Patrick Stumph, Miguel, Catarina, Antonio, and Tim (my one time housemate with Elie). David Gibbs house was they social centre, and had many BBQ where everyone was invited and the atmosphere was high. Patrick supported me through some personally difficult times, and I with him. As well we would cycle with our friend Rosanna, and Matt M. All these amazing nights out, and great memories made me so happy in Southampton. I will always remember my time as one where I grew up as a confident independent individual and this was all thanks to my friends.

My last thank you is to my amazing boyfriend Matt Ellis. We didn't meet until I was near the end, but his support was never ending. Always making allowances for lab work in date nights (one memorable night when we went to the lab 11 pm after the cinema), and putting up with my moaning. He supported me as I moved on from lab work: he kept on top of my writing, made me dinner and done the chores so I could keep writing and finish on time.

I couldn't have made it to the end without the incredible support from the amazing people around me. Thank you to everyone.

Abbreviations

3`UTR - 3` Untranslated Region

ACAC - Acetyl CoA Carboxylase

ADP - Adenosine Diphosphate

AFM - Atomic Force Microscopy

AGO1-4 - Argonaute 1-4

ALP - Alkaline Phosphatase

ATP - Adenosine Triphosphate

BMP - Bone Morphogenic Protein

BSP - Bone Sialoprotein

CBF-β - Core Binding Factor Beta

CFU-F - Colony Forming Unit - Fibroblastic

COX-2 - Cyclooxygenase 2

CTG - CellTracker Green

DKK1 - Dickkopf 1

DMSO - Dimethylsiloxane

EBL - Electron Beam Lithography

ECM - Extracellular Matrix

ECS - Embryonic Stem Cell

ERK - Extracellular Signal Related Kinase

FAK - Focal Adhesion Kinase

FGF- Fibroblast Growth Factor

GFP - Green fluorescent Protein

HA - Hydroxyapatite

HA/TCP -Hydroxyapatite/

Tricalcium Phosphate

hADSC - human Adipose Derived Stem Cell

hBMMNC - human Bone Marrow

Mononuclear Cell

HDAC5 - Histone Deacetylase 5

HSC - Haematopoetic Stem Cell

HSC70 - Heat Shock Cognate 70

ICAM-1 - Intracellular associated molecule 1

IL-6 - Interleukin 6

INF-γ - Interferon gamma

IPA - Ingenuity Pathway Analysis

IPSC- Induced Pluripotent Stem Cells

JNK - c-Jun NH2 Terminal Kinase

LC3 - Lightchain 3

LDH - Lactate Dehydrogenase

LFA-1 - Leukocyte Function Associated Protein 1

LINC - Linker of Nucleskeleton and Cytoskeleton

LOXL4 - Lysyl Oxidase Like 4

MAPK - Mitogen Activated Protein Kinase

MAPKK - MAPK Kinase

MAPKKK - MAPKK Kinase

miRNA - microRNA

MMP - Matrix Metalloproteinase

MSC - Mesenchymal stem cell

NO - Nitric Acid

NSQ - Nearsquare

OA - Osteoarthritis

OCN - Osteocalcin

OM - Osteogenic Media

OP - Osteoporosis

OPN – Osteopontin

OSX – Osterix

OXPHOS - Oxidative Phosphorylation

Pa - Pascals

PAAm – Polyacrylamide

PBS - Phosphate buffered saline

PCL - Polycaprolactone

PDMS - Polydimethysiloxane

PEG - Polyethylene Glycol

PFA - Paraformaldehyde

PL - Planar

PMMA - Polymethylmethacrylate

Pol II - RNA Polymerase 1

POSTN - Periostin

pri-miRNA primary miRNA

PS - Polystyrene

PTH - Parathyroid Hormone

RGD - Tripeptide Motif Arginine –

Glycine - Aspartic Acid

RISC - RNA Induced Siliencing Complex

rMSC - Rat Mesenchymal Stem Cell

sFRP3 - secreted Frizzled Related Protein 3

SNP - Single Nucleotide Polymorphism

SSC - Skeletal Stem Cell

TAZ - Transcriptional Coactivator with PDZ Binding Motif

TCA - Tricarboxylic Acid

TCP - Tissue Culture Plastic

TGF-β - Transforming Growth Factor Beta

TNF-α - Tumour necrosis factor alpha

VEGF - Vascular Endothelial Factor

YAP - Yes Associated Protein

Chapter 1: Introduction

Chapter 1 – Introduction

Sections of this Chapter have been published in *Budd E, Waddell S, de Andrés MC, Oreffo ROC. The Potential of microRNAs for Stem Cell-based Therapy for Degenerative Skeletal Diseases. Current Molecular Biology Reports. 2017;3(4):263-75* [1]. This paper is detailed in Appendix V.

1.1. Bone Anatomy and Disease

1.1.1. Bone structure and function

Bone is an organ, highly vascularised with the majority of cells in bone embedded in a mineralised tissue [2]. The skeleton serves a number of key physiological functions: i) movement through providing muscle attachment sites, ii) structural support for the body and protects organs including the brain and organs of the chest, iii) as a reserve for mineral and hormone homeostasis and, v) the bone marrow microenvironment is essential for haematopoiesis [2].

1.1.1.1. Types of bone

There are many types of bones, each with differing shapes depending on their main function in the skeleton. In general, there are five main types of bones: long, short, flat, irregular, and sesamoid, with the delicate bones of the auditory canal considered additional to this grouping [2]. The long bones offer structural and motile support for the skeleton and these include the femur, humerus and tibia (Figure 1.1). Long bones contain dual epiphyseal growth plates [2]. Short bones offer limited structural support, however, these bones, such as the tarsals of the ankles and carpals of the wrists, have a role in providing stability and movement [2]. Flat bones are strong, flat plates of bone which function predominantly to protect organs [2]. Examples of flat bones include the cranium, sternum, scapula ribs and pelvis. Irregular bones are miscellaneous bones which do not fall into other categories, such as vertebrae, mandible and sacrum. Sesamoid bones are embedded in tendons, with the most notable example being the patella, enabling movement and joint protection [2].

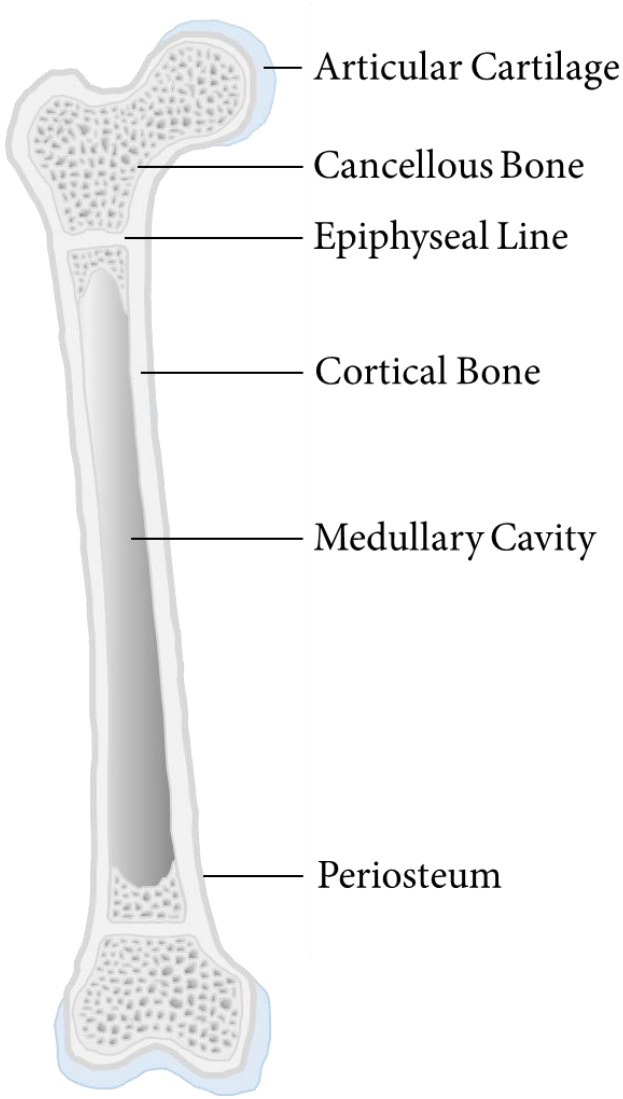

Figure 1.1. Anatomy of a long bone. *This is a cross sectional model of the femur. Compact, cortical bone is located at the edge of the bone and cancellous, spongy bone is located at the centre of the bone. The medullary cavity is found in the centre of long bones and stores bone marrow. Joints of the bone are protected with articular cartilage to allow for smooth movements.*

1.1.1.2. Bone macrostructure

Bone tissue is present in two forms: cortical (compact) bone and cancellous (spongy or trabeculae) bone (Figure 1.1). Cortical bone is a dense, strong, load bearing tissue which typically is around the outside of bones. Cancellous bone is comprised of a porous network of bone tissue with the spaces within filled with marrow. Long bones have a larger space in the centre of cancellous bone called the medullary cavity in which marrow is stored. Overall, the adult skeleton is composed of roughly 80% cortical bone and 20% cancellous bone [3]. However, different bones have varying ratios of cortical and cancellous bone. For example, the vertebrae have a ratio of cortical to cancellous bone of 75:25 and the femoral head a ratio of 50:50 [3]. Periosteum forms a thin layer of vascularised, fibrocollagenous connective tissue which surrounds the entire bone, except those areas covered by the articular cartilage at joints (Figure 1.1). The periosteum has a role in bone healing [4, 5].

1.1.1.3. Bone microstructure

Cortical and cancellous bone in adult bones are organised in a lamellar pattern, in which collagen fibrils are laid down in alternating orientation. It is this orientation of collagen fibrils that gives lamellar bone its strength, however the mechanism by which this is achieved is unknown [3]. Woven bone by contrast, the first bone laid down during skeletal development and bone healing after injury, where collagen fibrils are assembled in a random, disorganised manner, is weaker than lamellar bone [3].

Cortical bone has an outer periosteal surface and an inner endosteal surface (Figure 1.2A). Given that bone formation is greater on the periosteal surface, bone diameter increases with aging [3]. Coupled with this, at the endosteal surface bone resorption exceeds bone formation, leading to an expansion of the medullary cavity with aging [3].

Cortical bone is formed in circular units termed osteons, which consist of circular rings of concentric lamellae of bone around blood vessels (Figure 1.2A). Interstitial lamellae support bone between osteons. Osteocytes reside in osteons, in spaces termed lacuna. Osteocytes extend projections through canaliculi in bone matrix in order to communicate with other osteocytes/cells and exchange nutrients through blood vessels [3].

Cancellous bone is also organised into osteons with concentric lamellae, however these are semi-circular in shape (Figure 1.2B). Similar to cortical bone, osteocytes within the cancellous bone exist in lacuna and communicate through canaliculi. Cancellous bone is lined with endosteum. Trabecular osteons are approximately 35 mm wide in average [3].

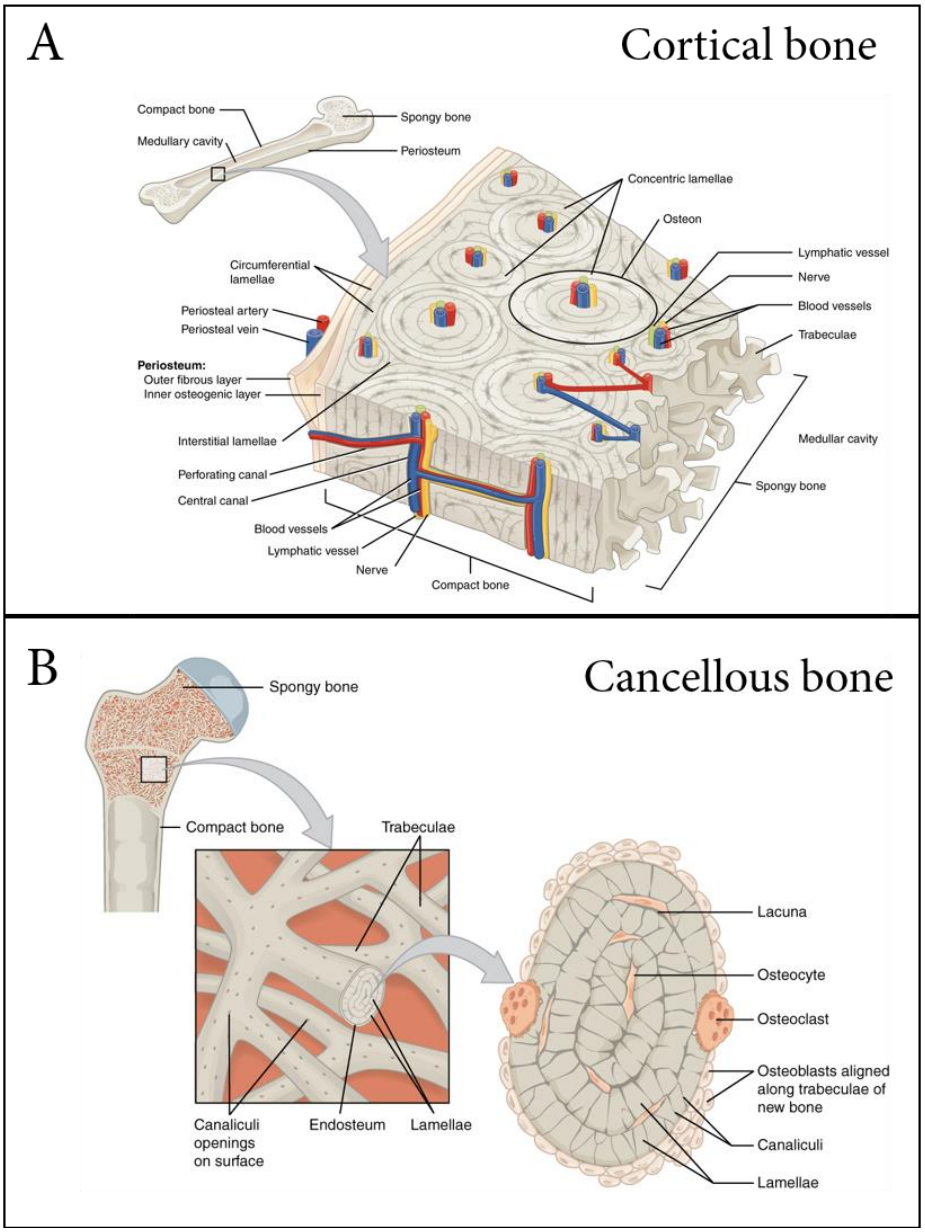

Figure 1.2. Schematic representation of inner structure of (A) compact bone and (B) cancellous bone. *Image taken from OERPUB, open access educational resource publication, http://oerpub.github.io/epubjs-demo-book/content/m46281.xhtml. Date accessed 10/02/2017.*

1.1.2. Bone Matrix

Bone tissue is composed of 60% inorganic salts, 30% organic matrix (protein) and 10% water [7]. Bone matrix is laid down by the osteoblast cell. This matrix can be renewed over time and repaired after injury by the osteoblasts and osteoclasts that reside in the bone. Mature bone is moderately hydrated with 10-20% water. Of its dry mass, 30% is made of collagen [2].

Of the several types of collagen found in the body, bone tissue is mainly composed of type 1. The Type 1 collagen molecule is a heterotrimer of two α1 chains and one α2 chain and is synthesised in the endoplasmic reticulum and Golgi apparatus within osteoblasts with the prodomain intact, preventing heterotrimer formation [8, 9]. The prodomain is cleaved outside the cell, allowing for collagen heterotrimer to form. Collagen molecules self-assemble into fibrils and then into large fibre structure where cross-linking strengthens the fibres. Bone mineral typically makes up 60% of the bone dry mass [2]. The majority of the mineral portion of bone is composed of crystals of hydroxyapatite (HA) ($Ca_{10}(PO_4)_6(OH)_2$) which are present between collagen molecules to strengthen the bone further [10]. HA forms due to the interaction of calcium phosphate ($Ca_3(PO_4)_2$) with water. Bone minerals give bone its hardness and rigidity making it brittle and prone to breaking. In contrast, collagen offers flexibility to bone, allowing bone to absorb shocks. The result is a tissue which is both strong, hard and with a degree of flexibility. In addition, bone matrix holds almost 99% of the body's calcium reserve and responds to body's metabolic demands for calcium [2].

Within the bone matrix are matricellular proteins, which have no direct role in bone strength, rather these proteins function as biological modulators to alter bone composition, for example osteocalcin (OCN), osteopontin (OPN) and bone sialoprotein (BSP) [11]. OCN is one of the most abundant proteins in bone, and is produced by the osteoblast. The absence of osteocalcin has been reported to lead to increased cortical bone thickness in osteocalcin-deficient mice, indicating a role for OCN in regulating bone formation through inhibition of bone formation [12]. Recently, there has been emerging evidence of a possible role for OCN in feedback between energy requirements and glucose metabolism [13]. OPN, another matricellular protein, is involved in directing osteogenic differentiation, controlling osteoblast numbers [14]. BSP is known to enhance osteoblast differentiation and matrix mineralisation and has a role in collagen nucleation [15, 16].

1.1.3. Cartilage in bone joints

The bone surfaces of synovial joints are covered in articular hyaline cartilage, which allows for movement without friction, to protect the joints and serves as a shock absorber [17]. Articular cartilage is avascular resulting in negligible regeneration with age, causing cartilage to wear down with age [18]. In patients with osteoarthritis (OA), cartilage wears down to very thin or completely away leading to exposure of the bone underneath [19]. As a connective tissue, cartilage is dominated by extracellular matrix (ECM), of which approximately 60% of dried weight is collagen [17].

1.2. Ossification: bone development in utero to early adulthood

Ossification is the process of laying down new bone matrix and occurs during infancy and continues to adolescence, determining skeletal size, and during all ages as a response of bone to injury. There are two types of bone ossification: endochondral ossification (conversion of cartilage to bone), and intramembranous ossification (osteoblast differentiation within mesenchymal tissues) [2].

Endochondral ossification is the process by which the skeleton develops in the embryo and the foetus (Figure 1.3). The skeleton of the embryo is initially composed of hyaline cartilage, formed by skeletal stem cells (SSCs) which commit to cells of the chondrogenic lineage [20, 21]. This cartilage template is gradually converted to bone during development in the utero. Bone formation occurs initially at the primary ossification centre. Within this centre, chondroblasts undergo hypertrophy and eventually die [22]. This generates large pores or lacunae within the centre. The lacunae become calcified and attract blood vessels from the periosteum surrounding the cartilaginous template [20]. The new blood supply brings in osteoprogenitor cells which differentiate to osteoblasts [20]. Osteoblasts form disordered immature bone matrix (woven bone) which is subsequently remodelled to form mature bone. At the periosteum, osteoblasts form a bone collar around the outside of the shaft. The medullary cavity is formed by osteoclasts breaking down newly formed bone. A secondary ossification centre occurs within the cartilaginous template around the end of long bones and starts to ossify. Ossification continues through the cartilaginous template until only articular cartilage, for joint movement, and epiphyseal cartilage, or the epiphyseal plate remain. The epiphyseal plate is the site of bone lengthening during adult skeletal development, and will remain as cartilage until bones have reached their full length in early adulthood, where upon

the epiphyseal plate is converted to bone [22]. Bone remodelling ensures formation of cortical bone in areas of high loading [23].

Intramembranous ossification occurs within mesenchymal tissue or fibrous connective tissue when SSCs differentiate directly into osteoblasts which lay down bone matrix. Intramembranous formation results in flat, dermal bones such as the bones of the skull, mandible and clavicle [2].

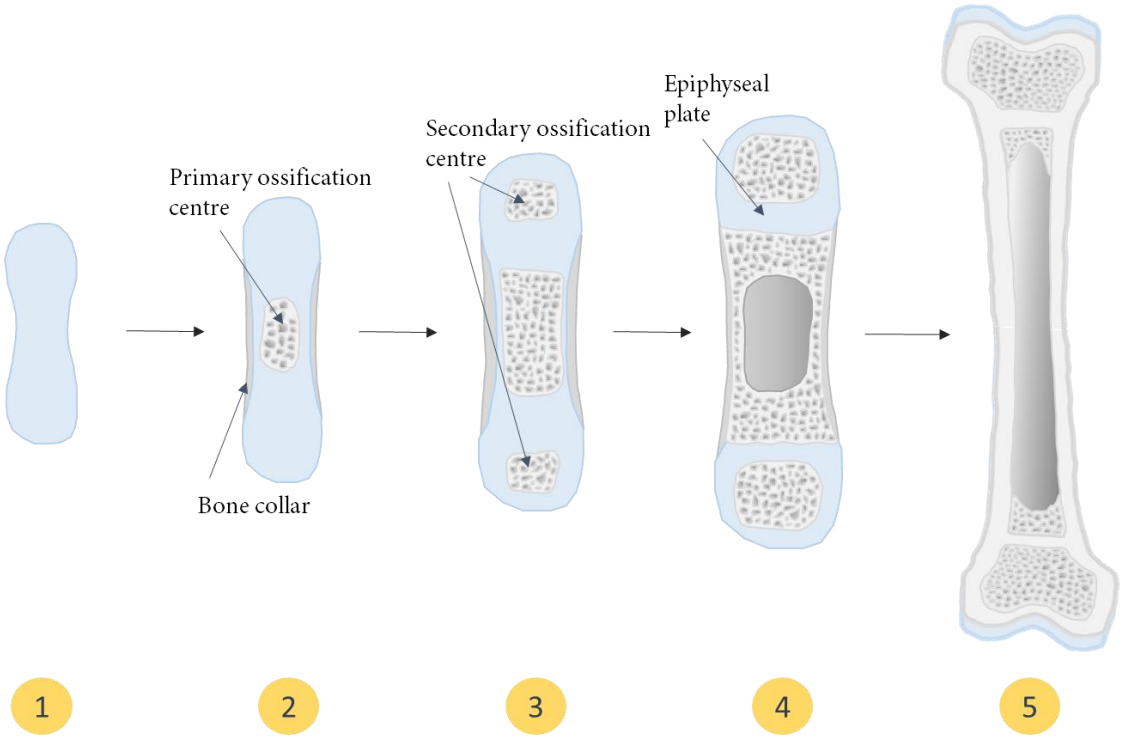

Figure 1.3. Formation of mature bone through endochondral ossification. *(1) First, a cartilaginous template is created by chondroblasts. (2) Next, chondroblasts enlarge and undergo apoptosis, leaving large spaces celled lacunae. This is infiltrated with blood vessels, which provides osteoblasts to the lacunae, giving rise to the primary ossification centre. During this time, blood supply to the periosteum brings in osteoblasts which create the bone collar. (3) Bone collar and primary ossification centre expands. At the end of bones, a secondary ossification centre is created. (4) Medullary cavity forms. Epiphyseal plate is visible. (5) Once bones reach their full potential, epiphyseal plate ossifies.*

1.3. Bone Remodelling

Bone tissue can initially, at the organ level, appear to be a static tissue, which remains largely unaltered throughout the lifetime of an individual. However at the cellular level, bone is continually remodelling in response to force, metabolic demands and nutritional requirements.

There are four main types of cells involved in bone remodelling and repair: osteoclasts, osteoprogenitors (originating from SSCs), osteoblasts, and osteocytes. The process of bone remodelling is described in detail in Figure 1.4.

Bone remodelling is triggered locally through the action of both osteocytes and bone lining cells. Systematic control over bone remodelling exists through hormonal regulation mainly by calcitonin, parathyroid hormone (PTH), vitamin D_3 and oestrogen [23]. The trigger for remodelling is not fully understood, however a growing body of evidence suggests osteocytes play a crucial role [24, 25], with osteocyte apoptosis, in particular, a key event in triggering bone remodelling [24, 26]. Osteocytes make up 90-95% of the cells in bone [24] and reside surrounded by bone matrix, and thus are ideally placed to sense the mechanical forces experienced through the bone [25]. Osteocytes produce signalling molecules including nitric oxide (NO), prostaglandins and sclerostin, which can modulate the activity of the bone-degrading osteoclasts [27].

Bone lining cells are flattened, quiescent osteoblasts on the surface of bones which are thought to have a role in attracting immature bone-degrading osteoclasts to bone [28]. The binding of intercellular associated molecule 1 (ICAM-1) on immature osteoclasts to leukocyte function associated protein 1 (LFA-1) on bone lining cells, induces gene expression changes resulting in mature osteoclast differentiation [28]. Bone lining cells withdraw from bone following induction of osteoclast differentiation [29]. Non-mineralised bone tissue components, which protrude from the surface of bone once occupied by bone lining cells, assist in osteoclast adherence [30]. Eck *et al*, have shown that matrix metalloproteinases-1 (MMP-1) and collagen 1 fragments present in the surrounding fluid can enhance osteoclast differentiation [31].

Osteoclasts are the only cell type which can degrade or resorb bone and appear to prefer attachment to mature bone [27]. Osteoclasts are large cells, originating from haematopoietic stem cells (HSCs) and comprising part of the monocyte-macrophage lineage [32]. Osteoclasts bind to bone through attachment of integrin $\alpha_v\beta_3$ which recognises vitronectin, OPN, BSP and fibronectin, all of which are present on the bone surface [33]. The osteoclast creates a sealing zone which localises the degradative process to the surface of bone thereby preventing release into the environment [34]. The region of osteoclast membrane present at the sealing

zone is characterised by a ruffled membrane, termed the ruffled border. At the ruffled border in contact with bone, proton pumps present within the osteoclast release H^+ ions, creating an acidic microenvironment which disrupts the structure of the mineral component of the bone matrix [35]. Added to this, is the release of lysosomal vesicles containing degradative enzymes including cathepsin K and matrix metalloproteinases (MMPs), which destroy the organic proteins [29]. Following bone resorption, the osteoclasts leave and bone lining cells remove digested matrix debris [36]. This prepares the fresh surface for the arrival of the osteoblast cell, which lays down new bone matrix.

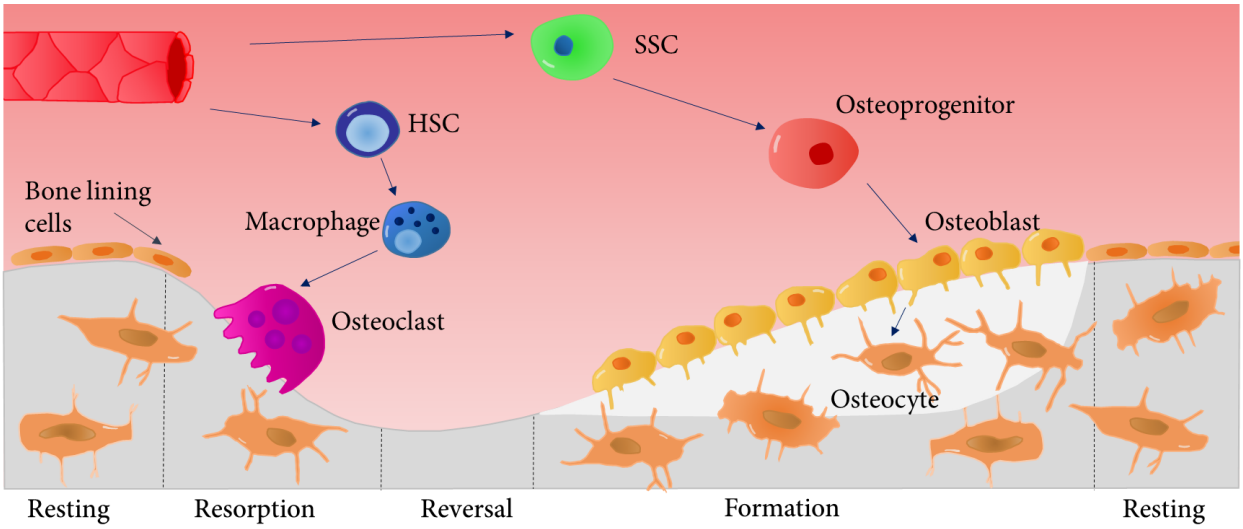

Figure 1.4. Schematic of bone remodelling. *During the resting phase, osteocytes remain within bone matrix and bone is covered by bone lining cells. Upon the trigger for bone remodelling, bone lining cells are removed and osteoclasts begin resorbing bone. When resorption is completed, osteoclasts leave and the bone goes through a phase of reversal of resorption to formation. During this phase, osteoblasts lay down new bone matrix which is then mineralised. After formation is complete, osteoblast differentiate into osteocytes and bone enters a resting phase. HSC – haematopoetic stem cell. SSC – skeletal stem cell. Dark grey indicates established bone. White indicates new bone formation.*

Osteoblasts originate from the stromal population within bone, and invade the space in remodelling bone which was taken up by the osteoclast. In quiescent bone, osteoblasts are present in greater numbers on the endosteal rather than periosteal side of bone, as well as osteons where bone is being remodelled [2]. Known to be important in osteoblast differentiation are Wnt and bone morphogenetic protein (BMP) signalling pathways. The function of the osteoblast is to produce new bone matrix and the cell is highly adapted to meet this function. Osteoblasts are known to produce mainly collagen type 1, and small amounts of collagen type V and proteins involved in regulation of bone formation (OCN, osteonectin, RANKL, osteoprotegrin, OPN and BSP to name a few) [23]. It is the production of collagen which makes osteoblasts important bone matrix generating cells. Osteoblasts also play an important role in bone mineralisation, through a number of mechanisms, including through the secretion of OCN, which binds calcium weakly, ensuring the local concentration of calcium is high [13]. In addition, alkaline phosphatase (ALP)-mediated cleavage of phosphate ions from proteins allows phosphate ion levels to increase [37], allowing for an increase in HA [2]. The dual role of osteoblasts in generating collagen type 1 and encouraging bone mineralisation allows for new bone formation.

The majority of osteoblasts undergo apoptosis following bone remodelling, however, a small number differentiate to osteocytes and are embedded in bone matrix [23]. During osteoblast differentiation to osteocytes, almost 70% of cell organelles and cytoplasm are lost, as a high secretory capacity is no longer needed, and cells form a star-like, stellar shape with numerous (up to 50) projections [23]. These projections pass through channels called canaliculi within the bone matrix and, allow osteocytes to communicate with other osteocytes and surface osteoblasts. The main body of the osteocyte is trapped in spaces termed lacunae within bone matrix and provides bone with a micro porous structure. Interestingly, osteocytes have the capacity to live for decades, as discovered in experiments by Frost *et al* [24, 38].

A careful balance is needed for bone remodelling to ensure maintenance of the skeletal system and gives bone its turnover. The process of bone remodelling can often be dysregulated during disease and aging, leading to loss or gain of bone mass and structure.

1.4. Ossification: bone injury and healing

Following injury, the majority of tissues heal with a connective tissue scar that does not have the same properties as the original tissue, which can lead to loss of function. Bone however, regains its properties after healing. Bone repair involves four stages: haematoma formation, soft callus, hard callus, and healed fracture remodelling [39, 40] (Figure 1.5). Immediately after injury, a haematoma is formed from disrupted blood vessels, within the area, which initiates an inflammatory response. The inflammation stage following injury goes through a similar process that occurs throughout the body, with recruitment of cells of the innate immune system (monocytes, lymphocytes, neutrophils and macrophages) [41]. These cells help to degrade debris and reorganise capillaries, and are guided to the injury site by cytokines and growth factors including vascular endothelial growth factor (VEGF), fibroblast growth factor 2 (FGF-2) and transforming growth factor-β (TGF-β) [39]. Tumour necrosis factor-α (TNF-α) and interleukin-6 (IL-6) are known to be important in enhancing osteogenic differentiation at the injury site [42]. The revascularisation at the injury site is also essential to the healing of a fracture. Following from inflammation, the fracture begins to form a fibrinous thrombus, a blood clot held together by fibrin. These factors help bring in additional immune cells from the blood and also recruit skeletal stem cells (SSCs), from the bone marrow and periosteum, into the damaged tissue. [4, 5]. Chen *et al* demonstrated, in *in vivo* experiments, an increase in SSC population size in response to skeletal injury, highlighting the essential role of the regenerative SSC in bone injury [21].

After this soft callus formation, repair moves to hard callus stage. Bone repair involves a mixture of endochondral and intramembranous ossification. During the beginning of hard callus formation, woven bone is laid down, which is characteristically more disordered than lamellar. There is a higher osteocyte density in woven bone compared to lamellar bone, with an increased lacunar density [6]. Given the proposed role of the osteocyte in initiating remodelling, this increase could result in accelerated remodelling in woven bone. The final stage, healed bone remodelling, involves reabsorption of mineralised bone by osteoclasts and replacement by osteoblasts to form lamellar bone, and the result is a healed fracture with the same mechanical properties as pre-fracture bone. Although fracture reparation typically follows the four stage process of fracture repair, some areas heal at different rates to others leaving the fracture with regions at different stages at any given time [41]. Bone repair is an efficient and complicated process, but remarkably, the majority of fractures heal without any problems. However, delayed healing can be the result of poor revascularization, age, mechanical instability, medication or pre-existing diseases and can result in severe complications for the patient.

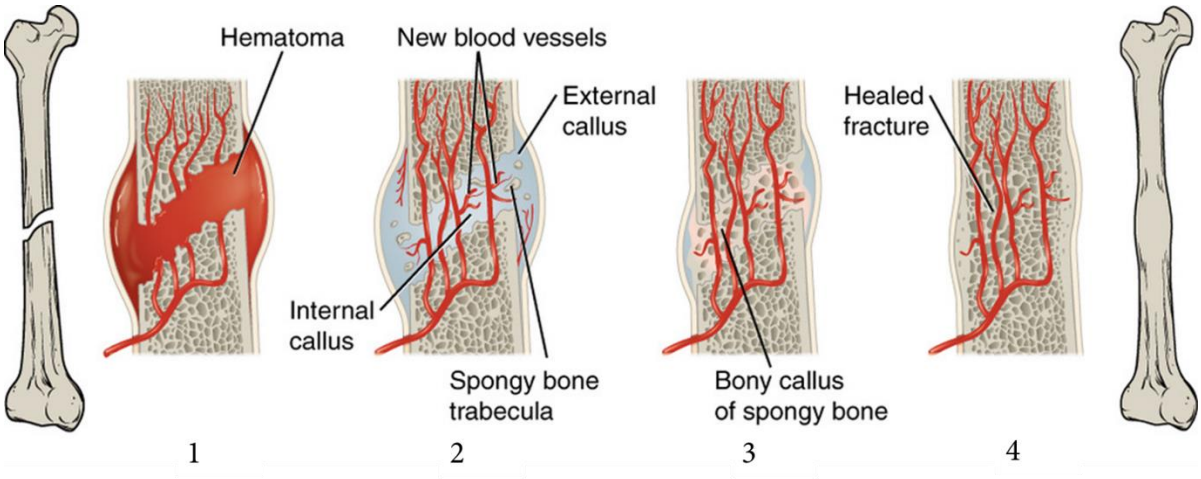

Figure 1.5. Schematic representation of stages of bone healing. *(1) Haematoma formation, (2) soft callus, (3) hard callus, and (4) healed fracture. Image from: https://www.boundless.com/biology/textbooks/boundless-biology-textbook/the-musculoskeletal-system-38/bone-216/bone-remodeling-and-repair-819-12062/images/stages-of-fracture-repair/. Accessed 11/01/2017.*

1.5. The aging bone

The human skeleton reaches peak bone mass at around 30 years of age and, thereafter, bone mass is gradually lost. ***Osteoporosis (OP)*** is a degenerative skeletal disorder, characterized by low bone mass and generalised disorder of the bone microarchitecture (Figure 1.6). OP is observed in men and women (in postmenopausal women, exacerbated by a fall in oestrogen production) and is a common cause of loss of bone mass and subsequent fracture [43]. It is estimated that 70% of inpatient fractures are a consequence of OP [44]. The regenerative capacity of bone is reduced with age, leading to a decrease in bone mass [45-47]. Bone remodelling and therefore the regenerative potential of bone is controlled by a careful balance between bone resorption, by osteoclasts, and bone deposition by osteoblasts. In OP, this process of bone remodelling is unbalanced with bone resorption exceeding bone formation resulting in the loss of bone mass observed in OP. The loss of regenerative capacity of bone is multifactorial including i) reduced stem cell potency/number, ii) increased osteoclastic bone resorption, iii) metabolic/factor imbalance and iv) reduced osteoblast function [47, 48]. In addition, the increase in bone marrow adiposity is believed to play an important role in OP, with osteoporotic patients exhibiting a higher ratio of adipose tissue to total tissue volume in iliac crest bone biopsies compared to healthy controls [49, 50].

Cell senescence is known to have an important role in aging tissues throughout the body, and has been shown to have specific role in the aging bone [51]. Replicative senescence due to telomere shortening is a key contributor to this process and gene therapy to increase telomerase levels has been successful at delaying aging in mice [52]. Interestingly, an

increase in reactive oxygen species which often accompanies aging, has been linked to an increase in adipogenesis of bone marrow stromal cells and a decrease in osteoblastogenesis.

Marrow adipose tissue is known to accumulate with age. Marrow adipose tissue can make up 70% of bone marrow by age 25 and continues to accumulate through life, and increase in marrow adipose tissue is correlated with a drop in bone strength [53]. It is known that during the aging process, bone morphogenic protein 2 (BMP-2) signalling in SSCs is altered to enhance adipogenesis and inhibit osteogenesis of SSCs [54]. This alteration in differentiation potential could have a role in changes in marrow adipose tissue content with age.

Osteocyte autophagy has been found to play a role in bone aging [55]. Autophagy is a self-degrading process by which cytoplasmic components are degraded in the lysosome. This exists as a protective mechanism to destroy damaged cells and remove them from the tissue, and therefore has anti-aging properties. Indeed, reduction of autophagy has been shown to increase aging [56, 57]. Osteocyte autophagy can be measured through biomarker microtubule-associated protein light chain 3 (LC3) which accompanies the accumulation of acidic vesicles within osteocytes [55]. LC3 was found to be significantly lower in older rat proximal tibia and correlated with a lower bone mineral density [55].

1.5.1. Degenerative bone diseases and current treatment approaches

Fractures associated with OP costs the United Kingdom around £1.7 billion per annum [58]. In North America, the estimated lifetime risk of fragility fractures is 17.5% for hip fracture, 15.6% for vertebrae fracture and 16% for distal forearm fracture among white women aged 50 [58], and patients are particularly vulnerable to fracture following a minor accident such as a sideways fall. When studying osteoprogenitor cells from patients with OP, it was noted that the osteoprogenitors proliferated slower and displayed a reduced osteogenic capacity compared to osteoprogenitors from healthy donors [47], reflecting the reduction of regenerative capacity of the bone with age. Added to this observation, the increase in bone marrow fat is thought to have a role to play in development of OP with osteoporotic patients, exhibiting a higher ratio of adipose tissue to total tissue volume in iliac crest bone biopsies compared to healthy controls [49, 50].

Currently, OP is treated with drugs which aim to increase bone density and, ideally, reverse the effect that OP has on bones before fracture. This can include bisphosphonate drugs which bind to HA crystals in bone [59]. The bisphosphonate Pamidronate was prescribed orally to patients with vertebral fractures daily [60]. It was found that following 5 years of treatment, total bone mineral density (BMD) increased by 14.3% in vertebrae, compared to 2.92 % in

patients given placebo [60]. There is promising hope for the anti-sclerostin antibody blosozumab. Sclerostin is produced by osteocytes and inhibits bone formation, therefore antibody neutralisation is thought to increase bone formation in osteoporotic patients [61]. In a clinical trial, blosozumab was found to increase BMD in the lumbar spine up to 17.7% in osteoporotic women, compared to a 1.6% decrease in BMD of the lumbar spine in osteoporotic women on placebo control [62].

Although these drugs are successful, the ever increasing aging population demands more treatment options.

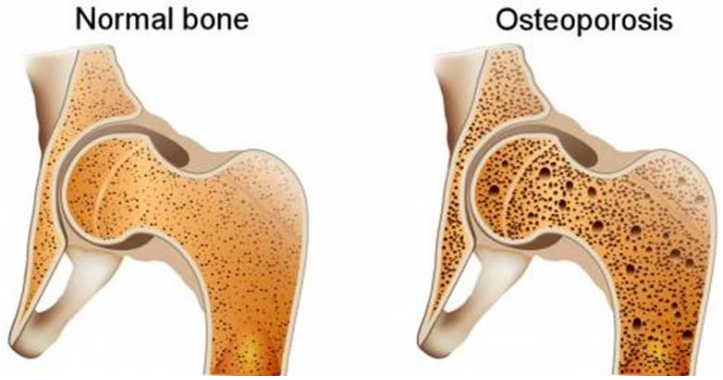

Figure 1.6. Degradation of bone density in osteoporotic bone. *Diagram shows cross section of a hip joint where both femur and ilium are more porous in osteoporotic bone. Image from: https://jeanhailes.org.au/health-a-z/bone-health/what-is-osteoporosis. Accessed 11/01/2017.*

Osteoarthritis (OA) is a prevalent chronic disease and can be described as a heterogeneous condition, which results in joint signs and symptoms associated with defective integrity of the articular cartilage and changes to bone at joint margins (Figure 1.7) [63]. It affects 15% of the population with an estimated lifetime risk of 40% in men and 47% in women [64]. Articular cartilage is composed of non-migratory and non-proliferative resident chondrocytes embedded within an avascular, alymphatic and aneural specialised ECM, factors which following injury are likely to account for the limited capacity of articular cartilage to intrinsically repair [17]. Articular cartilage injury is likely to be causative to the onset of OA. Damage to the articular cartilage may appear asymptomatic initially but it is extremely likely that over time degenerative changes will result. Messner *et al* demonstrated that athletes with isolated chondral lesions did not require treatment following initial injury. However, 14 years later some of the athletes displayed with a reduction of the joint space, indicating that despite the initial chondral lesions having been asymptomatic, degradation of the articular cartilage supervened leading to permanent knee damage [65]. Cartilage damage is typically succeeded with long term articular cartilage deterioration and OA.

Aging processes that contribute to development of OA are thought to also occur in the meniscus, ligaments, bone and synovium [19]. However, at the cellular level, epigenetic alterations in chondrocytes are known to take place [66] including demethylation of *MMP13* [67, 68] and expression of miRNA-146 [69] and miR-140 [70] as well as a whole host of mRNA and miRNA genes [71]. The risk of developing OA varies between joints but is most common in hands, feet, knees and hips [18]. Treatment for OA comes initially in the form of analgesics and anti-inflammatory drugs and, non-pharmacologic methods such as lifestyle changes and physiotherapy [72]. If symptoms do not improve with medication, surgical intervention may be required. Less invasive cortisone injections are performed, and if necessary, highly invasive joint replacement is performed [72].

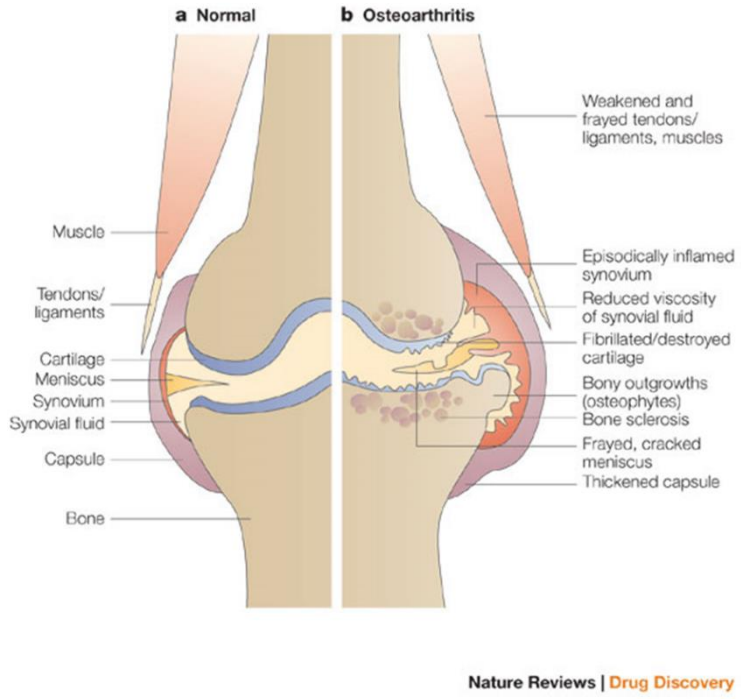

Figure 1.7. Comparison of normal and osteoarthritic synovial joint. *Inflamed synovium, degradation of cartilage, and reduced synovial fluid is illustrated in osteoarthritic joint (b). Image from [73].*

Both osteoporotic fragility fractures of major joints and osteoarthritic joints are treated with joint replacements. This procedure involves replacement of part of the joint or even the whole joint with a manufactured prosthesis and, is often the only option to restore function. Currently, estimated lifetime risk of total hip replacement at age 50 is 11.6% for women and 7.1% for men [74]. Joint replacement or arthroplasty is one of the most successful orthopaedic procedures and 90% of replacements are estimated to last at least 10 years [74]. UK estimated life expectancy at birth in the years 2010-2012 was estimated to be 78.9 years for men and 82.7 years for women (Office of National statistics UK,

https://www.ons.gov.uk/peoplepopulationandcommunity/birthsdeathsandmarriages/lifeexpectancies/datasets/lifeexpectancyatbirthandatage65bylocalareasintheunitedkingdomtable2ukandlocalareasinscotland, accessed 09/09/2018). With the number of total hip and knee replacements rising annually, and an estimated mean age of patients undergoing primary operations at 68.6 year old, there is a demand for definitive joint replacements [75].

1.6. Skeletal stem cells (SSCs)

Stem cells are defined by two characteristics: self-renewal and the ability to produce daughter cells with the capacity to become specialist cell types [76]. Self-renewal is cell division with maintenance of an undifferentiated state and can therefore increase the number of stem cells in a population. This is regulated intrinsically by cell signalling and energy demands and, by extrinsic factors including hormone signalling [77]. *OCT4, NANOG* and *SOX2* genes are known to be involved in molecular signalling which maintain stem cells an unspecialised state [78, 79]. The process of cells transforming to a specialised state is called differentiation (Figure 1.8). During this complex process, changes occur in signalling, gene expression, cell morphology and metabolism [80].

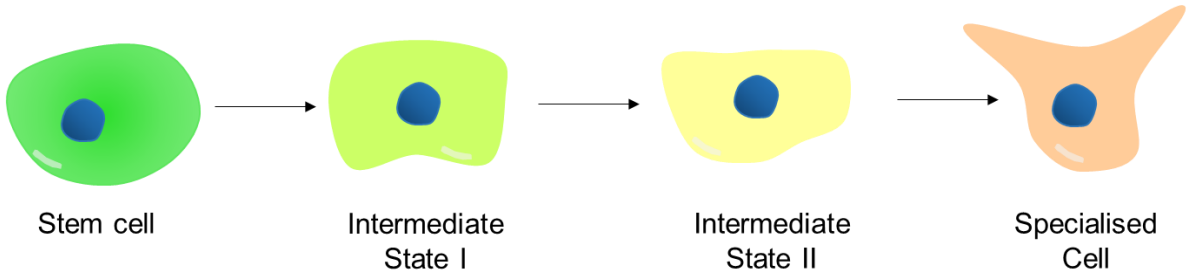

Figure 1.8. Schematic of stem cell differentiation to specialised cell. *An example of the intermediate stems involved during the complex process of stem cell differentiation to a specialised, fully differentiated cell.*

During early stages of development, embryonic stem cells have the potential to develop into endoderm, mesoderm and ectoderm tissue which will continue to form the entire organism (Figure 1.10). Mesenchyme tissue forms skeletal tissue (bone, cartilage, tendons, and ligaments), adipose tissue, muscle and connective tissue. SSC is the term given specifically to stem cells from bone able to generate into all skeletal tissues [81] (Figure 1.9).

SSCs were first identified by Friedenstein and colleagues in 1970s, who discovered a small sub-population of bone marrow cells with osteogenic potential [82]. These cells were distinguished from cells of haematopoetic lineage due to their strong adherence to tissue culture flasks and fibroblastic appearance [82]. In addition to this, Friedenstein and colleagues demonstrated that limited dilution seeding of SSCs could produce colonies of clonal origin and termed the colonies formed “colony-forming unit fibroblastic” (CFU-F) [83]. This ability to produce CFU-F is important as it indicates potential for self-renewal. Several years later, the SSC gained new found popularity when Pittenger *et al* published evidence of multipotent stem cells in bone marrow with the capacity to differentiate into adipocyte, osteocyte and chondrocyte lineages [84]. Following from these discoveries, a wealth of experiments have been conducted on SSCs and focus has also encompassed SSC interaction with biomaterials.

Recently, Chan *et al* published experiments aimed at identifying the SSC [21]. The authors isolated human SSCs from femoral tissue and defined the SSC population as $PDPN^{+}CD146^{-}$

$CD73^{+}CD164^{+}$ [21] The authors observed skeletogenic potential in SSCs derived from fetal, adult and induced pluripotent stem cell (iPSC) sources and discovered that SSCs isolated from adult skeletal tissue have a higher tendency to form bone, and SSCs derived from fetal and iPSCs has a higher tendency to form cartilage [21]. The authors aimed to study potential species similarities in SSCs and analysed gene expression, focussing on signalling pathways and genes associated with bone, in human and mice SSCs at the same developmental stage (18 weeks for human and e17.5 for mice) [21]. It was discovered that there was 66.4 % similarities in genes expressed in SSCs of humans and mice [21]. By looking at differences in gene expression, the authors could determine species divergence and identified WNT signalling pathway as human-specific, whereas genes such as *RUNX2* and *SOX9* were conserved between species [21].

SSCs are thought to be essential for maintenance of the self-renewing haematopoietic stem cell (HSC) and can act as regulators of the local bone marrow microenvironment. SSCs are thought to reside in the perivascular region, at the outer side of the endothelial lining of bone marrow sinusoids [85, 86]. This puts SSCs at an ideal position for bone regeneration during fracture and regulating the HSC niche. To study the co-habituation of SSCs and HSCs further, Chen *et al* injected a co-culture of SSCs and HSCs and transplanted these co-cultures into immunodeficient mice. The authors discovered that SSCs were essential to engraftment of HSCs [21].

SSCs have been suggested to lack expression of immune stimulatory factors such as major histocompatibility complex class II antigen, CD40, CD80 and CD86, supporting the idea of low immunogenicity [87]. Added to this, SSCs are known to have a suppressive effect on the immune system, through interactions with natural killer (NK) T-cells [88]. The presence of SSCs in cultures with cells of the innate immune system, NK cells, was found to reduce IL-5-induced secretion of IFNγ, IL-10 and TNF-α [88].

1.6.1. Terminology of Stem Cells

There has been debate in the literature regarding the name of the stem cells from bone marrow populations. The term mesenchymal stem cell (MSC) is used to describe a common progenitor of a wide range of “mesenchymal” tissues. It is commonly used when describing SSCs, which originate from bone marrow stroma. MSCs have the capacity to differentiate into “mesenchymal” lineages including osteoblast, chondrocyte, myoblast, adipocytes, fibroblasts and many more. These MSCs have been identified in adipose tissue, amniotic fluid, umbilical cord, dental pulp and menstrual fluid [89-91]. However, MSCs from certain non-bone marrow sources have not been shown to form mineralised tissue [92], making them poor choices for

the study of skeletal tissue differentiation. Following the identification of the SSC by Chan *et al*, it was discovered that SSCs can be found in skeletal tissue, BMP-2 treated adipose stromal cells, and iPSCs [21].

The term SSC refers to a self-renewing stem cells which resides specifically in the postnatal bone marrow and can differentiate into skeletal lineages (cartilage, bone, haematopoiesis-supportive stroma and marrow adipocytes) [81]. It is technically not a “MSC” as it cannot differentiate into all mesenchymal lineages. It is this cell which is responsible for the regenerative capacity inherent to bone. SSCs remain the preferred nomenclature in detailing, specifically, skeletal tissue differentiation from cells of postnatal bone marrow origin.

iPSCs, autologous fibroblast reprogrammed to pluripotent stem cells, are an attractive source for SSCs [93]. These cells have good differentiation potential and as they are autologous, therapeutic use would not evoke an immune response. However, we are only beginning to understand how to generate iPSCs and guide them to SSCs, therefore iPSCs are not, at this stage, a reliable source of SSCs, however extensive research is on-going to address this issue. [94].

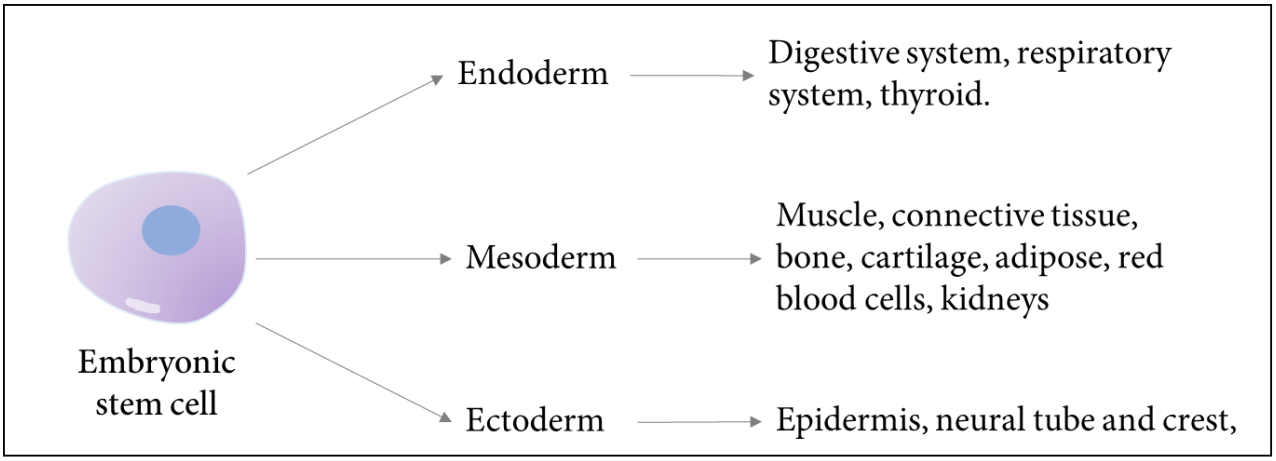

Figure 1.10. Lineage potential of embryonic germ layers. *Fate of endoderm, mesoderm and ectoderm germ layers in development from embryonic stem cells.*

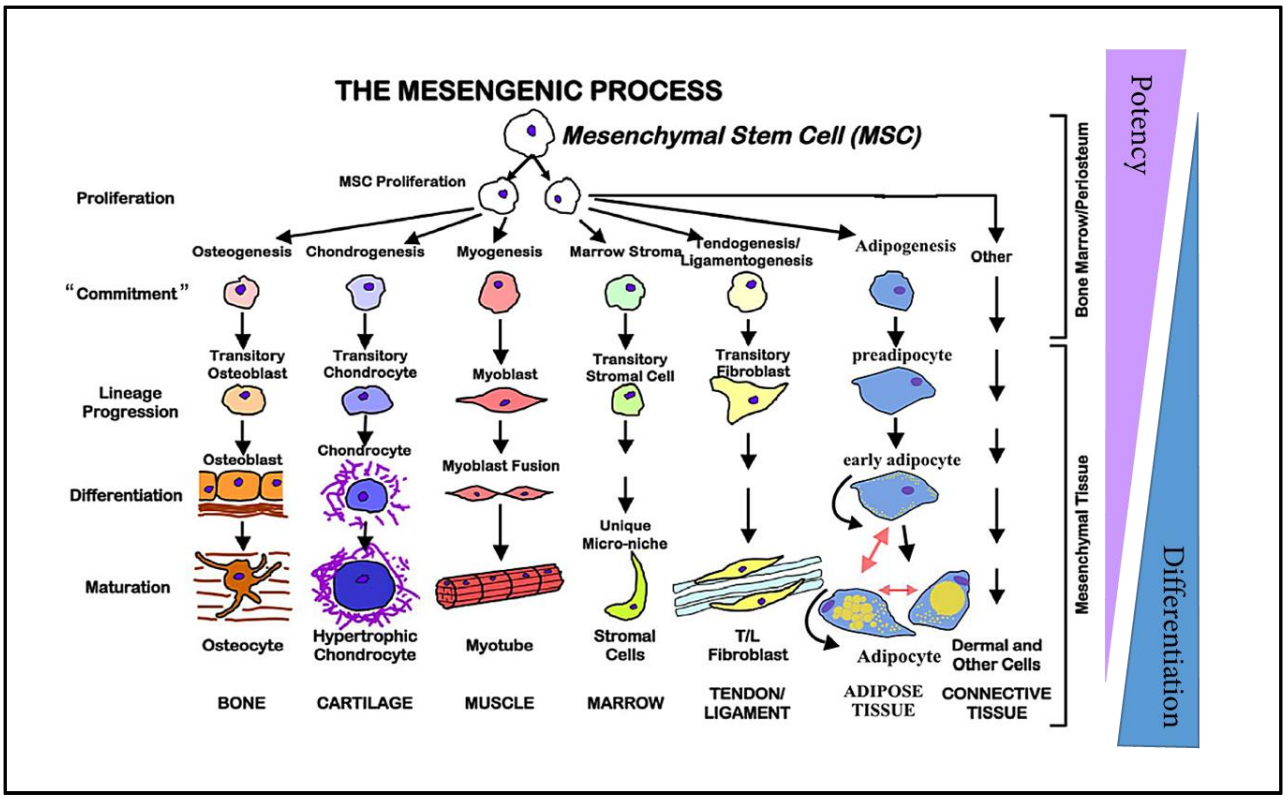

Figure 1.9. Detailed progression of mesenchyme tissue to terminally differentiated tissue. *Adapted from: http://quantitativemedicine.net/2015/05/30/the-amazing-mesenchymal-stem-cell, accessed 11/01/2017.*

1.6.2. SSC selection

The tissue culture plastic adherent bone marrow stem cells population is heterogenous and contains SSCs, erythroid cells, HSCs, lymphocytes, monocytes, osteoblasts, endothelial cells, fibroblasts and macrophages [95]. SSCs make up only a small percentage of this total cell number [95]. There has been great effort put into selecting SSCs from the general population. One method of bone marrow cloning involves isolating tissue plastic adherent cells and plating at low dilution to allow for CFU-F formation [85]. These CFU-F are then selected and their progeny cultured. This produces stem cells of true clonal origin which has to capacity to regenerate into skeletal origins [85].

The identification off a specific phenotype marker for SSC isolation would aid use of SSCs in the clinic. The International society for cellular therapy released in 2006 their position statement on MSC surface selection markers and included positive selection for CD105, CD73 and CD90 and negative selection for CD45, CD34, CD14 or CD11b, CD79α or CD19 [96]. Further to this, Chan *et al* recently discovered SSCs as identifying with the selection markers $PDPN^{+}CD146^{-}CD73^{+}CD164^{+}$ [21]. The use of these multiple markers can be impractical in the laboratory if large cell numbers are required. A true marker of a SSC should only be present in skeletal tissue and results in selection of a self-renewing cell.

STRO-1 remains one of the most widely used markers for SSCs enrichment and the binding of STRO-1 antibody can be used to enrich for the SSCs [97, 98]. Early studies by Gronthos *et al* demonstrated that in the presence of dexamethasone, ascorbate-2-phosphate and monopotassium phosphate, STRO-1+ SSCs developed a mineralised matrix, indicating the potential for osteoid formation and ultimately, under the appropriate stimuli, osteogenesis [98]. Since this early publication, osteogenic differentiation of adult SSCs has been studied using STRO-1+ SSCs [99]. The SSC specific marker STRO-1+ fractions reported to comprise 8.85 ± 4.66% of the total cell population recovered from density centrifugation [95]. Until recently, the epitope for STRO-1 was unknown. Through the use of western blotting and Tandem mass spectroscopy, STRO-1 antibody was found to bind to heat shock cognate 70 (HSC70) [100]. This is a molecular chaperone involved in protein folding and disassembly of clathrin coated vesicles. Although it is primarily located in the cytosol, the authors Fitter *et al* have described a cholesterol dependent membrane location of HSC70 [100]. The multipotential nature of STRO-1+ SSCs has been illustrated by Dennis *et al*, who demonstrated the osteogenic, adipogenic and chondrogenic potential of the STRO-1+ SSC population [101]. STRO-1 antigen, HSC70, expression is associated with an immature MSC phenotype and has greater immuno-modulatory properties [102, 103], making it ideal for selection of SSCs.

Through the use of dual-colour flow cytometry labelling STRO-1 and ALP, STRO-1+ population were found to have characteristics of MSCs and the authors noted expression of STRO-1 decreased as cells become ALP positive, progressing to differentiated osteoblasts [104]. It was concluded that STRO-1+ expression correlated with early osteoblast phenotype, and was absent in mature osteoblast populations [104].

Further to the work of Gronthos and colleagues, work in the Bone and Joint Research Group from Gothard *et al*, has investigated differences in the behaviour of STRO-1+ SSCs and CD146+ SSC populations [105]. Flow cytometry identified the CD146+ SSC population as comprising a smaller proportion of the total population than STRO-1+ SSC. Interestingly, both populations were found to behave similarly in terms of collagen/proteoglycan deposition and osteogenic gene expression [9]. STRO-1 enriched SSCs were found to exhibit increased expression of osteogenic markers *ALP, POSTN* (periostin) and *LOXL4* (lysyl oxidase like 4) compared to CD146+ and CD105+ subpopulations, suggesting STRO-1 enriched for a skeletal population with greater potential for osteogenic differentiation [105]. Nevertheless, it is important to note that the STRO-1+ population, derived from bone marrow stromal fraction, remains a heterogeneous population, displaying significant heterogeneity in marker expression and function [106]. Further to this, within the STRO-1+ population, there exists a subpopulation STRO-1^{bright}, which encompasses the selection of SSCs with the highest level of STRO-1 staining [107]. This population is known to have a greater number of CFU-F compared to total STRO-1+ population and is therefore more selective for a more clonal, less heterogeneous population [108]. Practically, this could present challenges as the STRO-1^{bright} population represents a smaller, rarer proportion of the total population, limiting numbers of cells available.

It should be noted that STRO-1+ selection is not specific for the SSC, and STRO-1 is known to bind to T cells, B cells, myeloid cells, and macrophages [109]. STRO-1 positive selection can be combined with negative selection of erythrocyte marker, glycophorin A and it has been shown that 95% of STRO-1+ cells were glycophorin A positive erythriod precursors [109]. In addition to bone marrow, STRO-1+ MSCs have been reported in adipose populations and have bone-forming potential [110]. While it is recognised STRO-1 selects for a heterogeneous skeletal cell population, when compared to other SSC selection markers, the STRO-1+ cell subset, represents a population with the capacity to differentiate along the osteoblast lineage. In addition, STRO-1 has been shown to be present in early osteoblast precursors and not mature osteoblasts [104], and thus, in the absence of better accepted markers, STRO-1 remains a useful selection marker for the study of SSC osteogenic differentiation.

1.6.3. Lineage commitment

The development of a terminally differentiated cell is the result of a change in phenotype from a stem cell to a specialised cell. During this process, the cell loses the ability to self-renew and gains the ability to perform specialised functions. Differentiation is triggered by both intrinsic and extrinsic factors such as growth factors, signalling stimuli, immune response, mechanical tension, and metabolic demand [111]. Differentiation is not a one-step process and instead involves formation of many intermediate stages between the stem cell to differentiated cell.

SSCs have the potential to differentiate into osteoblasts, chondrocytes and adipocytes [84]. The mechanisms which control this differentiation are highly complex and a variety of signalling pathways converge to orchestrate the highly ordered process of cell differentiation. Signalling pathways known to be involved include TGF-β, Wnt, Hedgehog, fibroblast growth factor (FGF), and Notch [112]. These signalling pathways, like differentiation, are complex and ordered. Signalling is initiated through an extracellular signalling molecule binding to transmembrane receptor, which induces changes in the cytosolic portion of the receptor. Inside the cell, the signal travels from protein to protein, usually resulting in protein expression changes that fuel differentiation. Major signalling pathways involved in SSC lineage commitment are described in Figure 1.11.

TGF-β comprises three isoforms TGF-β1, TGF-β2 and TGF-β3. BMP are members of the TGF-β1 family with an established role in osteogenic differentiation [112]. During signalling potentiation, BMP signalling molecules bind to kinase receptors which activate through cross-phosphorylation, subsequently initiating intracellular signalling [112]. BMP receptors activate SMAD transcription factors though phosphorylation, which induce gene expression changes of responsive genes [113, 114]. *RUNX2* is a major gene involved in controlling osteogenic differentiation and is a known target of BMP [113]. The importance of BMP in bone formation is described by the *Bmp2*$^{-/-}$ knock out mouse, which display spontaneous fractures [115].

Wnt family of proteins are glycoprotein ligands which bind to and activate the 7 transmembrane domain spanning Frizzled receptor and LRP5/6 c-receptor [116]. Binding of Wnt proteins to the receptor prevents the GSK3β from phosphorylating β-catenin. β-catenin phosphorylation targets it for degradation via the proteasome complex. Prevention of phosphorylation of β-catenin through Wnt binding allows β-catenin levels to stabilise and translocate to the nucleus. In the nucleus, the transcription factor β-catenin binds to it co-activator and induces expression of downstream genes such as *MYC, RUNX2* and *PPARG* [112, 117].

Notch signalling is not initiated by a soluble ligand, rather is activated by a membrane bound ligand, which binds to a transmembrane Notch receptor. Activation of the receptor results in cleavage of the cytosolic portion of the receptor and release of Notch Intracellular Domain, which translocates to the nucleus and activates expression of target genes [112]. Target genes includes *HES1*, which has a role in *OPN* expression [118].

Hedgehog proteins are secreted soluble factors, of which there are three types: sonic hedgehog, indian hedgehog and desert hedgehog. Activation of this pathway is known to be a trigger for adipogenesis, and results in expression of target genes including key regulator of adipogenesis *PPARG* [119]. Hedgehog signalling is inhibited during osteogenesis to prevent adipogenesis [120, 121]. FGF also have an important role in osteogenesis [51]. FGF are soluble ligands which bind to transmembrane receptors to activate the MAPK pathways [112]. FGF18 in particular is known to have a role in initiating osteogenesis during development [122].

The signalling pathways involved in differentiation communicate together in order to ensure the process of differentiation is performed properly. For example, Wnt has been found to communicate with BMP and hedgehog [123-125]. This cross talk is beginning to be elucidated although much research remains to be undertaken.

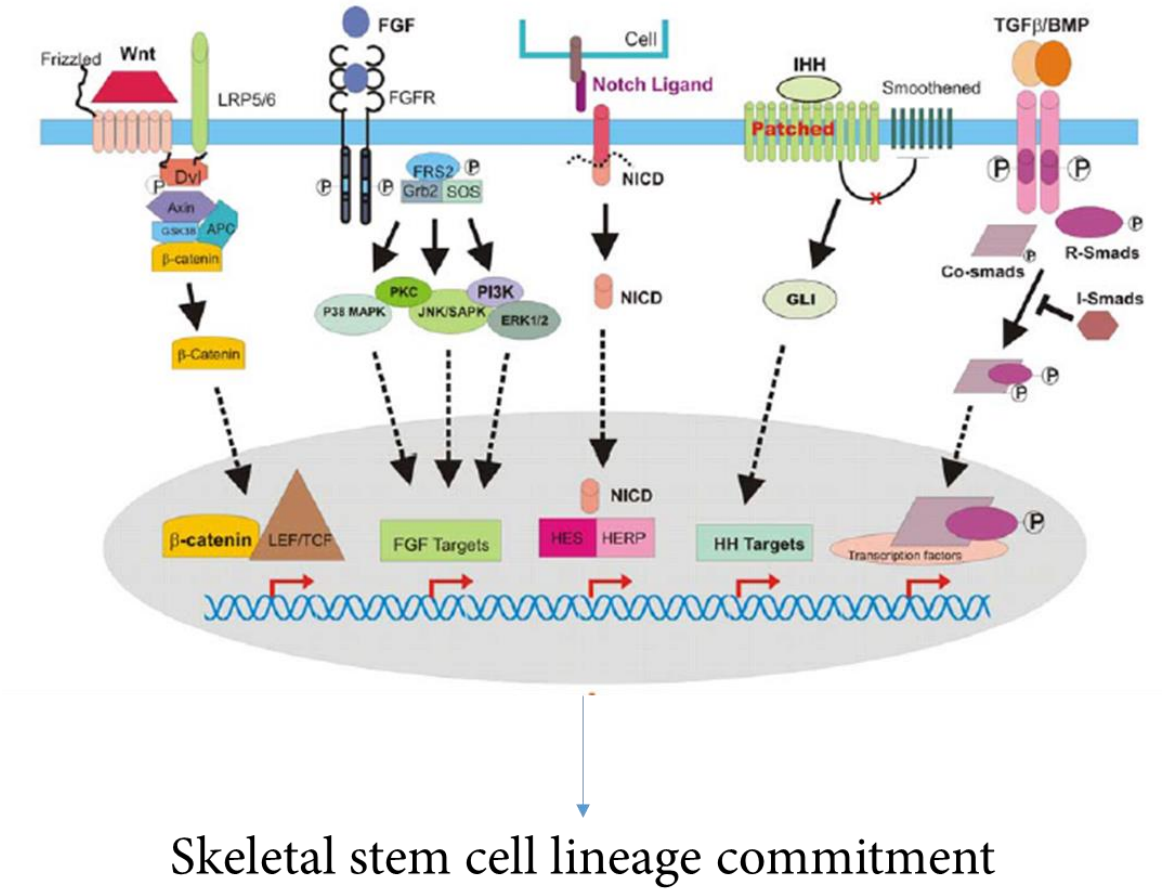

Figure 1.11. SSC lineage commitment involves multiple signalling pathways. *Wnt, FGF, Notch, Hedgehog and TGF-β pathways converge to control SSC differentiation. Figure adapted from [126].*

1.6.4. SSCs for treatment of bone disease

The remarkable ability of bone to remodel, coupled with the capacity of bone tissue to heal and to repair following fracture, supports the concept of a stem cell population within post-natal bone marrow. This has been ascribed to the SSC. SSCs are found within bone marrow stroma with high potential to differentiate into the osteogenic lineage and are responsible for the regenerative capacity of bone. The availability, plasticity and non-immunogenic properties of SSCs make them a promising prospect for therapeutic cell-based clinical applications [128]. The regenerative capacity of SSCs could be harnessed in the form of a cell therapeutic to regenerate the deteriorated bone and cartilage occurring during development of, for example bone disorders such as OP and OA.

Research focussing on SSCs, and bone and joint development, has centred on studying SSC progression down mesenchymal lineages and stabilisation of differentiation in order to understand the mechanisms of how cell therapies work. The importance of this research reflects the need for improved treatment for degenerative bone diseases and, understanding SSCs would allow for better application in the clinic. SSCs could potentially be coupled with tissue engineering to produce a highly effective cell/material based treatment.

Regenerative medicine aims to replace and repair injured tissues by harnessing the body's own capacity to repair through the use of stem cells [129]. Stem cells can be applied with or without biomaterials, which may be synthetic or natural, for example mimicking the ECM of the native tissue.

Ensuring maximal osteogenic differentiation, with minimal differentiation to other lineages, is one of the main challenges with using SSCs for clinical applications. Various proposed strategies have been suggested would ensure maximal osteogenic lineage commitment. These approaches include selection of a specific stage of osteoprogenitor subsets of SSCs. The ratio of *RUNX2/SOX9* expression was found to predict osteogenicity of SSCs [130], and could be used to select osteoprogenitor cells from a mixed population. In a second study, a transgenic *OCN* reporter construct using *OCN* promoter to express green fluorescent protein (GFP) was generated and transfected into MSCs [131]. Fluorescence increase correlated with OCN production and therefore osteogenesis [131]. Other approaches to select for osteoprogenitor cells includes using biomaterials designed to enhance osteogenic differentiation when SSCs are cultured on these materials. Examples of biomaterials includes nanosurface geometries [132, 133] and osteoconductive scaffolds [134].

In the area of musculoskeletal regeneration, one treatment option to repair bone defects involves the use of bone tissue to repair bone. This bone tissue can originate from the patient

(autograft) or from a donor (allograft). Coupling bone tissue with SSCs could provide the regenerative SSCs with ECM environment of bone tissue. In a study investigating the regenerative properties of stem cells mixed with bone tissue, SSCs were seeded onto bone allograft and this was compacted and used to fill pathological defects within the femur [135]. Further examination of this showed allograft containing SSCs displayed enhanced osteogenic activity versus allograft alone and, critically, the SSCs withstood the compaction process, illustrating the potential of this technique to improve efficiency of allografts. In a second study, 4 patients with large-bone defects were offered stem cell therapy where standard treatment had failed [136]. In these patients, autologous culture expanded SSCs were seeded onto a ceramic scaffold that was designed to match the defect [136]. No major complications were reported after surgery, and long term follow up of 6 to 7 years showed good integration of the scaffold [136]. Kim *et al* studied the effect of osteoblast injection into long bone fractures to examine accelerated healing [137]. Autologous osteoblasts were expanded from patients with long bone fracture, and injected into the site of fracture, with control group receiving no treatment [137]. It was observed that osteoblast injection enhanced fracture healing with little complication [137].

The success of these important, albeit small, clinical trials outlines the incredible potential SSCs have in the clinic for the treatment of bone fracture, bone defects and potentially degenerative bone diseases. In particular, culturing SSCs with a high osteogenic differentiation potential would prove important to generate the cell numbers required for cell-based therapy [138].

1.7. Mechanotransduction

Mechanical stimulation from extracellular materials is essential to the development and maintenance of the cytoskeleton. This sensing of the extracellular space can convert internally to intracellular biochemical responses. The perception of the mechanical properties of the ECM and subsequent intracellular signalling response is termed **mechanotransduction**.

Mechanotransduction is essential for correct development and function of almost all tissues in the body, however, in bone its importance is particularly relevant. This is due to the fact bone continuously remodels in response to changes in mechanical forces and, the demands of its function to ensure bone remains strong. It is due to mechanotransduction that cells within the bone can respond to an ever changing environment with appropriate adaptation. A good example of the importance of mechanotransduction to bone strength is during decreased mechanical loading during long-term spaceflights [139]. The reduction of loading on bone, and in that mechanical stimulation, leads to a decrease in bone mass [139].

The mechanical stimuli bones receive have alterations in magnitude, direction, duration and frequency, with applied forces ranging from compression, bending, twisting and shearing [127]. Osteoclasts within bone receive interstitial fluid flow and hydrostatic pressure, whereas for osteoprogenitors, mechanical stimulation from the matrix may be of more importance, as these cells reside in soft tissue [140].

To study the effect of mechanical stimulation of bone loading on MSC, Gharibi and colleagues seeded MSC on a calcium phosphate scaffold and subjected the scaffold to compressive force of 5.5±4.5 N and analysed gene expression via microarray [141]. The authors discovered after 2 hours of stimulation, 100 genes were differently expressed on mechanically stimulated compared to non-stimulated, indicating an immediate response of MSC to mechanical loading [141]. After 24 hours, increase in expression of osteogenic marker osterix was discovered, an early indication of osteogenic differentiation [141]. This work highlights the importance of mechanical stimulation on osteogenic differentiation.

A selection of signalling pathways activated during mechanotransduction includes integrin, MAPK, Wnt and Ca^{2+} and is described in **Figure *1.12***. It is the activation of these signalling pathways, and the cross-talk between these pathways, which results in the biological response to mechanical forces. In bone, responses can be on the tissue scale to remodel bone by either resorption or deposition of bone matrix, as well as a on the cellular scale to encourage proliferation, mobility and osteogenic differentiation of SSCs.

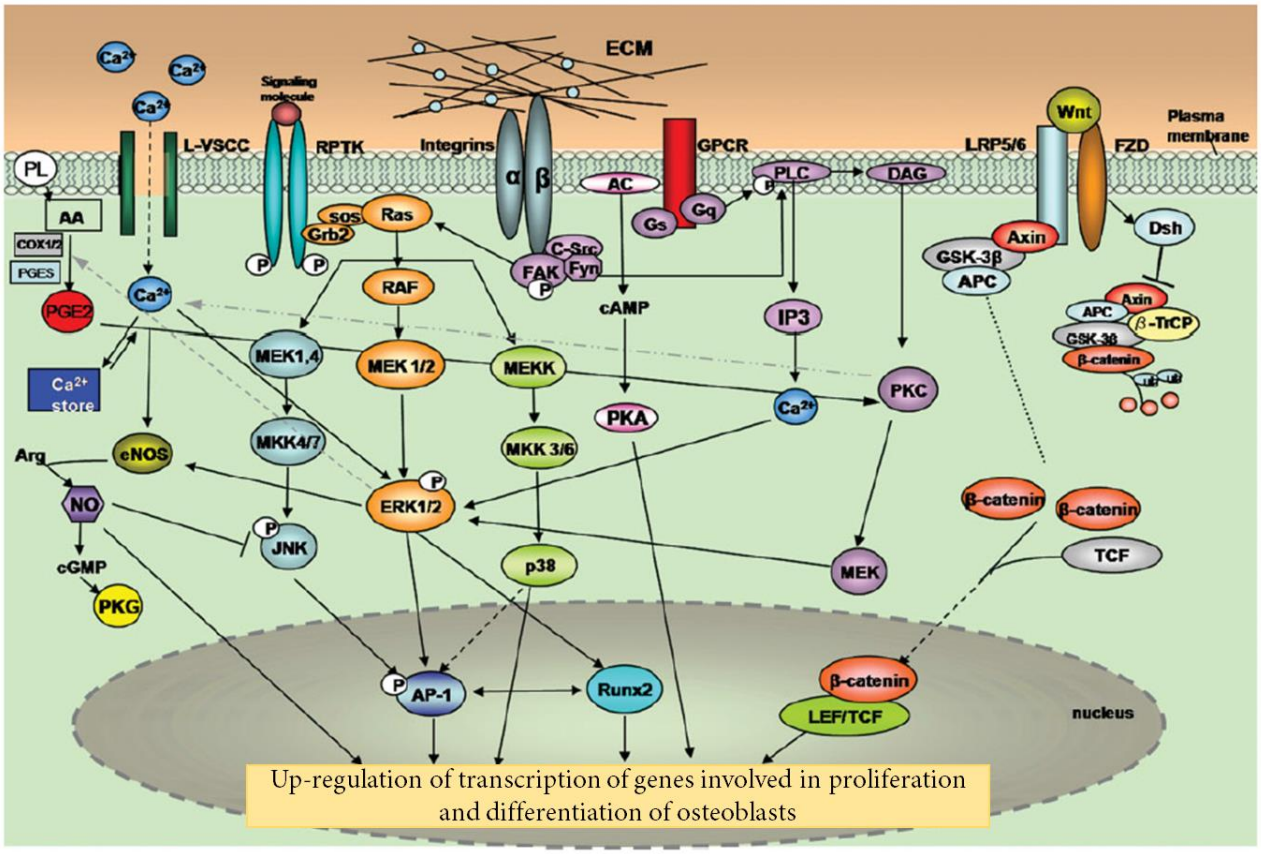

Figure 1.12. Schematic of signalling pathways involved in mechanotransduction in bone. *Figure adapted from [127].*

1.7.1. Signalling in mechanotransduction

1.7.1.1. Integrin signalling in mechanotransduction

The vast majority of cells in the body are exposed to ECM. Cells of epithelial or endothelial tissue, i.e. organs of the digestive tissue and the lungs, attach to a basement membrane, conferring polarity. Cells of connective tissue are typically surrounded by ECM, with no polarity, for example osteocytes in bone and chondrocytes in cartilage. The chemical and mechanical properties of the ECM control how the cell interacts with the ECM.

One of the major classes of cell receptors which confer cell-ECM interactions are integrins [142]. Integrins are heterodimeric proteins with one α and one β subunit. In vertebrates, the integrin family consists of 18 α subunits and 8 β subunits and 24 known different heterodimers (Figure 1.13). Integrins are transmembrane proteins with a large extracellular domain, which exists in two conformations: bent and open. The open conformation is traditionally viewed as the active form, when the protein is available for ligand binding [142]. All ligands bind to ECM components, with different combinations of integrin heterodimers binding different ligands

[142]. The α subunit is essential to ligand binding with the β subunit providing a supporting role [142]. The RGD tripeptide motif (Arginine (R)-Glycine (G) –Aspartic acid (D)) is a major integrin recognition sequence and is present in fibronectin, vitronectin and fibrinogen [142]. Collagen-binding integrins recognise the peptide sequence GFOGER present on the surface of collagens [142]. Inside the cell, the intracellular portion of integrins bind cytoskeletal proteins including focal adhesion kinase (FAK), talins and paxillin [142, 143]. Integrins can cluster to form focal adhesion complexes which enhance their signalling [143] (Figure 1.14). These complexes are highly ordered and connect through to the cytoskeleton via actin filaments. In this way, the cytoskeleton can respond to changes in ECM properties.

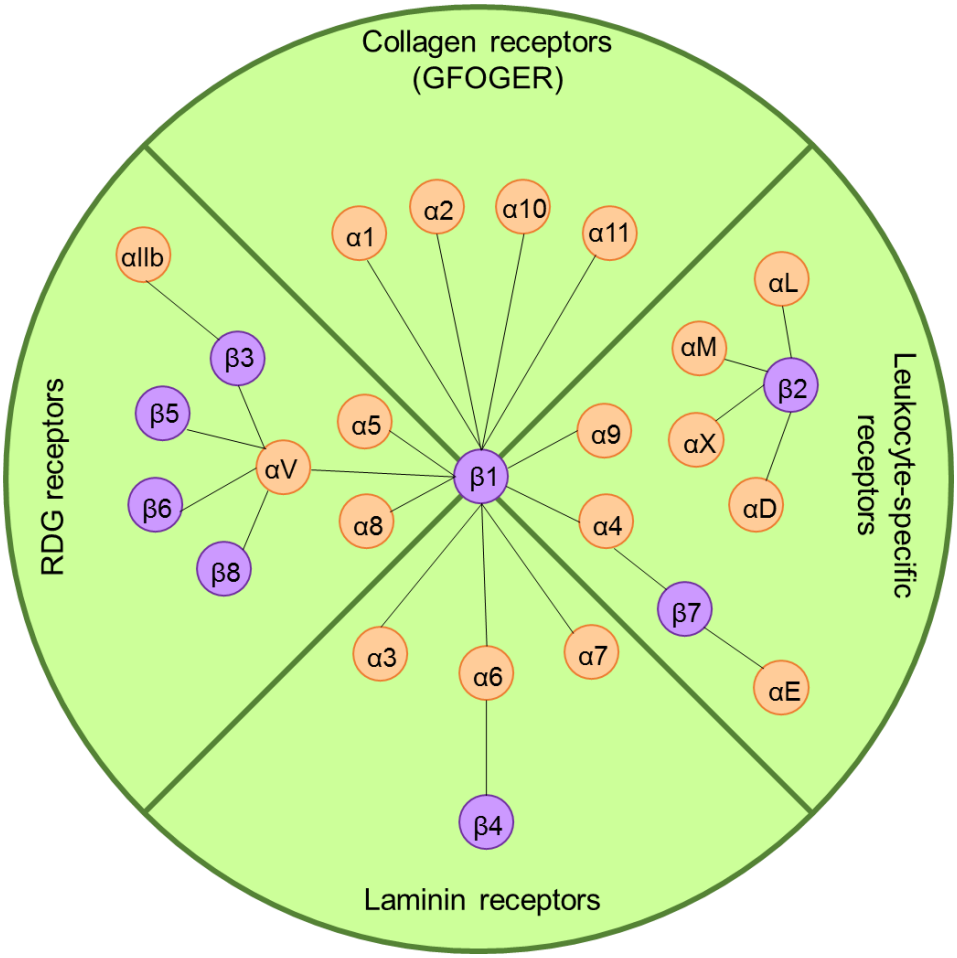

Figure 1.13. Representation of the integrin family. *A (orange) and β (purple) pairs are indicated by a black line. Integrins involved in either RDG receptors, collagen receptors, leukocyte-specific receptors and laminin receptors are contained within the appropriate area. Figure adapted from [142].*

Early experiments from Wang *et al* demonstrated integrin β1 induced focal adhesion formation through magnetic twisting of cell membrane [144]. Endothelial cells were allowed to bind beads coated with RGD peptide and transmembrane force transfer was observed [144]. Incubating the cells with inhibitor of actin polymerisation cytochalasin D lead to a decrease in force transfer and stiffening of the cytoplasm [144]. In addition to this, focal adhesion proteins talin, vinculin and α-actin were also found to be recruited to the RGD coated beads [144].

Integrins are essential in sensing ECM components and mechanical strength, as well as transmitting this to the cell. Any changes in these factors has the potential to alter cell behaviour. In particular, integrins are known to have a role in osteogenic differentiation of SSCs [143]. Expression of integrin subunit αv was found to be up-regulated during dexamethasone-induced osteogenic differentiation [145], leading to activation of focal adhesion kinase/MAPK signalling [145]. OPN contains an RGD motif and binds integrin αv/β1 [14]. Blocking this integrin through antibody neutralisation had a negative effect on osteogenic differentiation, skewing the balance towards adipogenesis [14]. Mechanical properties of the ECM are therefore important in controlling the balance between osteogenesis and adipogenesis of SSCs.

Further to this, the role of β1 in migration was studied in rat bone marrow derived MSCs (rMSCs) [146]. rMSCs migrated towards OPN in a concentration dependent manner and OPN had no effect on proliferation [146]. With OPN stimulation, an increase in *β1 i*ntegrin subunit was detected, relative to expression of control OPN surface receptor, CD44v6 at both the mRNA and protein level [146]. Similar to in previous study of Chen *et al* [14] blocking *β1 i*ntegrin through antibody neutralisation, OPN-mediated migration was inhibited [146].

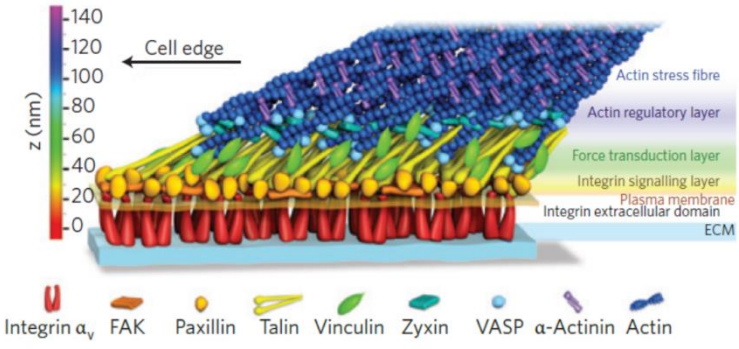

Figure 1.14. Integrin clustering to form focal adhesion complex. *Diagram indicates proteins involved in formation of focal adhesion complex. Modified from [147].*

1.7.1.2. Mitogen-activated protein kinase (MAPK) signalling in mechanotransduction

MAPK pathways link extracellular signals of mechanotransduction to intracellular signalling that control differentiation, proliferation, and migration to name a few [127]. MAPK pathways are composed of three levels of signal transduction whereby MAPK is activated through phosphorylation, activated MAPK kinase (MAPKK), which in turn activated MAPKK kinase (MAPKKK) [127]. There are three groups of MAPK cascades: extracellular signal-related kinase (ERK), the c-Jun NH_2-terminal kinase (JNK), p38 MAPK cascade [127]. One of the best characterised of these cascades is ERK. RUNX2 is known to be phosphorylated and therefore activated by ERK signalling [148], following *RUNX2* transcriptional induction by TGF-β [113]. RUNX2 is thought to have a role in mechanotransduction as its expression is known to increase during mechanical loading, through ERK and JNK cascades [148, 149]. Another target of ERK is the mechanically sensitive key enzyme in prostaglandin production, cyclooxygenase-2 (COX-2) [150, 151]. Wadhwa *et al* subjected primary osteoblasts from mice calvaria to steady fluid shear stress and found upregulation of *COX2* mRNA [151]. Inhibiting ERK phosphorylation using specific inhibitor PD98059 lead to a decrease in *COX2* mRNA levels [151].

1.7.1.3. Wnt Signalling in mechanotransduction

Wnt signalling has a well-established role in osteogenic differentiation, however, its role in mechanotransduction has only recently been uncovered. Sclerostin, gene name *SOST* is a known potent inhibitor of Wnt signalling and therefore bone formation. In wild type mice, a decrease in Wnt signalling was observed following mechanical unloading, along with increase in both *Sost* expression and bone loss [152]. When *Sost* null mutant was studied, mechanical unloading related bone loss was prevented and Wnt signalling was not altered [152]. Sclerostin is expressed from osteocytes to inhibit bone formation in osteoblasts [153]. Mechanical force, sensed by osteocytes, reduces sclerostin expression, and this leads to increased bone formation [153]. It could be postulated that osteocytes use sclerosin to communicate with osteoblasts, and inhibit the activity of osteoblasts. In order to investigate this, Tu *et al* designed transgenic *Sost* mice which overexpressed human *SOST* under and osteocyte specific promoter [153]. Attenuation of Wnt signalling was observed during overexpression of *SOST* under mechanical stimulation, relative to wild type mice, confirming the role of Wnt in mechanotransduction [153].

1.7.1.4. YAP/TAZ signalling in mechanotransduction

YAP (Yes-Associated Protein) and TAZ (Transcriptional coactivator with PDZ-binding motif) are two homologue transcriptional co-activators which, upon activation by dephosphorisation,

travel to the nucleus to induce expression of target genes [154]. YAP/TAZ signalling is a part of the Hippo pathway, which controls cell proliferation by contact inhibition [155]. Contact inhibition is the process by which cells cease proliferation on monolayer in a culture dish when there is no longer any space on the culture dish. Cell contact through for example cadherins activates Hippo signalling and leads to the prevention of nuclear accumulation of YAP protein, stopping YAP induced expression of cell proliferation genes [155, 156]. YAP/TAZ can sense mechanical stimulation. While on stiff substrates, YAP/TAZ are activated, with high nuclear accumulation and high transcription of targets genes compared to on stiff substrates [154]. Further to this, YAP/TAZ are known to be activated during osteogenic differentiation [157].

1.7.2. Cytoskeletal tension and mechanotransduction

The cytoskeleton of the cells is formed from actin fibres, myosin fibrils and microtubules which coordinate to control cell shape, movement and respond to biological signals. The close relationship between cytoskeleton, integrins and focal adhesion is one of the mechanisms by which external signalling results in changes in intracellular signalling, transmitting through the cytoplasm [158]. Tension within the cytoskeleton is known to be controlled by small GTPase RhoA and its effector ROCKII and results in myosin moving along actin fibrils, increasing cellular tension [159]. Cytoskeleton inhibitors were used to disrupt the cytoskeleton and examine the effect the integrity of the cytoskeleton had on osteogenic differentiation [159]. When C3H10T1/2 progenitor cells were exposed to cytochalasin D, an inhibition of actin polymerisation was observed only after mechanical stimulation, inferring that mechanical stimulation is essential to actin fibre formation [159]. The activation of RhosA/ROCKII pathways was measured by observing expression of downstream target, *RUNX2*, induction [159]. After mechanical stimulation, *RUNX2* expression was found to increase and cytoskeletal tension increased [159]. In addition to this, a decrease in adipogenic marker *PPARG* was observed during mechanical stimulation, illustrating the role mechanostimulation has in osteogenic differentiation [159].

Given integrins attach to the cytoskeleton through focal adhesion complexes, it could be postulated that integrins can, through the cytoskeleton, attach to the nucleus. The role integrins play in differentiation could be due, in part, to this link which allows changes in the shape of the nucleus, potentially altering gene expression. Maniotis *et al* used micromanipulation of integrins via microbeads to mechanically pull cells and alter cytoskeletal tension [160]. The authors noted both cytoskeletal and nuclear distortion when the microbeads were pulled [160].

1.7.3. Material stiffness and SSC differentiation

Given the importance of mechanotransduction on osteogenic differentiation, and the role of cytoskeletal tension, it is reasonable to hypothesise that the surface SSCs are cultured on *in vitro* will effect mechanotransduction signalling and SSC fate. Indeed this is the case and it has been confirmed that substrate stiffness has a big role to play in SSC differentiation [161].

1.7.3.1. Cell culture substrate materials

Polystyrene has been used as a cell culture surface for over 30 years [162], and is the most common material for cell cultures. Material properties can vary in terms of substrate topography, stiffness and surface chemistry. Substrate materials can have patterned substrates, and this variation in topography is known to affect stem cell behaviour. This is thought to affect how the cells adhere to the surface, which in turn alters intracellular signalling. The stiffness of a substrate is determined by its elastic modulus, or Young's modulus, which is independent of the dimensions of the surface and is measured in Pascals (Pa). Hydrogels can have a highly tuneable elastic modulus ranging from 0.5 kPa up to 740 kPa for polyacrylamide hydrogel [161]. Added to this, the surface chemistry will have a role in cell-surface adhesion. The chemistry of a surface is known to have a role in integrin binding and different integrins favour different surface chemistry [163]. Hydrophobic surfaces modified with $–CH_3$ methyl groups displayed low level of focal adhesion assembly, and highlights the importance of a hydrophilic surface in culturing cells [163]. When chemical modifications of glass culture surfaces were investigated, it was discovered that $–NH_2$ and –SH modifications promoted osteogenesis of SSCs [164].

1.7.3.2. Effect of material stiffness on SSC behaviour

In vivo, cells adhere to the ECM, which allows cells to sense their environment [165, 166]. Cells can bind to ECM proteins and, as well as altering molecular signalling, this allows for cells to recognise mechanical properties of the surface. Linking to this, when stem cells are cultured *in vitro*, the stiffness of material and shape of material is known to have a role in controlling cell behaviour including fate of stem cells, in particular osteogenesis [161].

Material stiffness and geometric cues have emerged as key factors in modulating stem cell differentiation, and as key properties regulating the stem cell niche environment. Trappmann

and colleagues reported that culturing MSCs on soft (0.5 kPa) polyacrylamide (PAAm) hydrogels increased Oil Red O staining, indicating adipogenesis, whereas culturing MSCs on stiff (115 kPa) PAAm hydrogels increased ALP staining, indicating osteogenesis (Figure 1.15) [167]. Previous consensus was that stem cell fate on hydrogels was controlled by stiffness of the hydrogel alone. Further to observations of the effect of material stiffness on MSC differentiation, Trappmann and colleagues, using collagen cross-linked hydrogels, demonstrated that mechanical feedback from the ECM had a role in controlling stem cell fate [161]. Soft hydrogels with a low level of cross-linked collagen resulted in MSCs exerting a low mechanical force on the hydrogel and subsequent differentiation to give adipogenesis. In contrast, stiff hydrogels with a higher level of cross-linked collagen, resulted in high mechanical force exerted by MSCs on the hydrogel and subsequent osteogenesis [161], highlighting the importance of a stiff substrate for osteogenic differentiation.

Further to this, Swift *et al*, studied the levels of nuclear lamin-A, a nucleoskeletal protein, during osteogenesis and adipogenesis on soft and stiff substrates [168]. It was noted that low levels of lamin-A were favourable for adipogenic differentiation on soft substrates, whereas high lamin-A levels were favourable for osteogenic differentiation on stiff substrates [168]. The nucleus, therefore, has the ability to sense material stiffness and mechanical stimulation and is altered as a result.

The effect of collagen tethering to hydrogels was investigated to determine if collagen tethering or hydrogel stiffness was the dominant factor [169]. In order to do this, PAAm hydrogels, either soft or stiff, were synthesised with a collagen covalently bonded to the surface of the hydrogel. The authors reported collagen tethering did not affect differentiation of adipocyte stromal cells [169]. However, altering the stiffness of hydrogel did have an effect, with a stiffer hydrogel enhancing osteogenesis [169]. For osteogenesis, the stiffness of a substrate is more important than collagen covalently bonded to the surface.

In conjugation with stiffness, it is known that cells can sense underlying materials with varying stiffness and therefore substrate thickness. To study this, a substrate material of glass with PAAm hydrogel on top was generated and the thickness of the PAAm hydrogel altered [170]. The behaviour of MG63 osteosarcoma cell lines cultured on these surfaces was studied in terms of cell area. It was found that cell area, both single cells and in colonies, decreased as thickness increased and these cells on thinner substrates can sense the glass underneath the hydrogel greater than cells on thicker hydrogels [170].

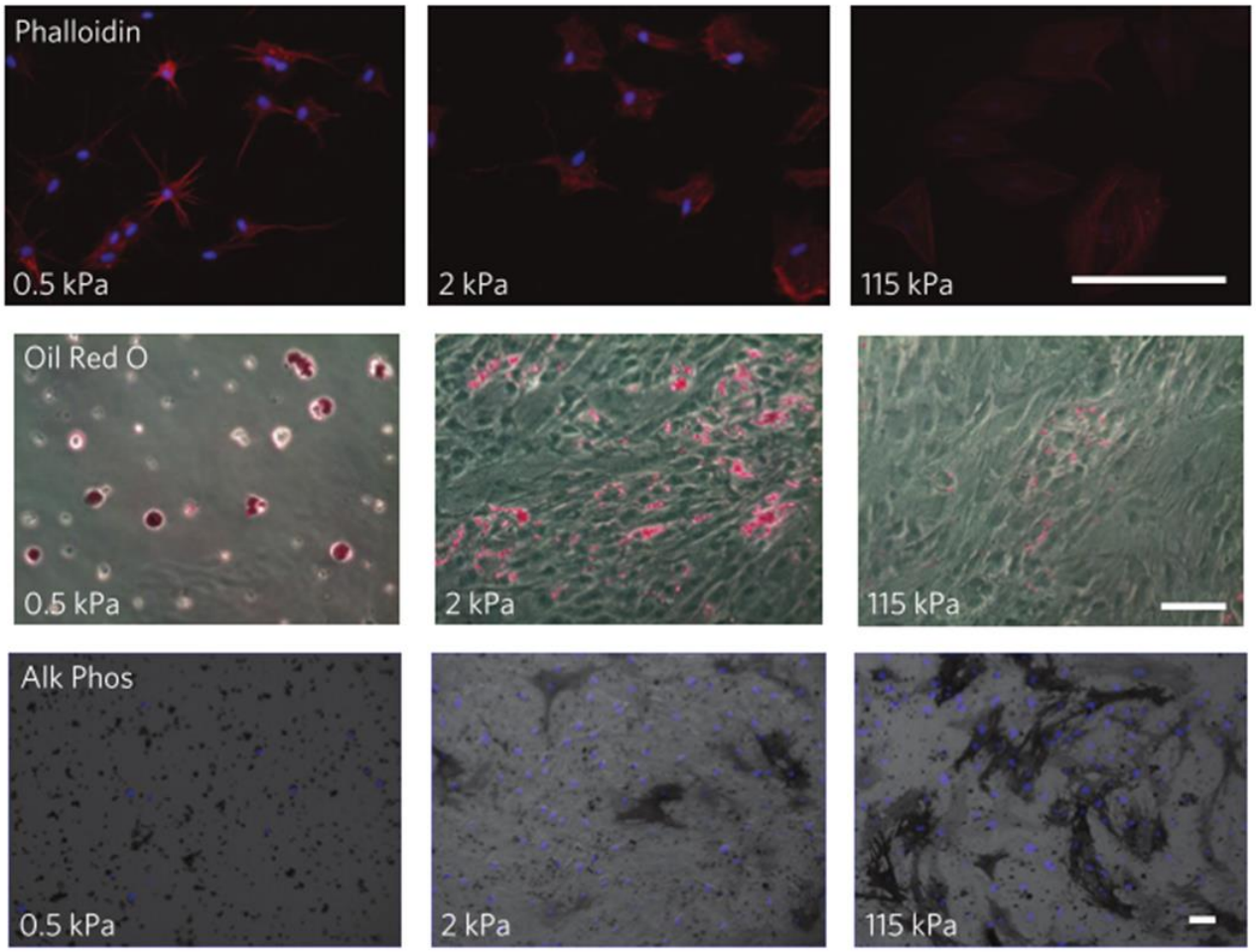

Figure 1.15. Influence of substrate stiffness on MSCs differentiation. *MSCs were cultured on PAAm hydrogels with elastic modulus detailed on each image. Cells were staining with phalloidin to visualise actin filaments. Oil Red O staining is an indicator of adipogenesis. Alk Phos (ALP) staining is an indicator of osteogenesis. Nucleus is counterstained with DAPI. Image modified from [161].*

1.8. Topography

A significant amount of research has centred on the development of materials with properties which display efficacy to induce osteogenic differentiation during culture. Materials including titanium, polycaprolactone (PCL) and poly(methyl methacrylate) (PMMA) have found application in culture of osteoblasts for potential use in regenerative medicine [132, 171, 172]. Recent developments, over the last decade, have indicated the potential of material surfaces displaying discrete topographical cues to modulate stem cell fate and function [173-175]. Topographical materials have surface features at both the micro- and nanoscale and recent work has centred on harnessing these properties to augment cell function [143]. Topographical features that enhance osteogenesis could be used as a culturing surface for growing SSCs for therapeutics, or incorporated into scaffolds to increase osteogenic differentiation around scaffold. In addition, topographical biomaterials could be modelled on the surface of orthopaedic implants to improve bone growth around the affected bone region after surgery and reducing the risk of failure of the implant due to loosening, subsequently offering the potential to prolong the lifespan of implants.

Cells process information about the shape of their environment as well as the stiffness of substrate. 2D surfaces stamped to create pitted shapes of either smooth flowers or sharp stars were used to show that SSC fate is controlled by shape of their environment [133]. The star shaped pits were found to promote osteogenesis when cultured in a media with 1:1 ratio of osteogenic and adipogenic factors, whereas SSCs cultured in flower shaped pits patterned monolayers with the same media were found to have an increased adipogenic fate [133]. In addition, SSCs cultured in star shaped pits had high, strong stress fibres at the points the star, and SSCs in flower shaped pits had few stress fibres (Figure 1.16) [133], indicating the important role of the cytoskeleton in osteogenic differentiation. Blocking integrin α1β5, an RGD binding ligand, caused an increase in adipogenic cell fate in both shapes [133]. Consistent with the positive role of Wnt signalling in osteogenesis, treatment with recombinant Wnt inhibitors Dickkopf1 (DKK1) and secreted frizzled-related protein3 (sFRP3) lead to decreased osteogenesis on star shapes [133]. The flower and star shaped on patterned monolayers could be said to create an environment for concentration of focal adhesions which could potentially result in either adipogenic or osteogenic differentiation. This work is a good example of the importance of patterns on culturing substrates to control osteogenesis.

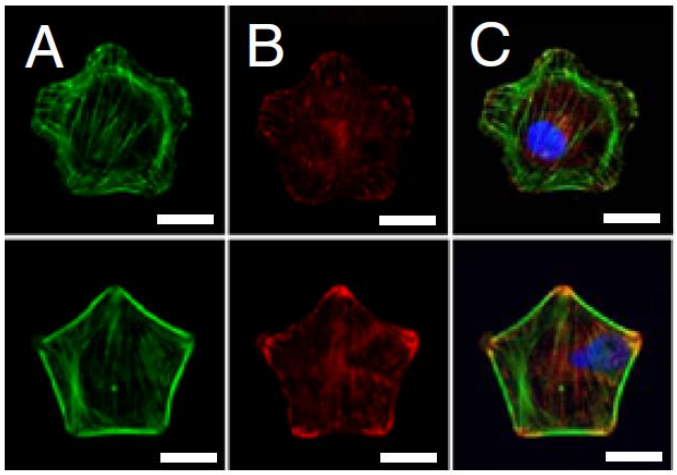

Figure 1.16. Immunofluorescent images of SSCs in flower and star shapes. *SSCs in flower (top row) and star (bottom row) shapes stained for F-actin (A- green), vinculin (B- red) and nuclei (C- blue, with F-actin and vinculin merged). (Scale bar, 20μm). Modified from [133].*

Stem cells have been shown to have the ability to sense the mechanical properties of the substrates upon which they are cultured, with a stiff substrate observed to be favourable for osteogenic differentiation. Further to this, small geometric changes on the micro- and nanoscale, or topographical modifications, can also have a large impact on stem cell fate. A variety of topographical surface features have been studied as potential biomaterials to control osteogenesis of SSCs [132, 173, 174, 176] with arrangements including pitted arrangements [132, 133, 175, 177], nanotubules [174], grates [178], hemispheres [179] and pillars [176, 180].

A study by Li *et al* looked at osteogenic differentiation on stiff and soft substrates with both pillar or groove topography and aimed to determine if substrate stiffness is a more dominant factor compared to topography for osteogenesis [176]. *RUNX2* expression, an indicator of osteogenesis, increased when SSCs were cultured on a stiff substrate compared to a soft substrate. Interestingly, expression was less varied between pillar and groove topographies indicating topography has less of an impact on osteogenic differentiation than stiffness, though nevertheless had an influence [176].

Furthermore, topography has been found to have an effect on nuclear deformation [181]. Wang *et al* reported alteration on nuclear area when fibroblasts were cultured on nanogroove substrates [181]. In a second study, nuclear deformation in MSCs was shown to increase with increase in height of topographical pillars, and this was maintained during differentiation [182]. Topography in this context, could have a similar effect on nucleoskeletal dynamics as material stiffness.

1.8.1. SSC osteogenesis on nanotopographical surfaces in the absence of chemical cues

Using osteogenic chemicals, it is possible to promote osteogenesis of SSCs. In order for SSCs to be used in a therapeutic context, osteogenic differentiation of SSCs needs to be controlled. However, *in vivo* it is difficult to control local concentrations of osteogenic chemical due to diffusion within the body making osteogenic differentiation after cell therapy challenging. As discussed in section 1.6.2., ideally, osteogenic stem cell fate would be promoted on biomaterials without the need for chemical cues, prior to treatment. This biomaterial could also be used in the body to promote osteogenic differentiation of local SSCs. There are studies using biomaterials with various topographical and mechanical properties that potentially offer such an approach [143, 174, 180].

Titanium metal is currently used in metal hip replacements and has a long history of use in surgery making it ideal for osteo-implants [183]. SSC fate was studied on a vertically aligned TiO_2 nanotube surface with varying diameters in the absence of osteogenic chemical promoters [174]. *OCN* and *ALP* were found to be upregulated on surfaces with 70 nm or 100 nm diameters, and to a lesser extent *OPN*, indicating osteogenesis in the absence of chemical cues [174]. Titanium nanopillar topographies have also been shown to induce osteogenesis in the absence of osteogenic factors. An increase in *RUNX2* and *OCN* expression in SSCs cultured on 15 nm high titanium nanopillars was observed compared to a planar surface without osteogenic media [180].

There are currently research efforts aimed at improving osteo-implants by offering an alternative implant material to titanium. Herath and colleagues studied the material zirconia as an alternative to titanium, and the effect of altering topography of zirconia on human osteoprogenitor cells [184]. Varying sintering time and temperature of zirconia powder resulted in alterations in the grain size of the zirconia surface and porosity and therefore topography [184]. The authors discovered that on both polished and grain-like surfaces, protein levels of osteogenic markers ALP and OCN increased, indicating potential osteogenic differentiation on all surfaces [184]. However, proliferation was highest on polished surfaces [184]. This work illustrates, again, that surface material and topography work together to alter cell behaviour.

Dalby and Oreffo's groups have cultured SSCs on stiff PCL surfaces with a pitted nanotopography generated using electron beam lithography (EBL) [132]. A disordered square, or near square (NSQ), arrangement of nanopits was found to promote osteogenesis as measured by increase OPN and OCN in the absence of chemical cues [132]. Higher levels of actin and myosin, and increased vinculin staining in SSCs grown on the surfaces indicates higher contractility and increased focal adhesions [177]. The cells therefore exerted a

mechanical force on the surface, similar to osteoblasts on bone, which, through mechanotransduction, lead to osteogenesis. In contrast, an ordered square arrangement prevented differentiation and retained the stem cell phenotype [175]. SSCs grown on this substrate exerted a lower force on the substrate than the disordered [177].

A varying range of nanotopographical surfaces have been shown to modulate osteogenesis. These surfaces could be modelled onto implants or scaffolds to be used with bone regeneration therapies, or to grow osteoblasts for cell therapy. SSCs have the potential to differentiate into other stromal lineages including adipocytes, chondrocytes, and osteoblasts, and use of these topographies offers new approaches to tissue modulation. Use of ordered square pitted nanotopography developed by Dalby and Oreffo, that maintains stem cell characteristics, would be valuable for high quality stem cell culturing to use as cell based therapies requiring SSC progenitors.

1.8.2. Nanotopography and integrin signalling

The signalling involved in stem cell response to topography is beginning to be explored and, it has become apparent that integrins play an important role in the mechanism by which nanotopography affects stem cell differentiation [143]. Dalby *et al* have postulated that the disordered square arrangement of nanopits enhances osteogenic differentiation by forcing integrins to cluster [143]. This ties in with studies which have detailed higher contractility and increased focal adhesion numbers when SSCs are cultured on the disordered square pits [177].

Indeed, nanospacing of RGD ligands was found to have a role in controlling lineage commitment of stem cells [185]. In published studies, RGD ligands were bonded to poly(ethylene glycol) (PEG) hydrogel with range of spacing from 37 nm to 124 nm apart. MSCs were subsequently cultured on these RGD modified PEG hydrogels under a 50:50 mixture of adipogenic and osteogenic media. It was discovered that a higher RGD nanospacing favoured osteogenic differentiation, and smaller RGD nanospacing favoured adipogenic differentiation (Figure 1.17) [185]. The authors noted that increased nanospacing lead to increased cell spreading which, in part could be leading to increased osteogenic differentiation on surfaces with large RGD nanospacing. Continuing from these experiment, the authors studied the effect of surface stiffness and RGD nanospacing [186]. In order to do this, RGD ligands were bonded to PEG hydrogels as before, however the stiffness of these hydrogels was altered to create a soft and stiff hydrogel. The authors found that both stiffness and RGD nanospacing had an effect on MSC behaviour, with large nanospacing and stiffer substrates favouring

osteogenesis [186]. Added to these observations, as previously described, Kilian *et al* used flower and star patterns to study the effect of shape and MSC behaviour (Figure 1.16). When the authors blocked integrin α1β5, they noted an increase in adipogenesis [133]. Dalby *et al* postulated integrin clustering promoted osteogenic differentiation [143], which apparently contrasts to published studies by Wang *et al*, 2013, and Ye *et al* 2015 [185, 186]. Taking into consideration experiments into RGD ligand spacing, it could be that integrins clustered with large spacing between them leading to the enhancement of cell spreading and osteogenic signalling.

As discussed previously, integrins connect to the cytoskeleton through focal adhesion complexes, and a key component of focal adhesion complexes is FAK. Teo *et al* cultured human MSCs on a nanogrooved substrate, with featured 250 nm apart, and found MSCs aligned to the direction of the nanogrooves [187]. When studying FAK, the authors discovered cells on nanogrooves had higher levels of phosphorylated FAK, indicating higher FAK activity [187]. When FAK was inhibited, inhibition of neuronal differentiation was observed through a decrease in neuronal markers [187].

Together, the studies discussed indicates the important role of integrins in stem cell response to nanotopography.

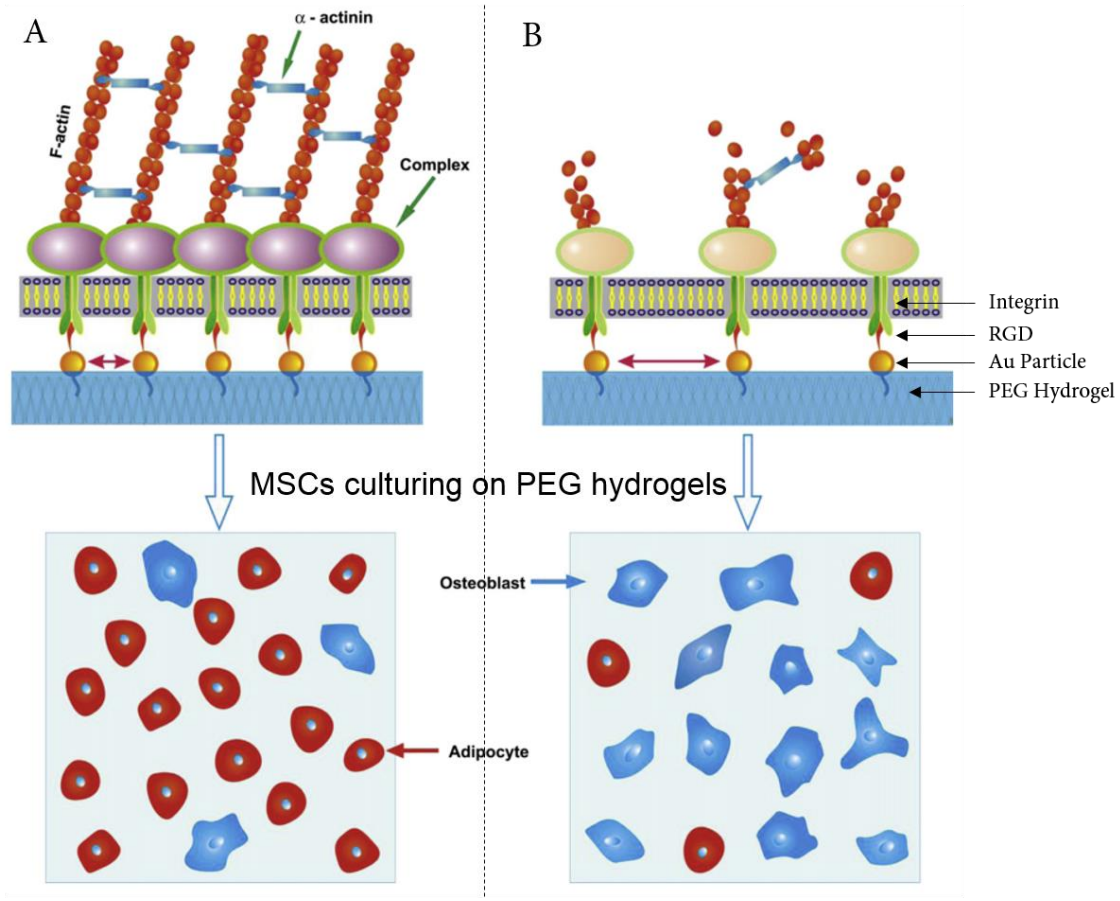

Figure 1.17. Effect of RGD ligand spacing on MSC differentiation. *RGD ligands were attached to PEG hydrogel via a gold particle. A – RGD ligands spaced close together increases focal adhesion formation. B – RGD ligands spaced far apart does not favour focal adhesion formation. Image modified from [185].*

1.9. miRNAs

MicroRNA (miRNA) are 20-22 base pair RNA oligonucleotides which bind to and negatively regulate translation of mRNA into protein. The basic structure of a miRNA and how it binds to mRNA is detailed in Figure 1.18.

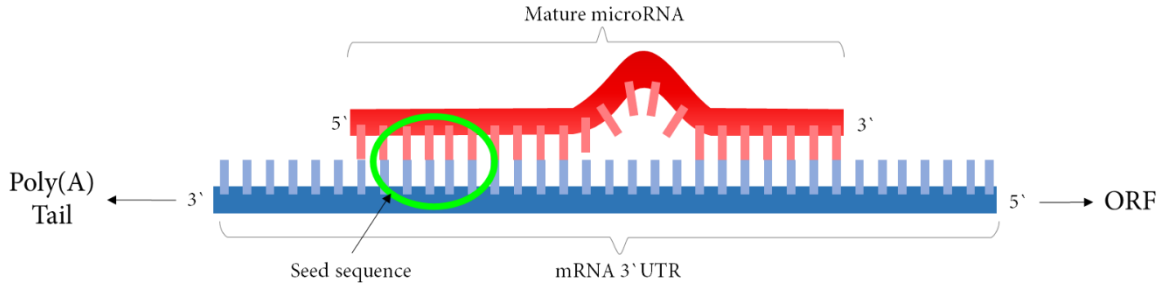

Figure 1.18. Schematic of microRNA binding to mRNA. *Ribose-phosphate backbone of either mRNA (blue) or miRNA (red) is indicated by thicker line. Nucleobases are indicated by light blue and light red rectangles. ORF- open reading frame. UTR – untranslated region. Direction of stand is indicated by 5` or 3`. Seed sequence is indicated by green circle.*

1.8.1. Discovery of miRNA

miRNAs were discovered in 1993 in the Ambros and Ruvkun laboratories when studying developmental genes *lin-4* and *lin-14* in *C. elegans* with Ambros studying lin-4 and Ruvkun focusing on lin-14 [188, 189]. In 1993, both labs independently published that *lin-4* negatively regulated *lin-14* though a previously unknown post-transcriptional mechanism, with lin-4 RNA imperfect base pairing to *lin-14* mRNA 3` untranslated region (3`UTR) [188, 189]. Initially this type of regulation was thought to only occur in *C. elegans*, as no lin-4 homologs were found. Indeed, it was not until 2000 when let-7, which had homologs in drosophila and humans was discovered, that miRNA research exploded [190]. Since then, a redesign of classical PCR primers to create stem-loop reverse transcription primers and improvements in next-generation sequences have allowed for easier detection of miRNA [191]. There has been significant effort put into the generation of target prediction programmes (TargetScan, and miRanda, and miRNA database, miRBase, created in 2002 now has over 25,000 entries) to aid miRNA research.

1.8.2. Gene expression regulation by miRNAs

miRNAs are found in the genome, either between genes (intergenic) or more rarely within introns (intronic). The biogenesis of miRNAs is described in Figure 1.19. Initially miRNA were believed to be transcribed by RNA Polymerase III as this transcribes tRNA, another small RNA, however it was discovered by Lee *et al* to be RNA Polymerase II (Pol II) [192]. Pol II produces

long primary-miRNA (pri-miRNA) from intergenic miRNA genes, which are modified with a 5'cap and polyadenylated similar to mRNA processing [193]. Shortly after transcription, the pri-miRNA base pairs to itself, forming a hairpin loop, which allows the miRNA to be recognised by RNAse III Drosha. Drosha is the catalytic component of the microprocessor complex, which includes DGCR8 in mammals and Pasha in other animals. DGCR8 restricts Drosha's substrates to improve cleavage accuracy. Drosha cleaves the pri-miRNA into one or more pre-miRNAs of about 60-70 base pairs in length removing the 5' cap and poly(A) tail [194, 195]. Poly cistronic miRNA or clusters of miRNA within the one pri-miRNA are common and allows multiple pathways to be regulated within one promoter, coordinating signals between pathways [196]. Cleavage by Drosha is essential to export from the nucleus because cleavage allows for recognition by nuclear export protein, exportin 5 [197]. Once in the cytoplasm, pre-miRNA is recognised by Dicer-1, a second RNase III enzyme, which removes the loop in pre-miRNA to produce a ~22 nucleotide mature miRNA duplex. The duplex is passed onto Argonaute proteins (AGO1-4), where the passenger strand is removed. AGO, together with supporting proteins, form the RNA-induced silencing complex (RISC) that directs miRNA to their target mRNA. The first 2-7 nucleotides, the so-called "seed sequence" at the 3' end of miRNA are the most important for determining target specificity [198, 199]. Imperfect base pairing of miRNA to mRNA 3`UTR impairs hydrogen bonding between miRNA and mRNA strands, which results in a structural bulge, disturbing the interaction between mRNA 5`-cap and poly(A) tail, which destabilises the mRNA [200]. This leads to deadenylation and the removal of 5-cap which induces silencing. Perfect, highly complementary base pairing results in activation of the endonuclease activity of AGO2 only, leading to degradation of miRNA and target mRNA [201]. This is known to power RNA interference approaches, and down regulate target mRNA, however it is unknown how large a role it plays in miRNA induced silencing [202].

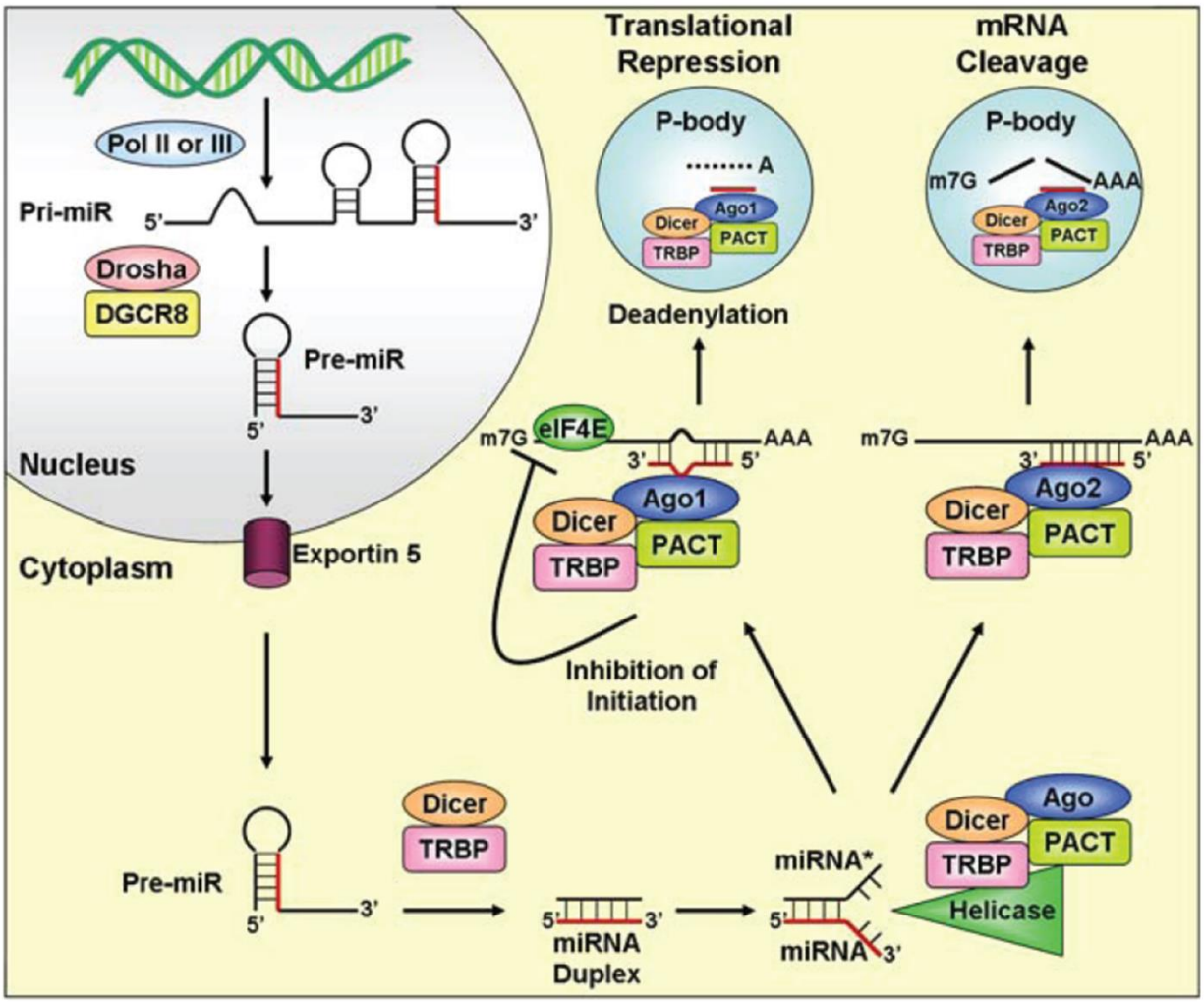

Figure 1.19. miRNA biogenesis. *In the nucleus miRNA are transcribed by RNA Pol II or III and cleaved into pre-miRNA and exported to the cytoplasm. Here, they are cleaved by Dicer and bound to the Argonaute complex. From this point, miRNA-mediated gene regulation can go in two directions: imperfect binding of miRNA to target induces deadenylation of target mRNA and transcriptional repression of that mRNA, or perfect binding of miRNA to target mRNA induces cleavage of target mRNA. Image modified from [203].*

1.8.3. miRNA-mediated regulation of osteogenesis

In osteogenesis, key miRNA can act as switches either retaining “stemness” or promoting differentiation to osteoblasts and, to date, a wealth of miRNAs known to be involved in osteogenesis have been identified (selection described in Figure 1.20 and Table 1) [1].

miR-2861, which targets histone deacetylase 5 (HDAC5), was identified from primary mouse osteoblasts and is conserved in humans. *In vivo* experiments using miR-2861 antisense oligonucleotides resulted in a reduction in bone mineral density in mice, illustrating miR-2861 role in bone formation [204]. Genome studies on patients with OP revealed a single nucleotide polymorphism (SNP) in pre-miR-2681, which corresponded with a decreased level of HDAC5 when the mutation was expressed in HEK 293 cells. The mutation, although common in certain families, is rare and so is unlikely to be disease causing in the wider population. HDAC5 was known to enhance *RUNX2* degradation, and therefore miR-2861, by targeting HDAC5, could in turn stabilise *RUNX2* levels. Further to this study, miR-3960, which was identified at the miR-2861 gene cluster, was found to target Hoxa2, a transcription factor controlling *RUNX2* expression [205]. *RUNX2* overexpression lead to an increase in miR-3960/miR-2861 levels and ChIP assays confirmed *RUNX2* could bind both miR-3960/miR-2861 promoters, suggesting that *RUNX2* could directly increase miR-3960/miR-2861 levels.

miRNAs have also been implicated in controlling the balance between osteogenesis and adipogenesis of MSCs. miR-637 levels increase during adipogenesis and decrease during osteogenesis of human MSCs isolated from bone marrow [206]. Importantly, miR-637 levels were higher in MSCs obtained from older patients with OP than from younger patients. This is consistent with the idea that an accumulation of bone marrow with age, resulting in a decrease of bone volume, contributes to OP and highlights the therapeutic potential of miR-637 inhibition as an OP treatment [207].

Wnt signalling is known to play a central role in osteoblast differentiation and miR-218 has been identified as a key regulator of this process [208]. Over expression of miR-218 in bone marrow-derived MSCs resulted in an increase in *RUNX2* expression and ALP activity, indicating an increase in osteogenesis [208]. This is achieved through miR-218 targeting Wnt inhibitors *Tob, Sost, Sfrp2* and *Dkk2,* leading to an increase in Wnt signalling. Studies using human adipose derived stem cells (hADSCs) revealed a feedback loop between miR-218 and Wnt signalling, with Wnt signalling having a positive effect on miR-218 expression [209].

Chen and colleagues performed a miRNA microarray on SSCs following osteogenic induction of cultures on 3D-spheroid cultures [210]. When compared to a control, an intense up-regulation of miR-34a was observed over 14 days and was confirmed using *in situ*

hybridisation. Inhibition of miR34a by use of an anti-miR34a led to an increase in osteogenic gene expression, whereas over expression of miR34a through pre-miR-34a transfection led to a decrease. Together, these results indicate miR34a is a negative regulator of gene expression during osteogenesis [210]. miR-34a achieved regulation through targeting JAG1 [210].

In a separate study, microarray analysis has been used to compare miRNA profiles expressed in fibroblasts against SSC populations derived from a variety of sources including adipose-derived stem cells, bone-marrow derived stem cells and umbilical cord-derived stem cells [211]. miR-140 was found to be enriched in all three cell sources. Luciferase assay confirmed BMP2 as a target for miR-140. miR-140 levels decreased during osteogenic differentiation to allow for osteogenesis, as marked by an increase in BMP2 protein, as well as osteogenic proteins ALP and osteocalcin. Here, microarray was successfully deployed to predict miRNAs involved in stem cell maintenance.

Activation of the Wnt pathway through inhibition of Wnt inhibitor GSK-3 is known to enhance osteogenesis [212]. Wang *et al* used microarray miRNA screening and miRNA target prediction software to identify GSK-3 as a target for miR-346 [213]. This was later found to be essential for GSK-3 inhibition and therefore Wnt-induced osteogenesis [213].

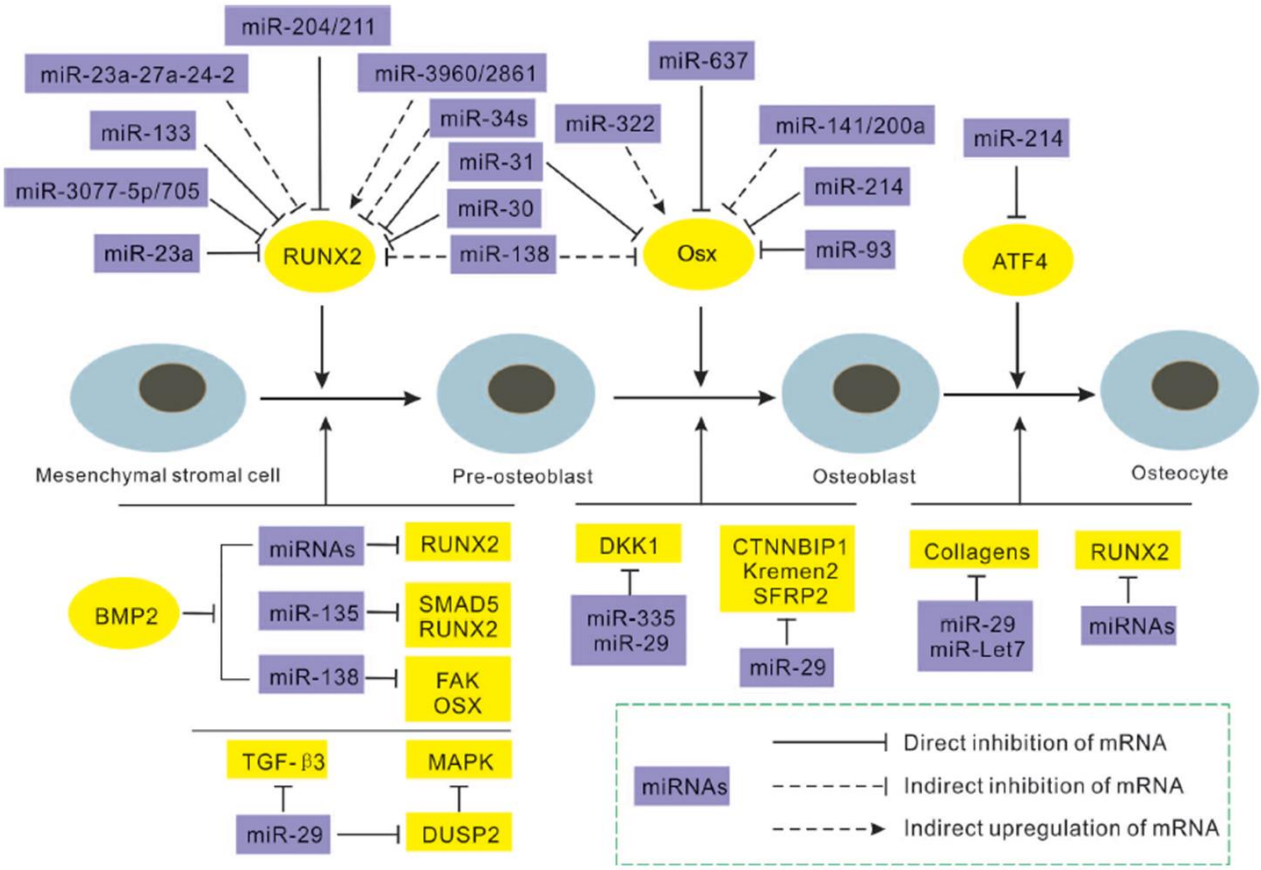

Figure 1.20. miRNAs known to be involved in osteogenesis. *miRNAs are in purple box and proteins in yellow box. Legend describe manner in which miRNA regulate protein expression. Modified from [214].*

miRNA	Positive or negative regulators of osteogenesis	Known targets
15b [215]	Positive	*SMURF1*
23a [216, 217]	Negative	*RUNX2*
23b [217]	Negative	*RUNX2*
27 [218]	Positive	*APC*
29b [219]	Positive	*COL1A1, COL5A3, COL4A2, HDAC4, TGFB3*
34a [210]	Negative	*JAG1, CCND1, CDK4, CDK6*
138 [220]	Negative	*FAK*
140 [211]	Negative	*BMP2*
154 [221]	Negative	*WNT11*
218 [208]	Positive	*SOST, DKK2, SFRP2*
637 [206]	Negative	*SP7*
2861 [204]	Positive	*HDAC5*
3960 [205]	Positive	*HOXA2*

Table 1. miRNAs involved in osteogenesis. *Highlighted are examples of miRNAs involved in osteogenic differentiation and whether the miRNAs are up or down regulated during osteogenesis. Known targets of miRNA are indicated.*

1.8.4. miRNA involved in SSC response to nanotopography

Given miRNAs have a major role to play in regulating osteogenic differentiation, it is highly likely miRNAs will play a role in SSC response to nanotopography. It is known that genome wide expression differs from dexamethasone-induced osteogenesis to nanotopographical induced differentiation [132]. Following from this concept, it should be expected miRNAs regulating SSC response to nanotopography will vary from those involved in osteogenic differentiation after culture in osteogenic media. Currently, there is little information as to how miRNAs control the cell-nanotopographical response.

Upon analysis of miRNAs dysregulated on osteogenic titanium nanotopographical surfaces displaying a pitted arrangement compared to a flat titanium surface, 40 miRNAs were found to be either up or down regulated [222]. Three miRNAs in particular were observed to be more than 5-fold downregulated: miR-4448, -4708 and -4773 [222]. miR-4448, -4708 and -4773 are known to target SMAD1 and SMAD4, key downstream transducers of BMP-2 signalling [222]. Downregulation of these miRNAs during osteogenesis allowed for accumulation of SMAD1 and SMAD4 mRNA, which enhanced BMP-2-mediated osteogenesis.

Expression of *RUNX2*-targetting miRNA on SSCs cultured on disordered square nanopits developed by Dalby *et al,* was thought to be involved in nanotopographically-mediated osteogenic differentiation [217]. miR-23b was shown to be down regulated in response to nanotopography, compared to flat control surface [217]. Furthermore, after cells were treated with the BMP-2 inhibitor noggin, expression of miR-23a returned to basal levels [217].

These few studies have highlighted the role miRNA have in controlling nanotopographical changes in cell behaviour. Thus, when designing nanotopographical-based SSC therapies, understanding miRNAs could help elucidate the mechanisms by which nanotopography controls SSCs.

1.8.5. Therapeutic use of miRNA for treatment of degenerative bone disease

The potential of miRNAs to augment bone formation has been demonstrated in a number of murine studies. With both miR-138 and miR34a, a hydroxyapatite/ tricalcium phosphate (HA/TCP) scaffold was utilised in order to localise stem cells subcutaneously. Chen *et al* used a similar approach to study the role of miR-34a, which is a negative regulator of bone formation [210]. MSCs were transfected with pre-miR-34a, anti-miR-34a and control miR and loaded onto HA/TCP scaffolds and implanted subcutaneously into immunocompromised mice. Implantation of the scaffold with MSCs transfected with anti-miR-34a resulted in a more than 3.5-fold increase in bone formation [210]. Eskildsen *et al* used lipofectamine to transfect pre-

miR-138, anti-miR-138, and control miR into MSCs [220]. The cells were loaded onto HA/TCP scaffold and implanted subcutaneously into immunocompromised mice. Implantation of the scaffold comprising MSCs transfected with anti-miR-138 resulted in a 2.2-fold increase in bone formation. While, implantation of the scaffold comprising MSCs transfected with miR-138 mimic resulted in a 6.7-fold decrease in bone formation, supporting the observation that miR-138 is a negative regulator of osteogenic differentiation and bone formation [220]. This approach, combining MSC primed with miRNA inhibitor or mimic and a scaffold, suggests translational strategies to localise stem cells to bone.

Li *et al* used a miRNA intravenous therapy approach, without the use of the scaffold, to investigate the role of the positive regulator of osteogenic differentiation, miR-2861, on bone formation in mice [204]. When antagomiR miR-2861 was intravenously administered to induce miR-2861 silencing, a decrease in femur mineral density and trabecular thickness was observed. Following on from this work, Li *et al* studied the role of miR-2681 in the development of OP in human patients with primary OP. The authors identified in a human sibling pair, both suffering from OP, an undetectable expression level of miR-2861 in their bone. A homozygous SNP in pre-miR-2861 was identified and was suggested to be accountable for negligible miR-2861 expression levels and likely to be the confounding factor in the pathogenesis of primary OP. The authors suggest that dysregulation of miR-2861 is likely to induce defective osteoblast differentiation and subsequently contribute to OP. This mutation was found to be heterozygous in the parents of the sibling pair and these family members also suffered from OP. However, when extended to a larger cohort of 369 patients, the same SNP in pre-miR-2861 was not identified, indicating that the SNP was uncommon and not reflective of the general osteoporotic population. Nevertheless, the importance of miR-2861 in osteogenic differentiation and OP was highlighted, indicating its potential as a therapeutic approach.

1.10. Cellular Metabolism

Cellular metabolism encompasses the processes by which cells extract energy from their environment and synthesise building blocks of larger macromolecules, and the macromolecules themselves. Cells use this energy for three main purposes: (i) movement, e.g. cellular movements and muscle contractions, (ii) active transport of molecules and ions into and out of the cell, and, (iii) biosynthesis of macromolecules from precursors. The First Law of Thermodynamics states that energy cannot be created or destroyed, however it can be converted from one form to another. Cells convert chemical energy held within bonds of certain molecules, to either kinetic or a different form of chemical energy, readily used by the cell [223].

Energy transformation from chemical to kinetic, electrical or alternate chemical energy, does not happen as one reaction, instead thousands of small reactions are taking place within every cell to control energy transformation and ensure the correct compounds are made to the cell requirements. In brief, we can divide the metabolic pathways into two types: catabolic reactions and anabolic reactions. Catabolism is the conversion of energy into biologically usable forms. In these reactions, fuel is broken down and energy currency is generated, along with water and carbon dioxide waste. Anabolic reactions require energy input. These use the energy currency produced in catabolic reactions to generate for example complex structures, movement of cell and cell contractility [223].

The energy currency used within cells is mainly adenosine triphosphate (ATP). ATP is composed of an adenine ring, ribose sugar and 3 phosphate groups. The phosphate bonds in ATP are high in energy, in particular the γ phosphate group at the outside of the molecule. This means the breakdown of these bonds by hydrolysis liberates a high level of free energy, in comparison to other phosphate (e.g. glycerol-3-phosphate). This is partly due to electrostatically unfavourable charge repulsion of 4 negative charges and effective binding of water to adenosine diphosphate (ADP) and inorganic phosphate [224]. This energy can be harnessed to drive anabolic reactions which require input of free energy. The main way the cell does this is through conversion of ATP to ADP and inorganic phosphate (Figure 1.21). This process can cycle in either direction and does so constantly within the cell when energy is transferred, making ATP a very effective energy currency. Additional nucleoside triphosphates including guanosine triphosphate, can also be used but ATP remains fundamental in energy exchange.

ATP is the principle energy donor for cells, however there is not a large or long term store of ATP. Levels within the cell are kept low and instead ATP/ADP is constantly turning over. ATP

is generated from food sources. There exists a complex pathway of enzymatic reactions which convert food macromolecules into sequentially smaller and smaller units. Respiration is the name given to the process by which energy is converted from food products to useable energy by the cell.

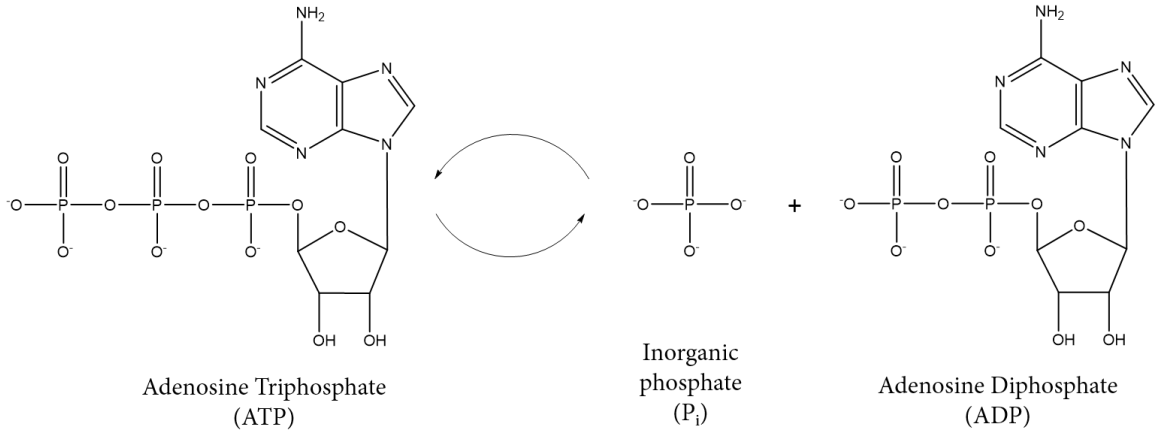

Figure 1.21. Conversion of ATP to ADP. *This catabolic process and the reverse anabolic process is the fundamental cycle by which energy is exchanged in cells.*

1.10.1. Glycolysis

Respiration can be thought of as existing in two stages: glycolysis and oxidative phosphorylation (OXPHOS). Glycolysis reactions occur without the need for oxygen and generates a low yield of ATP, and OXPHOS requires oxygen and generates a high yield of ATP. In brief, during glycolysis glycose is converted to pyruvate and yields 2 ATP and 2 nicotinamide adenine dinucleotide (NADH) per molecule of glucose (Figure 1.22). NADH is an electron carrier which can be later used to generate ATP during OXPHOS in the presence of oxygen. Further ATP can be extracted from pyruvate in anaerobic conditions through conversion to either ethanol or more commonly lactate (Figure 1.22). This is an important pathway in anaerobic bacteria, but is also used in humans when ATP needs exceeds the ability to provide oxygen, for example when short bursts of intense exercise are performed [225]. In order to generate the maximum yield of ATP possible per glucose molecule, oxygen is required.

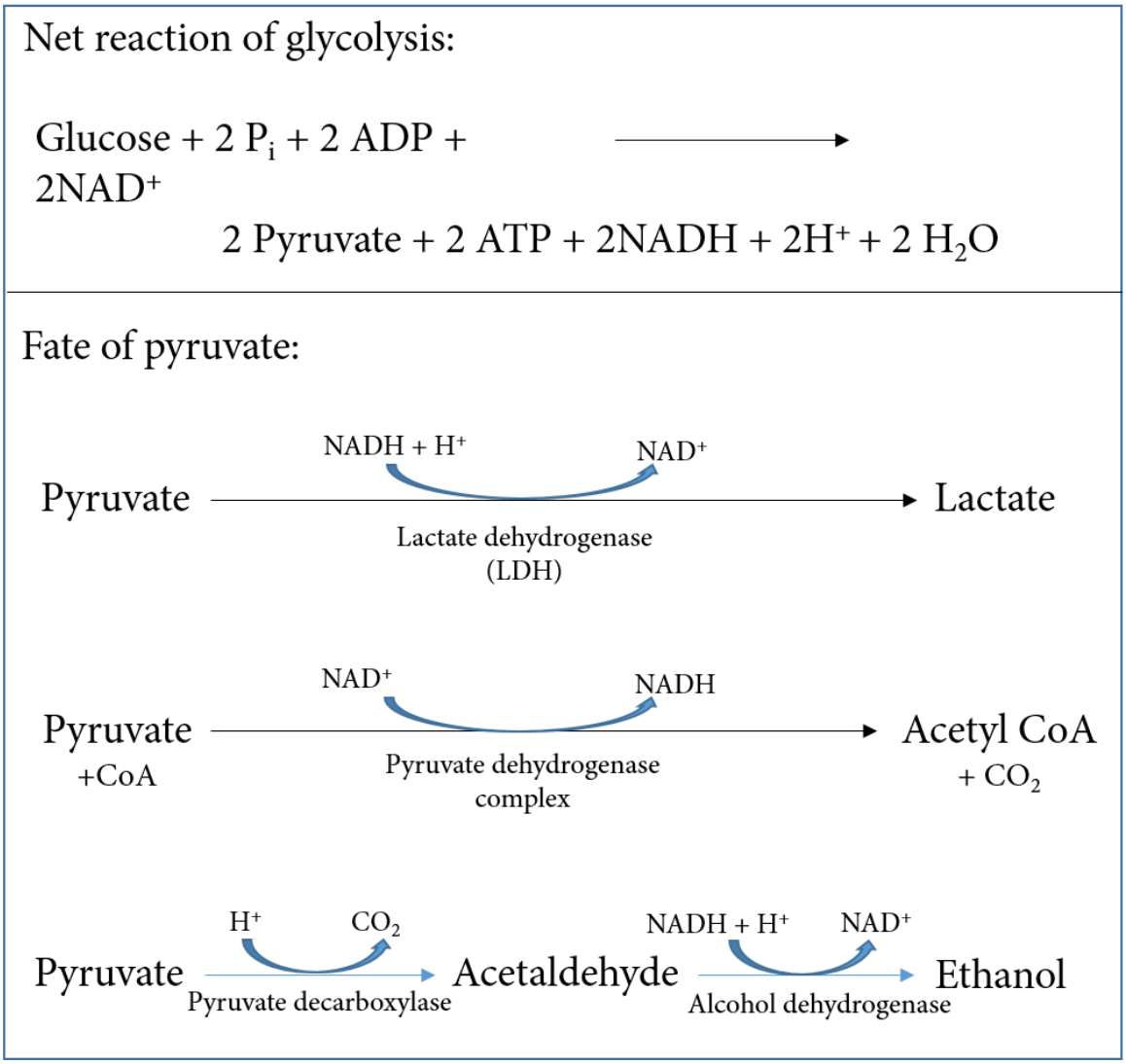

Figure 1.22. Anaerobic glycolysis. *The net reaction of glycolysis. The three fates of pyruvate generated in glycolysis. Below each reaction is the enzyme involved. Based on information obtained in [223].*

1.10.1.1. Aerobic Glycolysis

As well as glycolysis occurring under anaerobic conditions, glucose can be fermented to produce lactate in aerobic conditions, in the presence of oxygen. This is known as the Warburg Effect and has been documented in developing cells and cancer cells [226-228]. The rate of glucose metabolism to lactate is known to be 10-100 times faster than the complete oxidation of glucose in the mitochondria [228]. If demand of ATP is high, there could be a kinetic advantage of employing aerobic glycolysis.

1.10.2. Tricarboxylic acid (TCA) cycle

Only a small fraction of the potential energy of glucose is extracted in anaerobic glycolysis. To release its full amount, aerobic condition are required. To initiate this, pyruvate is converted to acetyl-coenzyme A (CoA) by pyruvate dehydrogenase. Acetyl-CoA is brought to the tri-

carboxylic acid (TCA) cycle (also called the citric acid cycle or Krebs cycle) in the mitochondria under aerobic conditions only. The TCA cycle is a circular series of enzymatic conversions and leads to net production of $3NADH_2$, 1 $FADH_2$ and 1 GTP, giving 12 ATP per molecule of pyruvate, or 24 per glucose molecule (Figure 1.24) [229]. The cycle starts when acetyl-CoA combines with oxaloacetate to produce the 6 carbon molecule citrate [230]. Citrate is slowly broken down to eventually reform the 4 carbon molecule oxaloacetate, ready to combine with acetyl-CoA and begin the cycle again. As well as pyruvate, the products of fatty acid oxidation feed into the TCA cycle to produce ATP.

1.10.3. Oxidative Phosphorylation (OXPHOS)

OXPHOS is the process in which ATP is formed when electrons are transferred from energy rich $NADH_2$, and $FADH_2$ to O_2 through a series of electron carriers. The electron carriers allow for control of energy transfer and is termed the electron transport chain. This electron transport chain pump protons and generates a pH gradient across the inner mitochondrial membrane (Figure 1.23). This is used to drive ADP phosphorylation to ATP through ATP synthase, the final step in OXPHOS. During the breakdown of each glucose molecule, 2 ATP and 2 NADH are formed in glycolysis, 2 NADH in pyruvate conversion to acetyl CoA, and 6 NADH, 2 FADH and 2 GTP during TCA cycle. Approximately 3 ATP molecules are formed per NADH and 2 ATP molecules per FADH. This gives a total number of ATP molecules produced per glucose molecule of (2+2x3+2x3+6x3+2x2+2)=38 ATP molecules [227].

1.10.4. Metabolism of stem cells

It is known that as stem cells develop and differentiate, the processes by which the cell utilises nutrients, or its metabolism, changes. Heightened aerobic glycolysis and a decrease in OXPHOS is a key feature of embryonic stem cells (ESCs). Multipotent adult stem cells in the stem cell niche are also known to undergo aerobic glycolysis as the primary energy generation mechanism, and are reprogrammed to focus on OXPHOS [231]. This reliance on aerobic glycosylation is known to switch to OXPHOS during differentiation [231]. This is associated with a change in redox status of the cell during differentiation from reducing environment to increased oxidative pathways [232]. During this time, the epigenetic landscape is known to shift to promote differentiation and this has been directly linked to metabolic reprogramming [233]. For example, in helper T cells, aerobic glycolysis is the primary means of energy generation. Lactate dehydrogenase (LDH) induction during the switch on of aerobic glycolysis was shown to increase acetyl CoA levels, enhancing histone acetylation and therefore transcription of interferon-γ [234]. Similar epigenetic modifications could be occurring during the differentiation of SSC.

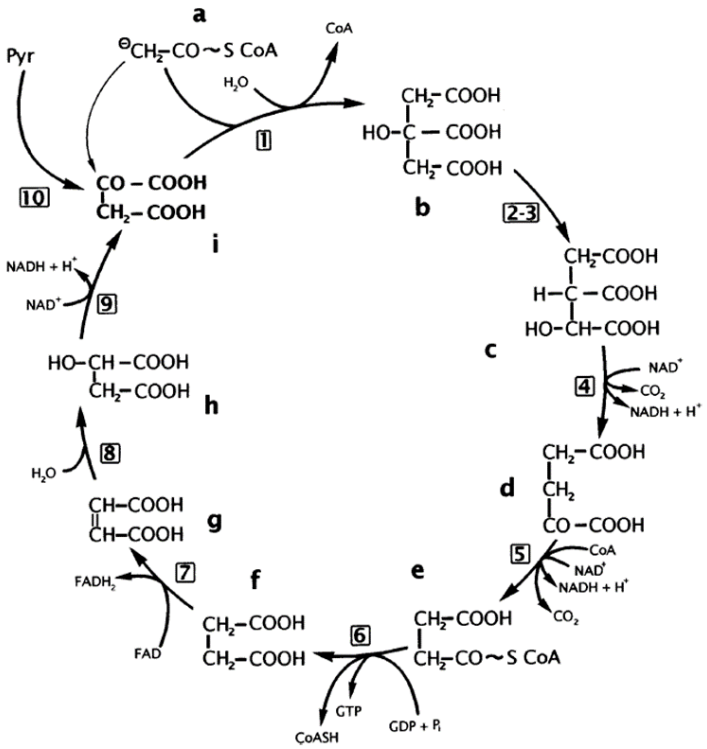

Figure 1.24. The tricarboxylic acid (TCA) cycle. *The cycle begins with (a) acetyl-CoA converted to (b) citrate, to (c) isocitrate, to (d) α-k-glutarate, (e), succinyl-CoA, (f) succinate, (g) fumarate, (h) malate, and finally converted to (i) oxaloacetate. The enzymes involved in this reaction are (1) citrate synthase, (2-3) aconitase, (4) isocitrate dehydrogenase, (5) α-ketoglutarate dehydrogenase, (6) succinyl-CoA synthetase, (7) succinate dehydrogenase, (8) fumarase, (9) malate dehydrogenase, and (10) pyruvate carboxylase. Image modified from [223].*

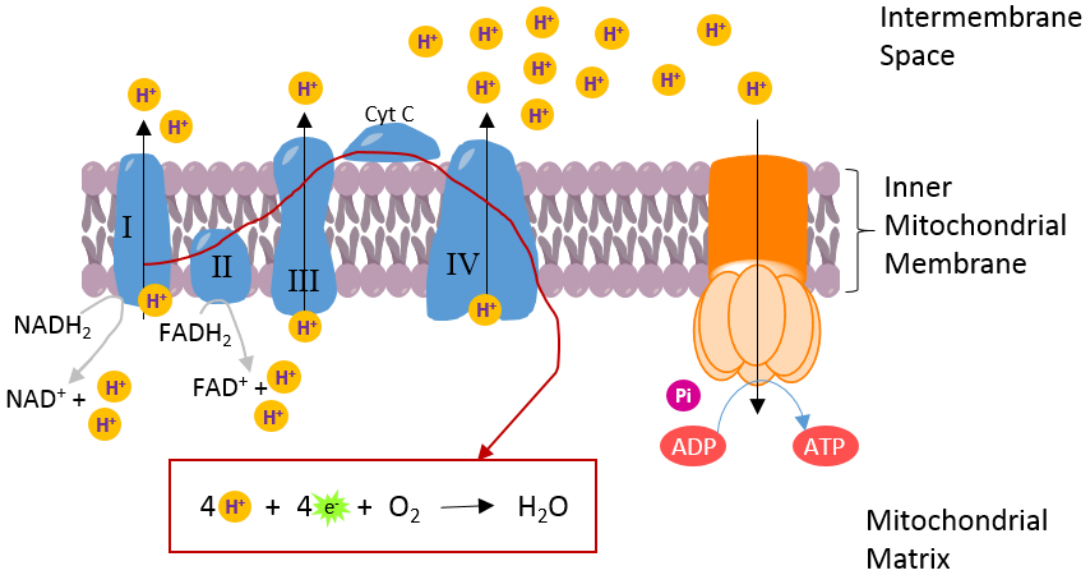

Figure 1.23. The electron transport chain and oxidative phosphorylation (OXPHOS). *Electron carriers $NADH_2$, and $FADH_2$ are brought to the electron transport chain on the inner mitochondrial membrane (IMM). Electron movement across complex I (NADH-Q oxidoreductase), II (succinate-Q reductase), III (Q-cytochrome c oxidoreductase), electron shuttle cytochrome C (Cyt C) to complex IV (cytochrome c oxidase). Complex I, III and IV pump electrons across the IMM, forming a pH gradient. This is used to power ATP synthase, which rotates to provide a hydrophobic compartment to allow for ATP generation. Image modified from [227].*

1.10.5. Metabolic reprogramming in SCCs during osteogenic differentiation

Curiously, the behaviour of the SSCs during differentiation to osteoblasts is thought to be different to the metabolic reprogramming usually observed in differentiating cells. Early experiments suggest bone consumed a large amount of glucose and produced lactate [235]. It was estimated that >80% of glucose consumed in bone tissue was converted to lactate [236]. In experiments, Wnt signalling has been known to stimulate aerobic glycolysis and glutamine catabolism, pathways which are associated with the Warburg effect [237-239]. Karner *et al* identified a glutamine dependent pathways which contributes to the TCA cycle, thereby generating energy [237]. Recently, Wu *et al* showed lactate promoted ALP activity and stabilised HIF1α expression and this was essential for osteogenic differentiation [240]. Collectively, these studies have suggested glycolysis plays an important role in energy generation during osteogenic differentiation. However, through investigation of mitochondrial biogenesis and bioenergetics, it was discovered that following osteogenic induction in bone marrow MSCs, number of mitochondria, levels of respiratory enzymes and oxygen consumption rate increased, indicating an enhancement of OXPHOS within differentiating cells [241]. Further to this, mitochondrial inhibitors impaired osteogenic differentiation [241]. Shum *et al* used bioenergetics profiling to show that during osteogenic differentiation, MSCs activate OXPHOS, but do not switch off glycolysis and instead maintain glycolysis levels similar to undifferentiated cells [242]. This revelation explains why experiments by Wu *et al* have found lactate to be of importance to osteogenic differentiation, and experiments by Karner *et al* showed Wnt signalling enhancing aerobic glycolysis. Metabolic reprogramming in osteogenic differentiation appears to not be a simple switch from glycolysis to OXPHOS and instead results in common ground between both mechanisms of energy generation.

1.11. Aims and Objectives

1.11.1. Research hypothesis

Biomimetic and synthetic material substrate topography can affect SSC fate and function upon culture in the absence of chemical cues. It is hypothesised that topographical features of three surfaces have the ability to alter SSC behaviour. These surface are: i) synthetically designed near square arrangement of nanopits, ii) substrates bioimprinted with SSC, and iii) the biomimetic topography of nacre shell.

Specifically this hypothesis will be broken down into:

I. Near square arrangement of nanopits can promote osteogenic differentiation of STRO-1+ SSC in the absence of chemical cues.
II. Bioimprinted substrates can alter STRO-1+ SSC behaviour.
III. Nacre and prism shell topography can promote osteogenesis differentiation of STRO-1+ SSCs.

1.11.2. Aims

The overarching aim of this work is: **"to understand changes in SSC behaviour, including osteogenic differentiation, in response to topography."** The topographical surfaces studied will be disordered square nanotopography, bioimprinted cell topography and shell surface topography.

This aim will be broken down into the following:

I. To examine molecular phenotype and behaviour of STRO-1+ SSCs following culture on discrete near square nanosurfaces. Specifically:
    a) To study the potential of NSQ nanosurfaces to differentiate SSCs to osteoblasts through expression of osteogenic markers.
    b) To investigate the miRNA profile of SSCs cultured on nanosurfaces in order to examine if any regulatory miRNA are involved in the modulation of SSC behaviour on discrete topographies.

II. To explore the response of human SSCs on select bioimprinted surfaces. Specifically:
    a) SSC response to two different bioimprinted surfaces, an immature (early) osteoblast phenotype and a mature (late) osteoblast phenotype bioimprinted substrates.
    b) SSC morphology on bioimprinted surfaces in comparison to flat surfaces derived from empty tissue culture plates.
    c) Proliferation and metabolic activity of human SSCs following culture on bioimprinted surfaces over 21 days.
    d) Molecular analysis (RNA and protein measurements) of human SSCs cultured on both early and late osteoblast bioimprint.

III. To examine molecular phenotype and metabolic profile of STRO-1+ SSCs following culture on nacre and prism topographies. Specifically:
    a) To study the potential of nacre and prism topographies to alter SSC size and shape
    b) To investigate expression of known regulators of osteogenesis in SSCs when cultured on nacre and prism topographies.
    c) To investigate the metabolic profile of SSCs cultured on nacre and prism topographies to examine similarities with metabolic changes occurring during osteogenesis.

Chapter 2: Materials and Methods

Chapter 2 - Materials and Methods

2.1. Materials

All cell culture consumables were purchased from Corning, UK and StarLabs, UK. All reagents used in the following methods described in this chapter and subsequent chapters are listed in Appendix I.

2.2. Cell Culture

2.2.1. Ethical Approval

Human bone marrow and femoral head samples were obtained after informed and written consent from patients undergoing routine hip replacement. Ethical approval was obtained from National Research Ethics Service (NRES) Committee Southampton and South West Hampshire LREC 194/99/1 (Study title: Bone formation in the young and aging skeleton).

2.2.2. Media

2.2.2.1. Basal media

Basal media consisted of Minimum Essential Medium Eagle - Alpha Modification (α-MEM) supplemented with 10% fetal bovine serum (FBS) (v/v) and 1% penicillin/streptomycin (P/S) and was used to maintain STRO-1+ SSCs under both control and experimental conditions.

2.2.2.2. Osteogenic media

Osteogenic media consisted of basal media supplemented with 10 nM vitamin D_3 and 100 μM ascorbic acid and was used to maintain SSCs under experimental conditions.

2.2.3. Bone marrow mononuclear cell isolation

Marrow samples were collected following routine hip replacement surgery and contained within universal tubes. If the marrow sample was too small to process to retrieve cells, cancellous bone was removed from the corresponding supplied femoral neck and broken into small pieces using orthopaedic bone nibblers and added to the marrow sample. The method used to release human bone marrow mononuclear cells (hBMMNCs) was previously described in Williams *et al*, 2013 [243]. To release hBMMNCs, the marrow sample was diluted in 10-15 mL of α-MEM and agitated aggressively. The marrow-α-MEM mix was transferred to a 50 mL falcon tube, and the process of diluting marrow in α-MEM and agitating repeated three times. The cell suspension was subjected to centrifugation (4 minutes, 100 x g, 18^{o}C) and resuspended in 20 mL α-MEM. Cell suspension was passed through a 70 μm cell strainer to remove debris. The cell suspension was then layered on top of 25 mL of lymphoprep

solution (Stem Cell Technologies, UK) in a separate 50 mL falcon tube. This was subjected to centrifugation (40 minutes, 200 x g, 18°C with the automatic brake off). hBMMNCs were collected from the "buffy coat" layer, at the interface between the lymphoprep and media. hBMMNCs were washed in 20 mL α-MEM by centrifugation (4 minutes, 100 x g, 18°C). Cells were resuspended and added to a T175 flask with 20 mL basal media. Media was changed 7 days after isolation and then after every 3-4 days until cells reached approximately 70-80% confluence, when the cultures were ready to seed for further experiments. All cells were maintained in static incubators at 37°C and 5% CO_2.

2.2.4. STRO-1+ SSC isolation by magnetic separation

STRO-1+ SSCs were isolated from hBMMNC population using MACS® magnetic separation (**Figure *2.1***) [243]. hBMMNCs were removed from the buffy coat layer after density centrifugation using lymphoprep™ and taken forward for magnetic separating to isolate STRO-1+ SSCs. hBMMNCs were collected in a 50 mL falcon tube and sufficient α-MEM was added to make the final volume up to 50 mL. The cell suspension was subjected to centrifugation (4 minutes, 100 x g). The cell pellet was re-suspended in 2 mL MACS® blocking buffer (α-MEM supplemented with 10% human serum, 1% BSA, and 5% FBS) and incubated at 4°C for 30 minutes, with regular mixing. The cell suspension was then made up to 10 mL with MACS® buffer (Phosphate buffered saline (PBS) supplemented with 2 mM EDTA and 0.5% BSA) and washed by centrifugation (5 minutes, 100 x g, 18°C). The cell pellet was then re-suspended in 500 µL STRO-1 hybridoma supernatant and incubated at 4°C for 30 minutes, with regular mixing. The cell suspension was washed three times in MACS® buffer and the cell pellet was resuspended in 200 µL MACS® rat anti-mouse IgM microbeads for 15 minutes at 4°C, with regular mixing. The cell suspension was then subjected to centrifugation (5 minutes, 100 x g, 18°C) and washed three times in MACS® buffer. After the final wash, cells were resuspended in 2 mL MACS® buffer. Cell suspension-MACS buffer mix was passed through MACS® cell separation columns in the presence of MACS® separator. Columns were removed from the separator and 5 mL MACS® buffer plunged through the column to release cells. The cell suspension was made up to 20 mL with α-MEM and washed twice through centrifugation (4 minutes, 100 x g, 18°C). After the final wash, cells were resuspended in 25 mL basal media for every T175 flask the cells were seeded in. Due to the high volume of cells which do not adhere to tissue culture flask after MACS isolation, the cell number was not counted. To estimate cell number, cell pellets were judged by eye and resuspended in the number of T175 was deemed appropriate to the estimated cell number. Media was changed

7 days after isolation and then after every 3-4 days until cells reached approximately 70-80% confluence. All experiments using STRO1+ SSCs were conducted on passage 1 cells.

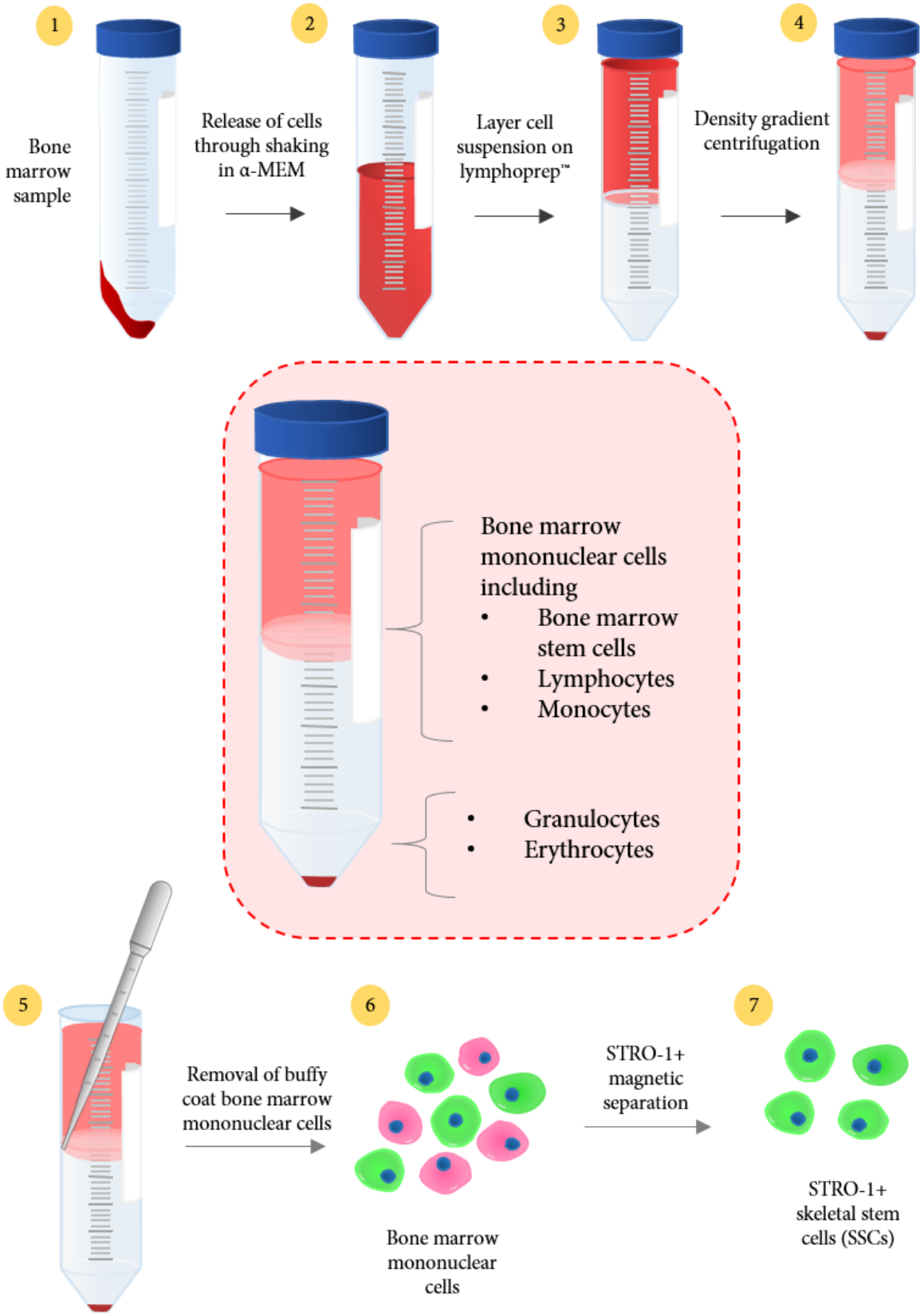

Figure 2.1. Protocol for STRO-1+ SSC isolation by magnetic separation. *1. Bone marrow sample supplied in tube. 2. Cells within bone marrow sample is released through aggressively shaking the sample in α-MEM. 3. Cell suspension subsequently layered over lymphoprep™ and 4. Subjected to density centrifugation. 5. After centrifugation, bone marrow mononuclear cells, located in the "buffy coat" are removed. 6. STRO-1+ SSC are selected from buffy coat fraction through magnetic separation 7. STRO-1+ SSC sample collected.*

2.2.5. Cell seeding for differentiation analysis

In order to generate a single cell suspension for accurate cell counting, SSCs were treated with collagenase IV [244]. SSCs were washed twice with PBS and incubated with 5 mL α-MEM supplemented with 1 mg collagenase IV for 45 minutes at 37°C. To release cells adhered to T175 tissue culture plastic flasks, cells were washed twice with PBS and incubated with 5 mL 1X trypsin for approximately 10 minutes. The flask was then given a sharp strike to release cells from the flask surface and 7 mL basal media added. The total cell suspension was pelleted through centrifugation (4 minutes, 100 x g, 18°C), and resuspended in 10 mL basal media. The cells present were counted using a haemocytometer and diluted to the appropriate concentration in media using Equations 1 and 2.

$$Total\ cell\ number\ = \frac{Average\ cell\ number\ per\ counting\ chamber}{\times\ volume\ cells\ suspeneded\ in\ (ml) \times 10'000}$$

Equation 1. Calculation for excess volume of media required in order to obtain correct media volume for seeding.

$$\frac{Volume\ of\ cell\ suspension}{required\ for\ experiment\ (mL)} = \frac{number\ of\ cells\ needed\ in\ experiment}{total\ number\ of\ cells\ in\ flask(s)} \times \frac{Volume\ of\ media}{cells\ resuspended\ in\ (mL)}$$

Equation 2. Calculation for correct volume of cell suspension to remove from cell stock for correct cell seeding.

Seeding density for STRO-1+ cells was selected based on previous group protocols and proliferation rate of STRO1+ SSC, as detailed in

Surface type	Plate defined by well number	Well surface area (cm^2)	Volume of media (mL)	Total cells/well
NSQ nanosurface	6	9.8	4	2, 000
Shell surface	24	1.9	0.5	500
Bioimprinted surface	6	9.8	4	2,000

[245]. Cells were grown in either basal or osteogenic media from the point of seeding and media changed every 3-4 days.

Surface type	Plate defined by well number	Well surface area (cm^2)	Volume of media (mL)	Total cells/well
NSQ nanosurface	6	9.8	4	2, 000
Shell surface	24	1.9	0.5	500
Bioimprinted surface	6	9.8	4	2,000

Table 2. Seeding densities detailed by surface area and volume of media used in chapters.

2.3. Molecular Biology

2.3.1. Cell lysis

Prior to cell lysis, cells were washed twice with PBS. 600 µL of lysis buffer Buffer RLT (Qiagen, UK) supplemented with 0.05% Reagent DX (Qiagen, UK) was added to a 6-well plate and cells scrapped with a filtered pipette tip. 350 µL of lysis buffer solution was added to 24-well plates. The cell lysate was transferred to a nuclease-free 1.5 mL tube and stored at -80°C prior to nucleic acid extraction. To lyse cells from any well with a nanotopographical surface contained within the well, the surface was moved to a new well containing 4 mL PBS with sterile forceps. PBS was removed and lysis buffer Buffer RLT supplemented with 0.05% Reagent DX was added to the well and surface scrapped with pipette tip. This was transferred to a nuclease-free 1.5 mL tube, as before, and stored at -80°C prior to nucleic acid extraction.

2.3.2. Nucleic acid extraction

2.3.2.1. RNA only extraction

RNA only extraction was performed using Qiagen RNeasy RNA extraction kit (outlined in **Figure *2.2***A). The Buffer RTL contains a high level of guanidine isothiocycanate, a protein denaturant and lysis chemical. RNA isolation was performed according to the manufacturer's protocol. Briefly, the cell lysate was thawed and equal volume of ethanol to the lysate was added to the cell lysate and mixed by pipetting. The lysate/ethanol mixture was loaded onto an RNeasy spin column which was placed in a 2 mL collection tube. The RNeasy spin column contains a silica membrane, which RNA strongly and specifically binds to. The column was subjected to centrifugation (1 minute, 8000 x g) and the supernatant discarded. Subsequent 700 µL aliquots were transferred to the RNeasy column and centrifuged under the same

conditions. Next two different buffers were transferred sequentially to the column to wash the column and the column was subjected to centrifugation (1 minute, 8000 x g) between washes. The first buffer, 700 µL of buffer RW1, contains ethanol and a guanidine salt to remove organic molecules such as carbohydrates, proteins and fatty acids that are not specifically bound to the silica membrane. Then 500 µL of buffer RPE was added to remove salt traces from earlier buffers and to clean the membrane prior to RNA elution. Next, the RNeasy spin column was transferred to a new 2 mL collection tube and centrifuged empty (1 minute, 8000 x g) to dry completely the column. To elute the RNA, the RNeasy spin column was placed in a new 1.5 mL collection tube and 33 µL RNase-free water was added directly on top of the membrane and centrifuged (1 minute, 8000 x g).

2.3.2.2. gDNA, RNA and miRNA combined extraction

RNA and gDNA isolation was performed using AllPrep DNA/RNA/miRNA universal kit (Qiagen, UK) with adherence to the manufacturer's protocol and is outlined in **Figure *2.2***B. As well as ensuring extraction of genomic DNA (gDNA) and mRNA, this extraction kit is specific for miRNA. In short, cell lysate was passed through an AllPrep DNA spin column with attached collection tube and centrifuged for 1 minute at 8000 x g to ensure all the liquid had passed through the column. AllPrep DNA spin column, containing gDNA, was transferred to a new 2 mL collection tube and stored at 4°C for no more than 60 minutes prior to gDNA extraction. RNA including miRNA is contained within supernatant. To the supernatant, 80 µL Proteinase K (concentration 20 mg/mL) was added and mixed by pipetting. A further 350 µL of 100% ethanol was added and mixed through pipetting. The mixture was incubated at room temperature for 10 minutes. After incubation, 700 µL 100% ethanol was pipetted into the mixture and mixed well. 700 µL of the mixture was transferred to an RNeasy spin column placed in a 2 mL collection tube. The RNeasy spin column contains a silica membrane which RNA strongly and specifically binds to. This was subjected to centrifugation (1 minute, 8000 x g) and the supernatant discarded. Subsequent 700 µL aliquots were transferred to the RNeasy spin column and centrifuged under the same conditions until all mixture has been passed thought the column. 500 µL Buffer RPE was added to the RNeasy spin column and centrifuged (1 minute, 8000 x g) and flow through discarded after centrifugation. Next, a mixture of 10 µL DNase I stock solution and 70 µL Buffer RDD was added directly to the RNeasy spin column membrane and incubated for 15 minutes at room temperature. After incubation, 500 µL Buffer FRN was added to the RNeasy spin column and centrifuged for 1 minute at 8000 x g. In order to ensure minimal miRNA loss, the supernatant was passed through the same RNeasy spin column again, centrifuged (1 minute, 8000 x g) and supernatant discarded. 500 µL Buffer RPE was added to the RNeasy spin column and centrifuged (1 minute, 8000 x g) and flow through

discarded after centrifugation. 500 µL 100% ethanol was added to the RNeasy spin column and centrifuged (2 minutes, 8000 x g) and flow through discarded after centrifugation. Next, RNeasy spin column was placed in a new 2 mL collection tube and centrifuged empty (1 minute, 8000 x g) to ensure no residual ethanol transfer. To elute RNA, RNeasy spin column was placed in a new 1.5 mL collection tube and 33 µL RNase-free water was added directly on top of the membrane and centrifuged (1 minute, 8000 x g).

gDNA contained within the AllPrep DNA spin column was washed with 350 µL Buffer AW1 by centrifugation (1 minute, 8000 x g). Next a mixture of 20 µL Proteinase K (concentration 20mg/mL) and 60 µL Buffer AW1 was added to the membrane of the AllPrep DNA spin column and incubated for 5 minutes at room temperature. After incubation, 350 µL Buffer AW1 was added to the AllPrep DNA spin column and centrifuged (1 minute, 8000 x g) and the supernatant discarded. 500 µL Buffer AW2 was added to the AllPrep DNA spin column, centrifuged for 2 minutes, 8000 x g and the supernatant discarded. Next, the AllPrep DNA spin column was placed in a new 2 mL collection tube and centrifuged empty (2 minutes, 8000 x g) to ensure no residual ethanol transfer. To elute gDNA, AllPrep DNA spin column was placed in a 1.5 mL collection tube, 53 µL Buffer ED was added directly on top of the membrane and centrifuged (1 minute, 8000 x g).

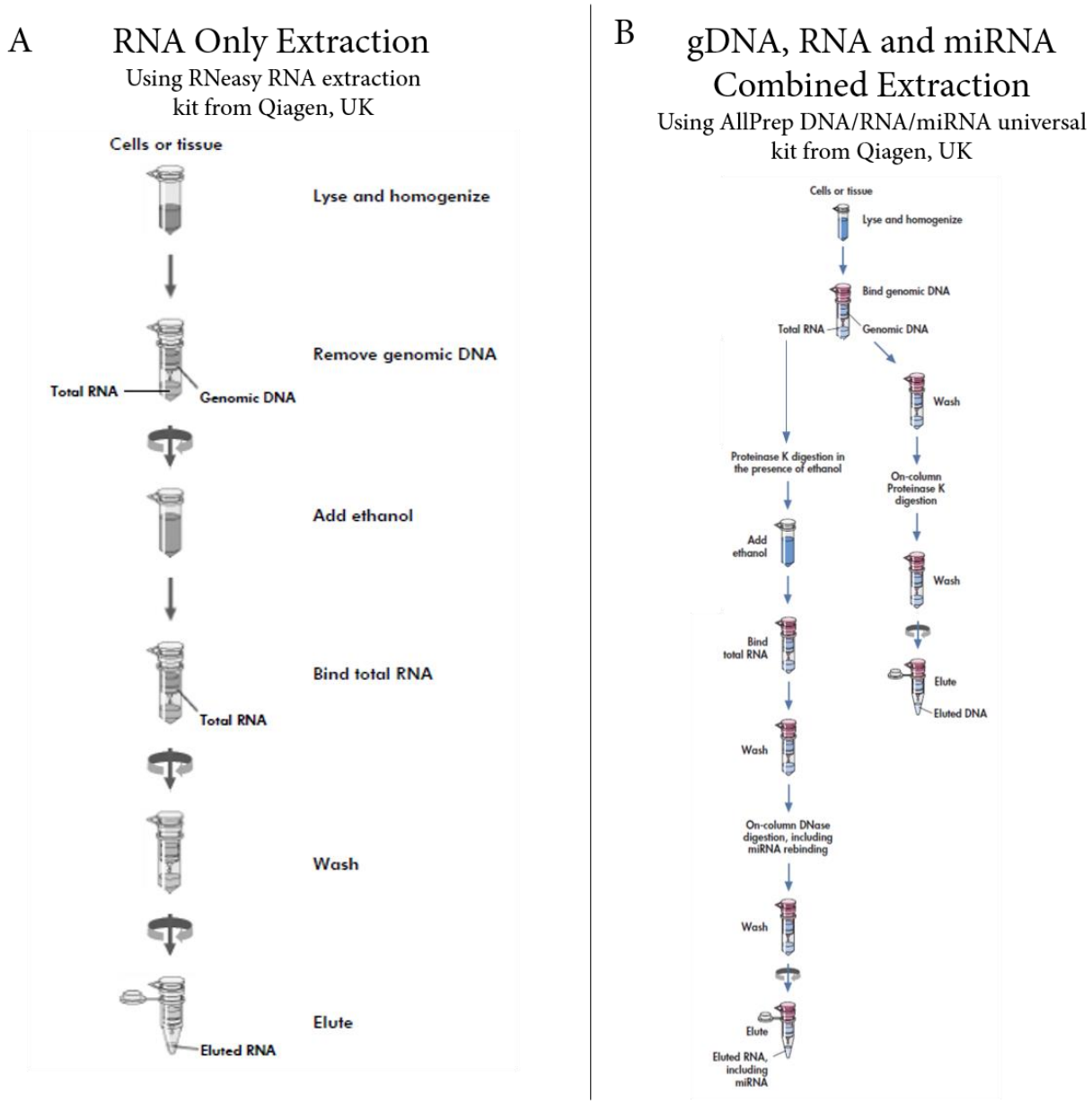

Figure 2.2. Schematic of nucleic acid extraction from cell lysates. *A - RNA extraction described in detail in section 2.2.2.1 RNA only extraction. This was performed using RNeasy RNA extraction kit supplied from Qiagen, UK. B - gDNA, RNA and miRNA extraction described in detail in section 2.2.2.2. gDNA, RNA and miRNA Combined Extraction. This was performed using AllPrep DNA/RNA/miRNA universal kit supplied from Qiagen, UK. Diagram A was obtained from RNeasy Plus mini handbook, Qiagen, accessed from https://www.qiagen.com/gb/resources/resourcedetail?id=c8cdc6bf-5bbf-4e3b-a0f4-476da9215012&lang=en. 28/11/2016. Diagram B was obtained from AllPrep DNA/RNA/miRNA Universal handbook, Qiagen, accessed from https://www.qiagen.com/gb/resources/resourcedetail?id=612cdf65-324c-4710-b0e7-186d9868b0bb&lang=en 28/11/2016.*

2.3.3. RNA and DNA Quantification

RNA and gDNA concentrations were measured using a NanoDrop™ 2000 spectrophotometer (obtained from Thermo Fisher Scientific Ltd (Paisley, UK)). The spectrophotometer quantifies the concentrations through absorbance of UV light at 260 nm. The NanoDrop compares this absorbance to a standard curve to enable calculation of concentration. A_{260}/A_{280} ratio determines protein contamination, and thereby RNA and DNA quality. A_{280} is the wavelength at which aromatic amino acids such as tryptophan, tyrosine and phenylalanine absorb UV. 1.5 µL of each sample was used to measure concentrations of RNA and gDNA.

2.3.4. mRNA quantitative reverse transcription polymerase chain reaction (qRT-PCR)

mRNA was converted to cDNA prior to analysis of gene expression through qRT-PCR using initially SuperScript® VILO™ cDNA Synthesis Kit Master Mix (ThermoFisher Scientific, UK). Later experiments used TaqMan™ Reverse Transcription Reagents (Thermofisher Scientific, UK). When using SuperScript® VILO™ cDNA synthesis kit, for each reaction, 2 µL of Master Mix and 1 µL of SuperScript® reverse transcriptase was added to 7 µL of RNA. RNA concentration was calculated to be constant across samples and sufficient RNase-free water was added if necessary. A minimum of 70 ng RNA and maximum of 500 ng RNA was used per reaction. The reaction mixture was incubated in a thermocycler at 25^{o}C for 10 minutes, 42^{o}C for 120 minutes to activate the reverse transcriptase and 85^{o}C for 5 minutes to terminate the reaction. Taqman™ Reverse Transcription Reagents utilised a master mix per reaction of 2 µL 10x TaqMan™ RT Buffer (PCR Buffer I), 4.4 µL 25mM $MgCl_2$, 4.0 µL deoxyNTPs mixture (2.5 mM each dNPT), 1 µL Random Hexamer (50 µM), RNase Inhibitor (20U/µL), and MultiScribe Reverse Transcriptase (50U/µL). This was added to 7.7 µL RNA sample. Similarly, RNA concentration was calculated to be constant across samples and sufficient RNase-free water was added if necessary. The reaction mixture was incubated in a thermocycler at 25^{o}C for 10 minutes, 48^{o}C for 30 minutes to activate the reverse transcriptase and 95^{o}C for 5 minutes to terminate the reaction. When using both kits, after reaction termination, the reaction was held at 4^{o}C until it was moved to -20^{o}C for storage.

qRT-PCR was performed using SYBR® Green PCR Master Mix (ThermoFisher Scientific, UK) initially and in later experiments GoTaq® qPCR Master mix (Promega, UK). For each 20 µL reaction, 10 µL SYBR® Green PCR Master Mix, (ThermoFisher Scientific, UK) 4 µL forward and reverse primer mixture (at 5 µM in stock, diluted to 1 µM in each reaction) (Sigma-Aldrich, UK), 5 µL RNase-free water and 1 µL cDNA were combined and mixed well. All primers used are detailed in Appendix 1. The final mixture was added to each well of a 96-well-plate. For the qRT-PCR run, Applied Biosystems (ThermoFisher Scientific, UK) Real Time PCR system

was set up to run first with two holding stages (2 minutes at 50°C, 10 minutes 95°C), followed by 40 cycles (15 seconds at 95°C, 1 minute at 60°C) where fluorescence of SYBR green/GoTaq was measured, and finally maintained at 4°C until the plate was removed from the machine. Data was analysed using 7500 Software version 2.3 (Life Technologies). Threshold for calculating Ct (cycle threshold) value was set at 0.2 and all samples normalized to expression of *ACTB*, as a housekeeping gene. The $2^{-\Delta\Delta Ct}$ method was used for relative quantification of gene expression [246].

2.3.5. microRNA qRT-PCR

microRNA expression was determined using TaqMan® microRNA assays. This assay works in two stages; a reverse transcription step using a specific stem loop primer followed by qPCR using a specific TaqMan® probe (**Figure *2.3***).

For each 7.5 µL reverse transcription reaction, 0.075 µL deoxynucleoside triphosphate (dNTP), 0.75 µL 10x reverse transcription buffer, 3.581 µL nuclease-free water, 1.5 µL stem loop primer, 0.5 µL MultiScribe® reverse transcriptase and 0.094 µL RNase inhibitor were combined in a well of a 96-well plate. To this, 1 µL of RNA sample, at a concentration of 10 ng/µL, was added and the reaction mixture mixed well through pipetting. The reaction mixture was incubated in a thermocycler at 16°C for 30 minutes, 42°C for 30 minutes and 85°C for 5 minutes to terminate the reaction. After this period, the reaction was held at 4°C until it was moved to -20°C for storage.

Each qPCR reaction was 10 µL and performed in triplicate. To set up each reaction, 12 µL TaqMan® universal PCR master mix, 7.7 µL nuclease-free water, 1.2 µL TaqMan® microRNA assay probe and 1.4 µL reverse transcriptase product were mixed well in a 200 µL tube. 10 µL of reaction mixture was pipetted into 2 wells of a 96-well plate. For the qRT-PCR run, Applied Biosystems (ThermoFisher Scientific, UK) Real Time PCR system was set up to run with an initial holding stage of 50°C for 2 minutes followed by 95°C for 10 minutes. Thereafter, the thermocycler was run at 95°C for 15 seconds and 60°C for 1 minute for 40 cycles and a final 4°C hold step. Threshold for calculating Ct (cycle threshold) value was set at 0.2 and all samples normalized to expression of U6 snRNA (non-coding small nuclear RNA) as a housekeeping gene. The $2^{-\Delta\Delta Ct}$ method was used for relative quantification of miRNA expression.

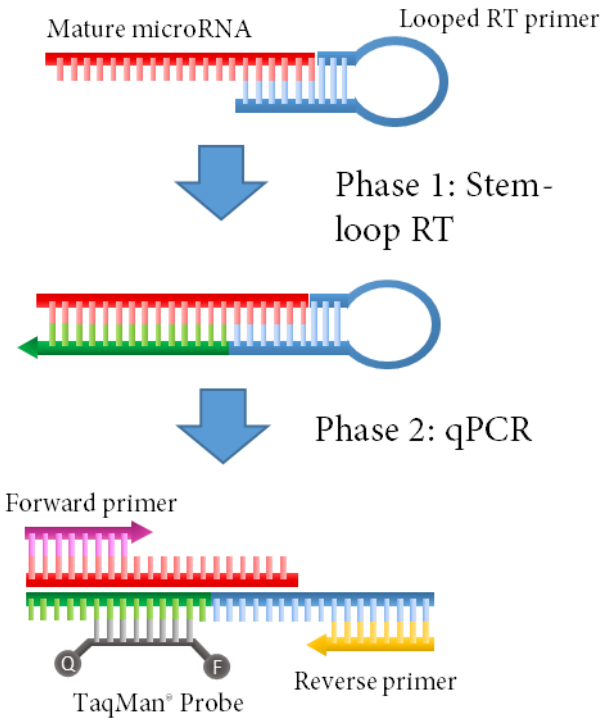

Figure 2.3 microRNA RT-qPCR. *Mature microRNA specifically binds stem looped RT-primer. Reverse transcriptase binds primers and elongates strand. During qPCR phase, strand is denatured exposing bases and allowing forward and reverse to hybridise and elongate. TaqMan probe binds to reverse strand and is released through the action of DNA polymerase, separating the fluorescent molecule from its quencher and thereby allowing it to fluoresce. The accumulation of fluorescence is measured as qPCR progresses and C_t during exponential phase of the reaction relative to housekeeping gene is taken as a relative measurement of gene expression. Image designed by the author, based on Figure 2. TaqMan® MicroRNA Assay mechanism, assessed from https://genome.med.harvard.edu/documents/qpcr/TaqManMicroRNAProductBrochure.pdf 14/11/2016.*

2.4. Metabolomic Activity- alamarBlue® Assay

The alamarBlue® assay is based on the enzymatic reduction of the indicator dye, resazurin, by viable, metabolically active cells. Resazurin is weakly fluorescently blue and is irreversibly reduced to highly fluorescent pink resorufin in the presence of enzymes which utilise the oxidative potential of NADH (**Figure *2.4***) [247]. The fluorescence of resorufin is therefore indirectly proportional to NADH present in the cell, and therefore metabolic activity.

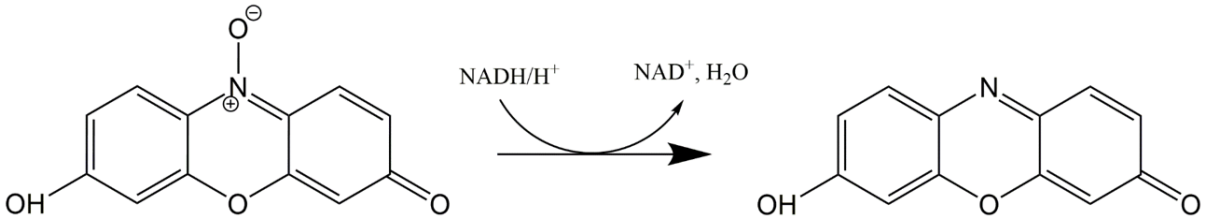

Figure 2.4. Chemical reaction of the reduction of resazurin to resorufin through oxidisation of NADH.

On the day of assay, media was aspirated from cells and the cells then washed with PBS. 10% alamarBlue® (Thermofisher, UK) in media (relevant media to experiment) solution was

prepared, mixed and added to well plate e.g. 200 µL reagent in 2 mL media for 6-well plate. The plate was incubated in the dark at 37°C, 5% CO_2 for 4 hours. After incubation, 125 µL of alamarBlue®/media mix was transferred to a black 96-well plate in triplicates. Fluorescence was measured in GloMax® Discover System plate reader (Promega, Southampton UK) with 530-560 nm excitation and 580-620 nm emission. When used in combination with PicoGreen cell quantity measurements, average fluorescence emission was divided by DNA (ng) to generate a standardised fluorescence per ng DNA reading.

2.5. Immunofluorescence

Prior to staining, surfaces or well plates were washed twice with PBS and fixed in 4% paraformaldehyde (PFA) (v/v) for 30 minutes at room temperature. 4% PFA (v/v) was then removed and surfaces or well plates washed twice with PBS, sealed with parafilm in PBS and stored at 4°C. Cells were blocked and permeabilised with blocking buffer composed of PBS, 0.3% Triton X-100 (Sigma-Aldrich, UK) and 5% Goat Serum (ThermoFisher Scientific, UK) for 60 minutes at room temperature with gentle rocking. Cells were then washed with PBS. Primary antibody was diluted at the concentration stated in **Table 6. Appendix I - Primary and secondary antibody pairings for immunofluorescence. Dilution used and company antibody was obtained from is detailed.**

. Antibodies were diluted in antibody dilution buffer consisting of PBS, 0.3% Triton X-100, and 1% BSA. A sufficient volume of antibody to cover the well plate was added (e.g. 200 µL for 24-well, 400 µL for 6-well plate). In order to minimise antibody usage when staining surfaces, a 50 µL droplet of antibody was placed on parafilm and the surface turned cell facing down onto the droplet, ensuring no bubbles were present. Primary antibody was incubated overnight at 4°C. After incubation, the surfaces were placed facing up in well plates and washed three times with PBS supplemented with 0.05% Tween 20 (Sigma- Aldrich, UK). Antibody was removed from the well plates and washed three times with PBS/Tween for 5 minutes each. Following from this, secondary antibody was incubated with the cells in the same way as primary. At this point, cells were counter stained with TRICT-conjugated phalloidin (diluted at 1:500) (FAK100, Part No. 90228, Merck-Millipore, UK). The secondary antibody was diluted in antibody dilution buffer (described previously) and incubated for 1 hour at room temperature. Following this, surfaces and well plates were washed three times in PBS/Tween for 5 minutes each. Cells were then incubated with 4',6-diamidino-2-phenylindole (DAPI) (dilution 1:100 in PBS) (ThermoFisher Scientific, UK) for 10 minutes at room temperature, using the same method previously described for antibody incubation. Cells were then washed three times with PBS/Tween. For storage before imaging, PBS/Tween in well plates were replaced with PBS. Surfaces were dried on non-cell side and placed on a glass slide with a droplet of fluoromount™ (Sigma-Aldrich, UK) and sealed with clear nail varnish. Surfaces were stored in the fridge, in the dark and imaged within 1 day.

2.6. Determination of DNA concentration in cell lysates

Quant-iT™ PicoGreen® dsDNA assay (ThermoFisher Scientific, UK) utilises PicoGreen's unique property of fluorescing only when bound to double stranded DNA (dsDNA). To generate standards of known DNA concentration, herring sperm DNA (Promega, UK) at 10 µg/µL was diluted in 1x TE buffer (100x TE buffer concentrate diluted in distilled H_2O) (Sigma-Aldrich, UK) to 50, 100, 250, 500, 750 and 1000 ng/mL, and 100 µL of each standard added to one well of 96-well plate. 10 µL of cell lysate was added to 90 µL 1x TE buffer. To this, 100 µL PicoGreen (diluted 1:200 in 1x TE buffer) was added. The plate was left to incubate at room temperature in the dark for 5 minutes. PicoGreen fluorescence was measured in FLx800 fluorescence reader (BioTek Instruments Inc., Swindon, UK) with excitation at 480 nm and emission measured at 520 nm. Using standard curve, DNA concentration in each sample was calculated in ng/mL.

2.7. Cell Spreading Analysis

2.7.1. Cell imaging using CellTracker™ Green (CTG)

20 µL of CellTracker Green (CTG) (Thermo Fisher, UK) was thawed and contents dissolved in 10 µL sterile demethly sulfoxide (DMSO). This was pipetted into a falcon tube containing 15 mL α-MEM. Media was removed from wells and washed once with PBS and CTG/α-MEM mix added to the well. Cells were then incubated in the dark at 37ºC for 1 hour. After this time, cells were washed with PBS and the media replaced with basal media, containing 10% FBS. Cells were imaged at the required time point. According to manufacturers, this dye stays within cells for 72 hours. In these experiments, where imaging took place over several days, cells were imaged within 3 days of staining. If more than 3 days had passed, cells were stained again.

2.7.2. Measuring cell area using image analysis software CellProfiler

To quantify cell area in an unbiased fashion, CTG images were processed using image analysis software CellProfiler 2.2.0 [248, 249]. The image process pipeline is detailed in Table 3. For image analysis, a minimum of 8 images per condition were used, and a minimum of 60 cells were used to generate average cell area. Each image was checked individually to ensure CellProfiler recognised cell correctly, and incorrect recognition was removed from analysis. As well as measuring cell area, CellProfiler can measure how spherical cells are and gives out a ratio of eccentricity. To do this, it measures the length and width of the cell and generates a ratio. A value of 0 is a perfect sphere and 1 is a straight line. Values between 0 and 1 are calculations of eccentricity of cell shape (Figure 2.5).

Process	Notes
ColourToGray	Creates a greyscale image – essential for downstream thresholding
IdentifyPrimaryObjects	• Primary object for measurement is cells • Segmentation process was completed using global thresholding strategy using MoG (mixture of Gaussian) thresholding method. • Typical diameter of object set at 30-90 pixels. • Automatic smoothing filter was used for declumping with a threshold correction factor of 1.00.
IdentifySecondaryObjects	• Secondary object for measurement is nuclei • Propagation method was used to identify secondary objects • Global threshold strategy was used with Robust Background thresholding method, with a correction factor of 1.0
MeasureObjectSizeShape	Selects primary objects to measure
DisplayDataOnImage	Displays value of cell area on image
ExportToSpreadsheet	Object shape parameters extracted to spreadsheet

Table 3. Pipeline of CellProfiler used to measure cell area of CTG stained cells

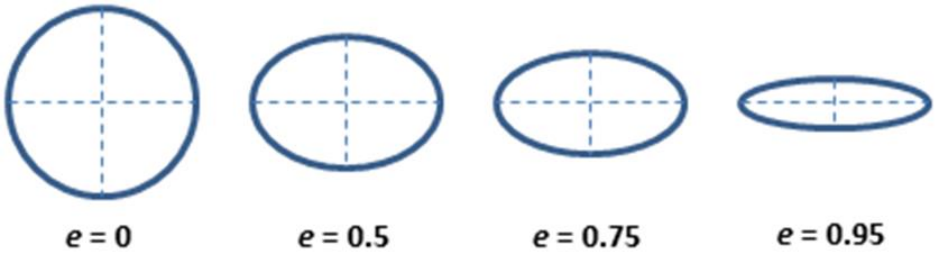

Figure 2.5. Example of CellProfiler eccentricity measurements. *e – eccentricity value calculated from example circular shapes. Image from https://s3.amazonaws.com/pnmresources/pID-500/topic-63028/1.14.14+CYTO+U+Webinar+Slides+%281+per+page%29.pdf. Accessed 10/03/2018.*

2.8. Image Capture

Sample images were captured using a Zeiss Axiovert 200 inverted microscope (Zeiss, Cambridge, UK) and Zeiss Axiovision software version 4.9. Light microscopy images were taken using an Axiocam HR camera and both phase and fluorescent images were captured using Axiocam MR, with the appropriate filter if necessary.

2.9. Statistical analysis

Statistical analysis was carried out using either paired t-test, or 2 way analysis of variance (ANOVA) using the statistics software GraphPad Prism version 7.01. Multiple two tailed paired t-test was chosen to analyse miRNA RT-qPCR data in which two groups of data were compared to determine if the mean data sets were statistically different. This test was chosen because the experimental design had a paired design. Here, the Bonferroni-Dunn post hoc test was performed. All other data sets were compared using two-way ANOVA and compared using Tukey post hoc test. This test was chosen as it compares three or more groups of data. Independent experiments were performed for statistical analysis a minimum of three times, each repeat with an independent patient and $p \leq 0.05$ was considered statistically significant.

Chapter 3: Effect of disordered nanotopographical cues on SSC behaviour

Chapter 3 - Effect of disordered nanotopographical cues on SSC behaviour

3.1. Introduction

Topography is known to affect human bone marrow stromal cells (reviewed in Dalby et al 2014 [143]) and is known to alter morphology and gene expression [250]. Studies on hemisphere embossed Polymethylmethacrylate (PMMA) nanotopographical surfaces have shown variation in human MSC behaviour down to 10 nm differences in morphology [251]. On these surfaces, filopodia were noted extended from the cell to the topographical substrate. In addition, MSCs were found to extensively spread on hemisphere substrates compared to control surfaces with cytoskeletal analysis demonstrating a higher tubulin and vinculin network. Interestingly, this change in the cell cytoskeleton network was accompanied by an increase in OCN and OPN protein expression, indicative of osteogenic differentiation of MSC on hemisurfaces [251]. This topographical induced modulation of cell phenotype indicates the potential to harness nanotopography at the nanoscale to study and modulate cell function and development of innovative surfaces at nanoscale resolution.

Electron beam lithography (EBL) technology has been used to fabricate a series of nanoscale patterns on cell culture surfaces. EBL involves the use of an electron beam to modify the topography of materials to produce the resultant patterns. This method is ultra-precise, with resolution published approaching 2 nm [252], and has the potential of being reproducible between batches and thus, providing commercial scale up is a real possibility. This technology has been utilised by Dalby and colleagues to produce a series of nanosubstrates with defined topography and introduce controlled roughness to surfaces. Initially an array of nanosubstrates were used, each modified with a discrete pattern of 120 nm diameter, 100 nm deep nanopits [132]. The patterns ranged from hexagonal, square, disordered square array with nanopits displaced randomly by up to 50 nm on both axes from their position in a true square (DSQ50) and random arrangements (Figure 3.1). In later studies, DSQ50 were referred to as near square (NSQ) and will be termed as such from now on.

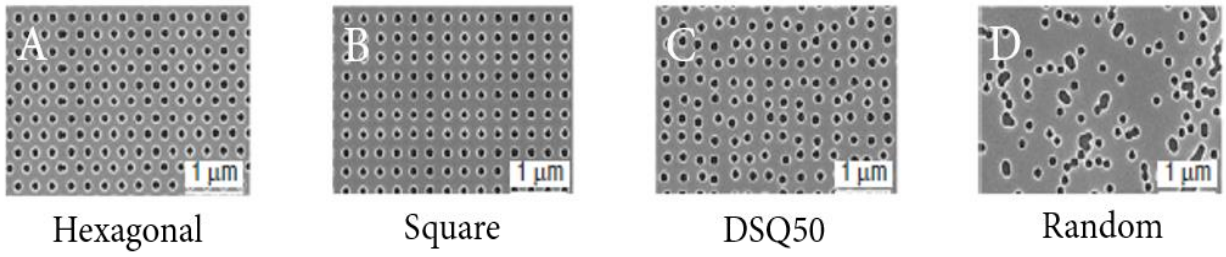

Figure 3.1. Nanosubstrates developed by Dalby et al (132). *Circular pits of 120 nm diameter, 100nm deep were embossed using EBL in patterns, all pits have either an absolute or average centre-centre spacing of 300 nm. A- Hexagonal array. B- square array. C- disordered square array with pits randomly distributed up to 50 nm from their true square position. D- Random distribution. Image modified from [132].*

STRO-1+ skeletal stem cells (SSCs) (termed mesenchymal stem cells (MSC) in this study) were cultured on these surfaces and compared to unselected bone marrow cells (termed osteoprogenitor cells in this study). The authors did not progress any studies with hexagonal nanosurfaces due to poor cell adherence. Enhanced expression of OPN and OCN protein was observed on the NSQ nanosurfaces, and the formation of mature bone nodules following 28 days culture [132]. Importantly, this was observed in the absence of chemical signals, demonstrating the power of a topographical approach to modulate cell phenotype [132]. Following from this observation, genome wide expression of mRNA osteogenic markers was investigated using microarray analysis. The results of the microarray evaluation showed that when STRO-1+ SSCs were cultured on flat, planar (PL) surfaces in the presence of osteo-inductive dexamethasone, there was an increase in expression of osteogenic markers [132]. However, there was also increase in the number of hits on STRO-1+ SSCs cultured on NSQ nanosurface in plain media [132]. A number of pathways related to bone development (fibroblast growth factor and epithelial growth factor signalling) were activated only on the NSQ nanosurfaces, indicating the potential for nanosurface-activated differentiation to induce a different set of cell changes in comparison to chemical stimulation.

Alterations in cell adhesion are known to contribute to gene expression changes and subsequently stem cell differentiation by affecting signalling from the cell membrane through to the nucleus [253]. It has been clearly established that the cytoskeleton forms a link between the cell membrane and the nucleus. Mechanical signals are transmitted from extracellular matrix (ECM) at the cell membrane, to cytoskeleton, to the nucleus via nucleoskeleton, which could affect gene expression [254]. STRO-1+ SSCs displayed larger focal adhesions when cultured on the NSQ nanosurface compared to PL control [177], an indication of high contractility within the cell. Enhanced focal adhesion generation was accompanied by an increase in p-myosin expression, indicating an increase in cytoskeletal tension [177]. Lamins, vital components of the nucleoskeleton, attach to the cytoskeleton via linker of nucleoskeleton

and cytoskeleton (LINC) complexes (Figure 3.2) [255]. The density of lamin A/C was studied to determine if NSQ nanosurface had an effect on nucleoskeleton [177]. Tsimbouri *et al*, discovered a lower density of lamin A/C network in this surface compared to PL control [177]. This change in density, and therefore lamin network, could be due to increased tension within the nucleus, possibly having an effect on chromosome positioning and subsequent differentiation. The authors postulated that the disordered arrangement forced integrins to cluster between the pits, allowing for high tensile strength within the cell, and triggering osteogenic differentiation [143].

Further to this, the metabolic rate of differentiating STRO-1+ SSCs on a NSQ nanosurface has been investigated through metabolomics studies [177]. It was found that cells on the NSQ nanosurface exhibited increased level of metabolites compared to planar control. This could possibly be due to extra metabolic demand from differentiating cells [177].

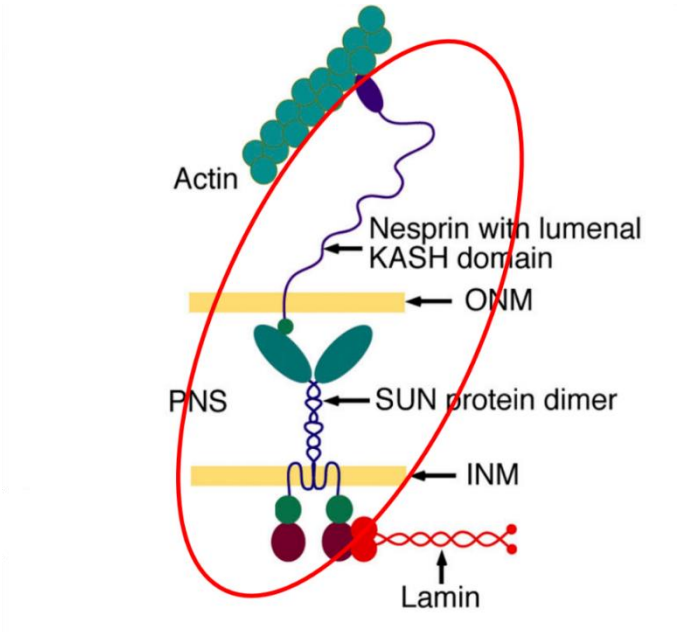

Figure 3.2. LINC complex diagram. *LINC complex (proteins included in red circle) connect actin of the cytoskeleton to nuclear lamins. ONM – outer nuclear membrane. PNS – perinuclear space. INM – inner nuclear membrane. Modified from Crisp* et al*, 2006 [255].*

In early experiments, Dalby et al studied an array of nanopitted surfaces and hexagonal arrangement and random arrangements were eliminated early on due to poor cell adhesion and lack of osteogenic induction respectively, with the NSQ surface found to be osteoinductive [132]. Nanofeatures were studied as it was known to have biological significance in the size of Type X collagen and fenestrated sinusoidal capillaries [143]. The aim was to identify a surface with controlled, reproducible topography which can influence osteogenic differentiation and through this the NSQ nanosurface was identified. The importance of the nanodisorder in the NSQ surface is thought to be due to the influence on integrin arrangement,

forcing integrins closer together. While there has been a wealth of knowledge discovered about the effect of NSQ topography on SSC behaviour, there is little information concerning the role of miRNAs in controlling differentiation.

3.1.1 Aims

Hypothesis:

NSQ topography can effect SSC fate and function, resulting in alterations in mRNA and miRNA gene expression.

The aim of this chapter was to examine molecular phenotype and behaviour of STRO-1+ SSCs following culture on discrete NSQ nanosurfaces. Specifically:

I. To study the potential of NSQ nanosurfaces to differentiate SSCs to osteoblasts through expression of osteogenic markers.
II. To investigate the miRNA profile of SSC cultured on nanosurfaces in order to examine if any regulatory miRNA are involved in the modulation of SSC behaviour on discrete topographies.

3.2. Methods

3.2.1. Nanosurface manufacturing

Nanosurfaces were generated and provided, using the microfabrication technique EBL, by the University of Glasgow (Professor Dalby and Professor Nikolaj Gaadegard). In these experiments, the selected polymer was PCL. The Young's modulus, a measurement of material stiffness, for the PCL nanosurfaces were not specifically calculated for these experiments but has been reported in published work to range from 343.9 to 364.3 MPa [256]. NSQ nanosurfaces contained 120 nm diameter pits, 100 nm deep in a square arrangement offset by 50 nm (Figure 3.3).

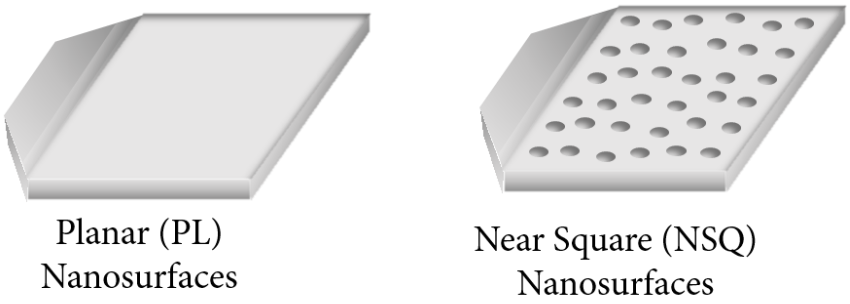

Figure 3.3. Diagram (illustrative only) of planar (PL) and near square (NSQ) nanosurface. *Pits shown in NSQ nanosurface are exaggerated for description purposes and are visible under SEM only.*

Substrates were generated in a three-step process: EBL, nickel die fabrication and hot embossing as discussed in detail in Dalby *et al*, (2004) [257]. Briefly, silicon substrates were coated with a resist, material that is sensitive to EBL, and the electron beam etched out the pattern. After this, samples were developed to remove areas modified by EBL. Following from this, nickel dies were made from the patterned samples, by first sputter coating with nickel and electroplating. PCL was then hot embossed with the nickel dies and left to cool.

3.2.2. Nanosurface culture preparations

Nanosurfaces were delivered sealed in plastic wallets by collaborators at the University of Glasgow and transferred to one well each of a 6-well plate using sterile forceps for sterilisation. Nanotopographical substrate samples were stored in 6 mL PBS supplemented with 5% antibiotic-antimytotic (ABAM, ThermoFisher Scientific, UK) for a minimum of overnight and washed twice in PBS prior to use. STRO1+ SSCs were prepared for seeding in 6-well plates as outlined in Section 2.2.5. and maintained in 4 mL basal media with a seeding concentration of 200 cells/cm^2. Surfaces were transferred to a new 6-well plate one day after seeding, to prevent interference from cells which adhered to tissue culture plastic (TCP) and not to

nanosurfaces, and the media replaced. At this point, media was changed on TCP control surfaces. Thereafter, the media was changed every 3-4 days.

3.2.3. miRNA microarray analysis

Applied Biosystems TaqMan® Low Density Array system was used to perform qRT-PCR miRNA microarrays, according to the manufacturer's protocol. Two patient samples, both females ages 69, and a day 21 time point was chosen for the miRNA microarray. Preliminary studies suggested culture for 21 days generated the highest degree of osteogenic differentiation and thus would provide, potentially, differences in miRNA expression in the microarray. cDNA synthesis and RT-qPCR amplification for microarray uses multiplex™ primer pools, which can detect up to 380 genes (as quoted by the manufacturer Thermo Fisher, https://tools.thermofisher.com/content/sfs/manuals/cms_053965.pdf, accessed 16/03/2018). 227 ng RNA was used for megaplex™ reverse transcription (RT) primers to generate cDNA. Briefly, per sample reaction, 0.8 µL megaplex™ RT primers (10x), 0.20 µL deoxynucleotide (dNTP) (100 mM), 1.50 µL Multiscribe™ reverse transcriptase (50 U/mL), 0.80 µL 10x RT buffer, 0.90 µL $MgCl_2$ (25 mM), 0.1 µL RNase inhibitor (20 U/µL) and 0.2 µL nuclease-free water were combined. To this, 3 µL RNA sample with concentration of 75.66 ng/µL RNA was added and mixed by pipetting. Megaplex™ RT was performed using 7900 system Real-Time PCR System (Applied Biosystems™, UK). The thermo-cycling conditions were set to run 40 cycles of 16°C for 2 min, 42°C for 1 min and 50°C for 1 second. After this, the cycler entered two hold stages, the first 85°C for 5 minutes and 4°C until plate removed from the system. Samples were stored at -20°C. 6 µL of cDNA was combined with 450 µL of 2x TaqMan™ PCR Master mix and 444 µL nuclease-free water, and loaded onto microarray card and assayed using a 7900 system Real-Time PCR System. Sequence Detection System v2.4 Enterprise edition (Applied Biosystems, UK) was used to analyse raw data and threshold set to 0.2. The $2^{-\Delta\Delta Ct}$ method was used for relative quantification of gene expression. From the three house-keeping genes available in the card (sRNA U6, RNU44 and RNU48), sRNA U6 was selected for comparison as this was the most stable and is commonly used for miRNA normalisation.

Hits to investigate from the miRNA microarray were selected manually by identifying miRNAs either upregulated or down regulated in both patients, relative to the housekeeping. Additionally, a literature check was performed to identify miRNAs known to be involved in osteogenic differentiation. On the basis of these two categories, 9 miRNAs were chosen for further investigation.

3.2.4. SEM preparation and imaging

Nanosurfaces were removed from packaging and mounted onto metal stubs using double-sided tape. Nanosurfaces were sputter coated with 7 nm platinum using Q150T turbo-pumped sputter coater/carbon coater (Quorum Technologies Ltd, East Sussex, UK). In order to ensure charge distribution, Electrodag 1415 (AGG3648, Agar scientific, Essex, UK) was painted from the edge of nanosurfaces to metal mounting stub. Samples were viewed using Quanta FEG 250 scanning electron microscope (FEI™, Eindhoven, The Netherlands). The SEM was controlled by xT microscope control software, which also allowed for image capturing.

3.3 Results

3.3.1 Nanosurface Image analysis

To study the patterns on the different nanosurface topographies, SEM was used. Samples were prepared and imaged as detailed in section 4.2.7. SEM imaging also allowed for quality control confirmation of the accuracy of EBL. **Figure *3.4*** illustrates images obtained with SEM of surfaces received during the initial stages of collaboration with University of Glasgow (October 2014). The PL nanosurface was observed to be smooth with some small scratches (Figure 3.4A-C). The size of the pits and disordered arrangement in NSQ nanosurface can be observed across all magnifications (Figure 3.4D-F). Although no images with STRO-1+ SSC on these surfaces were taken, given the size of the nanopits (120 nm diameter) and the average size of a STRO-1+ SSC (100 µm Figure3.5), it could be postulated that the nanopits would be so small as to be invisible next to the SSC. It was also apparent that the surface was clean and EBL modification had not resulted in detectable artefacts. However, under high magnification (Figure 3.4F), distortions in the modification were observed around the nanopits.

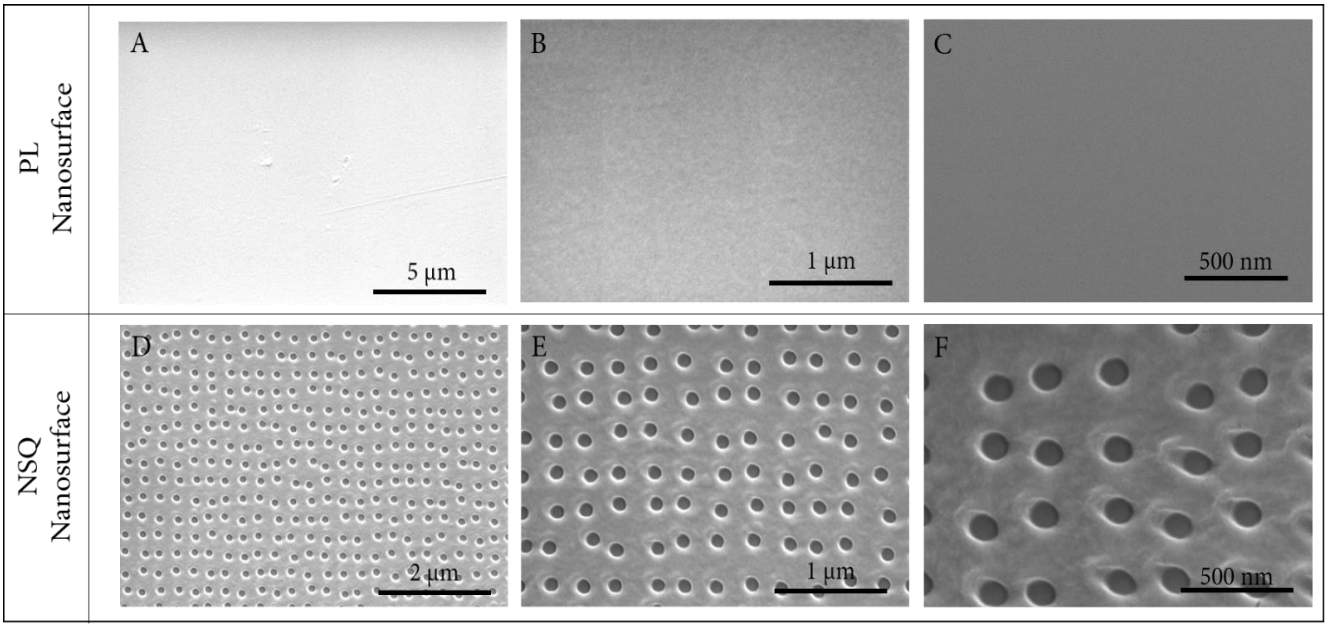

Figure 3.4. SEM imaging of nanosurfaces. *Surfaces were sputter coated with 7 nm platinum and viewed using FEI Quanta 250 SEM. A-C PL nanosurface. D-F NSQ nanosurface. The scale bar is shown in each individual image.*

3.3.2 SSC morphology on nanosurfaces

STRO-1+ enriched SSCs were cultured on the nanosurfaces as described in section 2.2.5 and cultured in basal media only (detailed in section 2.2.2). Images of cells proliferating on nanosurfaces and TCP surfaces were taken using a Zeiss light microscope at days 7, 14 and 21 post-seeding (Figure 3.5). The SSCs displayed a comparable morphology whether cultured on PL nanosurface, NSQ nanosurface or TCP (control surface). Cells displayed a spindle-like, stretched morphology across all substrates at day 7 (Figure 3.5A, D and G). By day 14, STRO-1+ SSCs had reached almost full confluence and cells were observed to be aligned (Figure 3.5B, E and H). This was maintained until day 21, with cells on all surfaces reaching 100% confluency (Figure 3.5C, F and I). At days 14 and 21, there were no clear distinctive differences in morphology on nanosurfaces and TCP control, as observed using light microscopy.

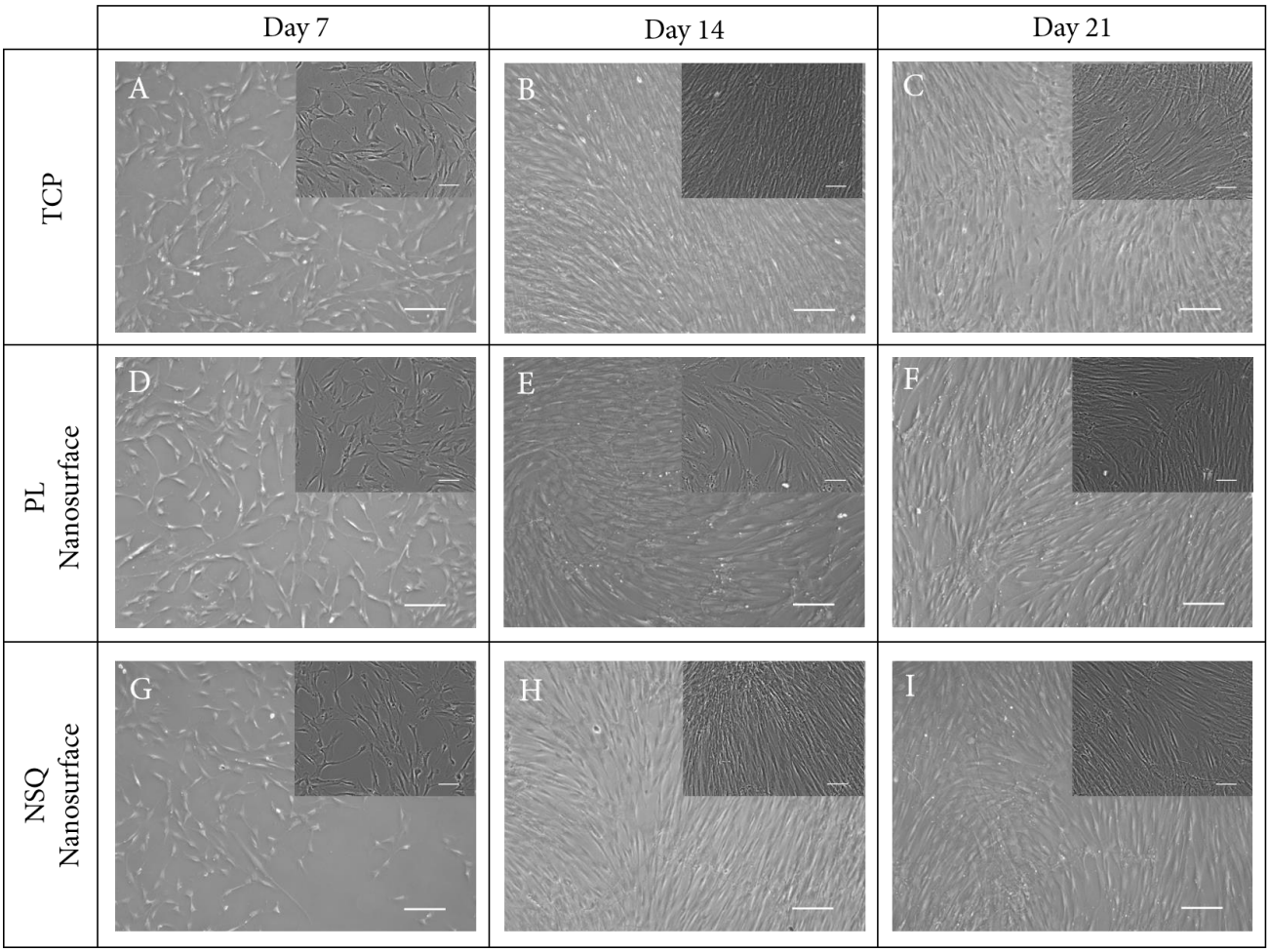

Figure 3.5. STRO-1+ SSC proliferation on nanosurfaces. *TCP (A, B and C). PL nanosurfaces (D, E, F). NSQ nanosurfaces (G, H and I). Images taken on day 7 (A, D and G), day 14 (B, E and H) and day 21 (C, F and I) post seeding. Larger image x5 magnification, scale bar 100 µm. Inset image x10 magnification, scale bar 200 µm.*

3.3.3 Expression of osteogenic markers on nanosurfaces

Following examination of cell morphology on the nanosurfaces, expression of selected osteogenic markers, following STRO-1+ SSC culture on nanosurfaces, was measured. STRO-1+ SSCs were cultured on PL and NSQ nanosurfaces as described in section 2.2.5. Patient donor samples comprised of 4 females aged 60-73 and one male aged 78. Cells were lysed at days 7, 14 and 21 and RNA extracted for RT_qPCR as described in sections 2.3.1., 2.3.2., 2.3.3., and 2.3.4. Overall, there was negligible difference in expression of osteogenic markers between PL and NSQ nanosurfaces (Figure 3.6) and expression of all osteogenic markers were noted to have increased over 21 days. Interestingly, on day 21, expression was marginally higher on NSQ nanosurfaces compared to PL nanosurfaces. For example, on day 21 expression of *OCN* on PL surface was observed non-significantly increase from 3.02 ± 1.57 and on NSQ 3.46 ± 1.42 and expression of *COL1A1* on PL surfaces was 2.82 ±1.02 and on NSQ 3.76 ± 1.19. Due to the high variability in expression between SSC donors, there was no significant difference observed between samples across the osteogenic markers examined. There was however significant up regulation of osteogenic markers expression temporally when measuring *ALP, RUNX2, COL1A1* and *OCN* mRNA levels. Thus, expression of *RUNX2* on PL surfaces from day 7 to day 21 (1.0 ± 0 to 3.1 ± 0.8), and NSQ surfaces from day 7 to day 21 (0.9 ± 0.08 to 3.3 ± 1.0) was observed to be significant ($p \leq 0.01$).

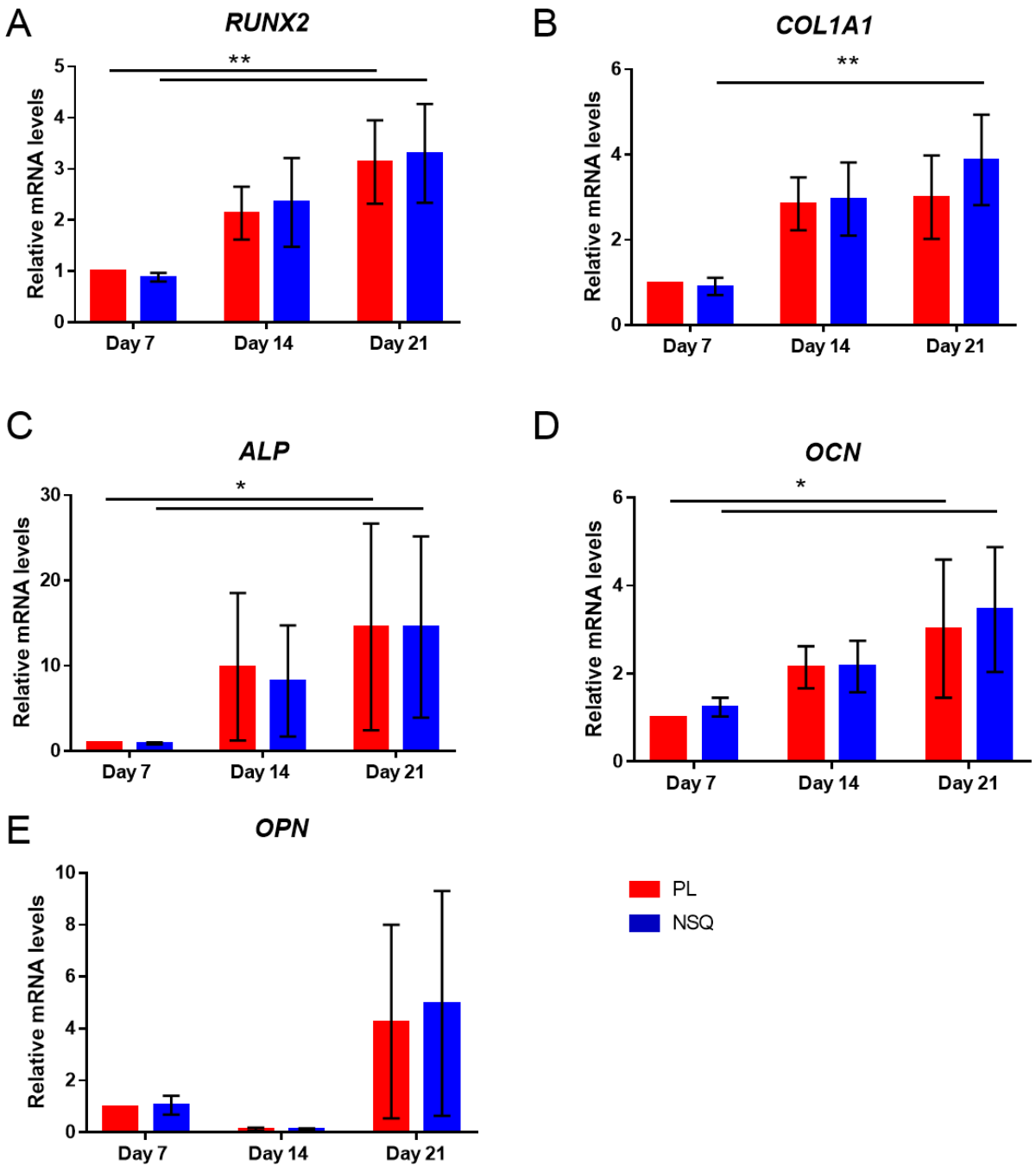

Figure 3.6. mRNA relative expression of osteogenic markers in STRO-1+ SSCs on nanosurfaces over 21 days. *PL nanosurfaces in red, NSQ nanosurfaces in blue. Expression measured on day 7, 14 and 21. Bar shows mean ± SD. Each sample was normalised to ACTB and relative to PL on day 7. N=5 individual patient samples. Analysed gene is displayed at the top of each graph. 2 way ANOVA was performed on data. * represents* $p \leq 0.05$. *** represents* $p \leq 0.01$.

3.3.4. Microarray measured miRNA expression on nanosurfaces

In order to study the microRNAs involved in change of behaviour observed on NSQ nanosurfaces, a whole genome approach was employed using microRNA microarray analysis. A day 21 time point was chosen to conduct the microarray as this was judged a likely point to observe any potential differentiation over the 21 day programme employed [250].

Two patient samples from experiments described in section 3.3.3. were selected (patients 4 and 5, both females aged 69), as these were observed to be maximally responsive to the nanosurfaces and showed the largest difference between NSQ and PL (Figure 3.6) (the microarray protocol is detailed in section 3.2.3). Expression of the miRNAs covered in the microarray are displayed in Figure 3.7A (patient 4) and Figure 3.7B (patient 5). miRNA with no x- or y-value displayed limited expression which was too low for microarray detection. A high ΔC_t value indicated miRNA which are expressed at a lower level, and a low ΔC_t value indicated miRNA which are expressed at a high level, relative to the control (U6 snRNA). In both patients, the miRNA expression displayed a linear, positive trend with negligible differences between ΔC_t value measured in NSQ surfaces and ΔC_t value on PL surfaces. Any outliers would indicate miRNAs expression significantly different on the NSQ surfaces to PL surfaces. The absence of outliers indicated comparable cell behaviour on NSQ surfaces to PL surfaces in both patients in these experiments.

From the results of the microarray analysis, 9 microRNAs hits were selected, displayed on the microarray scatter plot for patient 4 (Figure 3.8A) and patient 5 (Figure 3.8B). These miRNA were chosen as the miRNA were found to increase in expression on either the PL or NSQ surface and identified through literature search to be involved in osteogenic differentiation. The expression increase or decrease measured in the microarray between PL and NSQ was calculated using the $2^{-\Delta\Delta Ct}$ method and presented as a heatmap (Figure 3.9). These miRNAs miR-138, miR-20b, miR-23a, miR-133a, miR-218, miR-296, let-7f, miR-148b and miR-29a were found to be modulated on the nanosurfaces for both patients 4 and 5 (The functions of these miRNAs are described in **Table *4*** and discussed in section 3.4). Relative expression of miRNAs in NSQ nanosurfaces on day 21 varied across the nine selected miRNA between the two patients. Fold-change in expression of miR-138 and miR-133a on NSQ nanosurface compared to PL was comparable between the two patients (0.90 and 0.84 for miR-138 expression, and 2.48 and 2.57 for miR-133a expression). However for two miRNAs, miR-296 and miR-148b, fold-change in expression between the two patients was more widely distributed (miR-296 relative expression noted at 4.39 for patient 4 and 2.3 for patient 5, and miR-148b relative expression was 3.42 for patients 4 and 1.88 for patient 5).

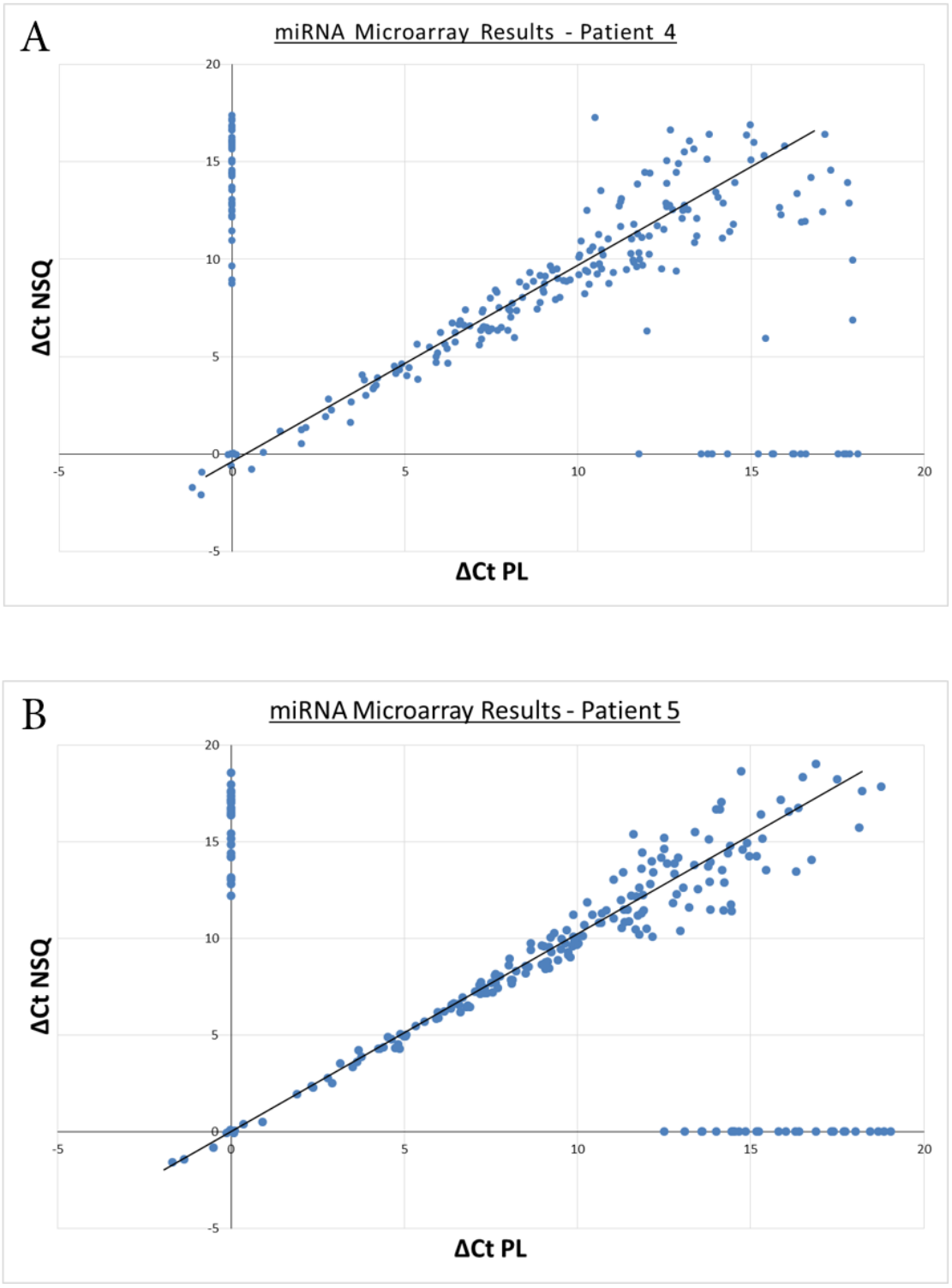

Figure 3.7. MiRNA microarray of STRO-1+ SSCs cultured on PL and NSQ nanosurfaces after 21 days of culture. *A - patient 4. B- patient 5. ΔCt was generated from the difference between sample C_t and U6 snRNA C_t. ΔC_t on PL surface on x-axis and ΔC_t on NSQ on y-axis. Each point on the scatter plot represents a different miRNA. Trend line in black.*

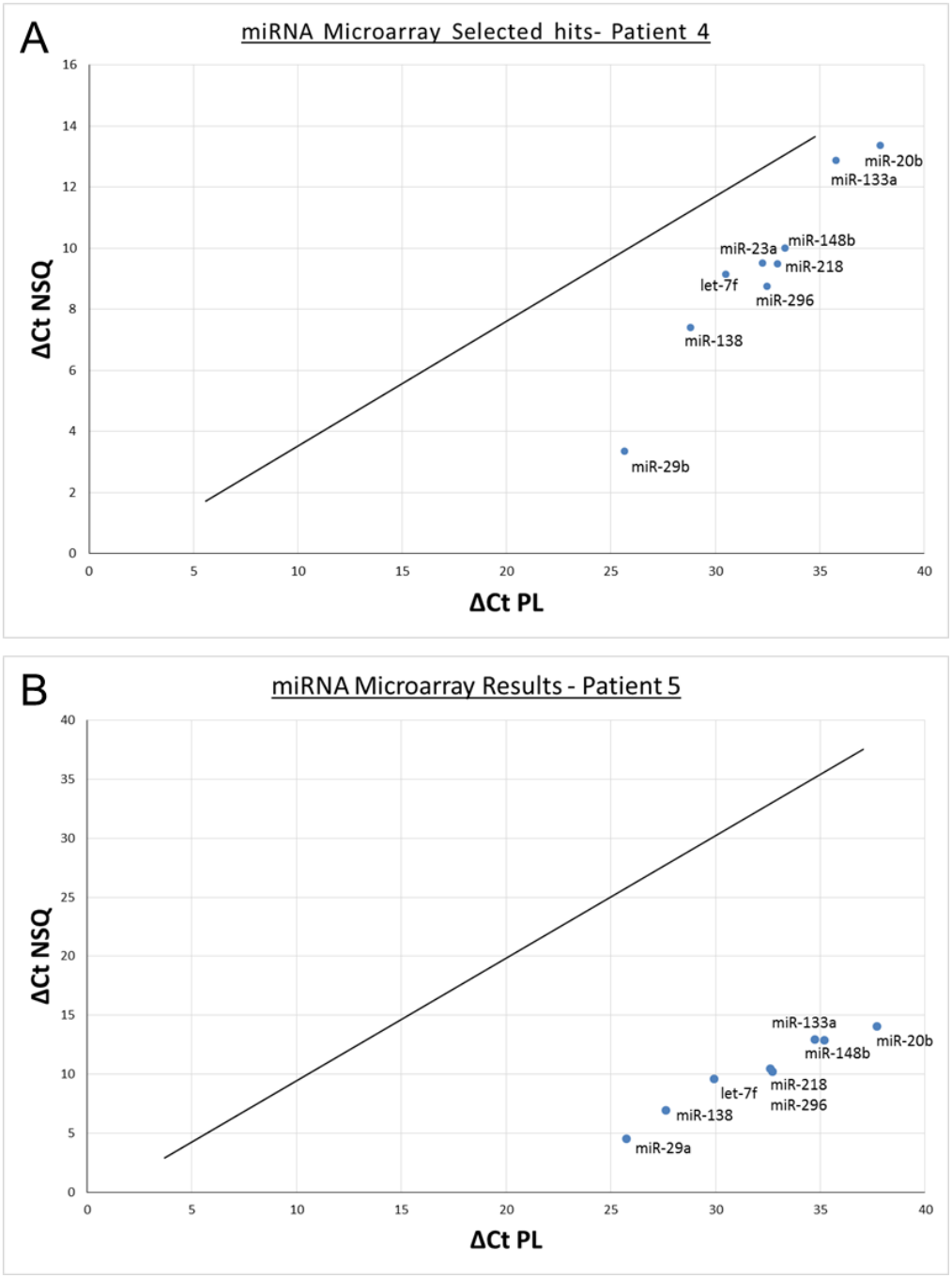

Figure 3.8. Hits from miRNA microarray of STRO-1+ SSCs cultured on PL and NSQ nanosurfaces after 21 days of culture. *A - patient 4. B- patient 5. ΔCt was generated from the difference between sample C_t and U6 snRNA C_t. ΔC_t on PL surface on x-axis and ΔC_t on NSQ on y-axis. Each point on the scatter plot represents a different miRNA and the miRNA is labelled on the bottom right of each point. Trend line in black.*

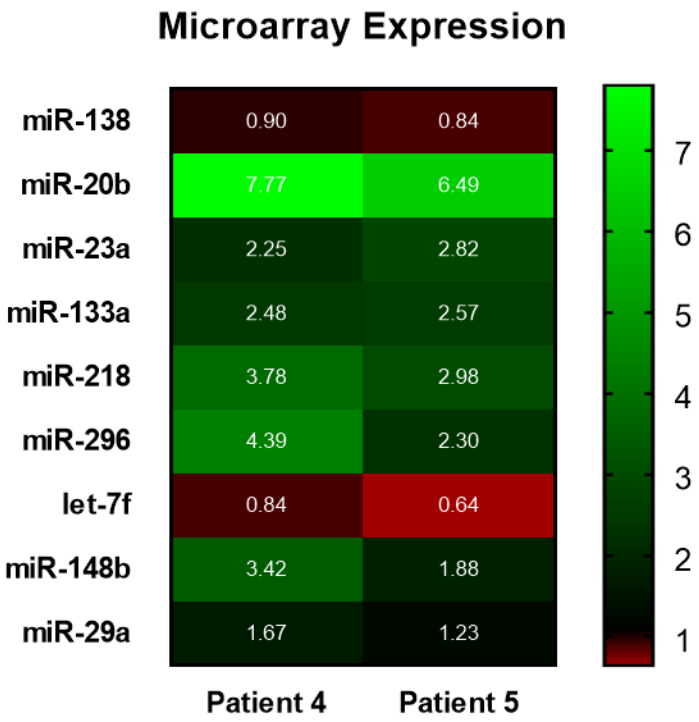

Figure 3.9. Heat map displaying relative expression of hits from miRNA microarray. *miRNA hits selected are listed on left. Patient samples are on the bottom. Inside each box is the relative expression of that sample. This was calculated using $2^{-\Delta\Delta Ct}$ method, comparing ΔPL to ΔNSQ relative to U6 snRNA. The key detailed in right-hand panel.*

miRNA	Positive or negative regulators of osteogenesis	Known target(s)	Functional outcome
miR-138	Negative	Focal Adhesion Kinase (*FAK*)	Down regulation during osteogenesis to prevent inhibition of FAK signalling [220].
miR-20b	Positive	*STAT3*	Through targeting of *STAT3*, self-renewal and proliferation is suppressed [258].
miR-23a	Negative	*SATB2*	*RUNX2*-mediated down regulation of miR-23a ensures up regulation of *SATB2*, *RUNX2* binding partner [259].
miR-133a	Negative	*RUNX2*	Down regulation of miR-133a promotes osteogenesis by prevention of miR-133a mediated inhibition of RUNX2 levels [260].
miR-218	Positive	Sclerostin (*SOST*), Dickkopf2 (*DKK2*), and secreted frizzled-related protein2 (*SFRP2*)	Through targeting of Wnt inhibitors, miR-218 stimulates Wnt signalling [208].
miR-296	Positive	Hepatocyte growth factor-regulated tyrosine kinase substrate (*HGS*).	Prevents HGS-mediated degradation of vascular endothelial growth factor receptor 2 (VEGFR2), thereby allowing angiogenesis to progress [261].
Let-7f	Positive	*AXIN2*	AXIN2 has a role in inhibiting Wnt signalling. Let-7f through down regulating AXIN2, stimulates Wnt signalling [262].
miR-148b	Positive	*WNT1* [263]	Delivery of miR-148b enhances osteogenic activity of SSC [264, 265].
miR-29a	Positive	*DKK1, SFRP2*	Through targeting of Wnt inhibitors, miR-29 stimulates Wnt signalling [266].

Table 4. Functional role of miRNA hits from microarray. *Table details negative and positive miRNA regulators of osteogenesis, any known targets, and the functional outcome of miRNA-mediated inhibition of targets.*

Validation of microarray results using RT-qPCR

All hits from the microarray evaluation were validated using RT-qPCR and highly specific probes to amplify and quantify specific miRNA as detailed in section 2.3.5 for miRNA RT-qPCR. In order to validate microarray hits from the detailed experiments, RT-qPCR was performed on RNA samples used for the microarray (Patient 4 and 5, PL and NSQ on day 21).

The relative expression results in Figure 3.10 indicated differences in miRNA expression measured by microarray and RT-qPCR. The greatest differences between microarray and RT-qPCR expression were noted for miR-20b expression (Figure 3.10B). Microarray expression in STRO-1+ SSCs on NSQ surfaces relative to PL was measured at fold-change of 7.77 and 6.49 for patients 4 and 5 respectively, in comparison to the fold-change 1.116 and 1.556 (for patient 4 and 5 respectively) measured in RT-qPCR. Occasionally, expression analysis measured using microarray was observed to be comparable to measurements derived using RT-qPCR. For example, miR-138 expression in patient 5 was measured at 0.84 fold-change in microarray and 0.949 fold-change in RT-qPCR (Figure 3.10A). Overall, significant differences in expression measurements between microarray and RT-qPCR, reflecting the differences in specificity of amplification and quantification of the two techniques, were observed.

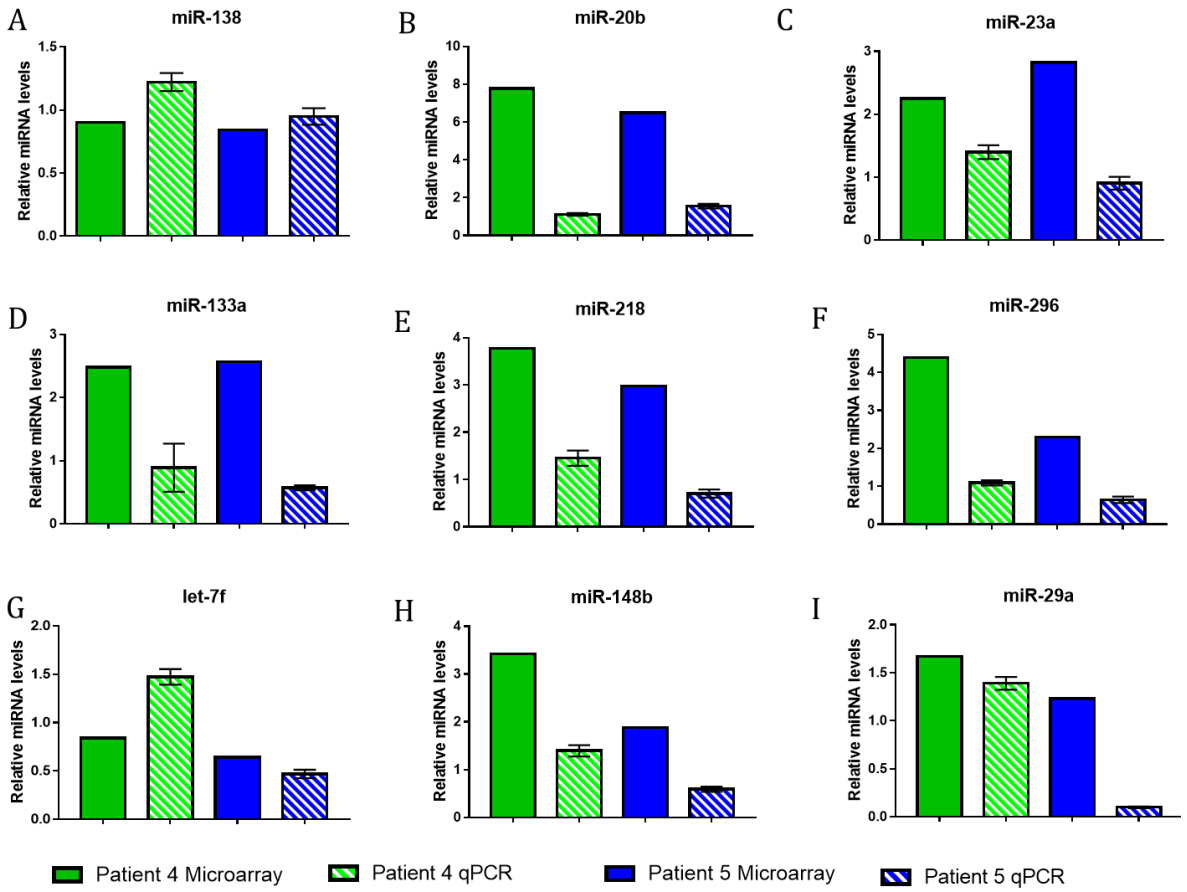

Figure 3.10. Validation of microarray hits using RT-qPCR. *Day 21 NSQ samples from patients 4 and 5 were analysed by RT-qPCR for expression of miRNA indicated on each graph and compared to expression measured by microarray. RT-qPCR was calculated using $2^{-\Delta\Delta Ct}$ method, comparing ΔPL on day 21 to ΔNSQ on day 21 relative to U6 snRNA. Patient 4 – green, patient 5 – blue, microarray expression – block colour, RT-qPCR expression – hashed colour. Microarray measured one value of expression. RT-qPCR was measured in triplicate and expression displayed as mean ± SD.*

3.3.5. Extension of data set to study STRO-1+ SSC on nanosurfaces

The expression of osteogenic markers in section 3.3.3 and microarray results in section 3.3.4 indicate possible upregulation of osteogenic mRNA markers and osteogenic miRNAs on the NSQ nanosurface. To generate a better picture of the cell osteogenic response to nanotopography, the data set was extended to include a further 7 patients, giving 12 patients in total. The mean patient age range in these 12 patients was 56-92 years of age with 7 female and 5 male patients. Similar to expression of osteogenic markers measured previously, STRO-1+ SSCs were seeded onto nanosurfaces as described in section 2.2.5. and cultured in basal media. Samples were taken on day 7, 14 and 21 for nucleic acid extraction, and RT-qPCR performed on the isolated RNA, as described in sections 2.3.1, 2.3.2, 2.3.3., and 2.3.4. The RT-qPCR results from patient 1 to 5 were then combined with the additional 7 patients.

The results in Figure 3.11 indicated, overall, negligible osteogenic induction on the NSQ nanosurface compared to PL surface and interestingly, expression was often higher on PL surfaces than NSQ surfaces. Expression of *ALP* on PL nanosurface on day 21 was slightly higher than NSQ nanosurface, at 15.7 ± 14.2 (Figure 3.11A) compared to 13.8 ± 10.0 on NSQ. *RUNX2* expression was found to be lower on NSQ surface (2.1 ± 2.3) on day 14, compared to PL nanosurface on day 14 (5.3 ± 10.4) (Figure 3.11B). However, by day 21 expression of *RUNX2* was measured at marginally higher on NSQ nanosurface compared to PL (6.6 ± 11.1 on NSQ compared to 5.7 ± 9.4 on PL). Expression of *COL1A1* and *OCN* was also found to be lower on NSQ compared to PL on day 14. *COL1A1* expression on NSQ nanosurface was measured at 10.8 ± 19.7 on day 14 and on PL nanosurface at 17.7 ± 34.5 (Figure 3.11C). *OCN* expression on NSQ nanosurface on day 14 was quantified at 1.6 ± 1.9 compared to measured expression of 5.4 ± 9.6 on PL nanosurface (Figure 3.11D). *OPN* expression was also higher on PL surfaces compared to NSQ (Figure 3.11E). Expression of *OPN* on day 14 was measured at 8.1 ± 16.0 on PL surface and 3.4 ± 7.1 on NSQ nanosurface.

Although there was no significant differences in expression of osteogenic markers between NSQ and PL surfaces, when examined at the same time point, expression of osteogenic markers was seen to increase significantly with time. Expression of *ALP* was found to have increased on NSQ surfaces from 0.8 ± 0.5 on day 7 to 13.8 ± 10.0 on day 21, ($p \leq 0.0001$).

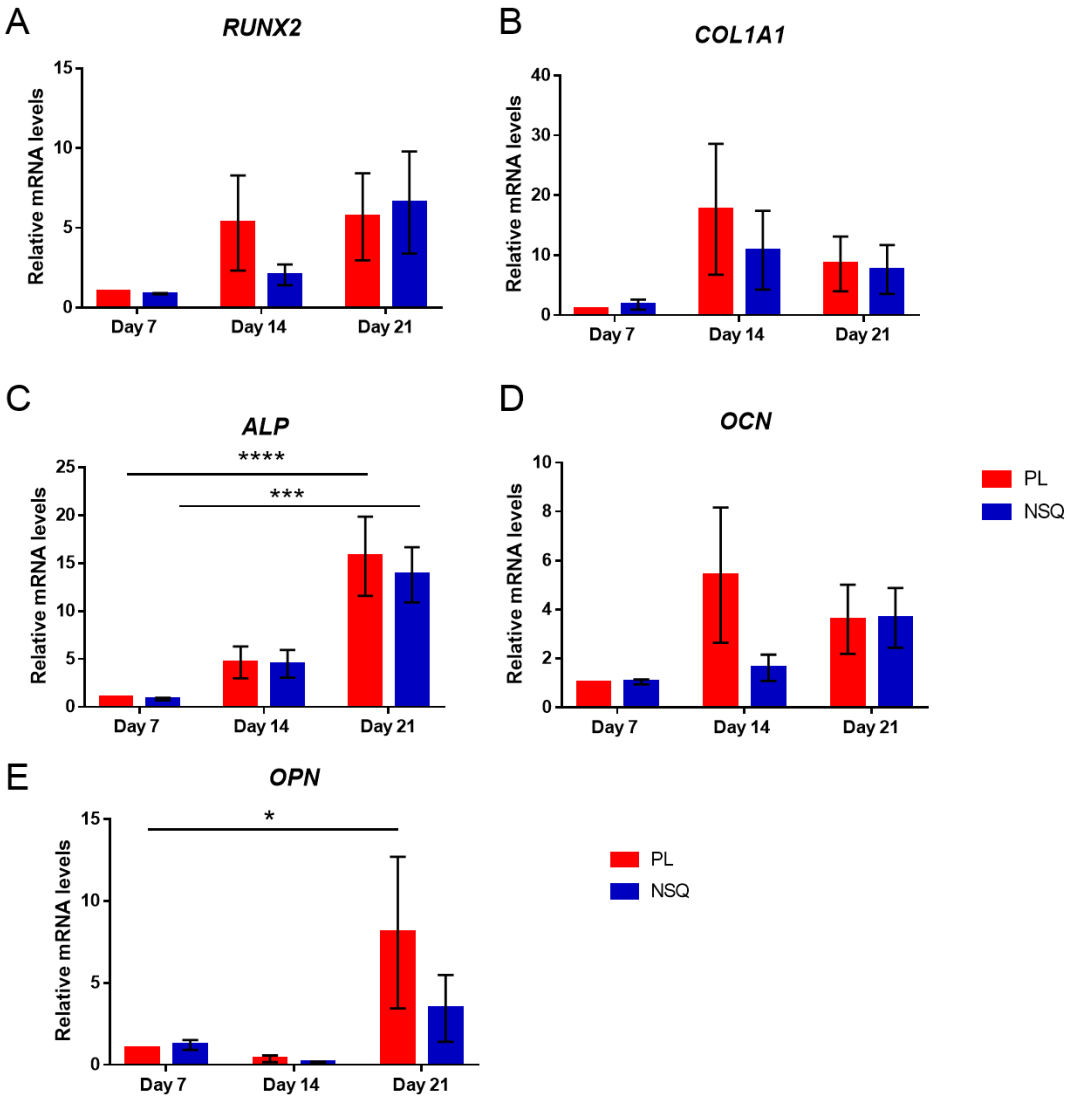

Figure 3.11. Expression of osteogenic markers on PL and NSQ nanosurface over 21 days measured in patients 1 to 12. *PL nanosurfaces in red, NSQ nanosurfaces in blue. Expression measured on day 7, 14 and 21. Bar shows mean ± SD. Each sample was normalised to ACTB and relative to PL on day 7. Analysed gene is displayed at the top of each graph. n = 12 patients. 2 way ANOVA was performed on data. * represents* $p \leq 0.05$.

Expression of osteogenic markers on NSQ nanosurface was found to be lower compared to PL surface. The expression of the nine selected miRNA from microarray was measured on both PL and NSQ nanosurfaces for patients 1 to 12. This could either confirm or challenge the lack of osteogenic induction of STRO-1+ SSCs on NSQ observed on the larger data set. RT-qPCR (protocol described in section 2.3.5) was performed on the additional 7 patients added to the data set, and combined with RT-qPCR results from the initial 5 patients.

The results on **Figure *3.12*** indicate small changes in miRNA expression on the whole 12 patient data set. For example in **Figure *3.12***E, expression of miR-218 on PL surface was measured at 3.7 ± 2.7 on PL and 2.9 ± 3.2 on NSQ. miR-138 and miR-23a are negative regulators of osteogenesis and so expression of miR-138 and miR23a should decrease during osteogenesis. In these experiments miR-138 was modestly decreased on NSQ surface (decrease in expression from 16.2 ± 24.2 on PL to 14.0 ± 16.7 on NSQ nanosurface) (Figure 3.12A). However, miR-23a expression was observed to increase from 1.9 ± 0.7 on PL to 2.1 ± 0.8 on NSQ nanosurface (Figure 3.12C).

Positive microRNA regulators of osteogenesis (miR-20b, miR-218, miR-296, let -7f, miR-148b and miR-29a) should increase expression during osteogenesis. All 6 positive regulators of osteogenesis were found to decrease on NSQ nanosurface compared to PL nanosurface. For example, expression of miR-296 decreased from 1.2 ± 0.8 on PL to 1.1 ± 0.5 on NSQ nanosurface (Figure 3.12F). Expression of miR-148b decreased from 5.2 ± 4.2 on PL to 4.8 ± 2.8 on NSQ nanosurface (Figure 3.12H).

These results confirmed the lack of osteogenic induction observed on examination of osteogenic microRNAs.

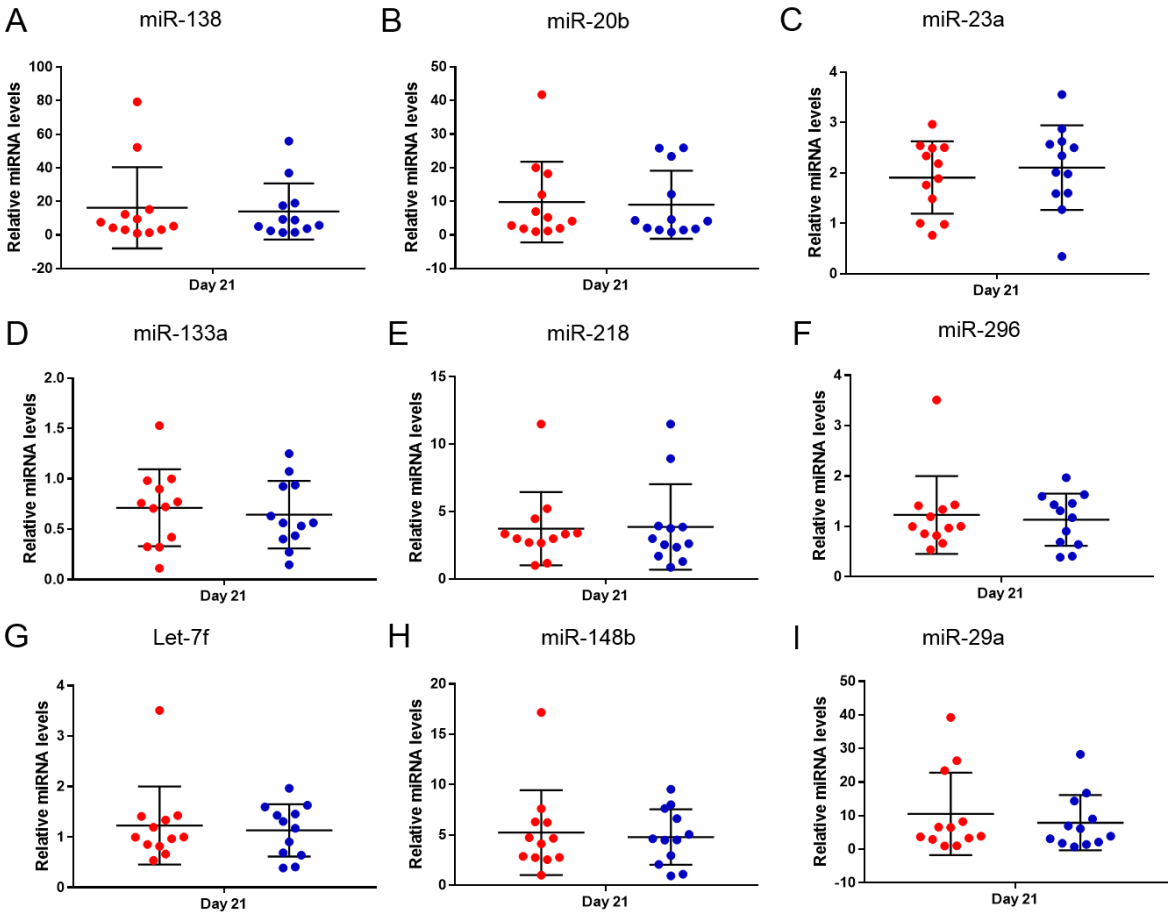

Figure 3.12. Expression of miRNA hits in STRO-1+ SSCs on PL and NSQ nanosurface 21 days in patients 1 to 12. *A-I displays expression of a different miRNA 21 days post seeding on both PL (red) and NSQ (blue) nanosurfaces. miRNA investigated displayed at the top of each graph and figure legend at the right of each graph. Middle horizontal line represents mean and vertical line represents SD. Expression is normalised to U6 snRNA and is relative to the lowest expressing patient on PL nanosurfaces on day 7. n = 12 patients. Paired t-test was performed on all data.*

3.3.6. Investigation of nanosurface features

Altogether the expression of osteogenic markers and miRNA induction indicate a possible lack of osteogenesis on NSQ nanosurface. This is in contrast to the published literature [132, 143, 175, 177, 217]. The striking lack of osteogenic response to the NSQ nanosurface following culture of SSCs was unexpected. As a consequence, the nanosurfaces were investigated further to determine if there were batch variation or alterations to the nanosurface which were different from initial surfaces received and imaged in Figure 3.4. Any significant variation or alteration in the quality of the surface of the nanosurfaces could explain the variability observed between the results obtained in these experiments and the results published in the literature, and as well as accounting for patient variation.

Surfaces were prepared for SEM imaging following protocols outlined in section 3.2.4. in the absence of cells. At the lower magnification imaging of Figure 3.13A, discrete but numerous areas of the surface in which no pitted arrangement was transferred was observed, as indicated by the white arrows. Upon higher magnification, it was revealed that non-pitted areas of the nanosurface were imperfect with (Figure 3.13B) a high degree of flecks/indentations, grooves and scratches on the nanosurface observed as indicated by the white arrows (Figure 3.13B). The nanosurfaces were noted to be of reduced quality with numerous and substantial imperfections. It should be noted here that Figure 3.13 showed representative, qualitative images, not an overall image analysis.

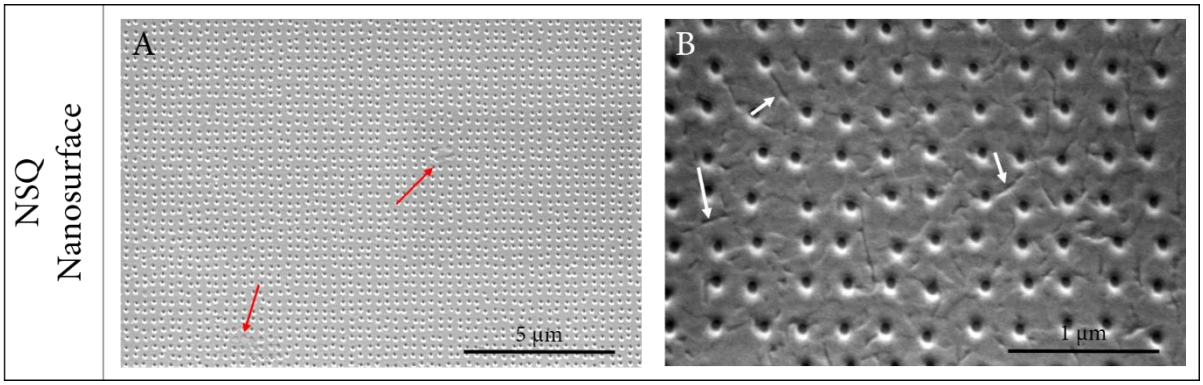

Figure 3.13. SEM imaging of nanosurface reveals imperfections on the NSQ pattern. *A- lower magnification. B – higher magnification. Red arrows on A indicate areas where features were not transferred correctly. White arrows on B indicate flecks/grooves, scratches and indentations on the surface.*

3.3.7. Expression of osteogenic markers and miRNA on clean nanosurfaces

Following the observations detailing imperfections in NSQ nanosurface, a new batch of nanosurfaces were received which were confirmed by SEM to have the same nanofeatures of nanosurfaces imaged in Figure 3.4. STRO-1+ SSC response to these new surfaces was examined in 4 patients (age range 43-56, 2 males and 2 females). In order to compare to previous experiments (12 patient samples dataset using possible imperfect surfaces) with experiments using clean surfaces, the same experimental set up was carried out to examine expression of osteogenic markers and miRNA hits from microarray, with 4 additional patient samples (names patients 13-16). Briefly, STRO-1+ SSCs were cultured on nanosurfaces for 7, 14 and 21 days and samples taken on these days for RNA extraction. RT-qPCR was performed on these surfaces to measure gene expression.

Expression of osteogenic markers for patients 13 to 16 is described in Figure 3.14. Expression of *ALP* increased to a peak on day 14 at 8.6 ± 11.1 on NSQ nanosurface and 9.9 ± 13.9 on PL nanosurface (Figure 3.14C). Expression of *ALP* decreased on day 21 on both surfaces to 6.3 ± 3.4 on NSQ and 6.7 ± 5.2 on PL nanosurface. *RUNX2* expression was found to increase on day 14, as seen previously in **Figure *3.12***. On day 14, *RUNX2* was measured at 4.6 ± 5.5 on NSQ and 4.9 ± 5.4 on PL nanosurface (Figure 3.14A). Expression remained until day 21 when *RUNX2* was measured at 4.2 ± 2.6 on NSQ and 4.5 ± 3.9 on PL. Expression of *COL1A1* was slightly higher on NSQ nanosurface (4.3 ± 5.0) compared to PL (2.6 ± 2.7) on day 21 (Figure 3.14B). *OCN* mRNA levels was lower on NSQ nanosurface at every time point (Figure 3.14D). Expression of *OPN* was also lower on NSQ nanosurface compared to PL on day 7 and day 21, however, expression difference were minimal on day 14 between NSQ and PL nanosurfaces (0.5 ± 0.4 on NSQ and 0.5 ± 0.3 on PL). Altogether, the expression of mRNA osteogenic markers did not increase on NSQ surfaces compared to PL surfaces on the “clean” nanosurfaces and patient to patient variation was apparent in these 4 patient samples.

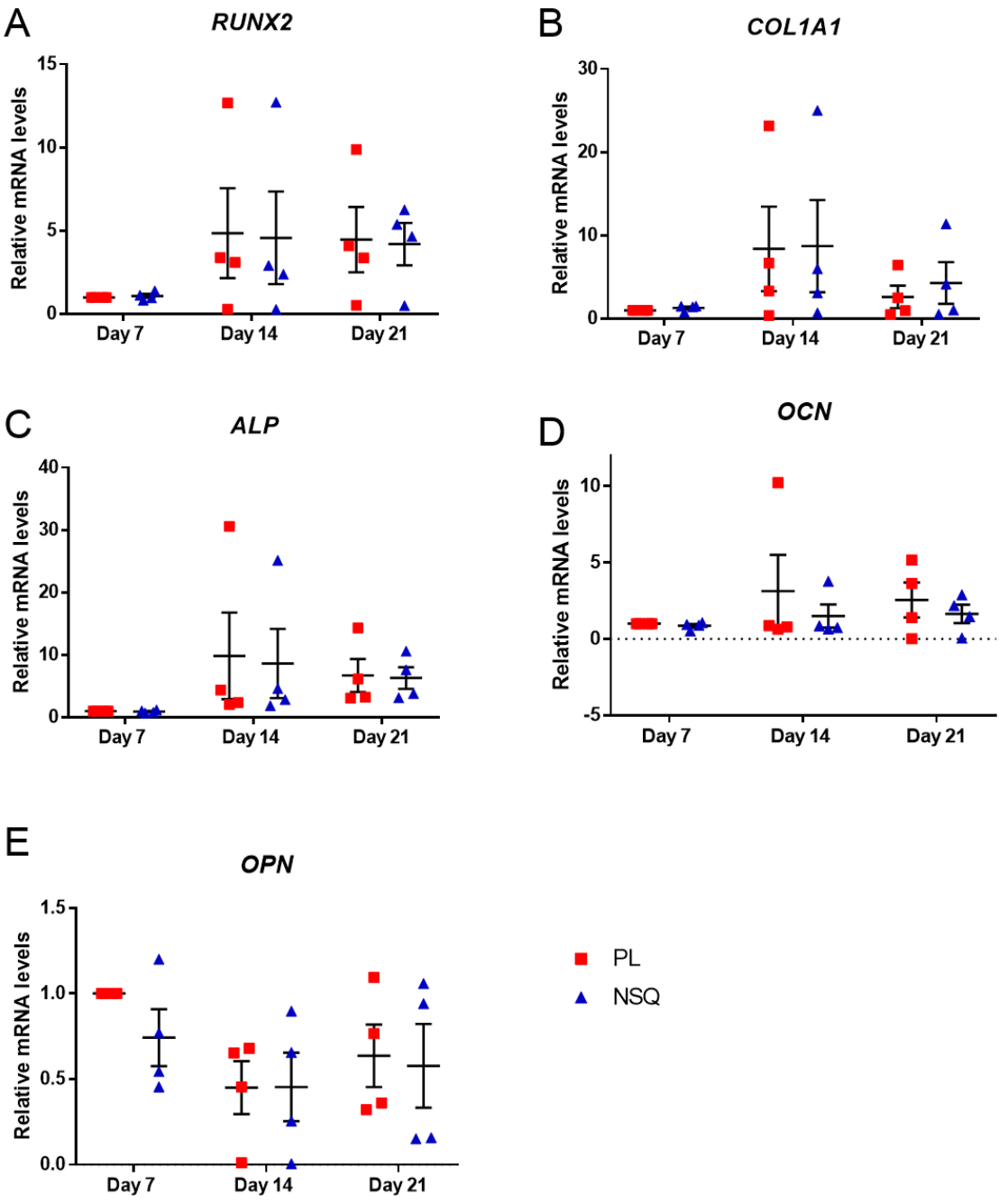

Figure 3.14. Expression of osteogenic markers on PL and NSQ nanosurface over 21 days measured in patients 13 to 16. *PL nanosurfaces in red, NSQ nanosurfaces in blue. Expression measured on day 7, 14 and 21. Middle horizontal line represents mean and vertical line represents SD. Each sample was normalised to ACTB and relative to PL on day 7. Analysed gene is displayed at the top of each graph. n = 4 patients. 2 way ANOVA was performed on all data.*

Following on from investigation of expression of osteogenic markers on patients 13-16, the same patient samples were assessed for expression of miRNA hits identified following microarray. RT-qPCR was performed on RNA samples from patients 13 -16 after 21 days culture on PL and NSQ surfaces.

The results indicated a wide distribution in miRNA expression. For example miR-29a expression in NSQ nanosurface varied from a fold-change of 0.9 in the lowest expressing patient to 4.5 fold-change in the highest expressing patient (Figure 3.15I) (mean 2.6 ± 1.5). Expression of negative regulator miR-138 was found to decrease from 2.3 ± 2.3 on PL to 1.6 ± 0.4 on NSQ nanosurface, as would be expected to happen if osteogenesis was occurring in STRO-1+ SSC on NSQ nanosurface (Figure 3.15A). However, this is one example and precludes conclusions as to whether STRO-1+ SSCs are differentiating along the osteoblast lineage on NSQ nanosurface.

Expression of negative regulatory miRNAs, miR-23a and miR-133a was found to increase on NSQ nanosurface. miR-23a increased modestly from 7.3 ± 7.3 on PL to 7.2 ± 8.0 on NSQ nanosurface (Figure 3.15C). miR-133a expression increased from 2.4 ± 1.6 on PL to 3.6 ± 2.7 on NSQ nanosurface (Figure 3.15D).

Expression of positive miRNA regulators of osteogenesis (miR-20b, miR-218, miR-296, let -7f, miR-148b and miR-29a) was mixed. MiR-20b and miR29a expression decreased on NSQ nanosurfaces (Figure 3.15B+I), when in previously published studies, expression of miR-20b and miR-29a was shown to increase during osteogenesis [267, 268]. Whereas, expression of miR-218, miR-296, let-7f and miR-148b all increased on NSQ nanosurface relative to PL. For example expression of miR-218 increased from 2.9 ± 1.9 on PL nanosurface to 3.5 ± 1.9 on NSQ nanosurface. This was also shown in published studies of osteogenic differentiation [269].

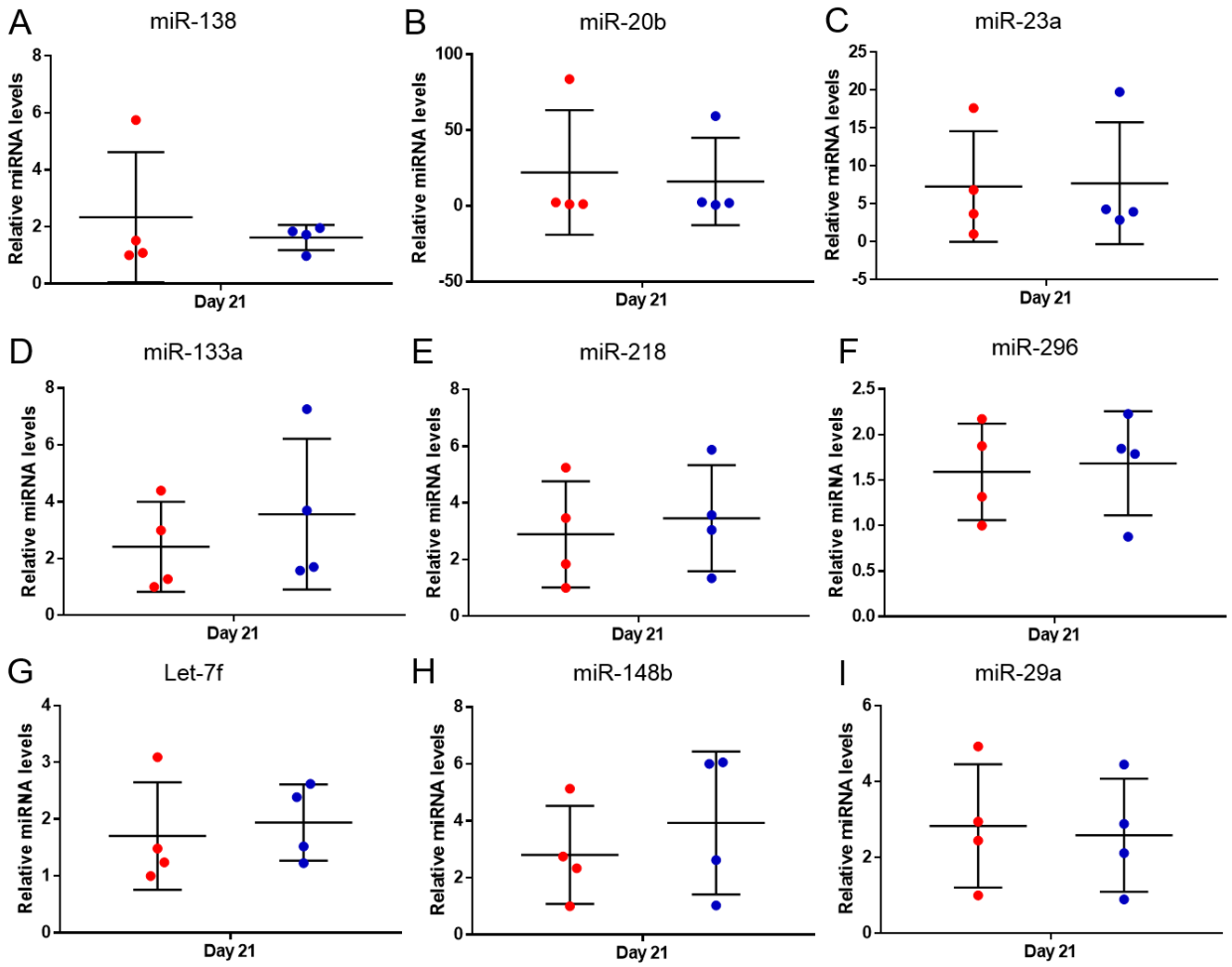

Figure 3.15. Expression of miRNA hits in STRO-1+ SSCs on PL and NSQ nanosurface 21 days in patients 13 to 16. *A-I displays expression of a different miRNA 21 days post seeding on both PL (red) and NSQ (blue) nanosurfaces. miRNA investigated displayed at the top of each graph and figure legend at the right of each graph. Middle horizontal line represents mean and vertical line represents SD. Expression is normalised to U6 snRNA and is relative to the lowest expressing patient on PL nanosurfaces on day 7. n = 4 patients. Paired t-test was performed on data.*

3.3.8. Patients responsive to NSQ nanosurface

While the previous results suggested that analysis from the 16 SSC patient donors (with perfect and imperfect surfaces), there was little induction of osteogenic differentiation following SSC culture on the surfaces, within the 16 patients, a subset of patients were observed to display a positive response to the surface. Detailed analysis of two patients, Patient 6 and 8 (M56 and F67 respectively), indicated upregulation of mRNA osteogenic markers.

Gene expression results from SSCs donated from patient 6 showed when comparing NSQ to planar surfaces, *RUNX2* was upregulated on NSQ ($p<0.05$) on day 14 (3.3 ± 0.2 on NSQ and 2.7 ± 0.1 on PL) and *ALP* was upregulated on NSQ ($p<0.0001$) on day 21 (10.9 ± 0.7 on NSQ and 8.6 ± 0.2 on PL) (Figure 3.16A). Both *OCN* and *OPN* were significantly upregulated on day 7 on NSQ compared to planar ($p<0.01$ for *OCN* expression (Figure 3.16E) and $p<0.0001$ for *OPN* expression (Figure 3.16G)). *ALP* expression was significantly downregulated on NSQ surfaces compared to planar ($p<0.0001$) on day 14 (6.5 ± 0.9 on NSQ and 8.8 ± 0.2 on PL) (Figure 3.16C). Furthermore, gene expression results from Patient 8 demonstrated an increase in expression of osteogenic markers. On day 21, there was a significant increase in expression of *OCN* and *OPN* ($p<0.0001$) on NSQ compared to PL. *OCN* expression increased from 1.6 ± 0.2 on PL to 2.4 ± 0.1 on NSQ (Figure 3.16F). *OPN* expression increased from 1.1 ± 0.1 on PL to 1.5 ± 0.1 on NSQ (Figure 3.16H). However, with the increased in expression on NSQ, there was also downregulation of osteogenic markers. From patient 8, on day 21, expression of *ALP* was downregulated on NSQ compared to planar ($p<0.05$) (3.2 ± 0.1 on NSQ and 3.7 ± 0.3 on PL) (Figure 3.16B). A decrease in expression of *OPN* in patient 8 was found on day 7 on NSQ surfaces compared to planar ($p<0.0001$) (0.5 ± 0.0 on NSQ to 1.0 ± 0.0 on PL surfaces) (Figure 3.16H). While both patients showed positive responses to the NSQ nanosurface in a number of genes, in neither was an increase in all five osteogenic markers found. Interestingly, there were several time points when expression was higher on PL surface compared to NSQ.

When analysing miRNA expression levels to identify the two highest positive responding patients, two different patients were discovered, patient 9 and 12. These patients showed an increase in positive osteogenic miRNA miR-20b, miR-218, miR-29a and miR-148b on NSQ surface (Figure 3.17). Expression increase measured for miRNAs on NSQ surfaces was different between patient 9 and patient 12. Thus, expression of miR-218 in patient 9 increased from 1.0 ± 0.2 on PL to 1.41. ± 0.1 on NSQ (Figure 3.17C). In patient 12, expression was observed to increase from 1.0 ± 0.1 on PL to 2.680 ± 0.13 (Figure 3.17D).

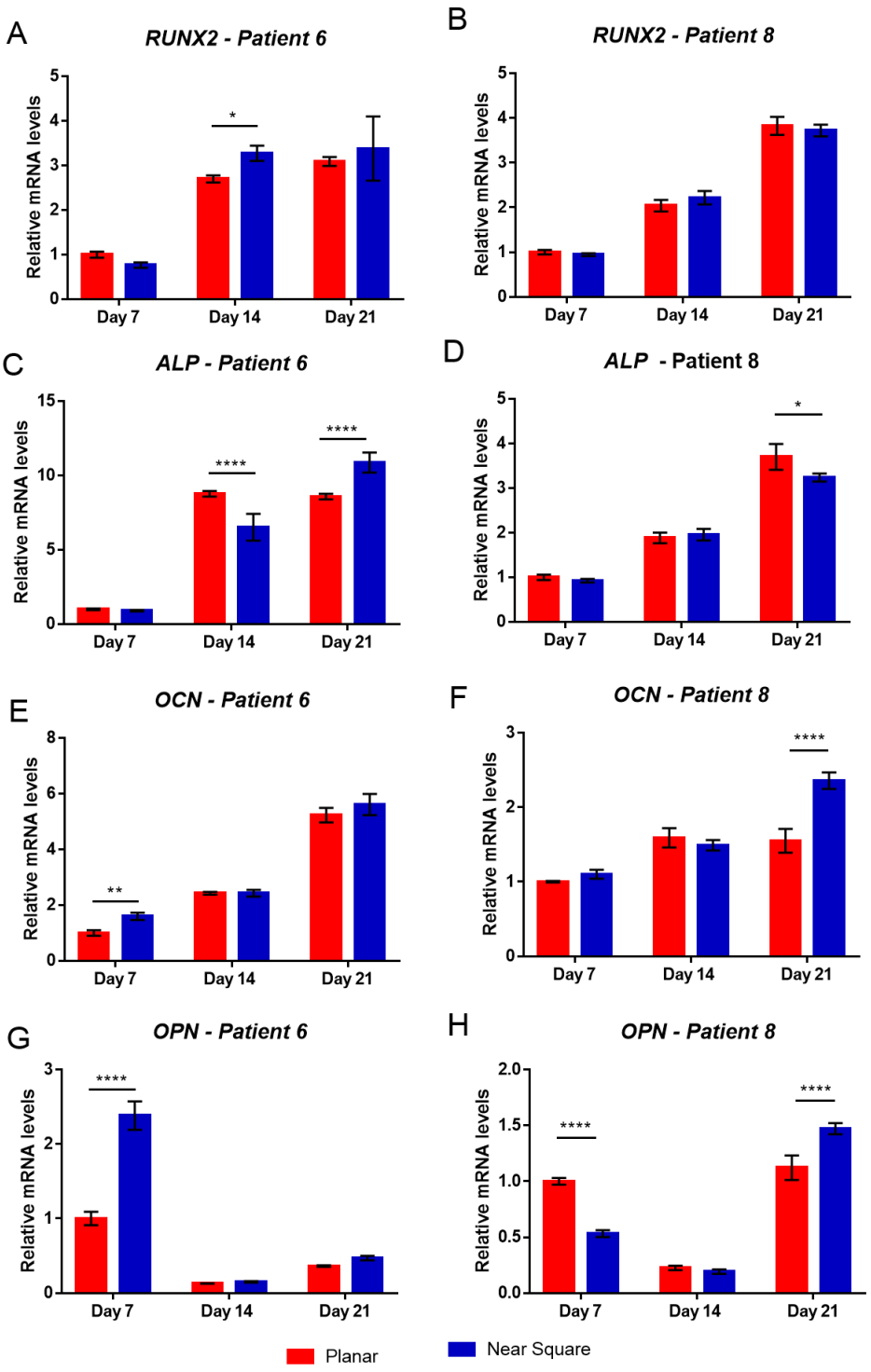

Figure 3.16. Expression of osteogenic markers of positive responding patients 6 and 8. *PL nanosurfaces in red, NSQ nanosurfaces in blue. Expression measured on day 7, 14 and 21. Bar shows mean ± SD. Each sample was normalised to ACTB and relative to PL on day 7. Analysed gene is displayed at the top of each graph. n = 4 experimental replicates. * represents p<0.05, ** represents p<0.01, **** represents p<0.0001.*

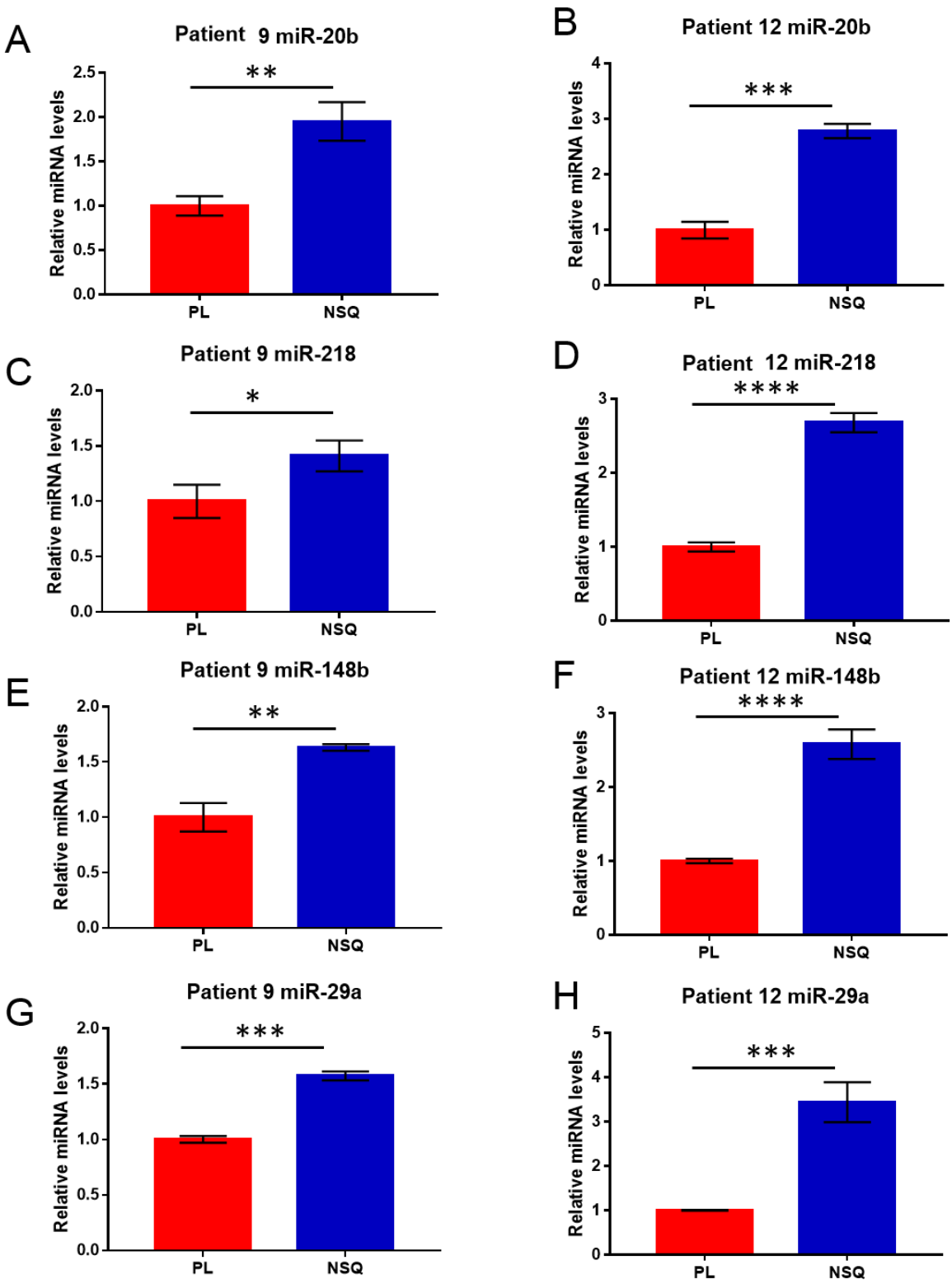

Figure 3.17. Expression of miRNA of positive responding patients 9 and 12. *PL nanosurfaces in red, NSQ nanosurfaces in blue. Expression measured on day 21. Bar shows mean ± SD. Each sample was normalised to ACTB and relative to PL on day 7. Analysed gene is displayed at the top of each graph. n = 3 experimental replicated. * represents p<0.05, ** represents p<0.01, *** represents p<0.001, ***" represents p<0.0001.*

3.4. Discussion

The results obtained showed a lack of osteogenic differentiation of SSCs following culture on NSQ nanosurface and no consensus on modulation of miRNA known to be involved in osteogenesis upon culture on discrete nanosurfaces. This was in contrast to previous literature [132, 143, 175, 177, 217, 270]. Examination of the surfaces using SEM, after studies to try and ascertain if any sample preparation issues, revealed that the nanosurfaces contained a number of surface flaws, significantly affecting the NSQ arrangement of nanopits. Following from this, clean nanosurfaces were obtained and when SSCs were cultured on these surfaces, there remained an inconsistent modulation of osteogenic differentiation on the NSQ nanosurface compared to PL with two patients, from a sample size total of 16, noted to display a positive response to the NSQ nanosurface.

There are a number of differences between the results described in this chapter and results published in papers, which may account for the apparent discrepancy, ranging from surfaces, media to cell culture. Experiments by Yang *et al*, 2014, displayed an increase in expression of osteogenic markers *RUNX2, ALP, OCN* and *OPN* relative to PL for 3 patient samples [217]. These published experiments were carried out using cultured MSCs derived from human bone marrow obtained from patients undergoing routine arthroplasty, although the authors did not specify which joint the tissue was harvested from. These cells could potentially represent a different sub-population of STRO-1+ SSCs to those used for experiments in this chapter, leading to variation in response to nanotopography. Furthermore, it is important to note the disease state of patients donating SSCs in the authors experiments remains unknown and variations in health of bone tissue could affect SSC populations, and therefore, patient response to the nanosurface. In the studies published by Yang *et* al, 3 patient samples were used for gene expression experiments, it is difficult to determine the response of MSCs over a wide population of patients or if the result obtained were solely a consequence of the chance selection of responding patients.

Other variables between experiments published by Yang *et al* and those conducted in this chapter include media content. α-MEM supplemented with 10% FBS and 1% P/S was found previously in Bone and Joint Research Group to be optimal for the culturing of STRO-1+ SSCs [271] and was chosen as the basal media in these experiments. This media type was also used in early studies with NSQ nanosurface by Dalby *et al* [132]. Published work by Yang *et al*, 2014 used DMEM (Dulbecco's modified eagles medium) plus 10% FBS, 1% sodium pyruvate, 1% non-essential amino acids and 2% penicillin. The media, α-MEM, used in the experiments discussed in this chapter contains sodium pyruvate and non-essential amino

acids. It is likely these components were added to DMEM in the work published by Yang *et al,* however is not explicitly stated and it is unknown exactly which type of DMEM is used. In another study by Tsimbouri *et al*, STRO-1+ SSCs were cultured in α-MEM supplemented with 10% FBS, 1% L-glutamine and antibiotics [177]. However, in the original studies using the NSQ nanosurface, authored by Dalby *et al,* the same media components were used as in the experiments discussed in this chapter [132]. The only difference between the media used by Dalby *et al* and in this chapter is the source of αMEM and, perhaps critically, FBS. Given that STRO-1+ SSCs have been shown in published data to be able to respond with a selection of different media types, it is likely that the components of cell media are not the predominant reason why the experiments described in this chapter did not demonstrate consistent induction of osteogenic differentiation.

Further to this, there are differences between cell densities in experiments discussed in this chapter and in published data. A density of 2000 cells per well or 200 cells/cm^2 was chosen for experiments as this was sufficient to allow cells to take cues for differentiation from the surface. Tsimbouri *et al* published a concentration of 1 x10^4 cells/mL and would have seeded using a minimum of 2 mL, giving a concentration of 20,000 cells per well [177]. In the original experiments by Dalby *et al*, a cell concentration of 10,000 cells/cm^2 was used. During experiments conducted in this chapter (Figure 3.5), cells proliferated at a faster rate than suggested in published literature and reached full confluence between 7 and 14 days, upon seeding at 200 cells/cm^2. It is likely that using seeding densities described in the discussed published papers, under the current protocols, cells would reach confluency within a few days and the high cell numbers could disrupt the cells and interfere with topographical interactions.

The single most significant observation resulting in the lack of response of SSCs on different nanotopographies is almost certainly a consequence of the poor quality nanosurfaces, received for these studies, during EBL biofabrication. As has been described in the literature, SSCs are exquisitely sensitive to nanoscale modifications. For example Dalby *et al* discovered that changing from a square arrangement of nanopits to hexagonal, had a dramatic effect of cell surface adhesion [132]. A perfectly square arrangement of nanopits has been reported to maintain stem cell phenotype [175]. A minor alteration to this arrangement, by offsetting the squares by 50 nm in random directions to produce a disordered NSQ arrangement, has been shown to push SSCs to differentiate into osteoblasts [132, 217, 272]. If these subtle changes to nanotopography could modulate cell phenotype, it is likely that the numerous imperfections to the NSQ surface could affect SSC differentiation and the observed lack of response to the surface.

The functions of osteogenic markers *RUNX2, ALP, COL1A1, OCN* and *OPN* vary within the cells and are discussed in full in Appendix II. In short, RUNX2 a master regulator of osteogenesis and belongs to a family of *RUNX* genes, all of which contain DNA binding runt domain (homologous to drosophila runt domain) [273]. RUNX2 forms heterodimers with core binding factor β (CBF-β) and specifically recognises a consensus sequence on target genes [274, 275]. RUNX2 is negatively self-regulated through the RUNX2 protein binding to *RUNX2* promoter regions, inhibiting expression [276]. As a master regulator, RUNX2 activates expression of *ALP*, *OCN*, and *OPN* [118, 277, 278]. RUNX2 has been shown to direct *ALP* expression through binding to ALP intron 1 [277]. Nuclear matrix targeting sequence was found to be essential for RUNX2 mediated induction of *ALP* [277]. The enzyme ALP works in bone by hydrolysing monophosphate esters in order to provide phosphates for HA. Thus, ALP has an essential role in bone mineralisation and is a useful marker for osteogenesis [37]. OPN and OCN have roles in controlling mineralisation. A decrease in osteoclast surface area in *ocn*-null mice suggests OCN has a role in bone resorption though osteoclast regulation [279]. In addition, OCN could have role in feedback between bone and metabolic demands of the body [13]. In contrast, OPN as well as a bone matricellular protein, has been found in a wide variety of biological tissues including, skeletal muscle, brain and kidney. OPN is aspartic acid rich, providing a high negative charge allowing OPN to bind to apatite crystals and inhibit bone mineralisation. OPN-null mice displayed normal bone development and morphology formation [280]. However, mineral content was higher in bones of null mice, confirming OPNs role of inhibition of bone mineralisation [281]. Osteoclast formation was higher in $opn^{-/-}$ bone marrow suggesting its role is with osteoclast differentiation [280]. OPN expression increased under mechanical stress, implying it could have a role in sensing mechanical stress and feedback to increase bone formation [282]. More recently, OPN has been found to have a role in inflammation [283, 284] and, high serum levels have been observed in chronic inflammatory diseases including Crohn's disease and cancer, and appears to regulate innate immune cells and T cells [283]. Collagen type I is essential for bone structure and health and therefore would be produced by osteoblasts which are actively laying down new bone tissue.

RUNX2, COL1A1, ALP, OCN and *OPN* were chosen here as they are established markers of osteogenic differentiation, activated over 21 days [285, 286]. When SSCs were first cultured on NSQ nanosurface and mRNA levels of these osteogenic markers investigated for only five patients, there was an up regulation of osteogenic markers compared to PL surface. This however was not significant, and at this early stage it was apparent there was a wide distribution in patient-to-patient response. When the data set was increased to 12 patients, with a view to reduce patient variation through increased patient numbers, there remained

patient-to-patient variation resulting in lack of osteogenic induction. When patients 13 to 16 were cultured on “good” nanosurfaces, expression of osteogenic markers was low on NSQ compared to planar and expression of miRNAs was mixed. Therefore, in addition to batch-to-batch variations with surface features, *patient-to-patient variation* would appear an important variable to consider in the differences observed between NSQ and PL nanosurface. Perhaps an interesting way to control this, could be to maintain consistency in the age and gender of STRO-1+ SSC donors used. It should be noted that in Figure 3.17, the variation between samples is smaller in comparison to other RT-qPCR based experiments (for example in Figure 3.11, Figure 3.14 and Figure 3.15). This is because in Figure 3.17, only one patient was studied and therefore the data represents the RT-qPCR analysis repeated three times. In Figure 3.17, the variation is small because the variation is representative of assay replicates and not biological replicates.

miRNAs regulate gene expression at the mRNA level through imperfect binding to 3`UTR of mRNA [287]. Significant up or down regulation of miRNA observed on NSQ could suggest a miRNA potentially involved in osteogenic differentiation. After performing a miRNA microarray with two samples investigating differences in miRNA expression between PL and NSQ in a genome wide scale, a discrete number of genes were found to be dysregulated. However, in general, the cells, in the current study, behaved similarly on PL and NSQ nanosurface, perhaps reflecting the lack in change of osteogenic marker expression between PL and NSQ. RT-qPCR to validate microarray gene expression results showed large differences in expression between PL and NSQ nanosurfaces, indicating potential issues with accuracy of expression measured using the microarray platform. There were individual indications of miRNA regulating osteogenesis in STRO-1+ SSCs on NSQ nanosurface (miR-218 and miR-148b in Figure 3.15). There was no consensus in miRNA response to nanotopography across the 9 miRNAs studied here, adding further evidence of a lack of osteogenic response of STRO-1+ SSCs to NSQ nanosurface.

miRNA microarray is a useful technique for analysing genome wide miRNA expression in a rapid and efficient manner. Validation of microarray hits is necessary in order to determine and confirm any obtained result. Zhang *et al* performed RT-qPCR on microarray hits for a selection of miRNAs [258]. The authors reported microarray over estimating the expression of miRNA compared to expression measured by RT-qPCR [258]. A similar effect was noted in microarray and subsequent RT-qPCR validation experiments detailed in this chapter. It is possible that miRNAs which do have a role in SSC response to the NSQ surface were not identified in the microarray and therefore not studied.

miR-218 has been identified in the literature as playing a role in osteogenesis through involvement in WNT signalling [208]. miR-218 is upregulated during osteogenesis and targets *DKK2* and *SFRP2*, negative regulators of WNT signalling. miR-218 therefore decreases the mRNA levels of these genes and up regulates WNT signalling, triggering osteogenesis [208]. miR-218 expression could be considered a positive control in order to study the osteogenic differentiation on nanosurfaces. miR-218 was found to be upregulated on patients 13 to 16. miR-29a has been reported to have similar targets to miR-218, targeting negative regulators of Wnt signalling, DKK2 and SFRP2 [266], and expression of miR-29a was found to down regulated on the NSQ nanosurface compared to PL in all patients, when it would be up regulated during osteogenesis. miR-138 was also reported to be osteogenic in the literature [220]. Previous reports suggest miR-138 targets *FAK*, a regulator of ERK1. Expression of miR-138 decreased in NSQ nanosurface compared to PL only in patients 13 to 16, indicating a lack of osteogenesis on nanosurfaces. There are a number of miRNAs involved in osteogenesis and it could be possible that an unidentified miRNA is controlling alterations in cell behaviour on the NSQ nanosurface.

The remaining targets from microarray have been found to have roles in angiogenesis, cytoskeleton organisation and DNA methylation [259, 261, 267, 288-290]. Specifically, miR-20b was reported by Zhang *et al* to be upregulated during osteogenic differentiation, to target the pluripotency marker *STAT3*, reducing *its* expression [258]. A selection of miRNA hits from the microarray were discovered to target *RUNX2*, including miR23a, miR-133a, and miR-218 [216, 259, 260]. miR-296 was shown to contribute to angiogenesis [261]. Let-7f targets *AXIN2*, which has been reported to play a role in the inhibition of β-catenin. By inhibiting *AXIN2*, the microRNA let-7f has a positive role in Wnt signalling and therefore osteogenesis [262]. Following a screen for miRNAs involved in osteogenesis of MSCs, miR-148b was found to up regulate osteogenesis [264]. miR-148b in combination with BMP-2 was found increase calvarial ossification in nude mice [265]. Due to the lack of significant differences between miRNA expression on PL and NSQ nanosurfaces, it is unclear if these miRNA have a role to play in variations in cell behaviour between the two surfaces. It is known that multiple miRNAs can target the same pathways and modest differences in expression of a miRNA can result in large changes in target mRNA levels [200]. Small changes in miRNA seen between NSQ and PL surfaces could result in enhanced changes in levels of target mRNA, and affecting the behaviour of SSCs.

Yang *et al* published, in a paper focussing on MSC response to NSQ nanosurface, a selection of experiments studying miRNAs which the authors observed from a targetscan database to target *RUNX2* and *osterix* (*OSX*) [217]. These included miR-23b, miR-96 and miR-143. In these experiments, after 5 days of culture, miR-23b expression was found to decrease and

RUNX2 expression was found to increase [217]. The experiments discussed in this chapter studied only one time point (day 21), which could explain the lack of observed differences in expression between NSQ and PL nanosurfaces. Interestingly, miR-96 and miR-143 were reported to be up-regulated in response to the NSQ surface, with this correlating with an increase in *OSX* expression. In this example, miRNA targeting had a positive role on target expression instead of the commonly seen negative regulation. The work published in this paper shows miRNAs are involved in the response of MSC to NSQ nanosurface. It is likely that miRNAs are also involved in regulation of SSCs response to nanosurface, however it was not found during the experiments in this chapter and due to lack of osteogenic response, it is unlikely these miRNAs will be involved in osteogenesis.

The mechanism by which nanotopography influence stem cell behaviour and proliferation still remains to be fully elucidated [291]. It is known that cytoskeleton and cell morphology changes in response to nanotopography are important and this has been speculated to be a driving force behind changes in cell fate and function [253]. The lack of changes in the morphology of STRO-1+ SSCs when cultured on NSQ nanotopography, as imaged in light microscope, is part of the overall picture, in this chapter, of cells displaying inconsistent and limited responses to the NSQ nanotopography. This could be studied further through immunofluorescence imaging of the cytoskeleton including actin filaments, and vinculin (a key protein in focal adhesion complex), and comparing the cytoskeleton between PL and NSQ surfaces.

In conclusion, two main factors are likely to have impacted on the limited SSC response to the examined nanotopographies – surface imperfections in nanosurface samples received from Glasgow and patient to patient variation in SSC quality. Initial gene expression studies suggested small changes in osteogenic marker expression on NSQ nanosurface. However, when the data set was increased to 12 patients, it became apparent that cell response was patient specific (patient 6 and 8). When 4 patients were cultured on newly fabricated, “good” NSQ nanosurface, there was a lack of osteogenic response. STRO-1+ SSCs are a heterogeneous population with patient-to-patient variation. Due to these over whelming issues, the decision was taken to not pursue STRO-1+ SSC response to NSQ nanosurface further. In summary, imperfections in the nanosurfaces precluded any conclusions to be drawn on the potential of NSQ or planar topographies for the modulation of SSC miRNA as a target to investigate SSC phenotype and any subsequent mechanism of action for cell phenotype/function alteration.

Chapter 4: SSC response to bioimprinted surfaces

Chapter 4 - SSC response to bioimprinted surfaces

4.1 Introduction

SSCs are known to respond to a wide variety of topographies including grooves, pillars and nanopits [132, 172, 292-294]. Topographies can alter stem cell behaviour including cell adhesion and cell shape, and topographies have been shown to modulate cell gene expression resulted in altered phenotype [178, 181]. A natural progression from the evaluation of NSQ nanosurface topographies presented in chapter 3 was to investigate alternative topographies to examine alternate surface topography variation on the modulation, if any, of STRO-1+ SSC phenotype and function. The development of many biomaterials depends on biocompatibility to generate specific and accurate biomaterials. Through the use of natural topographies, we can generate biomaterials which are more akin to what cells would experience *in vivo* and brings additional advantages of biocompatibility and possibly increased cell response [295]. Thus, topographies found in nature could provide additional advantages over synthetic topographies. One such alternative topography, to date unexamined using SSCs, are bioimprinted cell surfaces.

Cell-imprinting, or bioimprinting, involves generating topographical surfaces with imprints of the cell morphology created from a mould taken of cells grown in culture. Bioimprinting was previously developed as a soft lithography technique for examining surface features [296]. Certain cellular features such as cell membranes are extremely small and difficult to image using standard light microscopy techniques. In contrast, Atomic Force Microscopy (AFM) offers high resolution and thus AFM is capable of imaging delicate cellular features. However, the use of the scanning tip can result in structural damage to cells, making live imaging problematic. In order to visualise small features using AFM, without damaging cells, bioimprinting was used to generate a relief profile of the cells which could be imaged with AFM, leaving the cells of interest undamaged. This technique of soft lithography was used to visualise cell pores and microbeads attached to the surface of cells, with beads as small as 50 nm observed on the bioimprints [297].

A bioimprinting method was also used by DePorter *et al*, 2012 who were inspired by cell-imprinted bacterial detection systems [298]. The authors detail that cell-imprinted features were essential to cell adhesion on polyacrylamide hydrogels. The authors used established cell lines including HEK-293T, HeLa and MRC-9 cells to generate cell-imprinted hydrogels. The HEK-293T cells displayed a more condensed morphology on cell-imprinted polyacrylamide gels compared to TCP polystyrene. The method used to generate

polyacrylamide hydrogels in the work from DePorter and colleagues, involved the application of a 30% acrylamide gel poured on top of cells and incubated for 20 minutes at room temperature and subsequently washed, initially in 1 M sodium hydroxide and subsequently in 0.6 M sodium dodecyl sulphate, each for 1 hour. This approach, provided a simple, rapid method, with validation of resolution using SEM confirming details of less than 5 μm cell topography transferred to cell-imprints [7].

Since the advent of the powerful role of topography in controlling cell behaviour, it has been postulated that these bioimprinted topographies could be used as topographical surface cues to modify stem cell behaviour. Polyacrylamide hydrogels are by nature soft, while osteogenesis of SSCs has been reported to be favour stiff substrates [161]. Thus incorporation of a harder plastic cell-imprinted surfaces in contrast to a soft cell-imprint hydrogels, could provide SSCs with an environment more appropriate for their culture and for enhancement of potential osteogenesis. Murray *et al* developed a technique which eventually resulted in a polystyrene bioimprinted surface [299]. This technique involved replication first onto methacrylate and subsequently onto polymethylsiloxane (PDMS) and finally onto polystyrene (PS). This study reported replication resolution down to 430 nm. In further studies, Murray *et al* reported Ishikawa endometrial cancer cells preferentially adhered to areas of cell imprint and could sense the footprint of the original cell [300].

Following on from these studies, Mutreja *et al* at the University of Otago [301] removed the methacrylate step from the bioimprinting protocol designed by Murray and colleagues [300]. The authors used an initial mould with PDMS, with the added advantage that PDMS could i) transfer resolution down to 20 nm [300] and, ii) could be heat cured at 37°C making it suitable for cell replication without damage to cells [301]. In the study, Mutreja *et al* transferred PDMS imprint to a second PDMS imprint to generate features that had either a positive relief profile or negative relief profile [301]. These PDMS imprints were replicated onto a selection of polymers including PS. During the course of these studies, human nasal chondrocytes were bioimprinted in both positive and negative relief into PS [301]. The authors demonstrated that it was possible to visualise the bioimprint using an AFM, with resolution down to 3 nm resolution observed [301]. The authors cultured human nasal chondrocytes on these PS bioimprints and observed reduced cell area (limited cell spreading) on the bioimprinted surfaces compared to flat PS surfaces [301]. Other key findings from the study included the observation the cells were more compact on negative imprints compared to positive imprints, possibly as a consequence of the cells once located in concave depressions experiencing restricted cell spreading [301]. From these observations, it could be postulated that positive imprints would be more advantageous for osteogenic differentiation as this could allow for more cell spreading, a key factor in osteogenesis *in vitro* [302].

The majority of studies involving bioimprinted surfaces, to date, have focussed predominantly on design and characterisation of the bioimprinted surfaces. There has been a small number of studies published examining the effect of bioimprinted topographical surfaces on responses at the molecular level cell behaviour. Furthermore, while some studies have begun to characterise cell response using cell lines, there remains a paucity of information concerning primary cells, in particular SSCs, following their culture on bioimprinted surfaces, with no studies to date studying the effect of SSC bioimprinted surface on SSCs cultured on those surfaces.

This chapter used two different bioimprinted surfaces: those imprinted with the shape of SSCs differentiated to early osteoblasts (where differentiation of SSCs was stopped at 7 days and bioimprint taken), and a mature, or late osteoblast, (where differentiation of SSCs was stopped at 21 days).It was thought that the two different relief topographies, early and late osteoblast, would have a different effect on cell behaviour, with the early stage osteogenic-induced differentiated SSC promoting early stage osteogenic differentiation of SSCs cultured on that surface, and the late stage osteogenic-induced differentiated SSC promoting late stage osteogenic differentiation of SSCs cultured on that surface. A positive relief profile was chosen as previous experiments by Mutreja et al [302] indicated that cell proliferation was greater on this relief profile compared to a negative relief profile, with postulation that the negative relief profile limited cell spreading.

4.1.1. Aims

Hypothesis:

Topographical surfaces bioimprinted with differentiated SSCs (either differentiated to an early or late stage of osteogenic differentiation) can alter the behaviour of SSCs cultured on these bioimprinted surfaces.

The aim of this chapter is to explore the response of human SSCs on select bioimprinted surfaces. Specifically:

I. SSC response to two different bioimprinted surfaces, an immature (early) osteoblast phenotype and a mature (late) osteoblast phenotype bioimprinted substrates.
II. SSC morphology on bioimprinted surfaces in comparison to flat surfaces derived from empty tissue culture plates.
III. Proliferation and metabolic activity of human SSCs following culture on bioimprinted surfaces over 21 days.
IV. Molecular analysis and protein analysis of human SSCs cultured on both early and late osteoblast bioimprint.

4.2. Methods

4.2.1. Bioimprint generation

Two different conditions were selected for generation of bioimprints: cultures derived using day 7 SSCs to generate an early osteoblast phenotype and day 21 SSCs cultures, to provide a late osteoblast phenotype (Figure 4.1). To generate the bioimprints, STRO-1+ SSCs were seeded at a density of 2000 cells/well in 6 well-plates in osteogenic media (section 2.1.1). After 7 and 21 days of culture, cells were washed twice with PBS and fixed in 4% PFA at room temperature for 30 minutes. Four 6 well plates were used, with 2 plates at 7 days and two plates at 21 plates. Cells were then washed twice with PBS and 6 times with H_2O in order to remove traces of salt crystals which could affect the bioimprinting process. At this point, cells were air dried to prepare for shipping. Although this was essential of bioimprinting process, it could have introduced morpholoBioimprinting was performed at CReATE research group, University of Otago, New Zealand. Control blank non-bioimprinted surfaces were additionally generated following the same procedure.

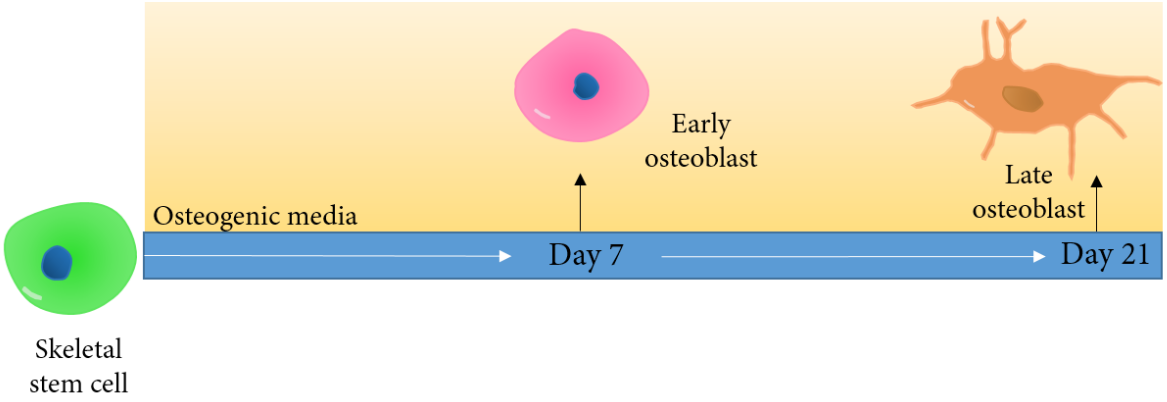

Figure 4.1. SSC samples taken for bioimprinting. *STRO-1+ SSCs were differentiated using osteogenic media and fixed at day 7 and day 21.*

The bioimprinting process aimed to replicate the positive relief profile of STRO-1+ SSCs on PS surfaces and is outlined in Figure 4.2. This followed a three step process: (1) a PDMS mould was taken of cells, then (2) PS mould was generated of the PDMS mould and finally (3) PS bioimprints were treated for cell culture.

(1) In order to ensure there was no condensation on the cells, prior to imprinting, the cells were left to air dry at room temperature for 1 hour and the PDMS prepared. PDMS was

made using SLYGARD® 184 silicone elastomer kit (Dow Corning New Zealand, Auckland, New Zealand). From the kit, one part “base” was mixed in a clean plastic container with one part “curing agent” (w/w). This process introduced bubbles into the mixture, which were subsequently removed by desiccation under vacuum for 30 minutes. This mixture was added to completely dry cells until the height of the mixture in the well reached approximately 5 mm. At this point, PDMS moulds for blank bioimprints were generated. In order to do this, PDMS was poured into the wells of a clean 6-well plate. As the pouring of the mixture into the well created additional bubbles, plates were placed under vacuum again for 30 minutes in order to completely remove any bubbles. The mixture was soft cured for 16-20 hours at 37°C, whereupon the PDMS moulds were removed from the plates using scalpel and forceps. In order for PDMS, and PS bioimprints subsequently made from them, to fit into a 6-well plate, PDMS moulds were stamped with a custom designed circular stamp which has a diameter of 30 mm, approximately 4 mm smaller than a well of 6-well plate. After stamping, PDMS moulds were hot cured at 80°C for 2 hours.

(2) PS was dissolved in a solution of gamma-butyrolactone (GBL) at 25% PS /75% GBL (w/w). Heating at 90°C and continuous stirring was required for PS to dissolve in GBL. PDMS moulds were cleaned with ethanol and placed imprint side up on a large glass petri dish. PS was heated slightly to reduce viscosity in order for it to be easier to work with. PS was gently poured onto the PDMS mould and spread with a pipette tip until the entire PDMS mould was covered in PS. The glass petri dish was placed on a hot plate and heated at 95°C for 4 hours, followed by 150°C for 12 hours. This allowed the PS to penetrate all the bioimprinted features and to ensure replication into PDMS mould and, secondly, for complete evaporation of GBL. The resulted PS bioimprint was thus pure PS.

(3) PS is hydrophobic and therefore not an ideal substrate for cell culture. To prepare PS bioimprints for cell culture, the PS was treated with sulphuric acid (H_2SO_4) (Sigma, NZ) at 99.99% purity (18.4 M). To do this, bioimprints were placed imprint-down in sulphuric acid using forceps for 10 minutes. After this, bioimprints were washed twice in water for 10 minutes and dried, first with paper towel and then overnight at 37°C. Surfaces were stored at room temperature. Before cell seeding, surfaces were washed twice in PBS and sterilised under UV light for 30 minutes.

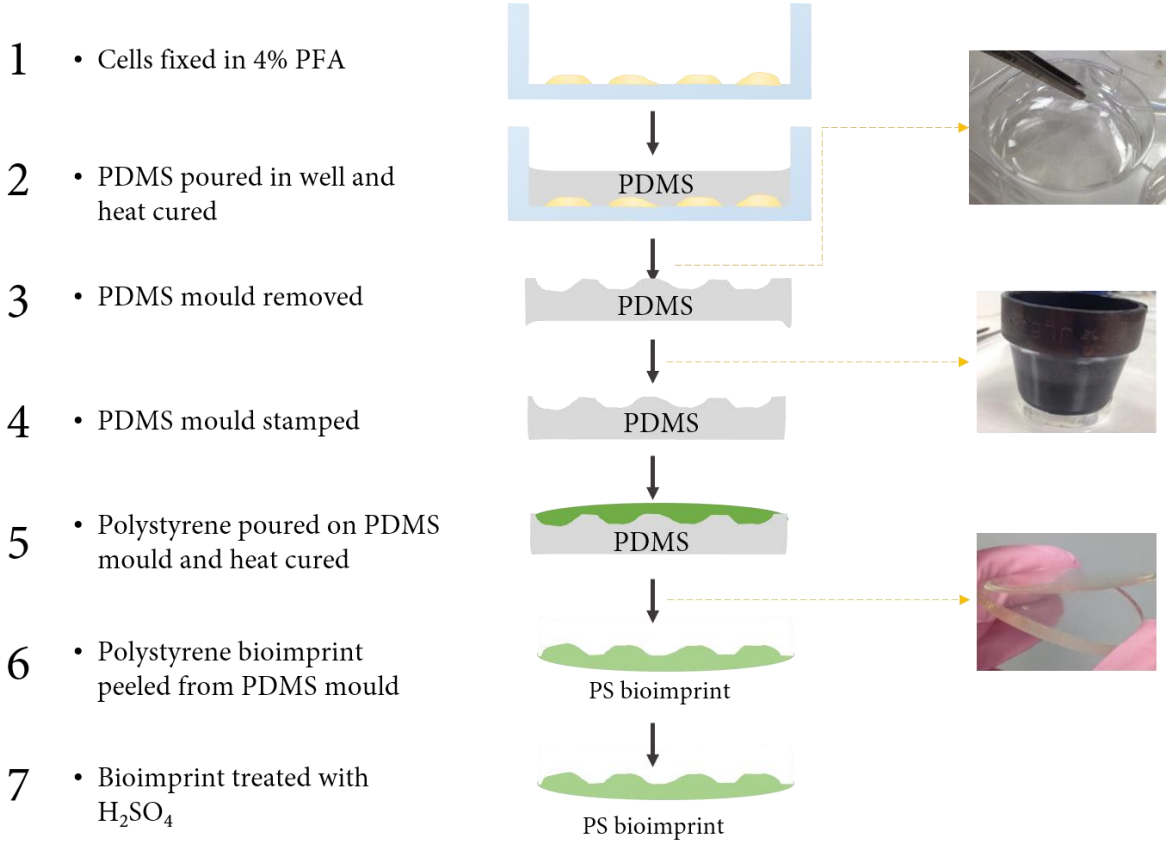

Figure 4.2. Bioimprint generation schematic *detailed in section 5.2.1 Bioimprint generation. 1. Cells were fixed in 4% paraformaldehyde (PFA) for 30 minutes and washed twice with PBS and 6 times with water and left to air dry before bioimprint. 2. PDMS was prepared at 10 parts base, one part curing agent, mixed together and poured onto the cells. PDMS was heat cured and 3. removed from well. 4. PDMS mould was then stamped to ensure PS bioimprints were slightly smaller than 6-well plate. 5. PS solution in 75% GBL was poured onto PDMS imprint side and heat cured. 6. PDMS mould was separated from PS bioimprint and 7. bioimprint chemically treated with sulphuric acid for cell culture. Control blank non-bioimprinted surfaces were also generated using this method. This process instead began in step 2 with PDMS mould created from an empty, clean well of 6-well plate. The process was then followed through as described in steps 2 to 7.*

4.2.2. Water contact angle

Water contact angle measurements were performed in static mode using the sessile drop method. A 2 µL drop of de-ionized water was pipetted on the sample surface which was mounted on an illuminated stage. The image of the droplet was captured (Edmond Scientific camera, NZ) and processed using drop-analysis software in Image J (1.47v, NIH, USA). Measurements were performed on 5 sports per surface and two surfaces used for each measurements.

4.2.3. Atomic force microscopy (AFM)

To examine the replication of the cell detail from PDMS to PS, AFM was performed using a Digital Instruments Dimensions 3100 Scanning Probe Microscope (Veeco sigital instruments by Bruker). Samples were scanned in tapping mode using ACT-SS super sharp AFM probes with a force constant of 40 N m^{-1} and tip radius of < 4 nm. Images were processed using Nanoscope v6.12rl software.

4.2.4. Cell imaging using CellTracker™ Green

20 µL of CellTracker Green (CTG) (Thermo Fisher, UK) was thawed and contents dissolved in 10 µL sterile DMSO. This was pipetted into a falcon tube containing 15 mL α-MEM. Media was removed from wells and washed once with PBS and CTG/α-MEM mix added to the well. Cells were then incubated in the dark at 37°C for 1 hour. After this time, cells were washed with PBS and the media replaced with basal media, containing 10% FBS. Cells were imaged at the required time point. According to manufacturers, this dye stays within cells for 72 hours. In these experiments, where imaging took place over several days, cells were imaged within 3 days of staining. If more than 3 days had passed, cells were stained again.

4.3. Results

4.3.1. Bioimprint characterisation

Using the protocol described in section 4.2.1. positive relief profile of bioimprinted PS surfaces were generated using early stage osteogenic differentiated STRO-1+ SSCs (cultured for 7 days - termed early osteoblast) and late stage osteogenic differentiated STRO-1+ SSCs (cultured for 21 days - termed late osteoblast).

Light microscope images of the bioimprint alone, showed the shape and morphology of the bioimprinted features (Figure 4.3). Bioimprinted cells displayed similar features to the morphology of osteogenic differentiated STRO-1+ SSCs imaged in Appendix II. Spindle shaped processes from fibroblast shaped cells were observed. Cells imprinted in early osteoblast bioimprint were noted to be less elongated and to display a more spread morphology relative to the late osteoblast cultures. Early osteoblast bioimprint features were observed to be sparse and features spread further apart than late osteoblast cultures with areas of surface which did not contain bioimprinted features (Figure 4.3A+B). In contrast, bioimprinted features in late osteoblast bioimprints were extensive, covering predominantly the whole surface (Figure 4.3C+D). Small scratches could be seen on the surface of the blank bioimprint as a consequence of damage from handling the surfaces.

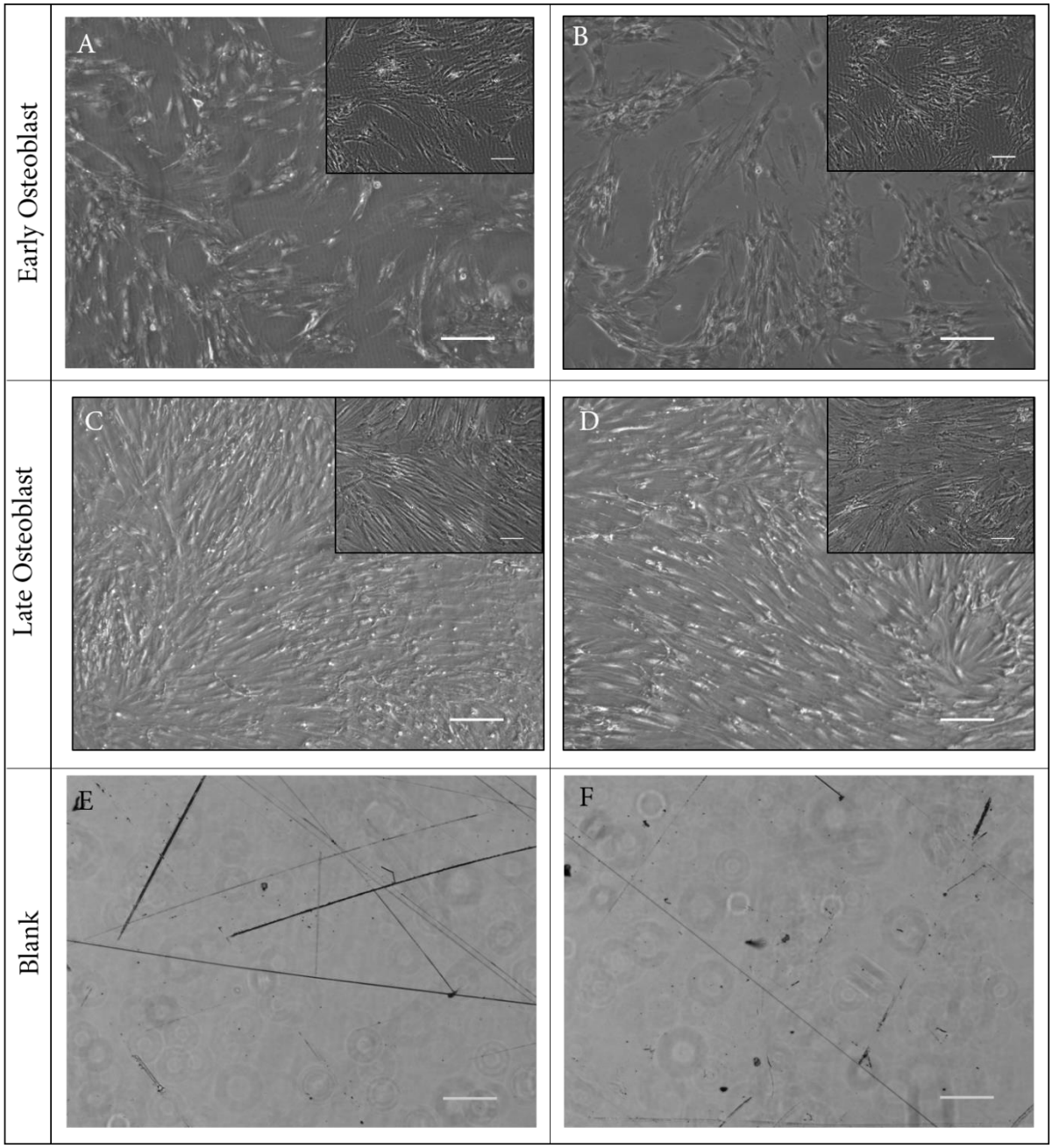

Figure 4.3. Light microscope images of bioimprinted surfaces. *A and B early osteoblast bioimprint. C and D late bioimprint, E and F – blank bioimprint. Scale bar in larger image 200 µm. Scale bar within inset image 100 µm.*

Water contact angle experiments were performed to provide an indication of the wettability of the sample and to also gain an indication of the presence of topographical features. Experiments were performed using the protocol described in section 4.2.2. The results show that the early and late osteoblast bioimprint display reduced water contact angle compared to the flat blank bioimprint (Figure 4.4) ($p \leq 0.0001$). This was expected as a lower water contact angle is associated with increased surface roughness.

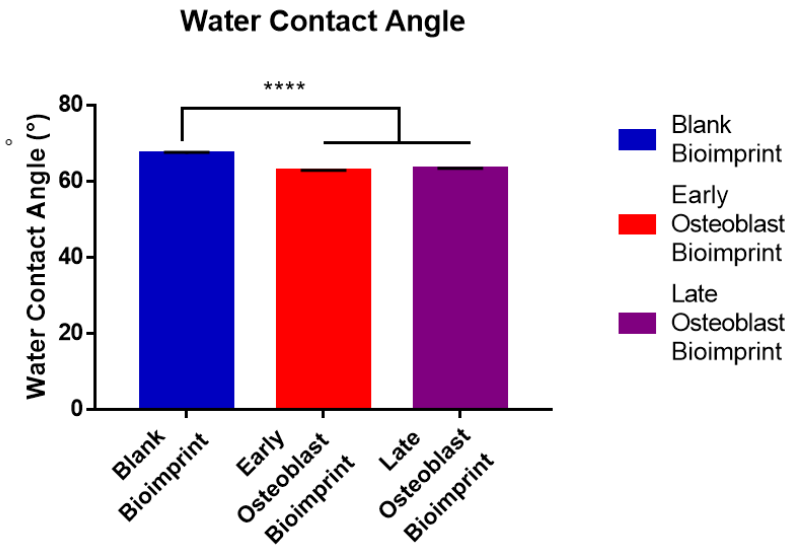

Figure 4.4. Water contact angle for blank, early and late bioimprint surfaces. *Bar represents mean ± SD, n=5 measurements. One-way ANOVA was performed on the data. ****p≤0.0001.*

The generated bioimprints were imaged using AFM to obtain information on cell measurements in 3D (Figure 4.5), as described in section 4.2.3. From cell height measurements, it was observed that the early osteoblast bioimprints were slightly higher, with features reaching approximately 1.5 µm (Figure 4.5A-C). Following culture over 21 days and differentiation of the STRO-1+ SSCs (late osteoblasts), the bioimprints were observed to display a shallower relief profile, with maximum features reaching approximately 700 nm, as measured using z-scale unique to each AFM image (Figure 4.5D-F). Within the early osteoblast bioimprints, the nucleus of each cell was observed as a distinct tall, circular object. However, as the cells began to differentiate further, the nucleus was noted to be shallower with respect to the cytoplasm in the day 21 late osteoblast bioimprints. At this late stage, cells were denser and the boundary between cells less defined. Interestingly, the level of detail transferred to bioimprints in both early and late osteoblast bioimprint could be seen in the form of actin filaments (white arrows) (Figure 4.5C+F).

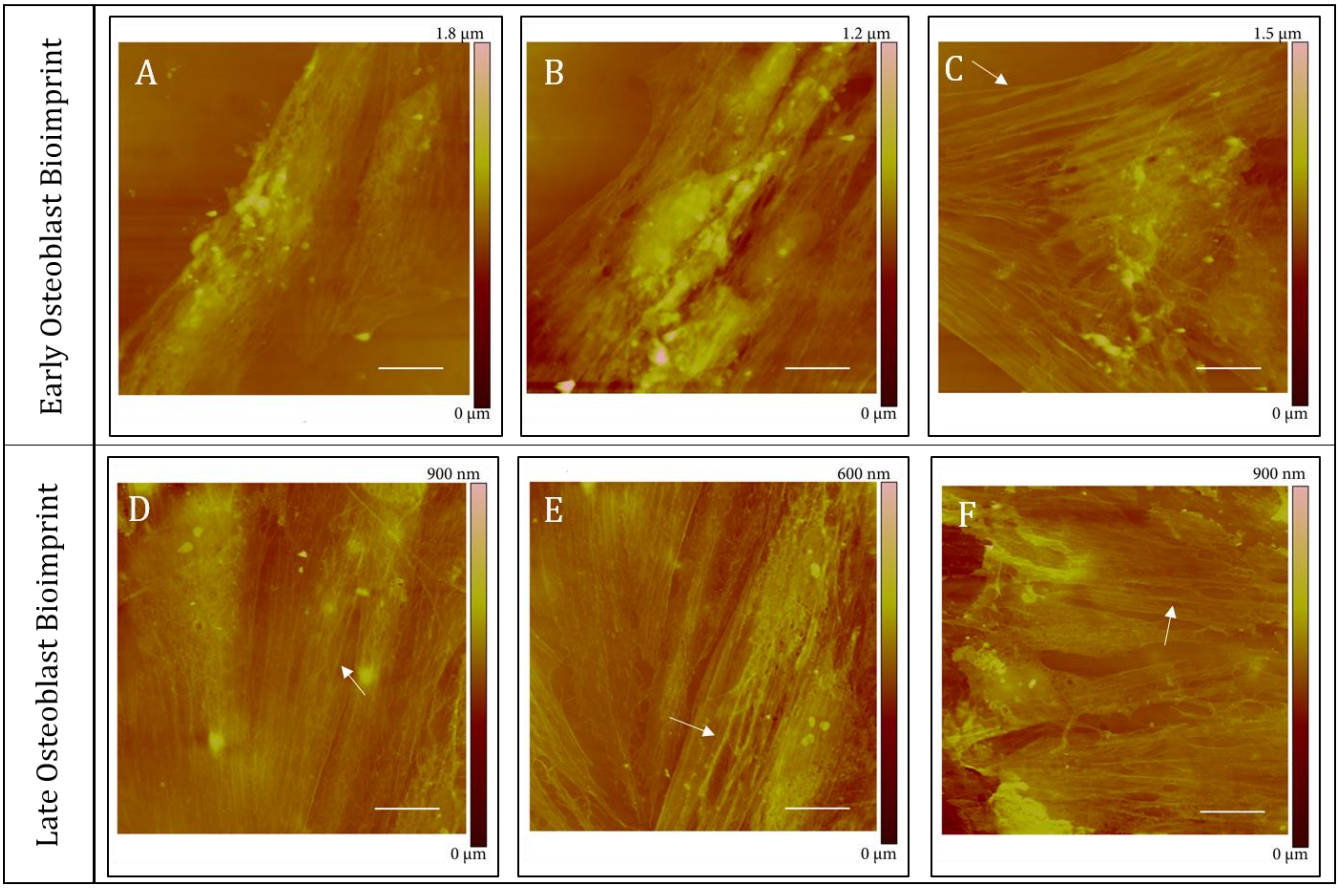

Figure 4.5. Atomic force microscopy (AFM) images of early and late osteoblast bioimprints. *(A-C) Early osteoblast bioimprint. (D-F) Late osteoblast bioimprint. Scale bar is 20 µm. White arrows indicate actin filaments. Z-scale is unique to each image and indicated at the right of each image. Images were generated using the protocol described in section 5.2.2.*

4.3.2. STRO-1+ SSC morphology on bioimprinted surfaces

STRO-1+ SSCs were isolated from human bone marrow as described in section 2.3.2 and cultured on bioimprinted surfaces as described in section 2.5.1. As observed in Figure 4.3, bioimprinted features were visible under light microscopy, making it difficult to distinguish between bioimprinted cell and live STRO-1 SSCs cultured on the surface. To aid visualisation of cells growing on the surface, CellTracker™ Green (CTG), a non-toxic, fluorescent dye (taken up by viable cells) was used (Figure 4.6A-H). Following culture of STRO-1+ SSCs on early and late stage osteoblast bioimprints, the bioimprints could be seen behind cells. The STRO-1+ SSCs appeared to grow randomly with respect to the bioimprint features. When the cells were cultured on late osteoblast bioimprints (Figure 4.6G and H), STRO-1+ SSCs displayed an elongated morphology in contrast to cells cultured on TCP (Figure 4.6A and B). SSCs did not appear to adopt the spindle-like processes characteristic of osteoblasts on either early or late osteoblast bioimprints and did not appear to adopt the shape of the improinted cells.

Following on from these initial observations, quantification of images were undertaken to understand the behavioural differences when SSCs were cultured on bioimprinted surfaces. In order to do this, images of SSCs stained with CTG were processed using CellProfiler software as detailed in section 2.7.2. Both cell area and cell elongation were measured at both days 4 and 7 in culture. The measurements showed that cell area falls for all samples between days 4 and 7. However, between samples, there was not measured difference in cell area between TCP, blank bioimprinted surface or early or late osteoblast bioimprinted surfaces at either day 4 or day 7 time point (Figure 4.7A). Cell eccentricity measurements indicated that on day 4 cells were more elongated and on day 7 this changed slightly to cells becoming more spherical (Figure 4.7B). However, as with cell area measurements, cell eccentricity does not change between surface topography at either day 4 or day 7 time points.

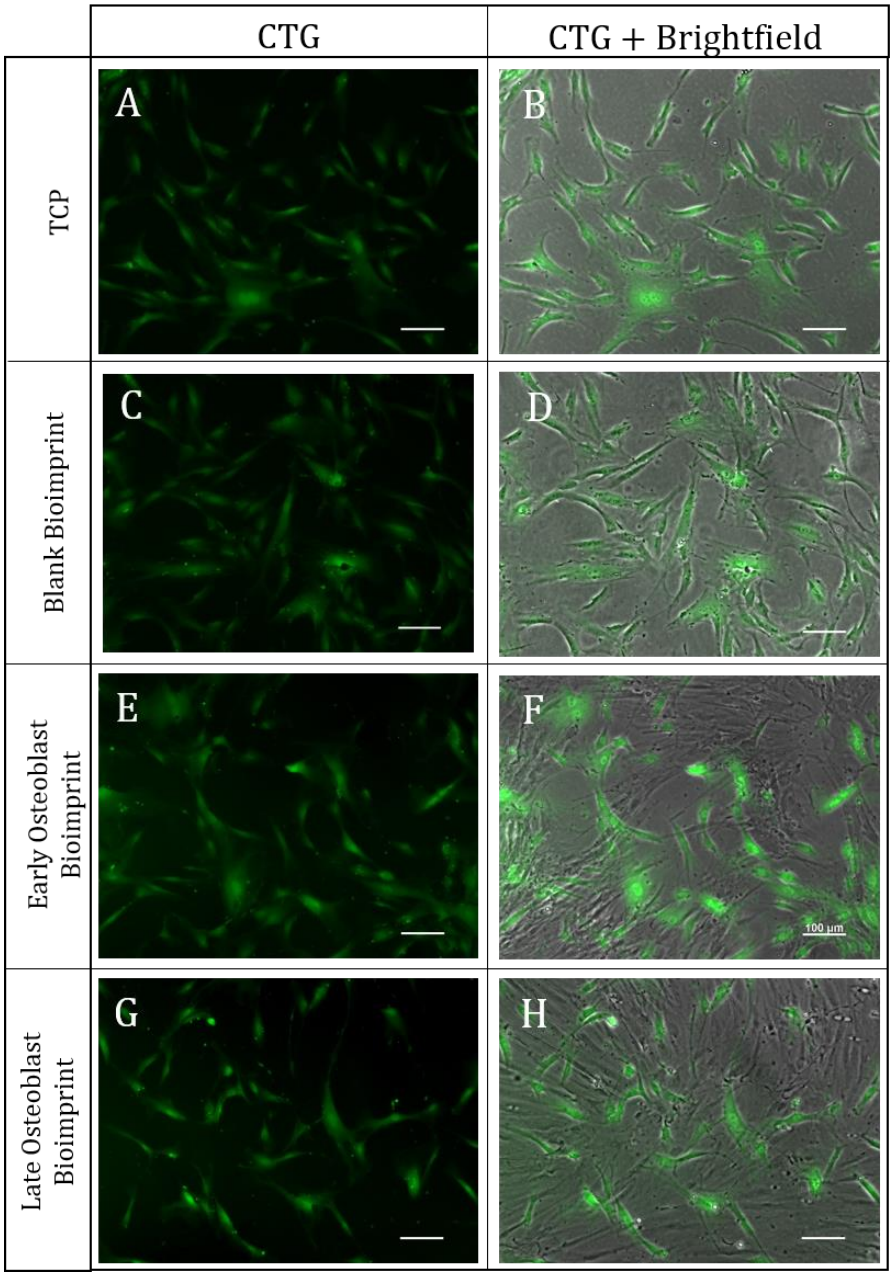

Figure 4.6. STRO1+ SSCs cultured on bioimprinted surfaces stained with CellTracker™ Green (CTG) 7 days after seeding. *CTG - CellTracker™ stained cells, CTG + Brightfield – CTG images with brightfield overlay. TCP – tissue culture plastic (A+B). Blank – non-bioimprint control surface (C+D). Early osteoblast – surfaces bioimprinted with early stage osteoblasts (E+F). Late osteoblast – surfaces bioimprinted with late stage osteoblasts (G+H). Scale bar - 100 µm.*

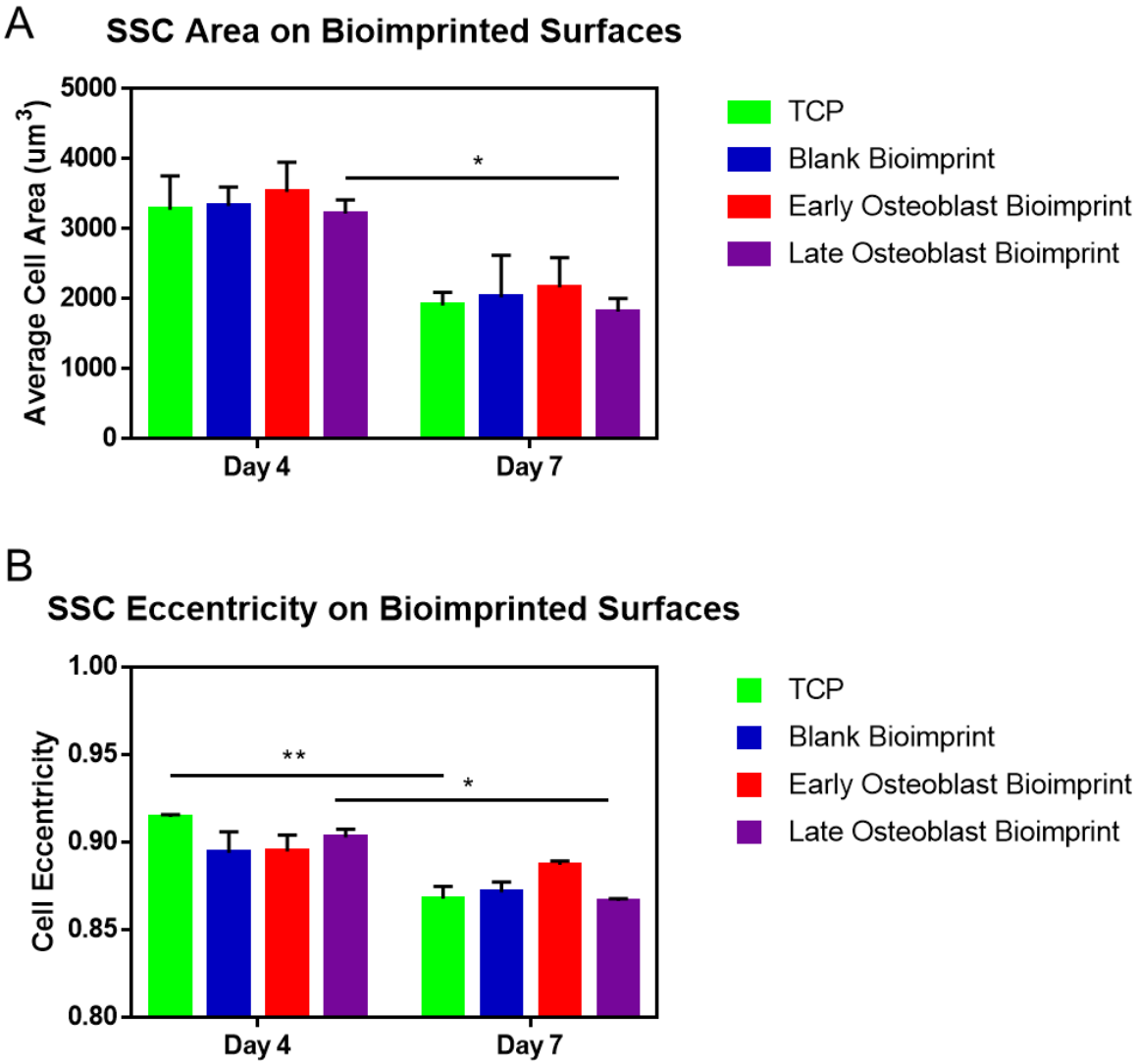

Figure 4.7. SSC morphology on bioimprinted PS surfaces. *(A) Cell area and (B) eccentricity measurements for SSC cultured on TCP, blank, early osteoblast or late osteoblast bioimprinted surfaces on day 4 and 7. Bar represents mean ± SD, n=3 patients. A minimum of 80 images were analysed per condition per patient. 2 way ANOVA statistical test was used to compare groups. * = p<0.05, ** = p<0.01.*

4.3.3. Metabolic activity of STRO-1+ SSCs on bioimprinted surfaces

Initial CTG images to monitor STRO-1+ SSC growth on these surfaces, indicated the cells grew more slowly on bioimprinted surfaces compared to STRO-1 SSCs on TCP. This was further investigated using quantification of DNA with PicoGreen fluorescent marker. STRO-1+ SSCs were seeded onto bioimprinted surfaces and samples taken on day 7, 14 and 21 for DNA quantification as detailed in section 3.2.

The results in Figure 4.8A demonstrated, overall, reduced DNA content in bioimprinted samples relative to STRO-1 SSCs cultured on TCP. DNA content was observed to increase between day 7 to 21 on all samples with bioimprints including blank surface. Thus, STRO-1+ SSCs cultured on the early osteoblast bioimprinted surfaces displayed increased in DNA content from day 7 (117.0 ± 32.5 ng DNA/mL of cell lysate) to day 14 (268.6 ± 69.8 ng DNA/mL of cell lysate) and finally to day 21 (494.8 ± 129.9 ng DNA/ml of cell lysate). STRO-1+ SSCs displayed a higher DNA content on day 7 on late osteoblast bioimprint on day 7 (139.8 ± 24.2 ng DNA/mL of cell lysate) compared to early (117.0 ± 32.5 ng DNA/mL of cell lysate) and blank (101.6 ± 44.0 ng DNA/mL of cell lysate) bioimprint. This however did not carry through to later time points and at day 14, proliferation was comparable between the three bioimprinted samples (blank bioimprint – 255.2±86.5 ng DNA/mL of cell lysate, early osteoblast bioimprint – 268.6±69.8 ng DNA/mL of cell lysate, and late bioimprint – 280.7±91.6 ng DNA/mL of cell lysate). DNA content in STRO-1 SSCs cultured on TCP plateaued on day 14 and remained unchanged at day 21. Interestingly, on day 7 and day 14, STRO-1 SSC proliferation was higher on TCP compared to bioimprinted surfaces. On day 21, however, DNA content on the two bioimprinted surfaces was observed to be non-significantly higher than TCP (TCP 422.3 ± 91.9 ng DNA/mL of cell lysate, blank bioimprint – 473.8 ± 74.0 ng DNA/mL of cell lysate, and early osteoblast bioimprint 494.8 ± 129.9 ng DNA/mL of cell lysate) (Figure 4.8A).

DNA content provides key important information on cell proliferation on bioimprinted surfaces, although the metabolic profile is unclear. In order to do this, alamarBlue® reagent was used. This dye was reduced in metabolically active cells to a fluorescent dye which could be measured and the methodology is detailed in section 2.4. The fluorescence measured was divided by average DNA content and plotted in Figure 4.8B. STRO-1+ SSC activity on TCP showed a slight dip inactivity on day 14 (280.6 ± 63.9) however recovered by day 21 (329.0 ± 88.9). Cells cultured on bioimprints showed the reverse, with activity increased on day 14 compared to days 7 and 21. For example on early osteoblast bioimprints activity was 206.4 ± 125.0 on day 7, increased to 370.5 ± 218.0 on day 14 and decreased to 230.1 ± 96.6 on day 21 (Figure 4.8B). It was apparent on these experiments, there was a large variation in the

measured metabolic activity of the STRO-1+ SSCs isolated from the 3 patients studied, similar to observations made in Chapter 3 about patient to patient variation.

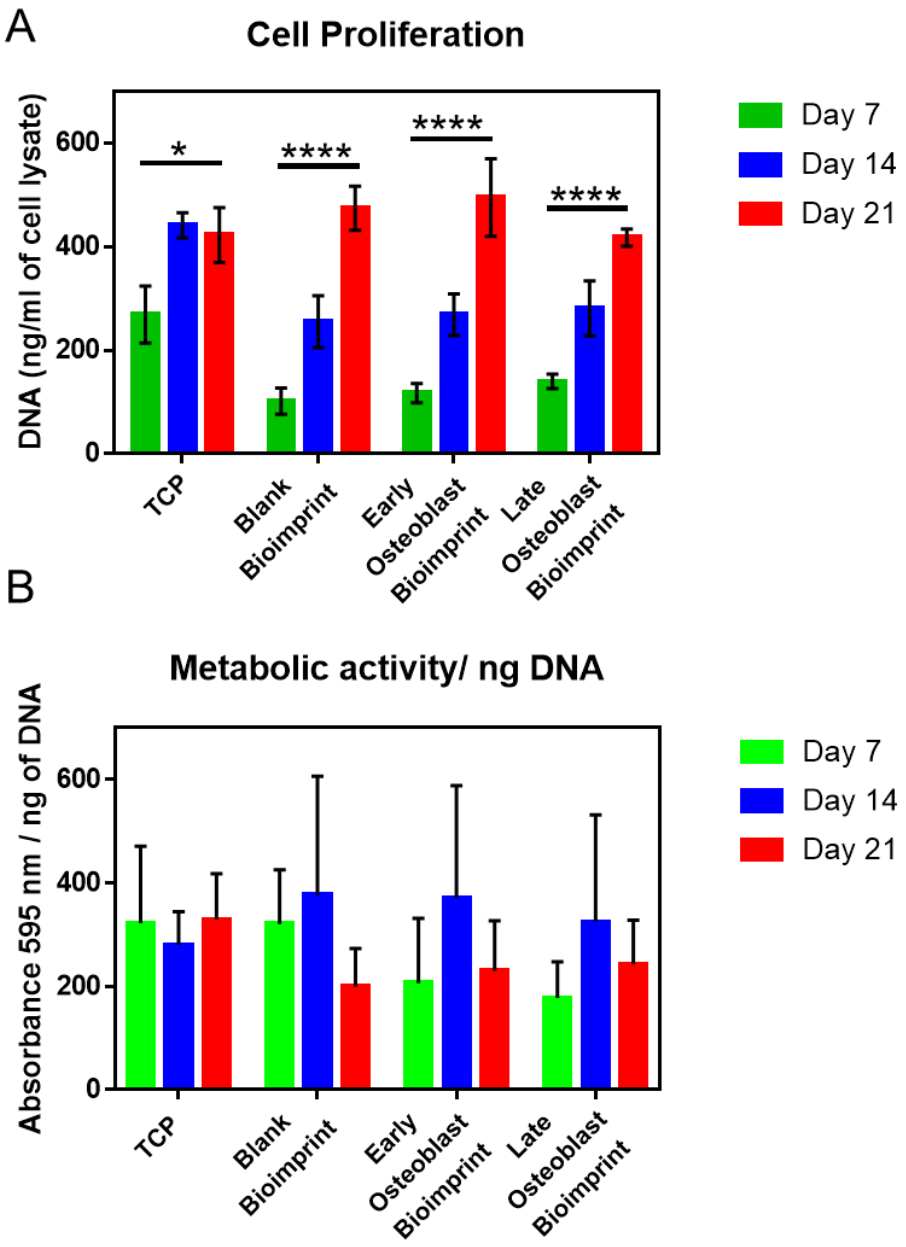

Figure 4.8. Metabolic activity of SSCs cultured on bioimprinted surfaces. *(A) Cell proliferation measured as DNA content of STRO-1+ SSCs cultured on blank bioimprint, early stage osteoblast bioimprint, late stage osteoblast bioimprint and TCP (tissue culture plastic). DNA content was measured using PicoGreen dsDNA assay on days 7, 14 and 21. (B) Absorbance of converted alamarBlue® reagent at 595 nm per ng DNA. Cells were treated with alamarBlue® and after 4 hours, absorbance of fluorescence measured. Cells were cultured in basal media. n=3 patients, bar represents mean, error bars represent SD. 2 way ANOVA was performed on the data. * p≤0.05, ****p≤0.0001.*

4.3.4. Molecular analysis of STRO-1 SSCs on bioimprint surfaces

Following analysis of STRO-1 SSC proliferation on the bioimprint surfaces, modulation of gene expression that could accompany the observed changes in proliferation were studied. STRO-1+ SSCs were cultured on bioimprinted surfaces and samples taken on day 7, 14 and 21 for nucleic acid extraction as detailed in 2.2.1-4). Given STRO-1+ SSCs have previously been shown to differentiate down the osteoblast pathway (Appendix II), the current work examined if osteoblast bioimprints induced osteogenic differentiation of STRO-1+ SSCs following cultured on the bioimprints.

Expression of osteogenic markers *RUNX2, ALP, COL1A1, OCN* and *OPN* was measured on days 7, 14 and 21 on bioimprinted surfaces and compared TCP control using two media types. Expression is detailed first to compare with STRO-1+ SSCs cultured on TCP in the absence of osteogenic media, or basal media, (Figure 4.9) with a total of 6 patients, and secondly to compare with STRO-1+ SSCs cultured on TCP in the presence of osteogenic media (TCP OM) with a total of 3 patients (Figure 4.11). The reason for this is because experiments were first performed with only TCP in basal media and then later, TCP in osteogenic media (OM) was added on.

For the initial 6 patients, expression of *RUNX2* increased with time for SSC cultured on TCP ($p \leq 0.05$), early osteoblast bioimprint ($p \leq 0.01$) and late osteoblast bioimprint ($p \leq 0.001$) (Figure 4.9A). Expression of *RUNX2* on blank bioimprint however did not increase with time. Expression of *COL1A1* was comparable between SSC cultured on TCP and early osteoblast, and late osteoblast bioimprint (Figure 4.9B). Expression on blank bioimprints was higher compared to the other three, with expression on day 21 measured at 123.3 ± 137.6 compared to 12.3 ± 16.7 relative expression on late osteoblast bioimprints. *ALP* measured on day 7, day 14 and day 21, was comparable between the bioimprinted surfaces and TCP across all three time points. For example, *ALP* expression was measured on day 14 at 10.6 ± 8.4 for TCP, 9.1 ±7.2 for blank bioimprint, 9.1 ± 5.6 for early osteoblast bioimprint, and 7.8 ± 7.4 for late osteoblast bioimprint (Figure 4.9C). Expression of the osteogenic markers *OCN* and *OPN* was consistently higher on blank bioimprinted surfaces. *OCN* expression peaked at 14.5 ± 9.7 on day 14 and *OPN* expression rose to 12.4 ± 8.2 on day 21, both on blank bioimprint. Accompanying this, expression of *OCN* and *OPN* in STRO-1+ SSCs was lower on early and late bioimprints than blank bioimprints. *OCN* expression on day 14 was measured at 3.9 ± 5.9 on early osteoblast bioimprint and 2.9 ± 3.8 on late osteoblast bioimprint (Figure 4.9D). *OPN* expression on day 21 was also observed to be lower on early and late osteoblast bioimprinted surfaces, at 3.0 ± 2.9 and 3.1 ± 3.6 respectively (Figure 4.9E). Significant differences were discovered in expression of *OPN* on day 21 between blank bioimprinted samples and both

early and late osteoblast bioimprinted samples ($p \leq 0.01$), and between blank bioimprint and TCP (≤ 0.001). There appeared to be little consistent difference in osteogenic response of STRO-1+ SSCs between early osteoblast bioimprint and late osteoblast bioimprint.

To relate to *COL1A1* gene expression data, immunofluorescence was used to visualise COL1A1 protein concentration (Figure 4.10). The results indicated that on day 21, protein expression of COL1A1 was approximately similar between TCP, blank, and late osteoblast bioimprint. There was a slight increase in COL1A1 protein level on early osteoblast (Figure 4.10E)

The current results do not indicate whether an increase in osteogenic marker expression would result in changes in function of SSCs. Expression increase observed in the presence of OM, and therefore osteogenic differentiation would give an indication on the necessary fold increase for SSC osteogenic differentiation. In order to understand if the increases in osteogenic marker expression observed on bioimprinted surface has implications on the biological function of SSCs and possible differentiation, SSCs were cultured on TCP in the presence of OM. The increase in expression of osteogenic markers in OM can then be compared to expression increases observed in SSCs on bioimprinted surfaces. This was shown as a separate graph as cultures using OM were only performed on 3 patients, and not the full 6 patients detailed in Figure 4.9.

Expression of *RUNX2* observed on day 21 was approximately 3 fold-change lower on blank bioimprints (5.9 ± 5.0) than TCP OM (15.7 ± 9.6) (Figure 4.11A). A similar expression difference was observed on with *COL1A1* expression. Expression of *COL1A1* on day 21 measured at 10.7 ± 11.6 on late osteoblast bioimprint and increased to 33.4 ± 9.8 (Figure 4.11B) ($p \leq 0.01$). *ALP* expression was found to increase from day 7 to day 21 in all samples similar to expression profile observed in Figure 4.9. Expression of *ALP* was higher on TCP OM (31.2 ± 17.1 on TCP OM on day 21, compared to for example 19.7 ± 10.7 on day 21 on blank bioimprints). *OCN* expression was found to increase approximately 10 fold in the presence of OM (Figure 4.11D). Expression was measured on day 21 at 59.9 ± 32.3, compared to 5.8 ± 5.5 on early osteoblast bioimprints ($p \leq 0.001$). Levels of *OPN* measured showed less dramatic differences in expression between samples in OM and samples in basal media. Expression of SSC in TCP OM on day 21 measured at 5.6 ± 2.7 and blank bioimprints at 3.6 ± 2.2.

The expression of osteogenic markers increased in the presence of OM and this differed for each gene. Due to patient variation, the expression profile for each gene was different in the larger patient set (Figure 4.9) compared to the smaller patient set (Figure 4.11).

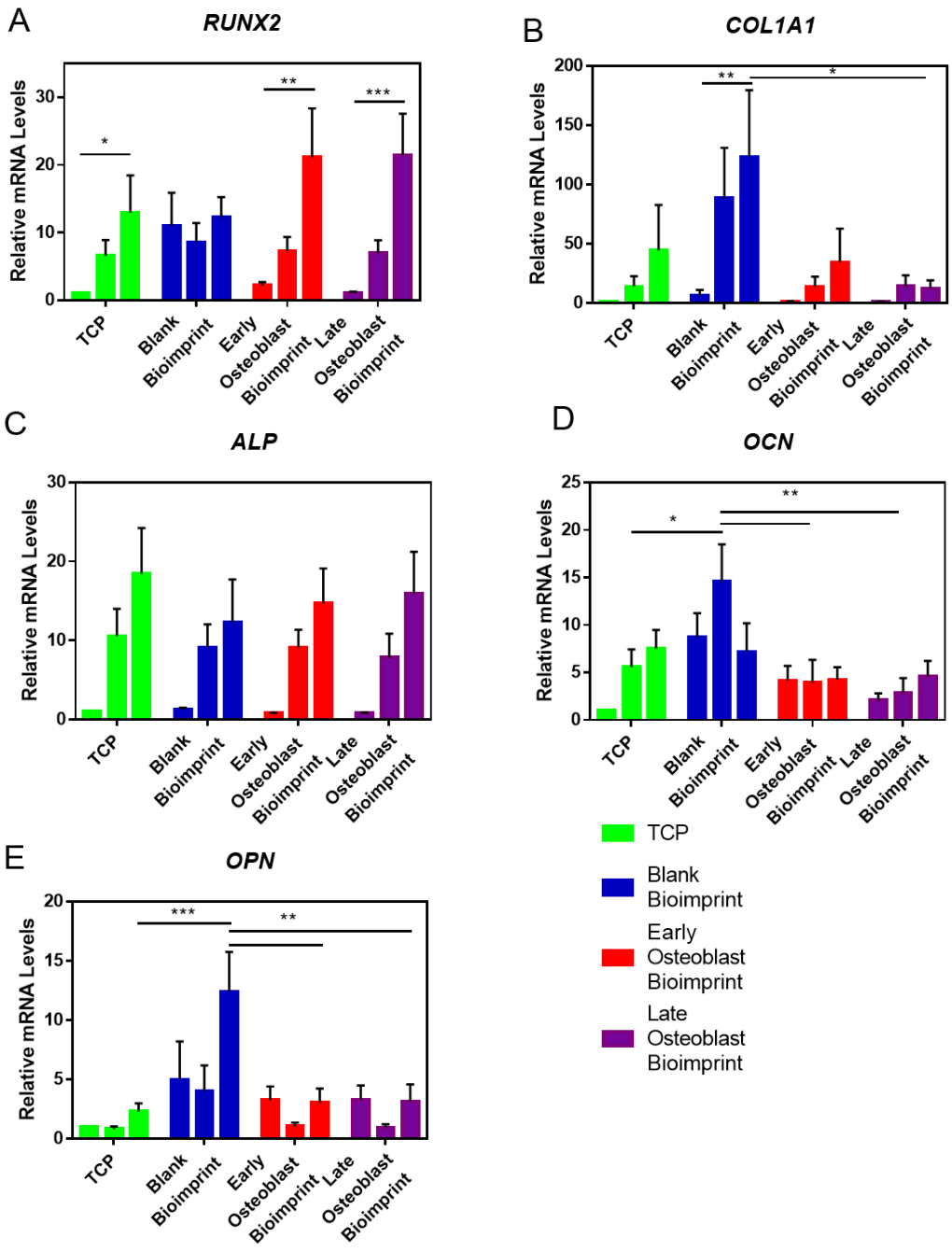

Figure 4.9. Expression of osteogenic markers in STRO-1+ SSCs cultured on bioimprinted surfaces on days 7 to 21, with TCP control in basal media. *STRO-1+ SSCs were cultured on blank bioimprint, early stage osteoblast bioimprint, late stage osteoblast bioimprint and TCP. First bar in each group represents day 7, second bar represents day 14 and third bar represents day 21. Bar represents mean and error bars represents SEM. Each sample was normalised to ACTB and relative to TCP on day 7. Name of gene expression measured is displayed at the top of each graph. n = 6 individual patients donors. Legend is at bottom right.*

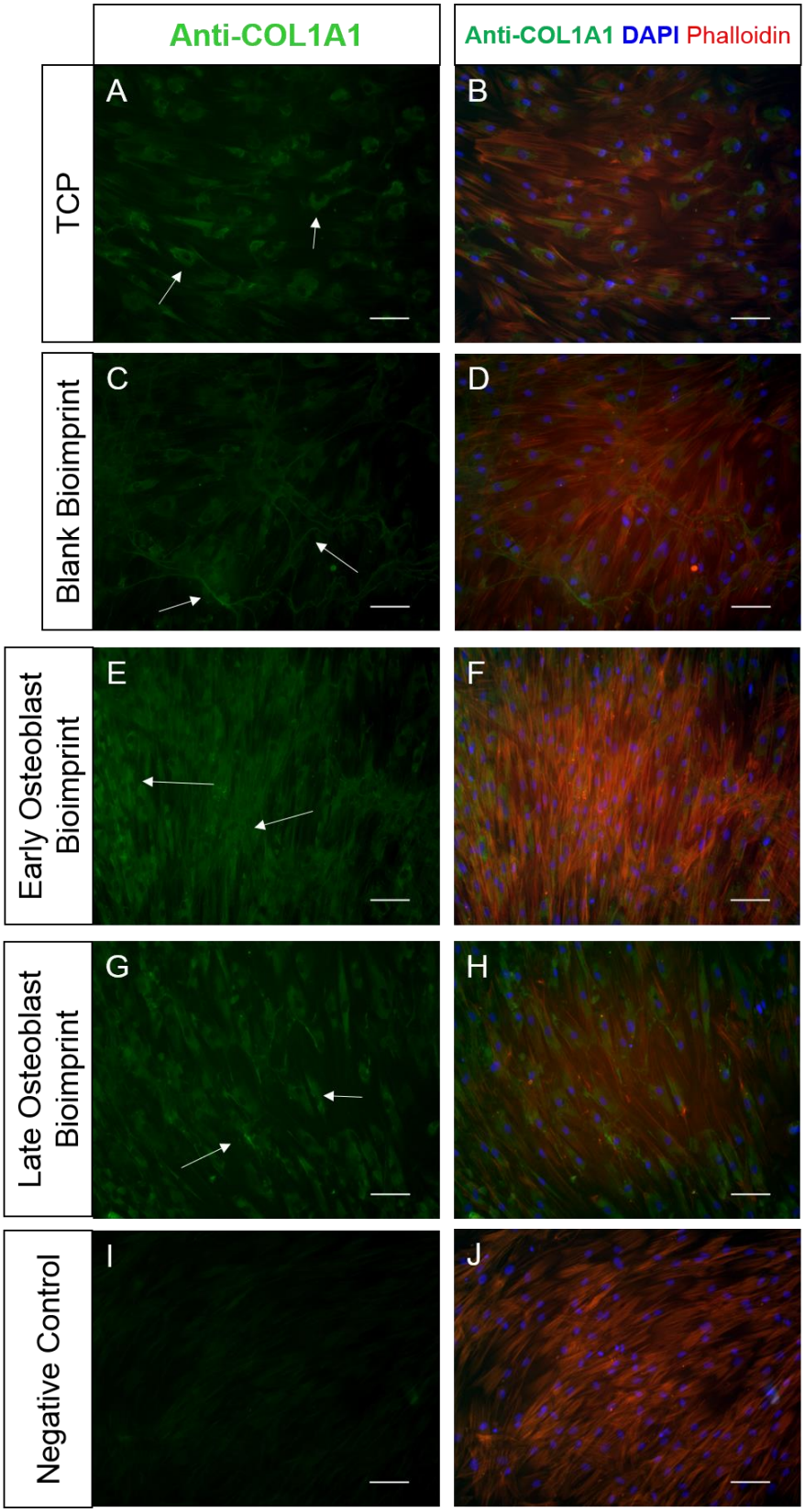

Figure 4.10. Collagen type 1 immunofluorescence staining of STRO-1+ SSCs at day 21. *Images of STRO-1+ SSCs stained with anti-COL1A1 antibody (green) (A, C, E, G and I) and anti-COL1A1 (green) DAPI (blue) and phalloidin (red) (B, D, F, H, and J) on TCP (basal media) (A+B), blank bioimprint (C+D), early osteoblast bioimprint (E+F), late osteoblast bioimprint (G+H) and negative control without anti-COL1A1 (I+J). n = 2 patients, Representative images shown.*

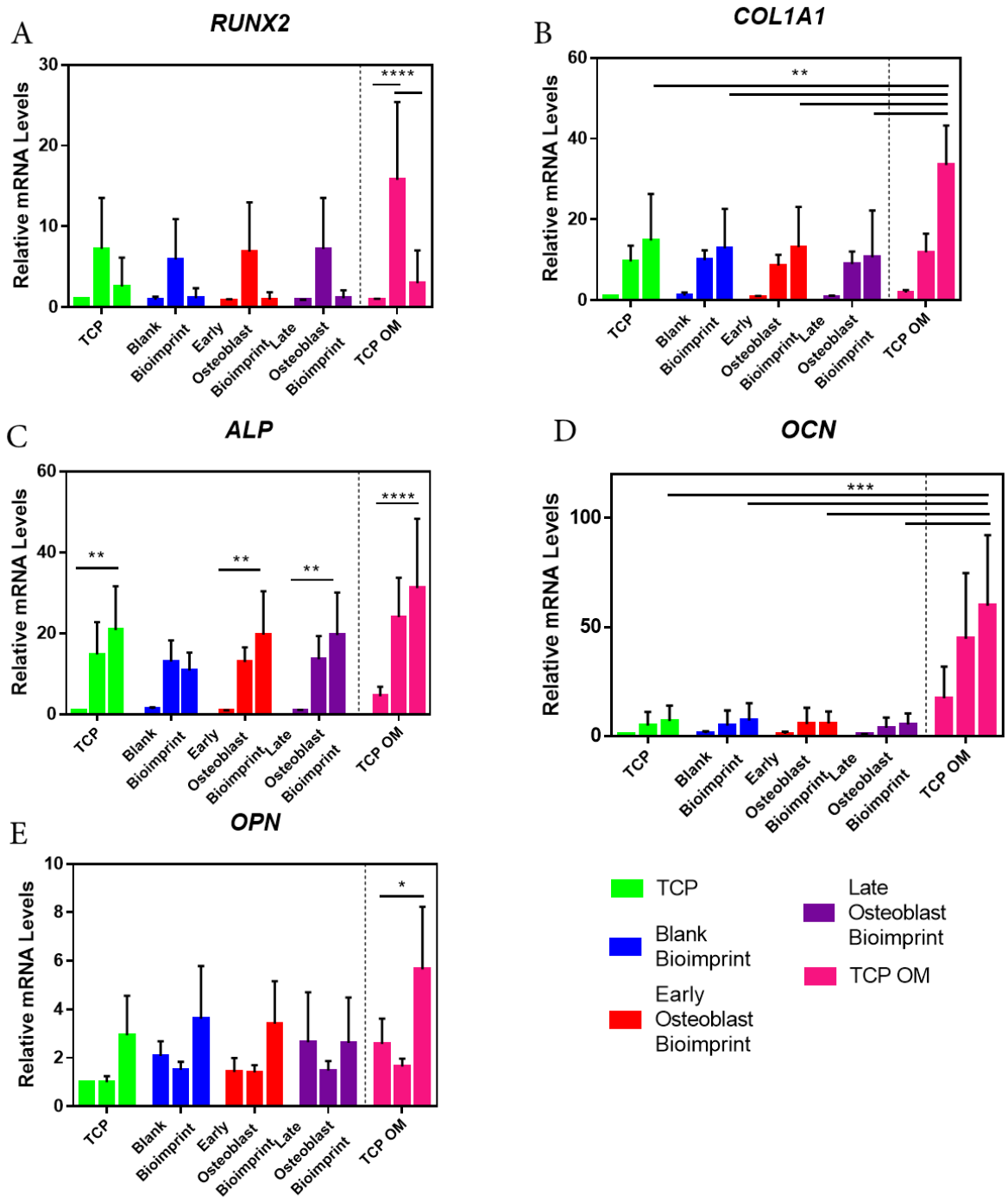

Figure 4.11. Expression of osteogenic markers in STRO-1+ SSCs cultured on bioimprinted surfaces on days 7 to 21, with TCP control in osteogenic media. *STRO-1+ SSCs were cultured on blank bioimprint, early stage osteoblast bioimprint, late stage osteoblast bioimprint, TCP and TCP with osteogenic media (TCP OM). First bar in each group represents day 7, second bar represents day 14 and third bar represents day 21. Bar represents mean and error bars represents SEM. Each sample was normalised to ACTB and relative to TCP on day 7. Gene expression is displayed at the top of each graph. n = 3 individual patient donors. Legend is shown bottom right.*

4.4. Discussion

The current studies demonstrate, STRO-1+ SSC behaviour was altered in response to bioimprinted surfaces. Morphological quantification demonstrated cells displayed a similar area and eccentricity on TCP compared to bioimprints, and between bioimprints blank, early and late, cells were also behaving similarly. From the cell proliferation results, it could be concluded that STRO-1+ SSCs proliferated at a slower rate on bioimprinted surfaces compared to TCP and, metabolic activity suggested that SSCs are less metabolically active on bioimprints compared to TCP. Concerning STRO-1+ SSC proliferation and metabolic activity, it could be postulated that the results observed were a material effect instead of a bioimprint-mediated effect, influencing cell proliferation and metabolic activity. In gene expression studies, osteogenic markers in STRO-1+ SSCs were not found to be up regulated compared to TCP OM. There was however, up regulation of *COL1A1*, *OCN* and *OPN* in STRO-1+ SSCs cultured on blank bioimprint, suggesting a special role of the flat, non-bioimprinted surface in upregulating these markers. The current observations indicate, the bioimprinted surfaces have an entirely undiscovered role on STRO-1+ SSCs behaviour, with the material from the bioimprints modulating STRO-1+ SSC behaviour.

Several studies have been published comparing the effect of surface stiffness and topography on cell behaviour. Li *et al* concluded that although both stiffness and topography have an effect on osteogenic differentiation, stiffness if the predominant regulator in osteogenic differentiation and topography plays a less important role [303]. Similarly Wu *et al* showed that when studying maintenance of embryonic stem cell stemness, stiffness is more important than topography [304]. A similar effect could be at play with the bioimprints, where the stiffness and chemistry of the bioimprints seem to be more important than the topography. Bioimprinted topography is not a regular pattern, so it could be that the cells are less responsive to the pattern, which is irregular. This was observed with the CTG images, where the cells were not associating with the bioimprinted features on the surfaces.

PDMS is commonly used as a polymer to replicate features at high resolution [305]; PDMS is known to be non-toxic to cells, making PDMS ideal for replication of cellular features [306]. Indeed, AFM images showed that there was a high level of fine detail which transferred over to the bioimprint. Several studies have also published the high resolution PDMS can transfer to PS surfaces [297, 301]. As PDMS is soft and flexible, PDMS was easily removed from both wells containing cell during the first stage of bioimprinting and, in later stages of bioimprinting, removed from PS bioimprinted surface.

PDMS is by nature highly hydrophobic, and following plasma treatment became hydrophilic, tolerating cell attachment [306]. In the experiments discussed in this chapter, features replicated on PDMS were transferred to PS. PS is traditionally used as a cell culture material for STRO-1+ SSC growth, however is hydrophobic. In these experiments, PS was treated to ensure cell attachment could occur. This was achieved by introducing an oxidised surface either through addition of hydroxyl groups (-OH) or sulphate groups (SO_3H) and in the experiments discussed in this chapter, sulphate groups were added. Sulfonation is known to be a highly effective way of preparing surfaces for cell culture [307]. Early studies indicated that sulphuric acid treatment should be combined with other treatments in order to generate the high number of hydroxyl groups required for cell attachment [162]. Water contact angle experiments in this chapter showed that wettability on the bioimprinted surfaces was slightly higher than in previously published generated bioimprints [301]. Thus, for blank bioimprinted surfaces, the result 67.03 ± 0.43 where as in published wettability results for the blank bioimprinted surface, a result of 66.8 ± 0.7 was obtained [301], indicating a decrease of wettability in surfaces used in this chapter compared to published results. The results obtained on sulphuric acid-treated bioimprinted surfaces were noticeably lower than the published results for water contact angle experiments on the hydrophobic PDMS (measured at 102.2 ±1.4 in [301]). Given that PDMS is more hydrophobic than PS, this would be expected. It should also be noted that bioimprinted surfaces did not float in media, suggesting sulphuric acid treatment was sufficient for cell culture preparation.

It was not studied if the sulfonation used on bioimprinted surfaces was as effective as commercial tissue culture treatment on TCP surfaces used in these experiments. If the sulfonation was not as effective as in commercial TCP surfaces, this could be the main reason behind why the cells responded to the PS bioimprinted surfaces with a material effect instead of a response to the topography.

Results of cell morphology indicated a decrease in both cell area and cell eccentricity from days 4 to day 7, and that this did not change between surface types. The reason for the decrease observed in both parameters could be due to the fact initially cell density on the surfaces was low, and thus cells had spread and elongated on the surface. With culture, cell density on the bioimprinted surfaces increased, leading to a decrease in cell spreading. Cell measurements were stopped at day 7 as after this time, cells became confluent and subject to contact inhibition. Importantly, when the cell membrane is unclear and indistinct, the CellProfiler software was observed to be prone to error and to avoid any issues, data collection was stopped at day 7. It was unknown if during these experiments there was a continuous drop in cell size as culturing progresses as this was not measured, however it is likely to

continue to drop as available area decreases. Because there was not a difference between the surfaces, cell area was not calculated in OM.

When cells proliferate in culture, there is an initial lag phase followed by an exponential growth, limited typically by nutrients or space. TCP is specifically designed for cell attachment and optimal cell proliferation, so proliferation on these surfaces is understandably faster compared to the bioimprinted surfaces. STRO-1+ SSCs on TCP reached a plateau on day 14 and cell number remained at that level to day 21. However, when studying the metabolomic activity, it was observed that the activity remained approximately the same from day 7-21 so although cell numbers increased, their metabolomic profile did change. On the bioimprints, cell proliferation and metabolomic activity, were predominantly comparable blank, early osteoblast and late osteoblast. The cell culture proliferation lag phase was greater on bioimprinted surfaces and, in fact, cell number did not show a plateau. By day 21, SSCs number reached approximately the same number on bioimprinted surfaces as STRO-1+ SSC number on TCP. This could be the maximum number of SSCs which could be accommodated on the 9.8 cm^2 area of 6-well plates. It could be hypothesised that should culture time have been extended beyond 21 days, a plateau would have been seen in SSCs cultured on bioimprinted surfaces. The reason for the slow culture growth on bioimprinted surfaces could be due to the chemical nature on the surfaces, inhibiting culture growth, or a change in cell differentiation on the surfaces as a consequence of cues detected and subsequent utilisation of nutrients. The metabolomic activity on the bioimprinted surfaces reached a peak on day 14, this could be due to the exponential growth of the culture at this time point.

Gene expression data showed that when in OM, SSCs are capable of osteogenic differentiation and the observed increase in expression differed for each gene. In general it was observed that SSCs on all surfaces have the same pattern of expression, but this was increased significantly in the presence of OM. There is a characteristic peak of *RUNX2* expression on day 14 in all samples and a gradual increase in *ALP, COL1A1, OPN* and *OCN* expression towards day 21. It appears that SSCs cultured in basal conditions are still showing a degree of osteogenic response, regardless of the surface type. This was also shown in Appendix II where a comparison between SSCs cultured in osteogenic and basal media showed an increase in expression of osteogenic markers over 21 days. Within the larger data set of 6 patients (Figure 4.9), it could be seen that the blank bioimprinted surface resulted in an increase in expression of *COL1A1, OPN,* and *OCN.* However, this increase disappeared when studying only the smaller data set for comparison in the presence of OM (Figure 4.11). It can therefore be concluded that this increase in expression is patient specific and is therefore not observed in every patient. In addition, given the level of expression of osteogenic markers did not increase when SSCs were cultured on the bioimprinted surfaces, it is known

that the surface did not induce osteogenic differentiation. From the gene expression results, it can be concluded that the cells did not alter their behaviour between the topographies of the bioimprinted surfaces.

It is important to note that the bioimprinted surfaces are not all identical. The surfaces were generated from two 6 well plates for each time points, and therefore a total of 12 wells were used to generate all the bioimprints used in this chapter. In each well, and the bioimprints created from these wells, there will be variation in cell density and individual cell morphology and therefore, although cells cultured on the bioimprints are exposed to similar features, there is considerable variation between the bioimprinted surfaces. The surfaces used in each experiment were chosen at random for each experiment. This means there is little consistency between the bioimprinted surfaces, which is a strong contributing factor to the variation observed in the experiments described in this chapter, as well as patient to patient variation.

In conclusion, analyses of cell morphology and gene expression indicate that cell behaviour was unaltered in response to bioimprinted features. In contrast, cell proliferation was reduced following culture on bioimprinted surfaces, and, critically, metabolic activity was also altered on bioimprinted surfaces compared to TCP control. Therefore, the current studies suggest PS bioimprints have a minimal effect on cell behaviour and, with the data set of patients examined and techniques used, this minimal effect was insufficient to affect osteogenic differentiation.

Chapter 5: Enhancement of SSC osteogenesis on shell topographical surfaces

Chapter 5 - Enhancement of SSC osteogenesis on shell topographical surfaces

5.1. Introduction

The majority of this chapter was published in "*Waddell SJ, de Andrés MC, Tsimbouri PM, Alakpa EV, Cusack M, Dalby MJ, Oreffo, ROC. Biomimetic oyster shell–replicated topography alters the behaviour of human skeletal stem cells. Journal of Tissue Engineering. 2018;9:2041731418794007*" [308]. This paper can be found in Appendix V.

Currently in orthopaedic medicine, there is an unmet need for bone tissue to treat fractures and bone degeneration in an increasing aging population [309-311]. SSCs offer the potential to improve musculoskeletal repair given their capacity to differentiate into bone [312]. However, before SSCs can be used in the clinic, delineation of the developmental pathway and, critically, elucidation of the specific processes in SSC differentiation into osteoblasts are required.

A wealth of data has illustrated the role of topographical surface patterns, including patterns such as grooves, ridges, pits, and pillars and their ability to act as cues to direct differentiation of stem cells [132, 292, 293, 313]. The mechanism by which this occurs is yet to be fully understood. However, it is thought that integrins and cytoskeletal components together with intracellular signalling mechanisms play an important role [143]. In particular, integrin organisation and arrangement is of importance in transducing signal pathways to direct cell differentiation and function for enhancement of osteogenic differentiation [314]. Seminal studies over a decade ago have demonstrated that a regular nanotopographical arrangement with slight offset can increase focal adhesion formation, and modulate osteogenic differentiation [143]. Interestingly, the majority of topographical designs studied to date, have been machine generated. Application and lessons from nature in the use of a biomimetic approach could provide additional advantages over existing topographical designed approaches and bring unexplored surface patterns for which design may not readily replicate.

The surface of the *Pinctada maxima* (*P. maxima*) oyster shell, on initial observation, appears distinct from bone tissue and yet there are important similarities [315]. Nacre, the substance lining the inside of *P. maxima* and other bivalve mollusc shells, and bone are both composed of an inorganic, mineralised matrix and an organic fraction composed of proteins. The organic fraction provides a scaffold and biological signals which promote crystallisation. This allows for a substance which is strong and yet displays considerable flexibility. In bone, 70% of dry

weight is composed of inorganic mineralised calcium phosphate in the form of HA [3]. Nacre however, has a much greater proportion of inorganic mineralised matrix (97% of dry weight), which is mainly in the form of the calcium carbonate mineral, aragonite [316].

The potential for nacre and bone interactions was first noticed in 1931 when ancient Mayan skulls were discovered with dental implants composed of nacre [315]. This demonstrated the biocompatibility of nacre with bone. This phenomenon was studied further by Lopez and colleagues many decades later in 1991, who showed that, not only could human osteoblasts grow on nacre but also, after prolonged culture, osteoblasts produced a mineralised tissue matrix between osteoblasts and nacre chips [317, 318]. Histological analysis of the composition of this tissue found that the tissue adjacent to the bone chips contained a HA-rich mineralized matrix. Interestingly, the mineralised tissue formed next to the nacre chips was composed of lamellar sheets which closely resembled those of nacreous shell. Raman spectroscopy allowed for confirmation of aragonite crystals present in the matrix [317]. Bone regeneration initiated by nacre was proven in experiments in ovine bone defects, rabbit defects and human maxillofacial defects, illustrating the powerful role of nacre in bone regeneration [319-322].

As nacre appeared to enhance bone regeneration in published *in vivo* studies, it could be hypothesised that nacre has the ability to drive SSC osteogenesis, leading to enhancement of bone regeneration. To date, only a limited number of studies have examined the role of nacre in directing osteogenesis from SSC populations.

Nacre matrix was found to lead to an increase in expression of ALP in rat BMSC [323]. Further to this, bone marrow derived human SSCs cultured with nacre chips displayed an increase in ALP activity, indicating osteogenic differentiation [324]. Thus, it could be hypothesised that the nacre shell may provide SSCs with an ideal topography for SSC differentiation or/and provide a chemical environment to enhance differentiation. A previous study aimed to separate the topography from the chemistry by replicating nacre topographical features into PCL and studied the behaviour of commercially available MSCs on the PCL replicas [325]. The authors studied the crystallinity of the mineralised matrix formed when MSC were cultured on the PCL nacre replicas. The results detail that MSCs produced a mineralised matrix with higher crystallinity than chemically induced osteogenic differentiation, indicating a different pathway of differentiation [325].

In this chapter, a similar approach of using PCL replicas is taken to study the topographical effects of the nacre region of *P. maxima,* as well as the topography of the calcite prisms which form the outer layer of *P. maxima* shells (Figure 5.1). In addition, the current studies have used PCL replicas to examine the role of the topography from the prism region of *P. maxima*,

which is also composed of calcium carbonate crystals and forms in the region where the two sections of the shell join together. Interestingly, the role of the topography from this part of the shell is less well understood and the current study has examined the role of this material and the topography of this material in modulation of SSC behaviour. The cell source used in the current studies were human primary bone marrow-derived SSCs from an aged population, clinically relevant for studying bone regeneration therapies. The effect of nacre and prism topography has not been studied on this SSC population and will inform translational and bone formation in human bone populations.

Although the powerful effect of the nacre material chemistry in inducing bone regeneration has already been established, it is not known if this is due to the effect of the chemistry of the shell or of the topography of the surface. Since the powerful role of topography to control and refine differentiation is known, the topography of the nacre surface could have a similar effect here of inducing the bioactivity of nacre and therefore directing and controlling bone regeneration. To date, the osteogenic effect of a solid 2D nacre and prism surface on primary SSC behaviour and function remains unknown and the experiments discussed in this chapter set out to delineate and examine this further. In order to distinguish the chemistry of nacre and prism substrate from topography, a soft lithography approach was used to develop cell culture surfaces with nacre and prism topographical features but without the surface chemistry of nacre or prism shell regions. As the *P. maxima* shell nacre topography is known to enhance osteogenic differentiation, potential for direction towards osteogenesis will be studied through observations of alterations in cell morphology, gene expression markers and metabolomics following SSC culture on the topographical surfaces. The topography of these bioimprinted surfaces could provide mechanical and topographical cues to alter SSC behaviour, potentially towards an osteogenic fate.

5.1.1. Aims

Hypothesis:

Both nacre and prism topography can effect SSC fate and function, resulting in alterations in mRNA and metabolic profile. Nacre topography can enhance osteogenesis of SSCs.

There is currently very little known about the effect nacre topography can have on primary ages STRO-1+ SSCs, with previous studies using MSCs suggesting nacre topography can enhance osteogenesis. The effect the topography of the prism surface has on SSCs is unknown.

The aim of this chapter was to examine molecular phenotype and metabolic profile of STRO-1+ SSCs following culture on nacre and prism topographies. Specifically:

I. To study the potential of nacre and prism topographies to alter SSC size and shape
II. To investigate expression of known regulators of osteogenesis in SSCs when cultured on nacre and prism topographies.
III. To investigate the metabolic profile of SSCs cultured on nacre and prism topographies to examine similarities with metabolic changes occurring during osteogenesis.

5.2. Methods

5.2.1. Surface Generation

PCL prism and nacre topographical surfaces were fabricated as outlined in Figure 5.1 and the fabrication process detailed in [325]. This fabrication process was performed at University of Glasgow by Carol-Anne Smith and Vineetha Jerwara. Shell surface was first washed and air dried thoroughly. Following this, PDMS at 1:10 mixture was degassed and poured onto the shell and cured at 60°C for 1 hour. Following this, the PDMS was removed from the shell. Next PCL beads were washed in methanol and air dried. These beads were melted on a 80°C hot plate and the PDMS stamps pressed onto the molten PCL. This technique is known as hot-embossing. The PCL was then removed from the heat and allowed to cool at room temperature before the PDMS was removed, leaving positive replica of the shell topographies. Following this, the surfaces were stamped into 1 cm^2 circles and plasma treated to prepare for cell culture. At this stage, surfaces were packaged and posted to University of Southampton. Prior to culturing, surfaces were sterilised under ultraviolet light for 30 minutes and washed twice with sterile PBS.

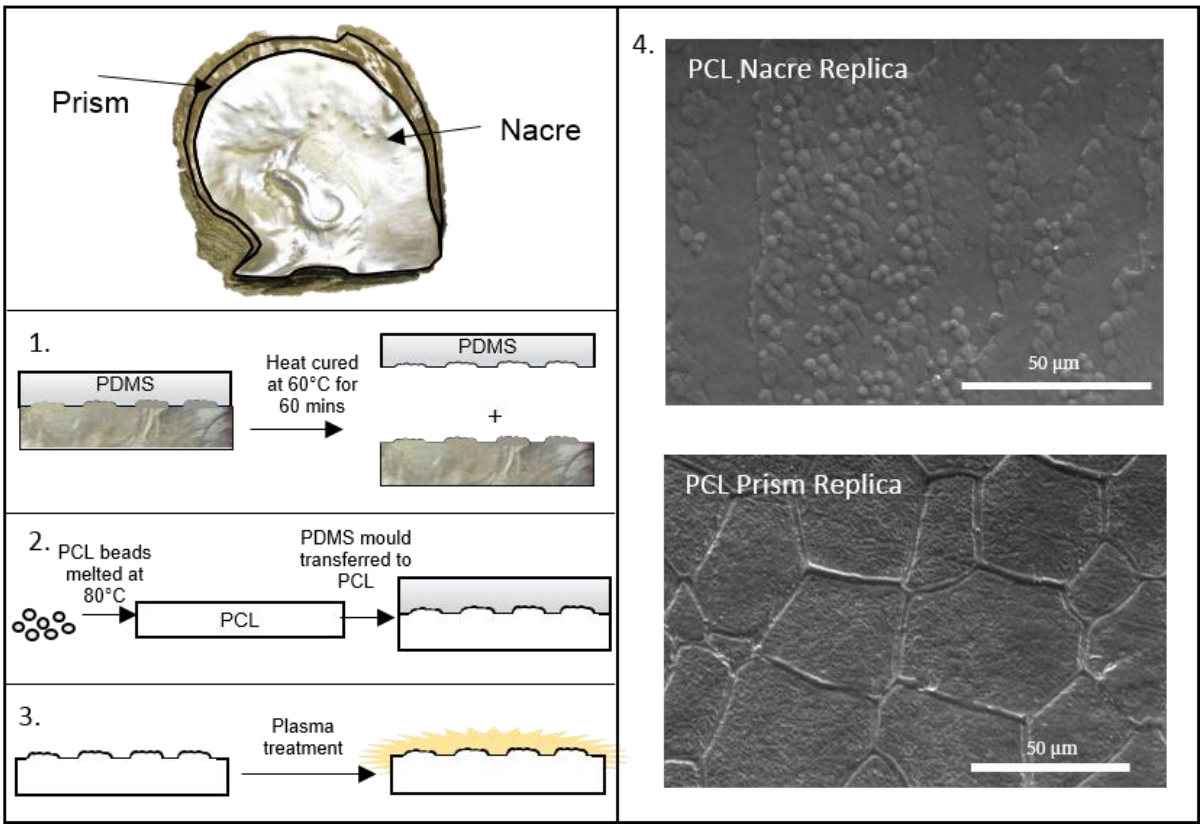

Figure 5.1. Schematic of biofabrication of PCL topographical surfaces. *1) Polydimethylsiloxane (PDMS) was poured on shell and heat cured at 60°C for 60 minutes. The mould was then removed from the shell. 2) Polycaprolactone (PCL) beads were washed in methanol and left to air dry. PCL beads were then melted at 80°C and PDMS mould transferred to molten PCL and features replicated using hot embossing. At this point, flat control PCL surfaces were generated using glass slides. When the PCL had cooled, the PDMS stamp was removed. 3) PCL topographical surfaces were prepared for cell culture with plasma treatment. 4) SEM images of PCL replicated nacre and prism topographies. To prepare for SEM, surfaces were sputter coated with 7 nm platinum.*

5.2.2. Scanning Electron Microscopy (SEM)

Surfaces were washed in sterile water and left to air dry. Surfaces were then sputter coated with 7 nm platinum using Q150T turbo-pumped sputter coater/carbon coater (Quorum Technologies Ltd, East Sussex, UK). In order to ensure charge distribution, Electrodag 1415 (AGG3648, Agar scientific, Essex, UK) was painted from the edge of surfaces to metal mounting stub. Samples were viewed using Quanta FEG 250 scanning electron microscope (SEM) (FEI™, Eindhoven, The Netherlands). The SEM was controlled by xT microscope control software, which also allowed for image capturing.

5.2.3. Metabolomics

Metabolites were extracted on days 10 and 21 post seeding. Metabolite extraction process was performed as published in Alakpa *et al* [325]. Surfaces were washed twice with chilled PBS. 400 µL chilled extraction buffer (chloroform:methanol:water, 1:3:1 (v/v)) was added to surfaces and agitated with shaker at 4°C. Samples were transferred to screw cap vials and centrifuged at 12,000 rpm for 20 minutes at 4°C to pellet cell debris. Supernatant was then transferred to screw cap vials. An liquid chromatography-mass spectrometry (LC-MS) system was used. Metabolomics analysis was performed at Glasgow Polyomics Centre, University of Glasgow by Isabel Vincent and Erin Manson with 10 µL aliquot of supernatant. Hydrophilic interaction liquid chromatography (HILIC) was carried out on UltiMate 3000 RSLC system (ThermoFisher Scientific, UK) using ZIC-pHILIC 5 µm column (150mm × 4.6 mm). The mobile phase was composed of 20 mM ammonium carbonate in either water or acetonitrile. A linear gradient was run for 24 minutes at 20% in water/80% acetonitrile, followed by change to 92%water/8% in acetronitrile for 8 minutes, before being brought down to 20 % water/80% acetonitrile. Orbitrap QExactive (ThermoFisher Scientific, UK) was used for MS analysis in polarity switching mode, within the mass range *m/z* 70-1050. Metabolite identification used Glasgow Polyomics Centre in-house XCMS/MzMatch/IDEOM pipeline using a set of standards to define mass and chromatographic retention times [326]. Peak intensities were normalised to protein concentration using BSA assay (ThermoFisher Scientific, UK). Ratios for each metabolite were calculated using peak intensity, relative to flat control surfaces and these were used for statistical analysis.

5.2.4. Statistical Analysis

Cell area measurements were performed with patients 51, 52 and 56, and data represented as mean ± SD. Gene expression experiments were performed with patients 51, 52, 56 and 71 and data represented with mean ± SEM. 2-way ANOVA followed by Tukey's post hoc was performed on results of cell area measurements and gene expression analysis. Patient female 56 was used for metabolomics experiments and performed in triplicates, with data represented as mean ± SD. One-way ANOVA followed by Dunnett's post hoc was performed on metabolite

intensity peak ratios. Principle component analysis was carried out using MetaboAnalyst 4.0. [327]. *P* values less than 0.05 were considered significant.

5.3. Results

5.3.1 Morphological changes on shell topographies

STRO-1 enriched SSCs were cultured on nacre and prism replicated PCL topographies and control flat surfaces, cultured under basal conditions, and the cell area measured at days 4 and 7, to ensure that cell density remained sufficiently low to allow for accurate single cell measurements. As these PCL surfaces are opaque, cells were stained with CellTracker Green and imaged using fluorescence imaging (Figure 5.2A-F) as described in section 2.7.1. Following on from imaging, cell images were processed using CellProfiler as detailed in section 2.7.2, and measurements for cell area and eccentricity were taken. On day 4, there were negligible differences in cell area between nacre, prism and control flat topography (Figure 5.2G). On day 7, as expected, there was a higher density of cells on the surfaces as the SSCs proliferate and an overall decrease in cell area was observed. From day 4 to day 7, average cell area decreased from 3250.9 ± 617.32 μm^2 to 2195.0 ± 359.0 μm^2 ($p<0.001$). On day 7, an increase in cell area on nacre surfaces (2472.2 ± 447.8 μm^2), compared to flat (2097.0 ± 220.1 μm^2) and prism (2015.9 ± 298.0 μm^2) was observed. However, due to patient variation between SSC samples, this did not reach statistical significance. Interestingly, there was negligible, insignificant differences between eccentricity of SSCs both with time and between surfaces (Figure 5.2H) and therefore cell elongation did not alter on topographical surfaces.

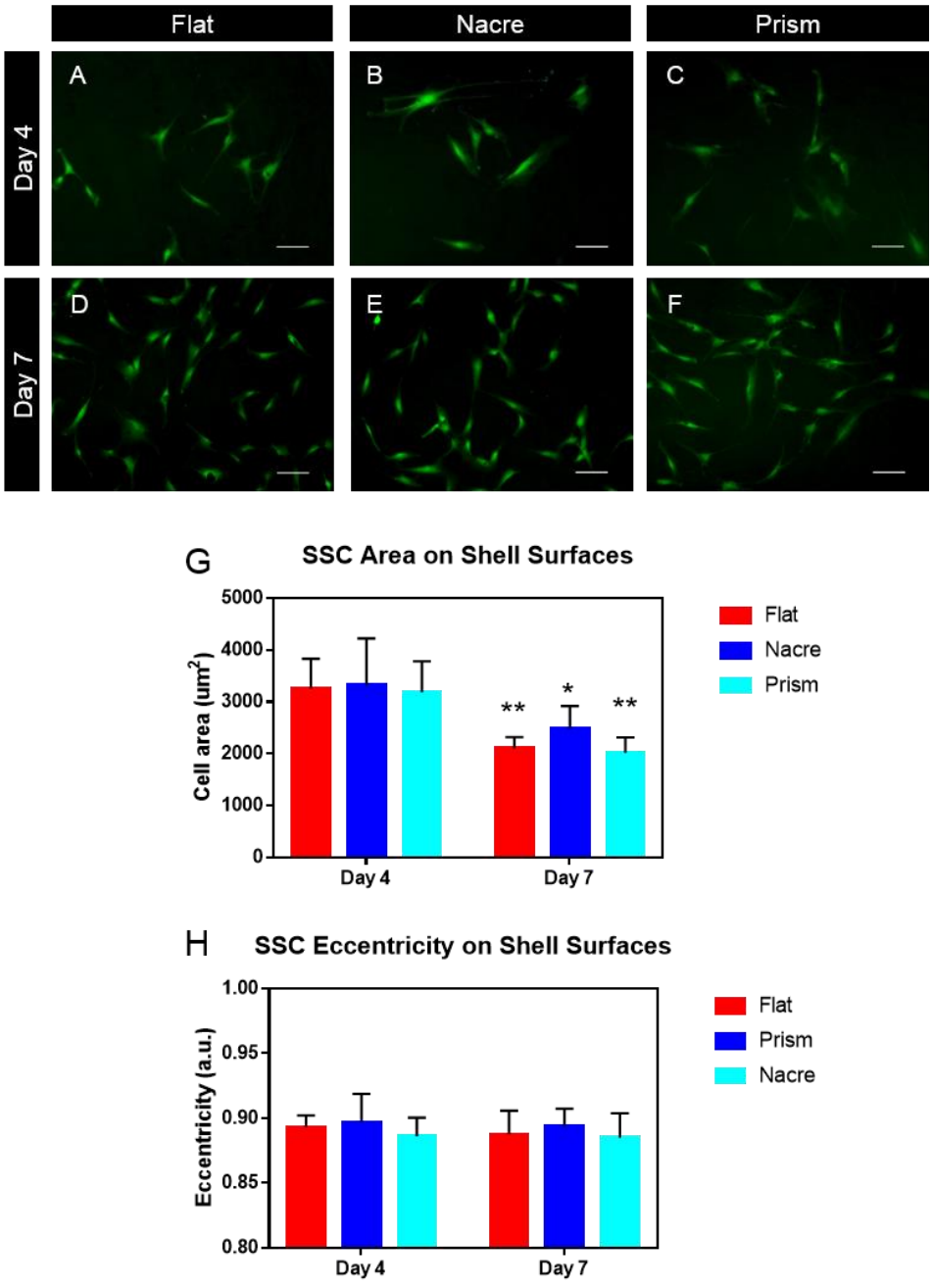

Figure 5.2. Morphology of SSCs cultured on nacre, prism and flat topographical surfaces. *Cells were stained with CellTracker Green and imaged at day 4 (A-C) and day 7 (D-F). Mean cell area (μm^2) was calculated at day 4 and day 7 (G). Eccentricity of SSC (a.u.) was calculated at day 4 and day 7, (n = 3 patients – females aged 51, 52 and 56), * = p<0.05, ** = p<0.01.*

5.3.2. Enhancement of osteogenic markers on shell topographies

To investigate osteogenic differentiation on the PCL topographies, expression of a range of early to late osteogenic markers were examined over 28 days of culture and compared to SSCs cultured on flat PCL surfaces under osteogenic conditions (Flat OM) (Figure 5.3A-E). A 28-day culture was chosen as osteogenic differentiation can take up to 28 days to reach full maturation and full examination of any potential osteogenic differentiation. *RUNX2* expression did not vary between the topographical surfaces and flat control surfaces, however a decrease in expression in *RUNX2* was identified on nacre topographies on day 28 (Figure 5.3A). It was apparent that expression of *RUNX2* was considerably higher in SSC cultured under osteogenic conditions. *ALP* expression on nacre topographies was slightly higher compared to flat and prism topographies on days 14, 21 and 28 (Figure 5.3B) and these differences were found to be non-significant. However, the expression measured on nacre topographies on days 14, 21 and 28 was less than the increase in *ALP* expression observed in the presence of osteogenic media, and again these differences were found to be non-significant. Differences in expression between topographical surfaces at recorded time points was minimal for *COL1A1* expression. Interestingly, expression of *COL1A1* was found to be lower in the presence of OM compared to flat surfaces, at all time points.

On day 21, there was a non-significant increase in expression of *OCN* on SSCs cultured on both nacre (27.1 ± 15.2) and prism (21.8 ± 7.1) PCL topographies compared to the flat control (14.7 ± 3.7). On day 14 a non-significant increase in *OPN* expression was observed in nacre topographies (10.1 ± 7.4) compared to both prism (8.9 ± 5.4) and flat control (6.7 ± 3.7). This however is very small increase when compared to the increase in expression of *OPN* observed in the presence of osteogenic media (51.0 ± 14.7). It should be noted that there was a significant variation in expression from different SSC patient donors.

Expression of miRNAs known to be associated with osteogenesis, miR-138 and miR-218, were also studied on nacre and prism topographies. Measurement taken at day 21 indicated no significant difference between flat and shell topographies (Figure 5.4A and B). Further to this, expression was similar on flat, nacre and prism topographies when studying miR-138 expression, expression was similar between the three studied surfaces here (Figure 5.4A). Expression was measured as 1.1 ± 0.3 on nacre topographies and 1.1 ± 0.4 on prism topographies. For miR-218 expression, expression was measured to increase 1.4 ± 0.8 on nacre topographies however decreases on prism topographies to 0.8 ± 0.3 fold change in expression (Figure 5.4B). Immunofluorescence staining of OPN confirmed gene expression data, indicating an increase in OPN levels on days 14 and 21 comparing nacre topographies to flat control (Figure 5.4C).

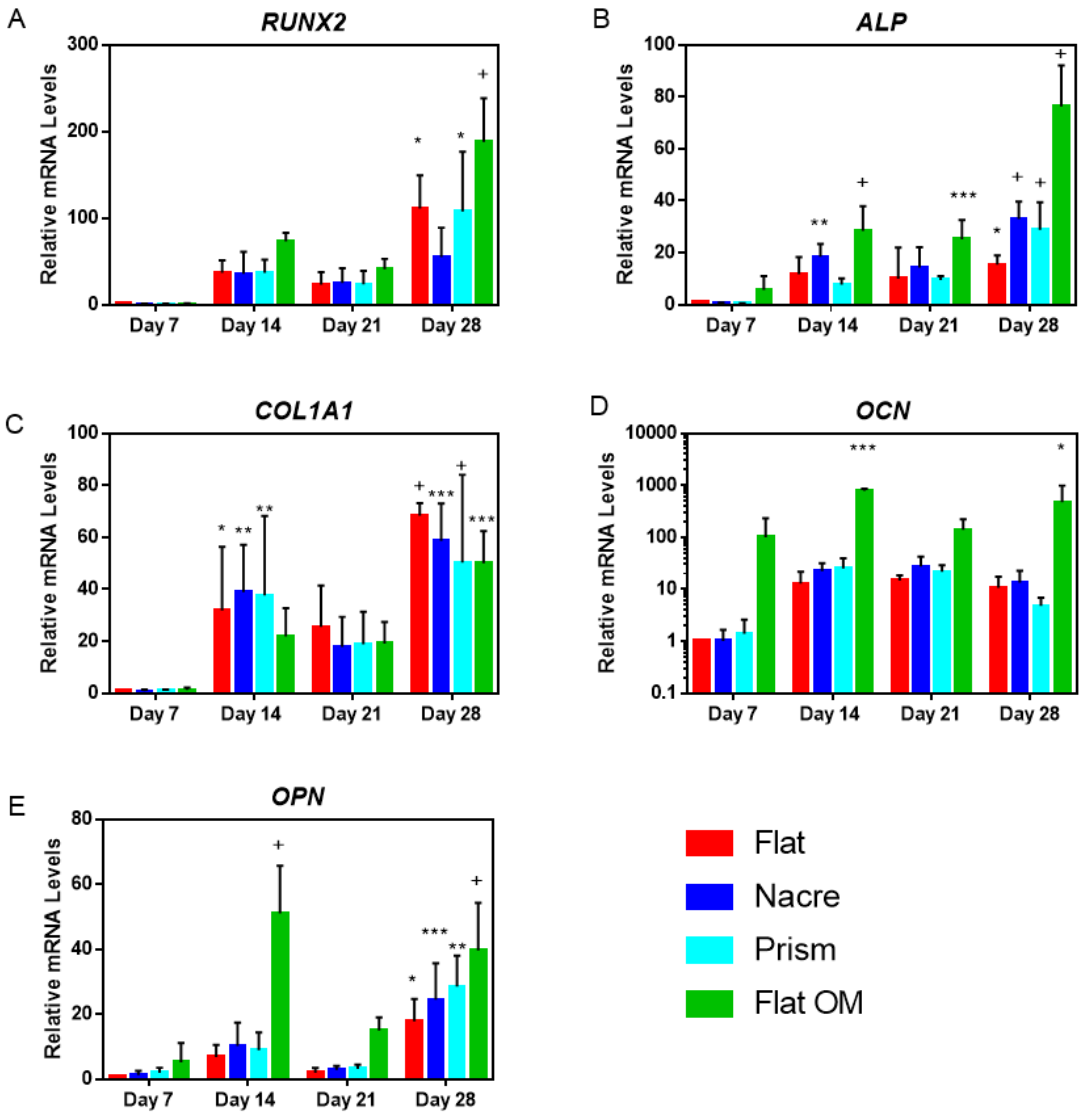

Figure 5.3. Changes in osteogenic mRNA and protein on shell topographies. *Expression of RUNX2, ALP, COL1A1, OCN and OPN mRNA in SSC cultured on nacre, prism and flat osteogenic media (flat OM) topographies over 28 days (A-E). n = 3 patient samples, 2-way ANOVA was performed on the data and every measurement compared to expression of relative mRNA level on flat surface on day 7. * = p<0.05, ** = p<0.01, *** = p<0.001, + = p<0.0001.*

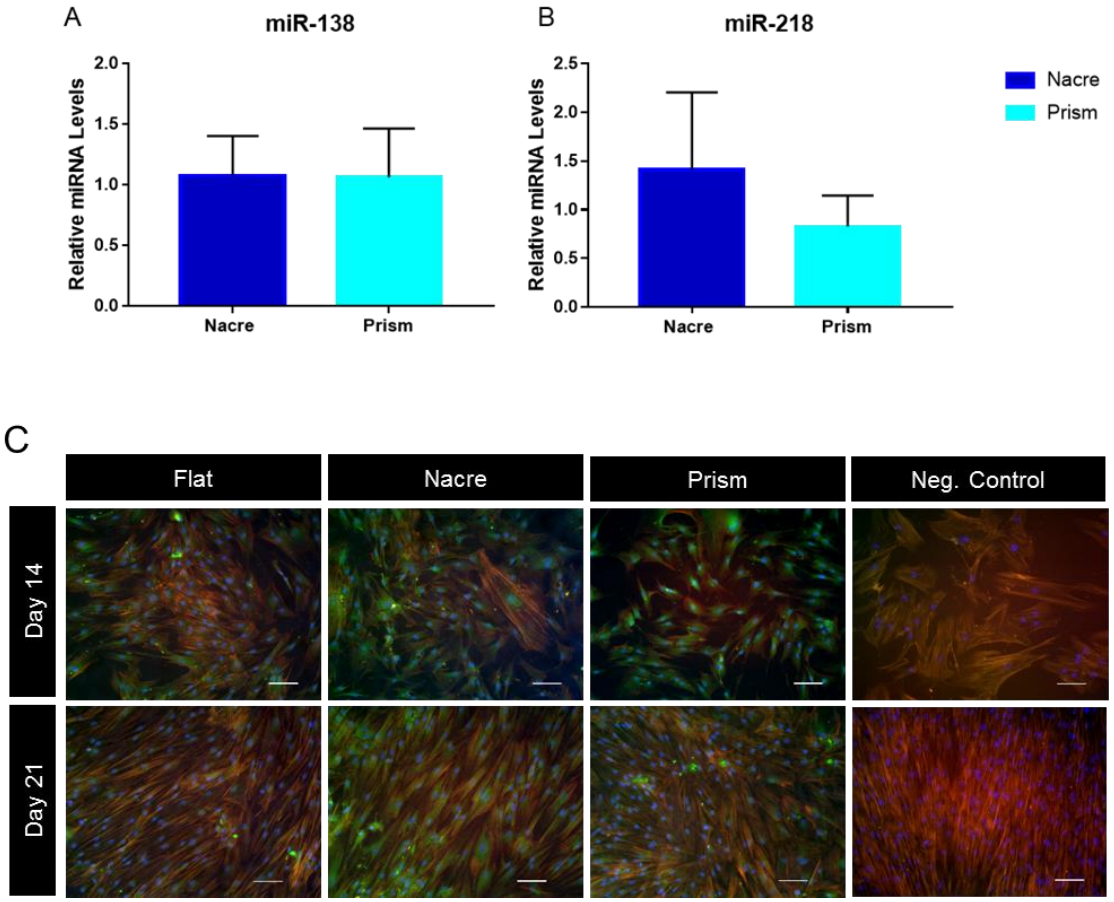

Figure 5.4. Expression of osteogenic miRNA and protein in SSCs cultured on shell topographies. *Expression of miRNA-138 (A) and miR-218 (B) on nacre (dark blue) and prism (light blue) topographies relative to flat topographies, following 21 day in culture. Expression was normalised to U6 snRNA expression using the* $2^{\Delta\Delta C_T}$ *method. n = 3 patient samples. (C) Immunofluorescence of OPN on days 14 and 21 on flat, nacre and prism topographies. Negative control is SSCs stained in the absence of anti-OPN antibody, cultured on standard commercial tissue culture plastic. White arrows indicate area of OPN protein. Scale bar = 100 µm.*

5.3.3. SSC proliferation and metabolic activity on shell topographies

Following on from alterations in expression of osteogenic markers on shell topographies, SSC proliferation while cultured on shell topographies was studied. To do this, SSCs were cultured on nacre, prism and flat control topographies along with flat OM conditions for 7, 10, 14, 21 and 28 days and samples taken for analysis. Absolute DNA concentration was measured using the methods described in section 2.6. The results (Figure 5.5A) indicated that on all topographies, SSC DNA and therefore cell proliferation had increased with time over 28 days, with increase from day 7 to day 28 significant with $p \leq 0.0001$. At each given time point, there was no clear topography which resulted in a higher or lower cell proliferation rate. For example on day 21 cell number was highest on prism topographies at 290.8 ± 54.4 whereas on day 28 cell number was highest on nacre topographies at 297.4 ± 22.3.

Following on from studying cell proliferation on the topographical surfaces, cell metabolic activity was measured using alamarBlue® reagent. The fluorescence increase obtained was divided by DNA concentration to indirectly quantify metabolic activity per cell (Figure 5.5B). The results indicated for all the surfaces SSCs were cultured on, metabolic activity peaks on day 10 and decreases to day 28. Although there was no significant difference between the surfaces at a given time point, there was significant decrease with time from day 10 to day 28 ($p \leq 0.01$) for each surface. It was apparent that on day 10, there was an increase in metabolic activity on nacre topographies (measured at 439.5 ± 64.8, compared to 283.4 ± 57.9 on flat OM surfaces). This increase although not significant, was maintained on day 14 for nacre topographies. However, by day 28 metabolic activity has dropped on all surfaces to 51.9 ± 16.5 on nacre topographies and 61.8 ± 44.0 on flat OM topographies.

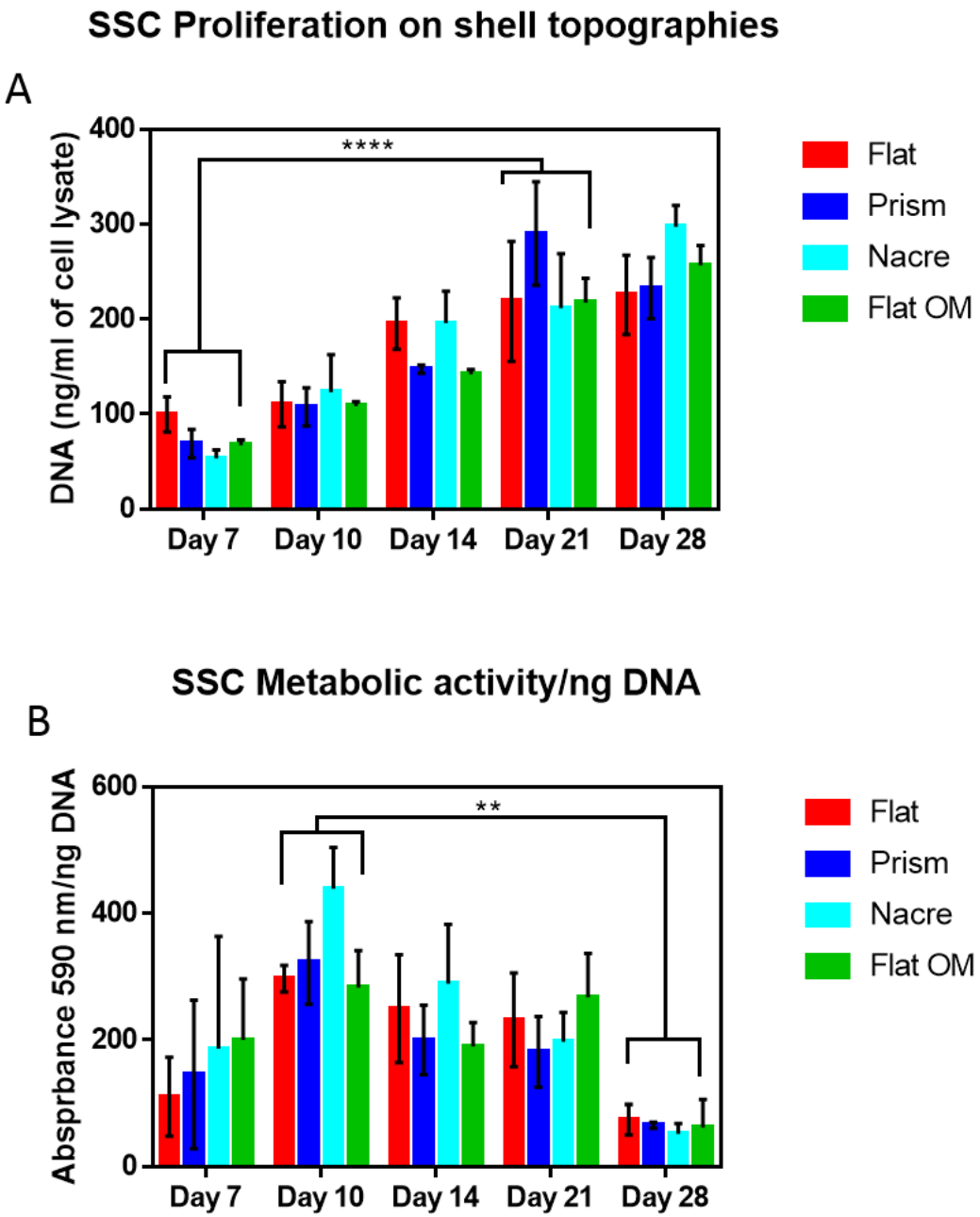

Figure 5.5. Proliferation and metabolic activity of STRO-1 SSCs cultured on shell topographies for 28 days. *SSC cultured on flat control (red), prism (dark blue), nacre (light blue) and flat osteogenic media (pink) surfaces for 28 days. (A) Measurements of DNA concentration determined using PicoGreen dsDNA binding reagent. (B) Measurement of metabolic activity, determined using alamarBlue® reagent, as a function of DNA concentration. n = 3 patients. ** =p≤0.01, **** =p≤0.0001.*

5.3.4. Cellular metabolomic profile of SSCs on shell topographies

To determine how metabolic pathways within SSC populations responded to the nacre and prism topographies, we performed metabolomics analysis using LC-MS on SSCs cultured on the shell topographies. For this experiment, day 10 and day 21 were chosen as during initial pilot studies, these time points displayed increased SSC metabolomic activity and therefore would reflect activity of metabolically active SSCs. We selected a 10-day time point for metabolomics to ensure that cell density was sufficiently low enough to avoid / minimise any cell interactions and ensure analysis was solely a reflection of the effect of the topography in the differentiation process of SSCs.

An overview of average metabolite intensity at day 10 detailed an increase in intensity on nacre topographies ($p<0.05$) and a decrease in intensity on prism topographies ($p=0.0455$) relative to flat control (Figure 5.6A-C). Interestingly, the metabolite intensity ratio was similar from nacre topography (2.32 ± 0.30) to flat control exposed to osteogenic media (Flat OM) (2.35 ± 0.26) (Figure 5.6A), and this was also observed on a heatmap displaying individual metabolites on day 10 (Figure 5.7). When this was analysed by carbohydrate- and lipid-associated metabolites, the similarity between nacre topography and flat OM remained (Figure 5.6B-C). At day 21, usually associated with differentiation towards a mature osteogenic phenotype, the metabolite intensity was altered in comparison to the day 10 (Figure 5.6D-F). Metabolite intensity on flat control and flat OM was observed to be similar (1.02 ± 0.28 and 1.16 ±0.31 respectively). Critically, an increase in metabolite intensity was only observed on day 21 on nacre topographies (1.54 ± 0.6) (Figure 5.6D). This is reflected in the heatmap of metabolites identified on day 21 (Figure 5.8). The heatmap also showed differences between the triplicates. SSCs on prism surfaces appeared to be more metabolically active at on day 21 (Figure 5.6D), compared to day 10 (Figure 5.6A) as the intensity compared to flat control increased from 0.58 ± 0.1 to 1.07 ± 0.1. PCA plots show linkage between flat OM and nacre, and flat and prism surfaces on day 10 (Figure 5.6G). However, this was lost by day 21 (Figure 5.6I). Individual metabolites L-creatine, L-glutamine, L-pyruvate and L-carnitine follow a similar result to the global trend (Figure 5.9).

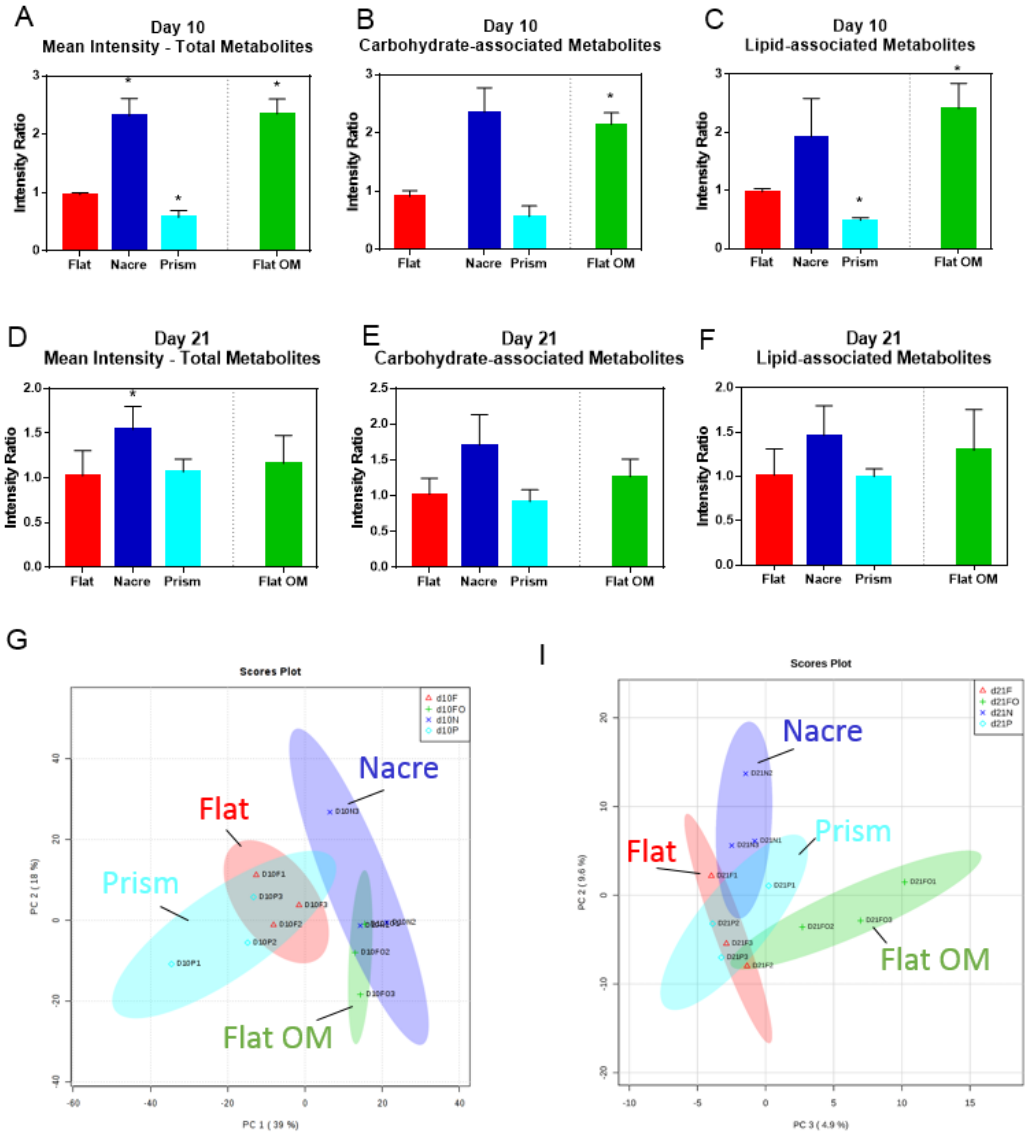

Figure 5.6. Metabolomic analysis of SSCs cultured on nacre and prism shell topographies. *Intensity ratio, relative to flat control, of total metabolites (A+D), carbohydrate-associated metabolites (B+E), and lipid associated metabolites (C+F) for days 10 (A-C) and 21 (D-F). Flat OM represents flat surface cultured in osteogenic media. Peak intensity ratio normalised to flat control, n = 3 replicates. PCA plots for day 10 (G) and 21 (I).*

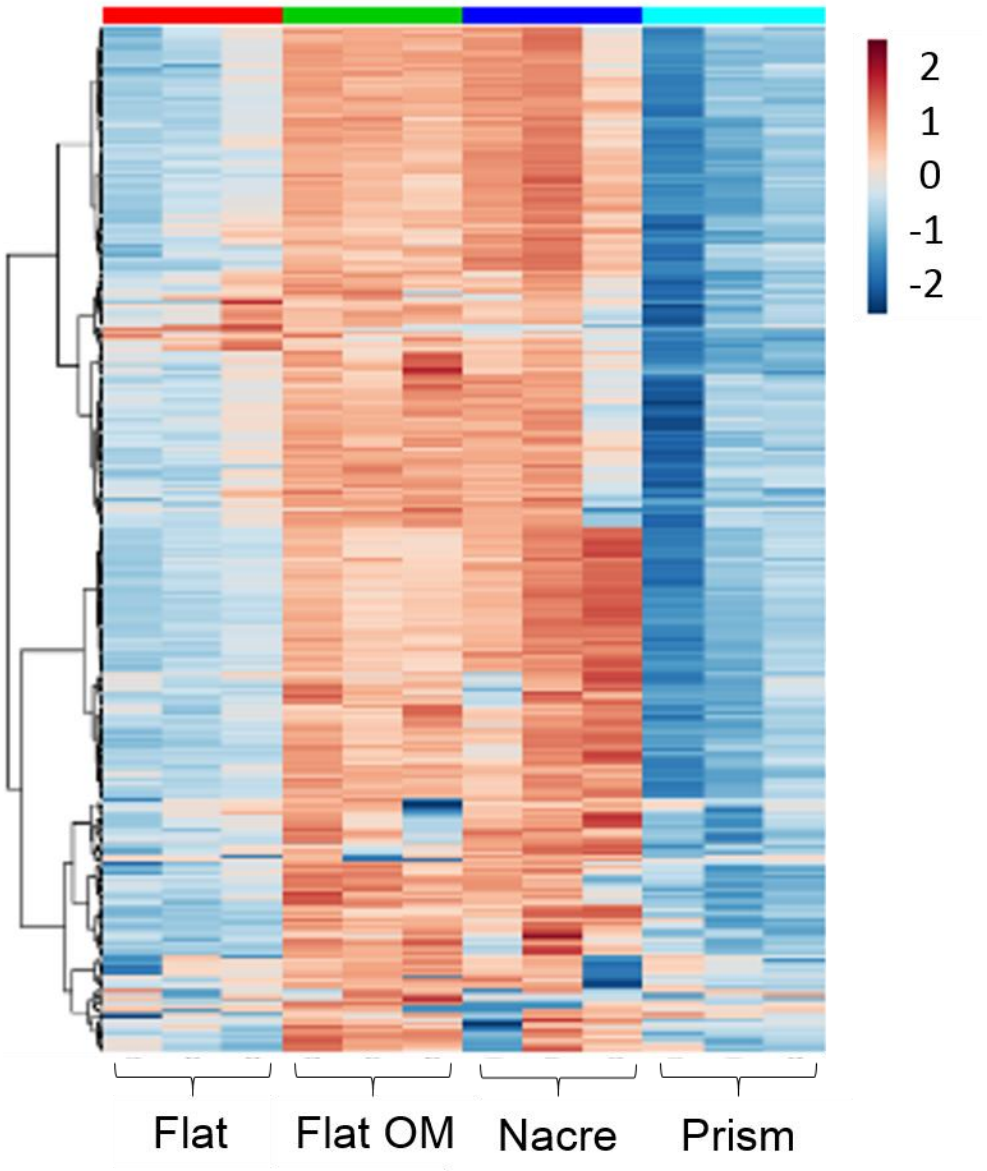

Figure 5.7. Heatmap of metabolites present in SSCs cultured on shell topographies for 10 days. *Heatmap generated using mean peak intensity using Metaboanalyst software. Each metabolite is represented by one box in the heatmap and for clarity, name of metabolite has been omitted. Metabolites were sorted into functional groups prior to heatmap generation. Legend upper right. Flat PCL surfaces, Flat Osteogenic Media (OM), Prism PCL replicas and Nacre PCL replicas.*

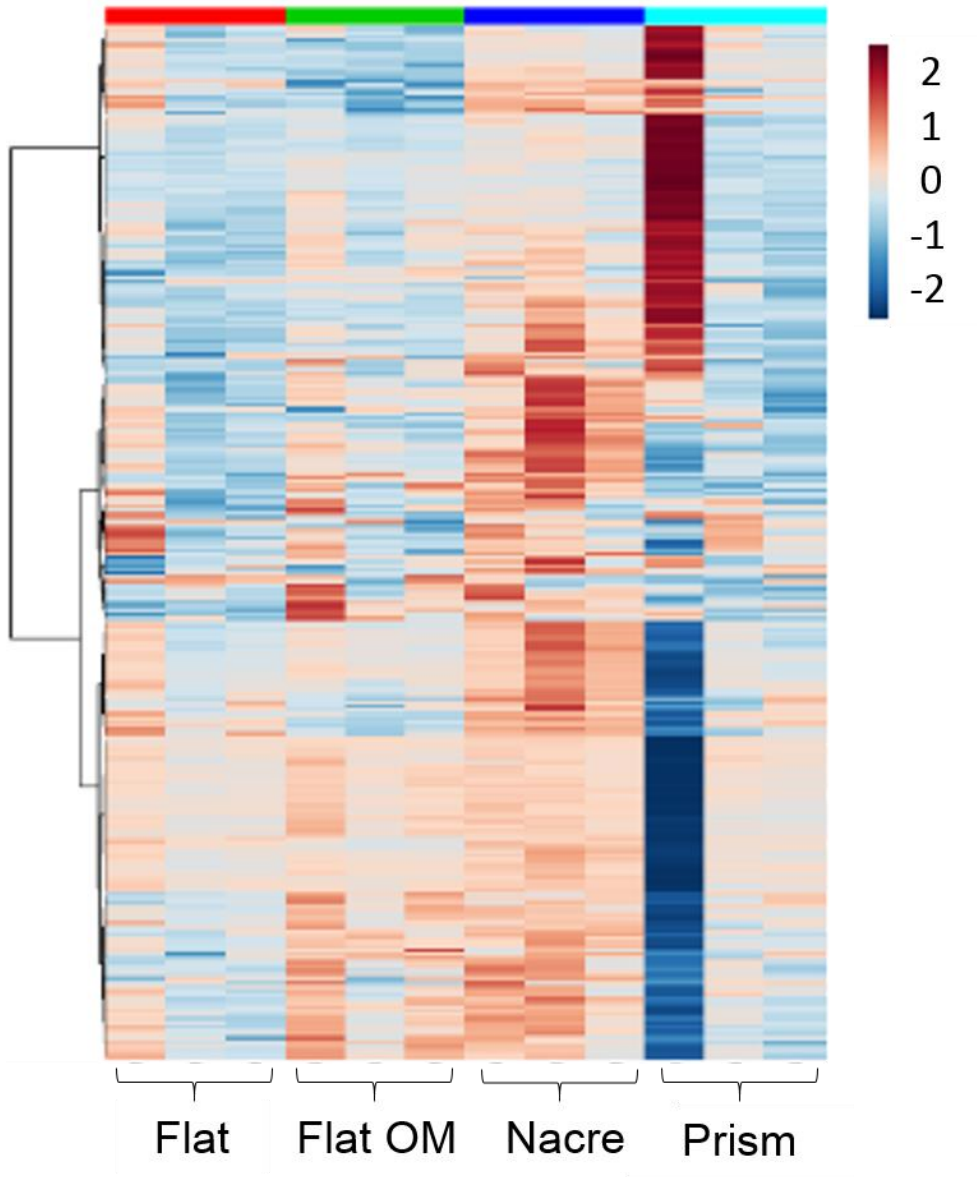

Figure 5.8. Heatmap of metabolites present in SSCs cultured on shell topographies for 21 days. *Heatmap generated using mean peak intensity using Metaboanalyst software. Each metabolite is represented by one box in the heatmap and for clarity, name of metabolite has been omitted. Metabolites were sorted into functional groups prior to heatmap generation. Legend upper right. Flat PCL surfaces, Flat Osteogenic Media (OM), Prism PCL replicas and Nacre PCL replicas.*

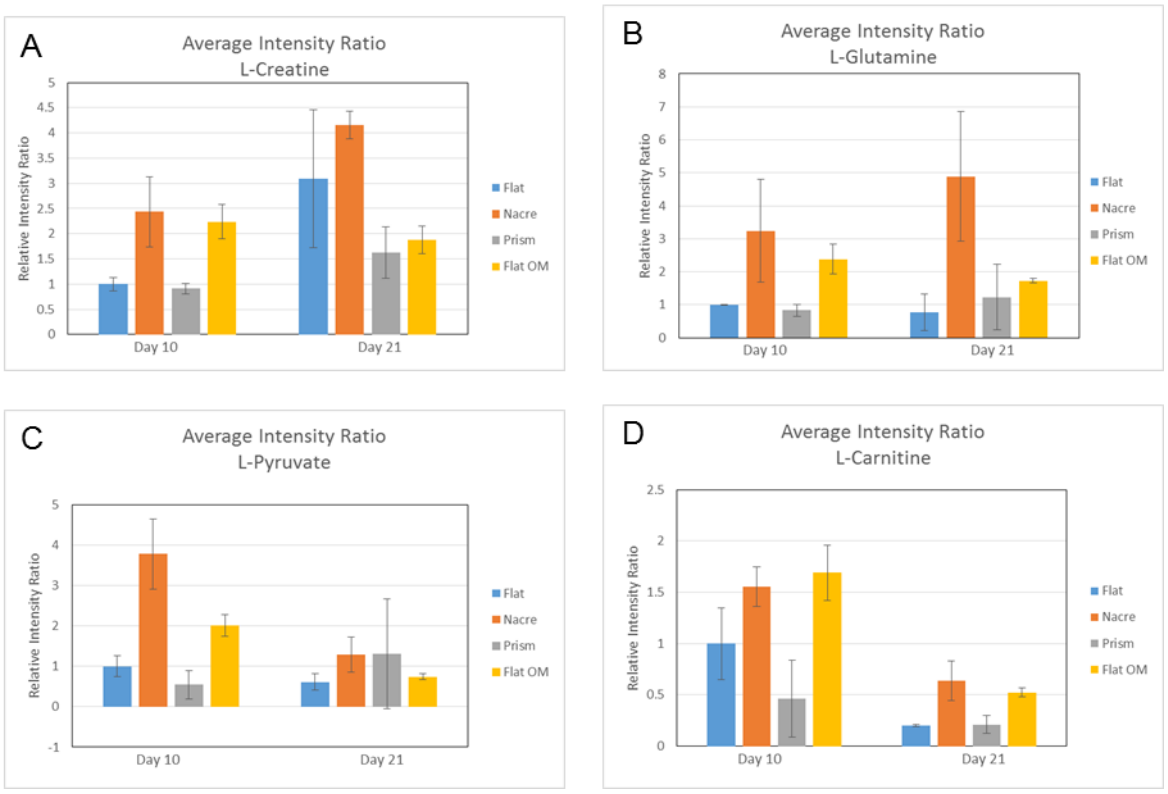

Figure 5.9. Average intensity of metabolites identified by metabolomics profiling in SSCs cultured for 10 and 21 days. *A - L-creatine, B - L-glutamine, C - L-pyruvate, D - L-carnitine. Samples of one patient were ran in triplicates and data is represented as mean ± SD.*

5.3.5. Identified networks and canonical pathways associated with changes in metabolites

Through the use of Ingenuity Pathway Analysis (IPA) software (Qiagen, UK), canonical pathways associated with nucleotide metabolism were analysed (Figure 5.10). IPA investigates all known metabolites associated with these pathways and if they are up on nacre and prism topographies or flat OM. The majority of metabolites identified were upregulated on nacre topographies and flat OM on day 10 (Figure 5.10A+C). On prism topographies, metabolites associated with nucleotide metabolism were down regulated (Figure 5.10B). As identified on analysing peak intensity, on day 21 an increase in metabolite intensity on nacre topographies was observed compared to metabolites on flat OM surfaces (Figure 5.10D+F).

Application of Ingenuity Pathway Analysis software (Qiagen, UK), demonstrated networks of associated metabolites generated including links to proteins known to be associated with metabolites from literature databases that predict the protein regulation / activation state. The network generated for nacre PCL topography and flat OM conditions were similar at day 10, indicating potential for a comparable cellular phenotype (Figure 5.11A+C). At day 21, the metabolomic networks generated for nacre topography showed enhanced activation in comparison to flat OM (Figure 5.11A+C). At day 10 on both nacre topographies and flat OM, key hubs associated with osteogenic differentiation were identified to be activated including ERK1/2, acetyl co-A carboxylase (ACAC) and collagen 1α, and increase in metabolites associated with the tricarboxylic acid cycle (TCA) cycle. On prism topography, the opposite was observed and the network generated displayed different activation levels (Figure 5.11). Here, at day 10 a predicted decrease in ERK1/2, ACAC and collagen 1α was discovered. Added to this, an activation of lactate dehydrogenase was observed in prism associated networks.

On networks generated for day 21 (Figure 5.12), it could also be seen that metabolic activity slowed down on flat OM surfaces. For example, there was a high number of metabolites including creatine displaying decreased levels relative to flat control surfaces (Figure 5.12C). This is compared to SSCs cultured on nacre topographies where level of metabolites was found to increase relative to flat control surfaces (Figure 5.12A). Although networks generated on nacre topography and flat OM conditions have variation in levels of metabolites, the predicted activation of proteins did not alter in numerous hubs. Collagen 1α and ERK1/2 and predicted decrease in activity of lactate dehydrogenase. Due to difficulties in generating the high number of samples required for metabolomic analysis, one patient (female aged 56) was used for this experiment and examined in triplicates.

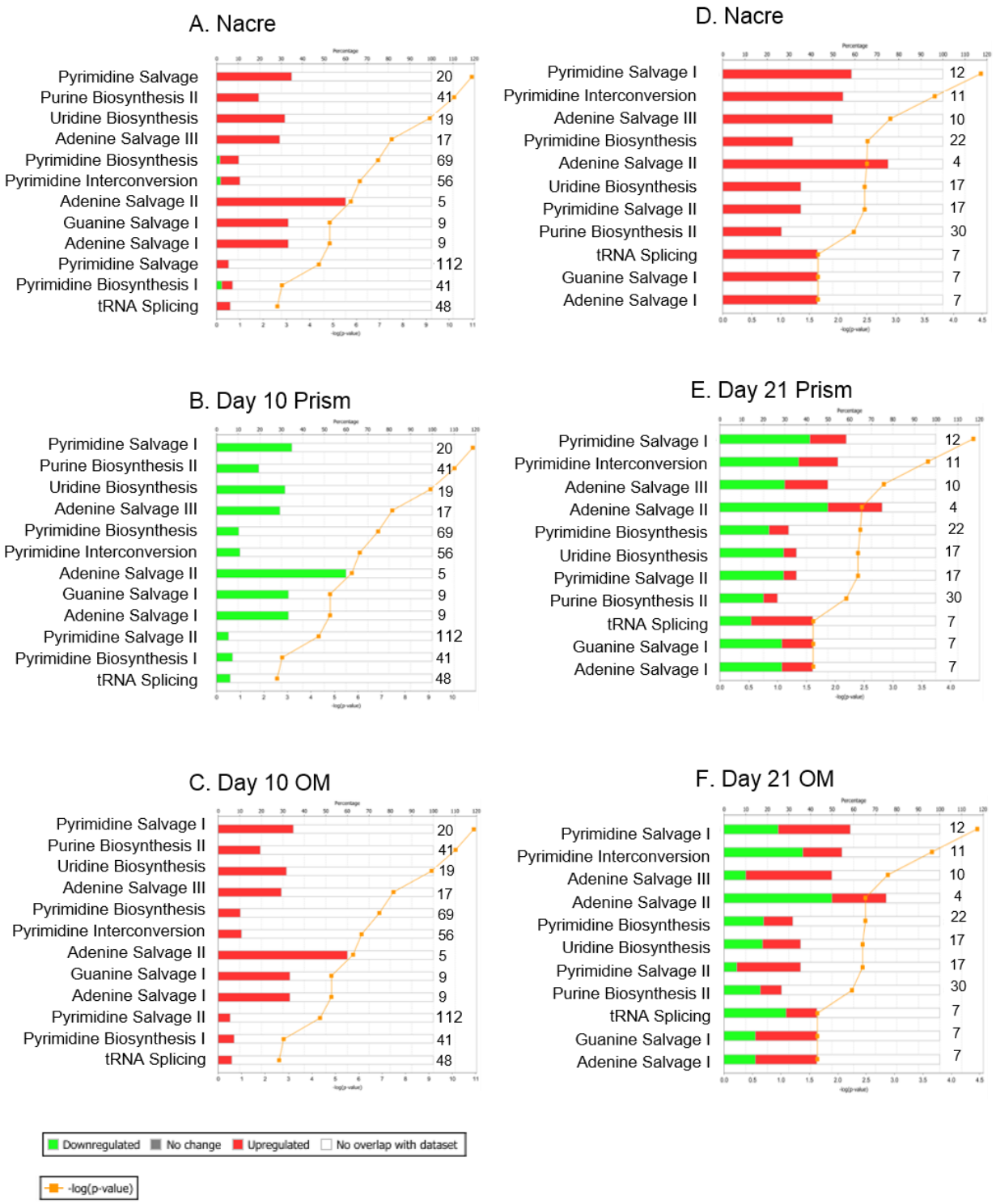

Figure 5.10. Nucleotide-metabolism associated canonical pathways for SSCs cultured on nacre, prism and control OM surfaces on day 10 and 21. *IPA generated canonical pathways associated with nucleotide metabolism for SSC on day 10 on nacre topographies (A), prism topographies (B), and flat osteogenic media control (C). Canonical pathways on day 21 on nacre topographies (D), prism topographies (E), and flat osteogenic media control (F). Shown in either red or green and on the numbers to the right of each bar was the number of metabolites identified in the sample out of all possible known associated metabolites. Threshold considered for the analysis was –log(p-value)>1.5. Legend on bottom left.*

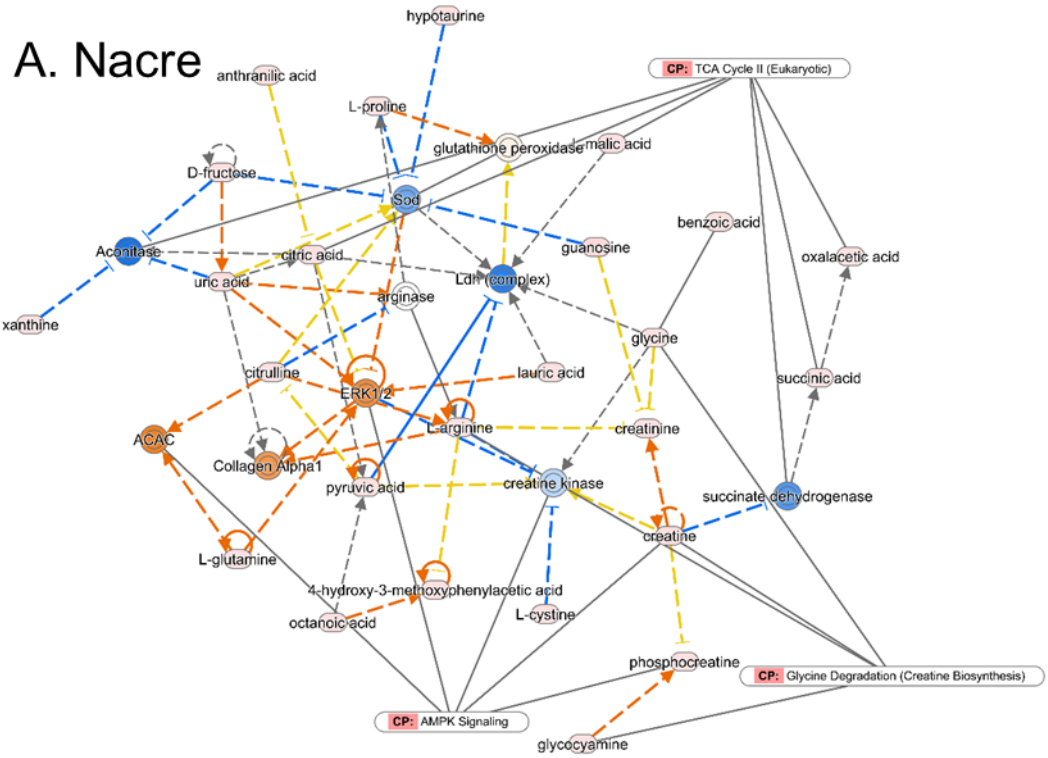
A. Nacre
hypotaurine
anthranilic acid
CP: TCA Cycle II (Eukaryotic)
L-proline
glutathione peroxidase
malic acid
D-fructose
Sod
benzoic acid
Aconitase
citric acid
guanosine
oxalacetic acid
uric acid
Ldh (complex)
arginase
xanthine
glycine
citrulline
lauric acid
succinic acid
ERK1/2
L-arginine
creatinine
ACAC
Collagen Alpha1
pyruvic acid
creatine kinase
succinate dehydrogenase
creatine
L-glutamine
4-hydroxy-3-methoxyphenylacetic acid
L-cystine
octanoic acid
phosphocreatine
CP: Glycine Degradation (Creatine Biosynthesis)
CP: AMPK Signaling
glycocyamine

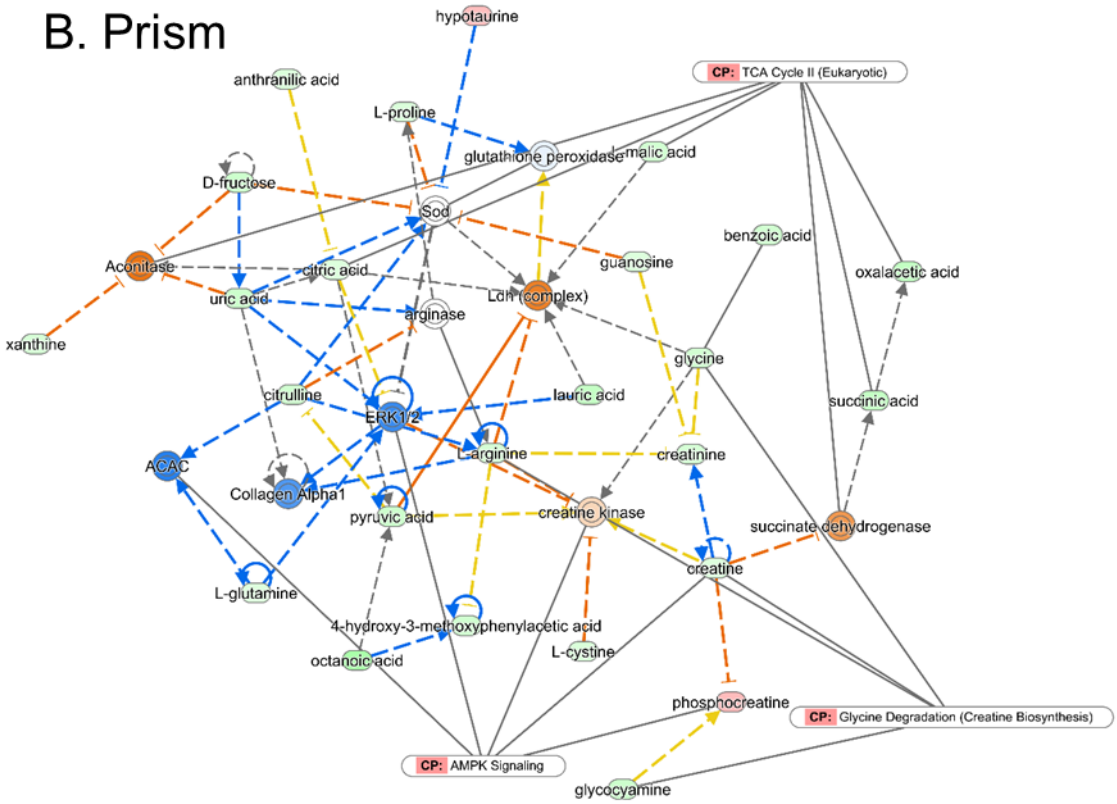
B. Prism
hypotaurine
anthranilic acid
CP: TCA Cycle II (Eukaryotic)
L-proline
glutathione peroxidase
malic acid
D-fructose
Sod
benzoic acid
Aconitase
citric acid
guanosine
oxalacetic acid
uric acid
Ldh (complex)
arginase
xanthine
glycine
citrulline
lauric acid
succinic acid
ERK1/2
L-arginine
creatinine
ACAC
Collagen Alpha1
pyruvic acid
creatine kinase
succinate dehydrogenase
creatine
L-glutamine
4-hydroxy-3-methoxyphenylacetic acid
L-cystine
octanoic acid
phosphocreatine
CP: Glycine Degradation (Creatine Biosynthesis)
CP: AMPK Signaling
glycocyamine

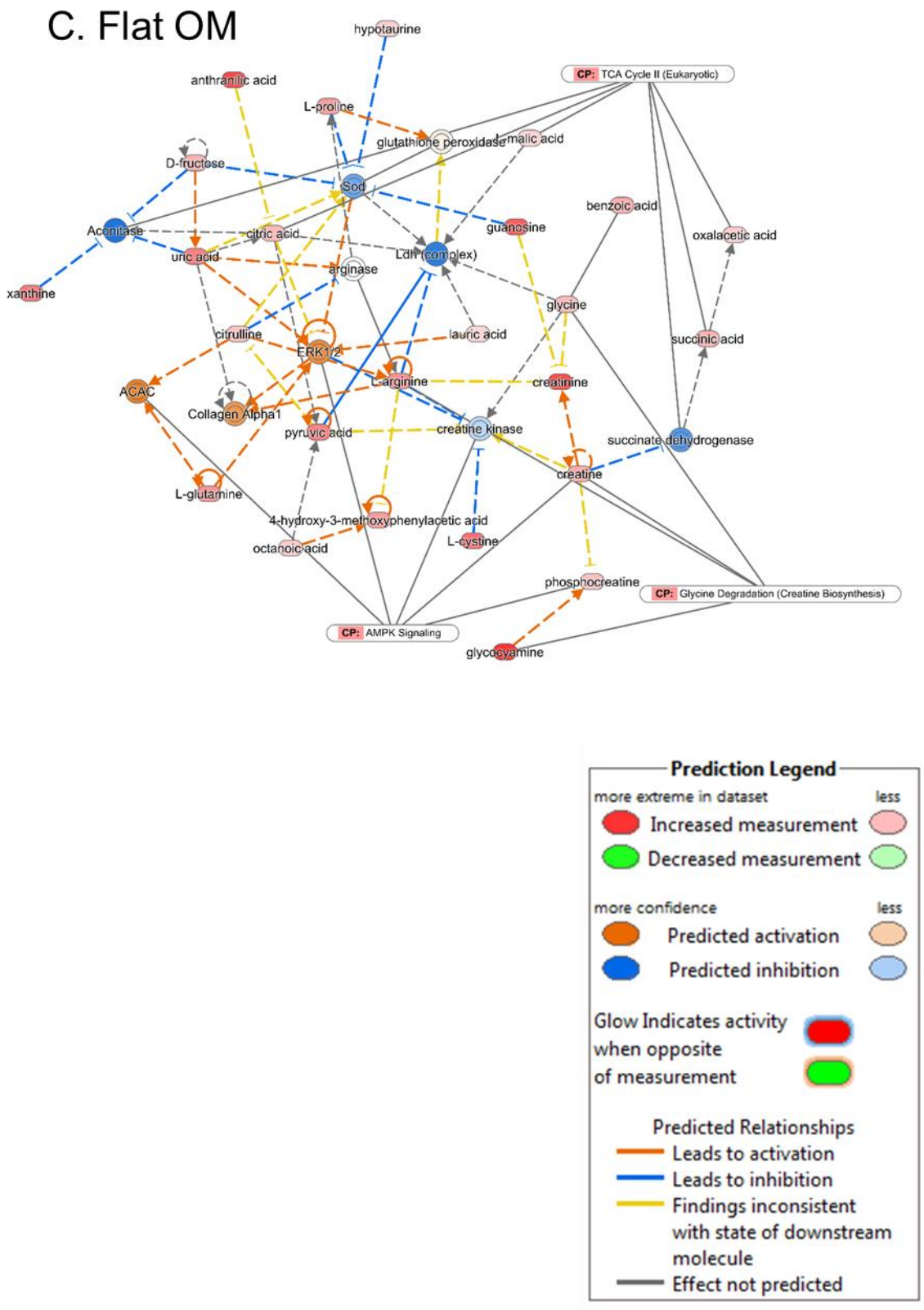

Figure 5.11. Metabolomic networks for SSCs cultured on nacre, prism and control OM surfaces on day 10. *IPA generated networks on nacre (A), prism (B), and flat osteogenic media control (OM) (C). Legend on bottom right.*

A. Nacre

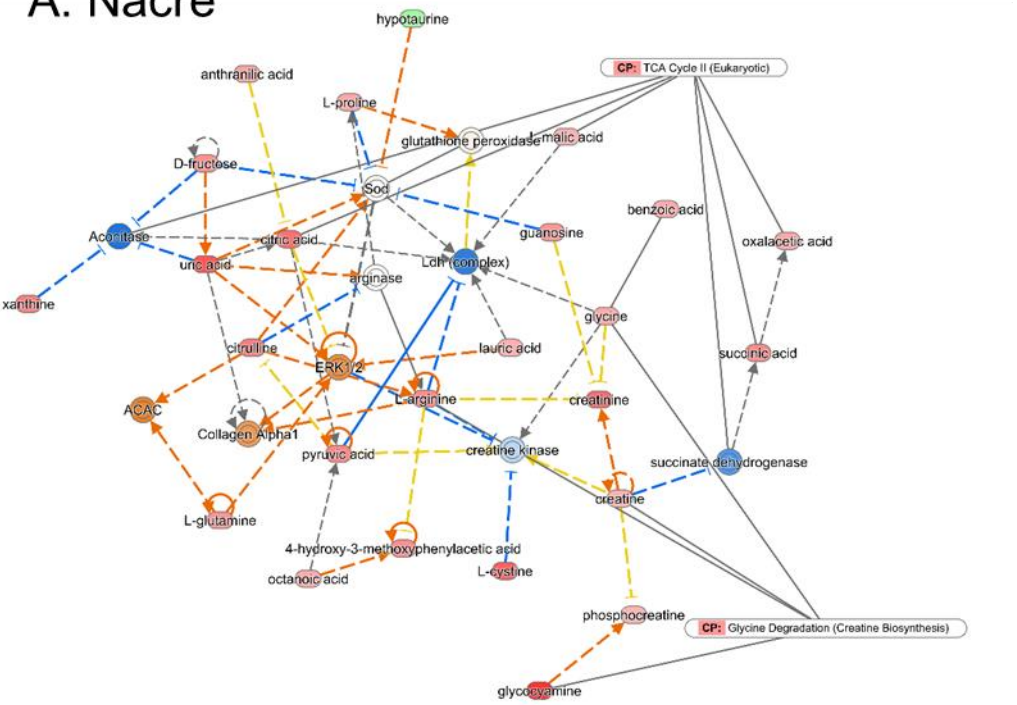

B. Prism

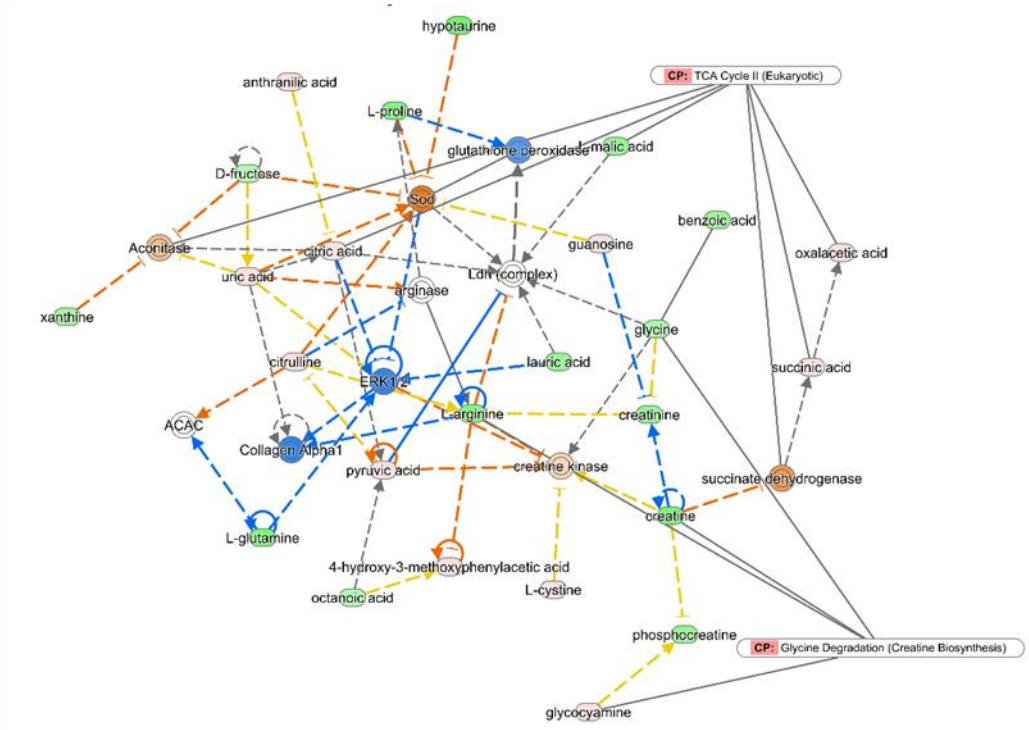

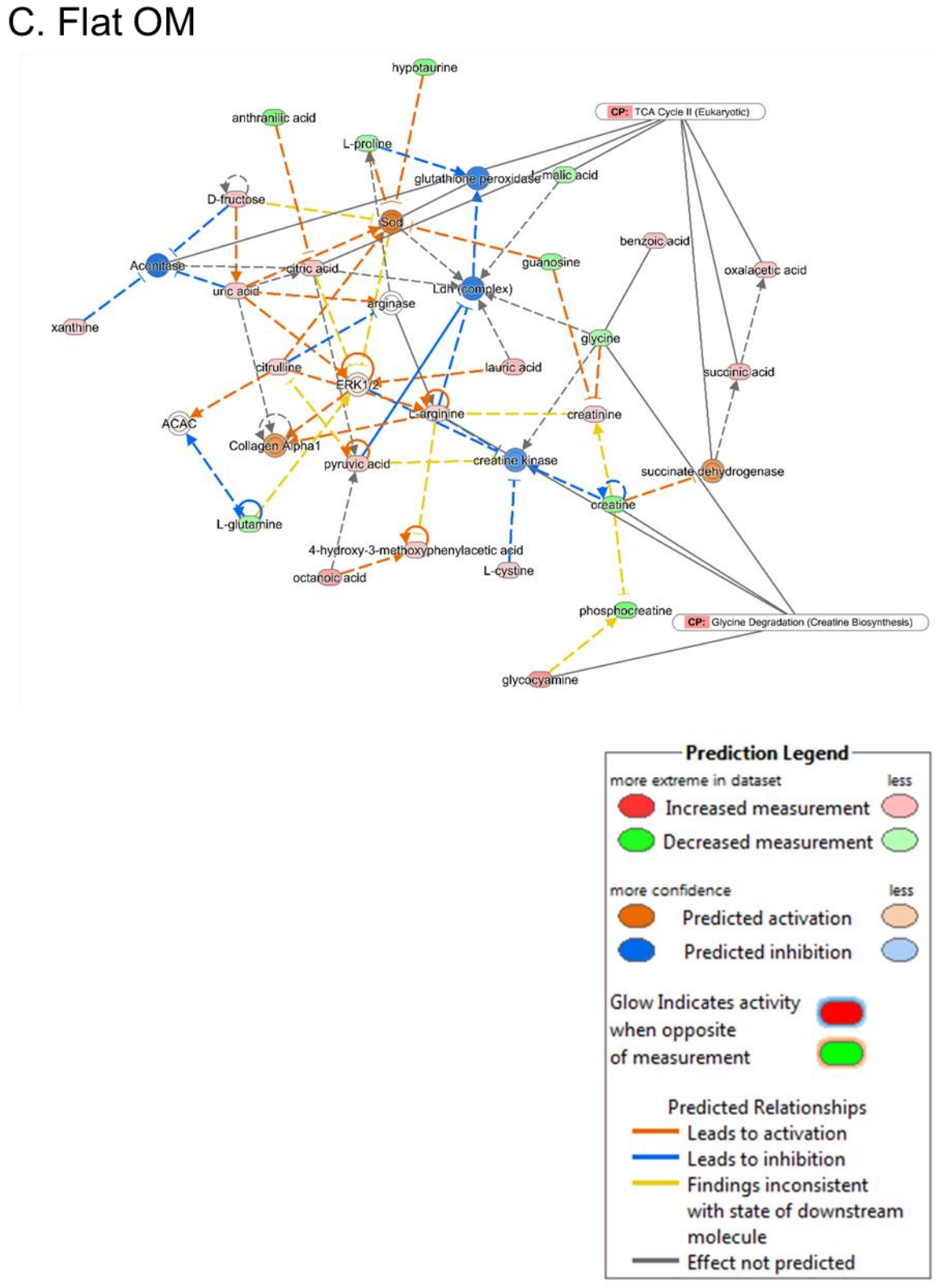

Figure 5.12. Metabolomic networks for SSCs cultured on nacre, prism and control OM surfaces on day 21. *IPA generated networks on nacre (A), prism (B), and flat osteogenic media control (OM) (C). Legend on bottom right.*

5.4. Discussion

The current study has demonstrated the ability of SSCs to respond to shell topographical surfaces. The nacre surface induced osteogenic differentiation of human SSCs, with an increase in *OPN, OCN* and *ALP* expression, compared to flat control PCL surfaces. Furthermore, the similarities in metabolic profile between SSCs on nacre surfaces compared to SSCs cultured in osteogenic media strengthens the potential for the nacre surface to induce osteogenic differentiation. In contrast, primary SSCs cultured on the prism surface presented a distinct and, significantly, a different response. On prism surfaces, a mixed increase in expression of osteogenic markers was observed, with an increase in *OCN* but not *ALP* compared to flat control without OM. Through the use of ingenuity pathway analysis for metabolomics profiling, SSCs cultured on prism surfaces displayed considerably less activity compared to flat control.

Previous studies have suggested an increase in cell area is observed during osteogenic differentiation [302]. In the current studies, a non-significant increase in cell area was observed on nacre surfaces, and demonstrated the ability of SSCs to respond to nacre topographical surface features. Examination of the expression of master bone-regulator *RUNX2*, indicated no effect of topography on gene expression. *RUNX2* is known to be expressed early on during osteogenic differentiation and functions to enhance transcription of bone associated proteins such as *ALP, OPN* and *OCN* [118, 277, 328, 329]. Given that an increase in *ALP, OPN* and *OCN* was observed, it could be speculated that an increase in *RUNX2* expression occurs at a time-point not investigated during this study. ALP, OCN and OPN are known to be indicators of osteogenic differentiation [222, 330]. The increase in expression of these markers in the current studies, supports the idea of potential osteogenic differentiation on the topographies. When comparing increases of observed expression to expression measured in flat OM surfaces, it is apparent that the expression observed on topographical surfaces is not as high as that identified during culture with OM. From this we can tell that chemically induced osteogenic differentiation is more powerful that topographical induced differentiation, though nonetheless topography has a moderate effect on gene expression.

SSC proliferation appears to decrease over time with DNA concentration reaching a plateau on day 21 and maintaining this until day 28. A similar effect was seen in Chapter 4 Figure 4.8A where cell number appeared to potentially reach a peak on day 21. The results obtained in Figure 5.5A suggest cell number does peak on day 21 with proliferation slowing after this. When comparing cell number to cell metabolic activity, it is apparent that during stages of cell proliferation on days 10-14, there is also an increase in metabolic activity. This metabolic activity decreases on day 21 to day 28 when proliferation has slowed down. It was thought

that proliferation slows down during differentiation and this was associated with an increase in metabolic activity. The results obtained in this chapter suggest that the day 21-28 slowdown of metabolic activity could be due to lack of cell division and in this result is not indicative of potential osteogenic activity.

When differentiating SSCs form specialised, terminally differentiated cells, the environment within the cell changes, including the way in which cells process metabolites [231]. The metabolomic profile of SSCs is known to change during differentiation with more energy as a consequence of OXPHOS pathways in the mitochondria as differentiation progresses [231, 331] and, accompanying this is an increase in energy-related metabolite intensity [332]. In the current studies, this change in metabolite processing was illustrated by the comparison between SSCs on flat control to flat OM where we observed an increase in metabolite intensity, increase in OXPHOS associated TCA cycle metabolites. The similarities between flat OM and nacre topographies in aspects studied including nucleotide processing canonical pathways and activation of network hubs supports the hypothesis of osteogenic differentiation of SSCs on the nacre topographical surface. Networks generated suggested an increase in TCA cycle components on nacre surfaces and flat OM, an indication of increased levels of OXPHOS. An increase in individual metabolites (creatine, glutamine, pyruvate and carnitine) observed has been linked to osteogenic differentiation [237, 333, 334]. Coupled with this, a predicted activation of Collagen α1 and ERK1/2 strengthens the case for osteogenic differentiation on the nacre topography [148, 335]. ACAC catalyses the conversion of acetyl-CoA to malonyl-CoA and therefore enhances the level of malonyl-CoA available, an increase which has been previously linked to stem cells progressing from a quiescence to differentiated state [336]. An increase in activation observed in the current study further details SSC differentiation on the nacre surfaces. Interestingly, at day 21, the metabolomic profile of SSCs on flat OM appears to be less active in comparison to the nacre topography. Since differentiation is promoted by two different mechanisms in these studies, either chemically or topographically, it is likely that the progression of differentiation is different on these surfaces which could explain the variation.

The nacre surface presents the cells with a nanodisordered feature arrangement, previously shown to be important for the induction of osteogenesis [132, 143]. This type of surface is believed to induce integrin clustering resulting in altered phenotype. Nacre is a natural surface and therefore the topography is distinct to machine-computer designed and generated topographies, which allows for further variation within the surface. It could be natural variation which allows nacre to provide the topographical cues necessary for osteogenic differentiation. In addition, when using the initial *P. maxima* shell as a mould, on the surface there was not only the natural topography of the shell, but also proteins produced by the shell. The resulting

PCL topographical mould is created via an intermediary PDMS mould and includes several washing steps. It is likely that during this time, the presence of these additions to the topography will have been removed, and only the shape of the proteins transferred during the soft lithography process, although it should be noted that this was not tested in the current studies and the effect of the presence of these proteins remains, currently unknown.

It has become apparent in recent studies that stem cells and wider bone regeneration processes benefit from a 3D environment [337, 338]. The use of a 2D topography, as in the current studies, could limit possible enhancement of osteogenesis observed in a 3D nacre topography environment. Future studies will evaluate the effect of a 3D nacre topographical environment on behaviour of SSCs.

To date, information on the role and function of the prism surfaces, remains limited and the potential to modulate skeletal cell function and cell behaviour remains poorly understood. As this topography is vastly different to the nacre, it is not surprising that it has a different effect on the cell. Cell area of SSCs on prism surfaces was similar to flat control, indicating a lack of response to the surfaces, at least in terms of cell spreading. Analysis of gene expression, demonstrated a significant increase in *OCN* expression. However, a similar result was not seen in other osteogenic markers tested including *ALP* and *OPN*, indicating lack of osteogenic response. Interestingly, there was an increase in *RUNX2* expression on day 28 however since *RUNX2* expression is usually expected early on in osteogenic differentiation, this is unlikely to indicate potential osteogenic differentiation. Analysis of the metabolic profile of SSCs on prism surfaces demonstrated a decrease in metabolomic intensity. An increase in predicted activation of lactate dehydrogenase rather than those linked to TCA cycle indicated the potential for stem cell maintenance on this surface [339]. Further to this, a decrease in nucleotide biosynthesis and ACAC suggests a quiescent population. The role the prism surface has remains to be fully elucidated, however the current results suggest the surface could provide topographical cues for maintenance of the stem cell phenotype.

In the current study, SSCs were obtained from residual tissue samples of patients undergoing routine hip replacement and there are variations in sample retrieval area and health of bone marrow, both of which can result in differences in cell behaviour and their ability to respond to biomechanical factors. This patient sample variation has been observed previously [95], and has led to observed variation within the samples analysed in the authors' experiments. A similar variation has been observed in the current studies and most apparent in gene expression studies. While this can complicate results of an experiment, these variations reflect the natural variation when using primary human tissue and emphasise the importance of using a clinically relevant cell population. It should be noted here that during these initial studies, a

small number of patient samples, a total of 4, was examined. This could have led to the observed sample variation and further studies should add to the current studies by increasing the number of samples examined to reduce experimental variation as a consequence of patient variability. Although the results discussed in these current studies showed enhancement of expression of osteogenic markers on nacre topographies and an increase in metabolomic activity of SSCs cultured on nacre topography, the results were not consistent for all mRNA investigated and, interestingly, for cell area. Additionally, analysis for the presence of mineralised tissue in the current work was not performed and future planned studies will address this issue. Another contributing factor to the variation observed in these experiments is the surface itself. The PCL surfaces were taken from PDMS mould of the surface of the shell. The PCL replicas were observed under SEM to have a pattern shown in Figure 5.1 throughout the surfaces. This was not examined using any other method, and quantification of how much of the surface is covered with the nacre and prism surfaces is important to understand the effect of the topography.

The enhancement of osteogenic differentiation of commercially available MSCs on nacre has previously been shown, and this was associated with mineral formation of a higher crystallinity compared to mineralised matrix produced from chemically stimulated MSCs [325]. The current study details nacre and prism effect on primary SSCs from donors who were undergoing routine total hip replacement for bone degeneration. Evaluation of a clinically relevant population, from aged patients suffering from degenerative bone disease, as in the current studies, confirm that nacre topography could induce osteogenic differentiation in the clinic. In order to translate these finding to the clinic, future experiments using nacre PCL replicated topography to investigate *in vivo* bone regeneration on 2D topography would be required.

This study demonstrates a role for nacre PCL topography from *P. maxima* oyster shells to induce osteogenic differentiation in human SSCs and progenitor populations. Increase in cell area, increase in *ALP, OCN* and *OPN* gene expressions, and increase in metabolites and close association with SSCs cultured in flat OM conditions illustrated the potential for the nacre surface to control osteogenic differentiation. Further to this, the current study improves understanding of stem cell response to prism topography. While the gene expression studies produced mixed results, metabolomics network analysis from SSCs cultured on the prism surface, indicate that there was a maintenance of the SSC phenotype on these surfaces. By studying cell behaviour using a clinically relevant population, we have shown the potential for nacre topography to be used for controlling osteogenic differentiation in patients with degenerative bone disease, and begun to understand the effects that the prism shell topography has on controlling SSC phenotype.

Chapter 6: Discussion and future directions

Chapter 6 Discussion and future directions

The work described in this thesis details the collection of experiments designed to explore the role of topography on human SSC behaviour and ultimately differentiation and function. A total of 3 different types of topographical surfaces were chosen: i) NSQ ordered disordered nanopits manufactured by electron beam lithography, ii) cell bioimprints manufactured to create topographical impressions of differentiated SSCs and, iii) PCL imprints of nacre and prism topographies taken from *Pinctada maxima* oyster shells. Each chapter of experiments is dedicated to one topographical surface type and describes in detail the experimental results and discussion relative to those experiments, and findings are summarised below.

Several studies have reported that NSQ nanosurface can induce osteogenic differentiation of SSCs in the absence of chemical cues [143, 177, 250, 272, 340]. The main aim of Chapter 3 was to further this work by identifying miRNA involved in osteogenic differentiation through the use of a microarray. Preliminary studies found a limited association between the NSQ surface and the upregulation of osteogenic markers, compared to cells cultured on a flat PL control. When 2 patient samples were selected for miRNA microarray analysis, it was apparent that at this stage there were similarities in miRNA expression profiles between SSCs cultured on NSQ and PL surfaces. When the data set were expanded to include a total of 16 patients, it could be observed that the NSQ nanosurface did not, in these experiments, induce osteogenic differentiation of SSCs in the absence of chemical cues.

Following on from this EBL-based machine generated topographical surface, cell bioimprinted topographical surfaces were pursued. Bioimprinted surfaces were generated through the use of moulds taken of the topographical profile of cells growing in culture. The rationale under examination was that bioimprinted surfaces of differentiated SSCs would induce behavioural changes in SSCs cultured on the bioimprinted surface. Two stages of differentiation were chosen to generate bioimprinted surfaces: day 7 “early osteoblast” and day 21 “late osteoblast”. Although a variety of analysis techniques were used to study the behaviour of SSCs including metabolic changes, cell shape changes, protein expression and gene expression, it was concluded that when compared to a flat surface, the bioimprinted topographical surfaces did not induce significant behavioural changes in SSCs.

Finally, the unique topography of *Pinctada maxima* was studied to extend recent published experiments suggesting the topography of this marine bivalve mollusc could enhance the mineralised matrix MSCs laid down following culture on topographical surfaces [325]. Two parts of the shell, nacre and prism, were studied for the effect of their topography on SSC differentiation. PCL imprints were used to study this topography. It was found that cell area

and shape were not altered on nacre or prism surfaces, compared to flat surfaces. Analysis of expression of osteogenic markers, demonstrated that they were increases in SSCs cultured on nacre topography, although this increase was not as large as changes observed in the presence of osteogenic media. Analysis of the metabolites, produced following culture of SSCs on nacre and prism topography, showed that the metabolic profile was similar to SSCs cultured on flat surfaces in the presence of osteogenic media. It was also observed that there was a reduction in metabolism when SSCs were cultured on the prism surface. Through examination of the various metabolites down regulated, in these samples, it was discovered there was potential evidence for maintenance of the human SSC phenotype on prism topographical surfaces.

6.1. The power of topography compared to chemical-induced topography

It was apparent during the experiments discussed in this thesis that two types of topographical surfaces, NSQ and bioimprint, had limited effect on behaviour of SSCs, compared to their flat, planar control counterpart surface. The reasons as to why the culture of SSCs on these surfaces resulted in minimal phenotypic changes was not fully explored in this thesis and reasons as to why more significant effects were not observed can therefore only be postulated. It could be that the surfaces are inducing discrete behavioural changes however, this was not identified during these experiments. It is possible that the shape of the topography of these surfaces was not sufficiently different to induce phenotypical changes in the human skeletal populations.

A common method to induce osteogenic differentiation in skeletal populations is through the use of biochemical modifiers [84, 98, 341]. Comparisons between chemically induced osteogenesis and topographical induced differentiation of SSCs in NSQ nanosurface was not studied in these experiments in order to focus solely and to isolate the effect of topography on SSCs. In published studies which reported an increase in osteogenic markers on SSCs cultured on NSQ nanosurfaces, comparison between chemical and topographical induced osteogenesis was studied [177, 250, 340]. Initial studies published in Journal of Nature Materials 2007 by Dalby *et al* showed that comparison of topographically-induced changes in gene expression measured by microarray, to those induced by the osteogenic agent dexamethasone, resulted in a distinct and different pattern of gene expression upregulation [250]. Dalby and colleagues in 2007 used gene macroarray expression and discovered that osteogenic gene expression for *OCN, ALP, ICAM1* and *TGFBR1* was higher in the presence of dexamethasone compared to without the chemical [250]. There was also an increase in the

osteogenic markers *OCN, ALP, ICAM1* and *TGFBR1* when MSCs were cultured on NSQ compared to without dexamethasone, however, this increase was not as large as in the presence of dexamethasone [250]. The authors indicated here that topography, although not as powerful at inducing a selection of osteogenic markers, resulted in a different pattern of upregulated genes, as identified in macroarray. These findings suggests that the mechanosensory pathways in MSCs, activated by topography, can produce changes in the skeletal cell, which are distinctly different to those activated by biochemical signals.

With this in mind, it is conceivable that the work in this thesis, detailed in chapter 3 had not identified changes in SSCs following culture on PL and NSQ nanosurface, and extending these experiments away from classic gene expression studies could identify alterations in SSCs on NSQ nanosurface. Nevertheless, it cannot be ignored that the gene expression studies performed in Chapter 3 strongly suggest limited biochemical and signalling differences in SSCs cultured on NSQ and PL nanosurfaces. The effect of biochemical inductors was compared to the effect of bioimprinted topography in this thesis. The results in Chapter 4 indicate that biochemical inductors produce a more powerful effect on osteogenic differentiation of SSCs compared to bioimprinted cell surfaces. Again with the bioimprinted cell surfaces, it could be concluded that cell bioimprints play a role in altering SSC behaviour however, this was not clearly delineated or observed in the experiments performed in this thesis.

Published studies in Acta Biomaterialia Journal in 2015 from Song *et al*, examining the effect of micro-post topography on stem cell behaviour, compared to biochemical inductors ascorbic acid and β-glycerol phosphate, have suggested that instead of examining chemical and topographical induced cell behavioural changes as separate, these should be viewed as working synergistically [342]. The published studies of Song and colleagues, found that expressions of osteogenic markers *ALP, OCN and COL1A1* increased on micro-post topography on basal media and further increased in the presence of osteogenic media [342]. This approach is more akin to what SSCs would experience in the body, where changes in chemical factors present in the environment, topography of the ECM, and indeed stiffness, all work together to control differentiation [143].

6.2. Effect of size of topographical features on SSC behaviour.

Bioimprinted cell surfaces, NSQ surfaces and, prism and nacre topographies clearly vary in shape, however there is also variety in the size of the topographical features present. NSQ features are on the nanoscale at 120 nm in diameter. The size of the nacre and bioimprinted topographies were not measured in these experiments, however can be estimated to be approximately 10-50 μm in length (using SEM images), and thus, to the cell, these topographies present as much larger features than nanoscale features. The size and ordered disordered distribution of the NSQ nanofeatures is thought to allow for clustering of focal adhesions [143, 177]. Due to the much larger size of nacre and bioimprinted topography, it can be concluded that a similar mechanism is not involved in these topographies. This is because relative to the size of the topographical patterns, focal adhesions are much smaller in size, whereas in the NSQ nanosurface, the focal adhesions are much larger relative to the size of the topographical pattern. Interestingly, the nacre topography can be seen from SEM images in Chapter 5, Figure 5.1 as displaying an ordered disordered topography, similar to NSQ, however at a larger scale. There is therefore a variety in the size, shape and disorder of topography in the surfaces studied in this thesis.

There has been a number of studies which have investigated the effect of size of topographical features on stem cell behaviour [343-345]. Costa-Rodrigues *et al* examined the effect of grain size of HA on osteoclasts, and found that osteoclasts were more responsive in terms of induction of osteoclast gene expression markers to microsize grains of HA than nanosize [343]. Zouani *et al* investigated the role of nanopatterned substrates ranging from depths of 10 nm to 100 nm [346]. The authors discovered that only on the larger 100 nm deep topography would the cell respond through an increase in actin stress fibre formation and cell area [346]. These studies from Zouani and colleagues indicate the importance of both shape and dimension of topographical features in controlling SSC behaviour. In the topographies studied in this thesis, the size of the topographical features in terms of depth, height and width, was not investigated. The results from studies published by Costa-Rodrigues *et al* and Zouani *et al* [343, 346] suggest that size of topographical features could potentially have an impact on response of SSCs to the surface and could be investigated when studying nacre and prism topographies in the future.

Interestingly, in this thesis, the effect of altering the height of the topographical features was not studied. Given previously described studies where the importance of topographical height was identified, it is possible that if the height of topographical surfaces studied in this these was examined, there could have been an effect of altering it on the measured SSC osteogenic differentiation.

6.3. Nature versus man-made: the impact on topography

The surfaces studied in this thesis range from the man-made NSQ surfaces, to the naturally produced nacre and prism PCL surfaces, with the bioimprinted surfaces created from natural cells growing *ex vivo* as a midpoint. The results in this thesis suggest that a designing topography based on natural materials offers a more promising strategy to controlled differentiation of SSCs.

There are several published studies using EBL generated NSQ nanotopography which detail osteogenic induction of SSCs on such surfaces in the absence of chemical signals [132, 143, 340]. Following analysis of these NSQ surfaces, as detailed in Chapter 3, patient variability and surface imperfections impeded determination as to whether immunoselected STRO-1+ SSCs populations differentiated along the osteoblast lineage into osteoblast cells. NSQ nanosurfaces are synthetic surfaces (in this study fabricated in PCL), a type of surface which is not naturally observed by cells. Dalby *et al*. described how the nanotopographical disorder of NSQ surface could induce osteogenesis through changes in cell integrin clustering, resulting in induced osteogenic signalling [143], therefore these studies describe an unnatural surface having an effect on stem cell differentiation.

In contrast, bioimprinted surfaces present cells with topographical cues derived from cell imprints and, is therefore a natural topography. Initial studies of STRO-1+ SSCs on surfaces with bioimprints of immature osteoblasts (day 7 early cell fraction) and mature osteoblasts (day 21 late cell fraction) indicate little observed variations in STRO-1+ SSC proliferation and osteogenic marker gene expression. Lack of differences in STRO-1+ SSC behaviour following culture on surfaces with bioimprinted topographical features compared to SSCs cultured on surfaces without topographical features, indicated a potential role of material properties such as surface chemistry and stiffness that enabled bioimprinted surfaces to affect SSC behaviour. The results obtained indicate SSCs do change behaviour with an observation of reduced proliferation on bioimprinted surfaces, both with and without topography, which could be a direct result of alterations in chemical and stiffness of substrate material.

When SSCs are cultured *in vitro* in tissue culture flasks, SSCs will grow on a 2D monolayer, which is perhaps not how SSCs would naturally grow like in the body. Following culture of SSCs on bioimprinted surfaces, the cells are exposed to 3D structures which could perhaps be found naturally in the body. Although the shape of cells and ECM proteins would be transferred to bioimprinted surfaces, the chemical stimulation and cues of the ECM to facilitate SSC differentiation are absent on the bioimprinted surface. Any changes in behaviour observed during SSC culture would be solely due to a topographical response. Further

experiments to those described in "Chapter 4: SSC response to bioimprinted surfaces" could be undertaken to further enhance the understanding of SSC behaviour on these surfaces, however during these early experiments, it would appear unlikely that there were any additional measurable alterations. A key issue with the use of bioimprinted surfaces is the absence of standardisation of the shape of the cells imprinted on the surfaces and therefore potential problems with reproducibility of the topographical surface. Thus each individual cell, on culture on the bioimprinted surface, presented with a unique and distinct topographical cue. However, through observing results over several surfaces, the pooled result would be representative of the response of SSCs.

Nacre and prism topographies originate from the natural shell of *Pinctada Maxima*. The bone-inductive properties of nacre shell have been known for some time and, the response of osteoblasts to nacre compound has been studied, with the nacre compound inducing mineralisation in the absence of chemical osteogenic inductors [317]. The first published study focussing on the effect of nacre powder on MSC osteogenic differentiation was published by Green *et al*., 2015 [324]. They studied protein levels of ALP using a histological stain and noted increased levels in the presence of nacre chips [324]. The effect of nacre chips on MSCs differentiation was compared to osteogenic media and, Green *et al* concluded that culturing MSCs in the presence of nacre chips lead to a higher level of ALP than osteogenic media [324]. These studies taken together strongly suggest the potentially powerful role of nacre on osteogenic differentiation. The mechanisms associated with STRO-1+ SSC response to nacre are largely unstudied and therefore remains elusive. In particular, the effect of nacre topography only on STRO-1+ SSCs, without the interference of the surface chemistry of nacre was unknown, prior to the experiments discussed in this thesis. Experiments in "Chapter 5: Biomimetic structures and SSC fate and function: effect of nacre and prism topography on SSC behaviour" confirm the powerful role of this natural surface in SSC differentiation.

6.4. The use of topography in the clinic

A natural progression from the discovery of the importance of topography in directing SSC behaviour is to take this into *in vivo* experiments which could hopefully progress to the use of topography in the clinic. A potential use of topographical features is in treatment of degenerative bone disease and here topographical features could be used to model the surface of osteogenic implants, with an aim to improve integration of implant with host bone and, hopefully, extend the lifetime of implants.

There have been a few studies which have examined the effect topographical features *in vivo.* Hulshof *et al* designed a study which used a TopoChip, a PLA (poly lactic acid) chip, coated in titanium, designed computationally to provide a high number of different surfaces to act as a high throughput screen of topographical patterns [347]. High throughput screening is commonly used in pharmaceutical industry in drug development and offers fast and efficient method of analysing a variety of surfaces. When MSCs were cultured on the TopoChip, and cell shape and ALP protein expression measured on the surface (through immunofluorescence experiments and image analysis software), a number of surfaces induced either a high or low level of ALP. The authors took these forward for *in vivo* experiments. The surfaces were modelled onto titanium and inserted into rat femurs. Topographical surfaces were tested by means of a "pull-out test" where the force required to remove the topography was assessed to quantify integration of the surface into bone [347]. An important discovery was that topographical surfaces which enhanced ALP expression *in vitro* also showed improved implant integration *in vivo.* Furthermore, topographical surfaces which did not enhance ALP expression *in vitro* displayed low bone integration *in vivo* [347]. This identification of correlation between *in vitro* osteogenic marker expression and implant integration *in vivo* supports the need for *in vitro* experiments, and following up with *in vivo* experiments, which aim to identify a clinically relevant topographical surface for bone implants.

SSCs have multipotency and with this entails plasticity, enabling them to differentiate not only into osteoblasts, but to other cell types [348]. It was described previously in section 1.6.2. the importance of substrate stiffness in controlling differentiation. Stiffness must be carefully considered when designing a surface to promote differentiation of SSCs in order to reduce the formation of unwanted cell types. When designing a surface which aimed to promote osteogenic differentiation of SSCs, selecting a soft substrate would, as suggested by numerous published studies, not result in osteogenic differentiation of SSCs and instead adipogenic differentiation [161, 169]. Therefore when designing a surface for osteogenic differentiation, a stiff substrate must be selected.

As well as taking into consideration surface stiffness, when designing a substrate to promote topographically induced differentiation, it is important to ensure your topographical substrate only promotes differentiation towards the linage you want promote. English *et al* studied the effect of nanogrooved topography on tenocytes first *in vitro* and then *in vivo* [349]. *In vivo* it was discovered that tenocytes, which form elongated shape, showed enhanced elongation and alignment on deeper nanogrooved substrates and noted a gradual increase over 10 days in expression of osteogenic markers including RUNX2 and osteonexin [349]. This was followed by English and colleagues up with two *in vivo* models, tendon model and subcutaneous model [349]. In the tendon model, the authors showed no formation of new

tissue on the implants. In subcutaneous model, there was no cell orientation to nanogrooved substrate, indicating a lack of tenocyte response to the nanogrooved substrate. In contrast to studies by Hulshof *et al* (discussed previously), English *et al* have shown that *in vitro* response to substrate topography does not correlate to *in vivo* responses [347, 349]. In experiments by English *et al*, the authors had identified substrates which appeared to differentiate away from the intended tenocyte lineage towards the osteogenic lineage [349]. The authors recognised that substrate stiffness could potentially have an effect *in vivo*. The studies by English *et al* [349] demonstrate that it is therefore important that when studying a topography *in vivo*, to analyse for a known response (e.g. for osteogenic differentiation if studying nacre topography), but also for differentiation towards an unwanted cell phenotype. Clearly, uncontrolled differentiation could have potentially dangerous effects in the clinic.

6.5. Future directions

The work discussed in this thesis aimed to explore novel substrates, as well as to identify new regulatory miRNAs using a previously detailed topographical substrate (NSQ). In the current work, it was discovered that NSQ surfaces had limited effect on SSC osteogenic differentiation and cell bioimprinted surfaces displayed limited effect on SSC behaviour. Given these observations, experiments centred on NSQ and cell bioimprinted should not be progressed further. In contrast, studies using nacre and prism topographies showed promising results, enhancing osteogenic differentiation of SSCs and potentially maintaining stem cell phenotype. With respect to nacre substrates, it has yet to be discovered how the nacre topography modulate SSC function. This could be examined through analysis of, for example, the Wnt signalling pathway by quantifying levels of non-phosphorylated β-catenin. Furthermore, a whole proteome approach could be used to quantify the proteomic profile, offering the opportunity to discover previously unknown regulators of the topographical response. Further to this, a wealth of information has established the role of focal adhesions in SSC response to topographical surfaces. In this thesis, it was not explored if focal adhesions played a role in the SSC osteogenic response to nacre surfaces - this could be examined using immunofluorescent staining and image analysis to quantify focal adhesion number and size. In addition, through the use of actin inhibitors such as cytochalasin d, the importance of the cytoskeleton in osteogenic response to nacre topographical surfaces could be studied.

Experiments in this thesis indicate that the metabolic activity of SSCs is upregulated in response to nacre topography and this metabolic profile was similar to SSCs cultured under osteogenic conditions. Although this technique was valuable to assess the metabolome, the

individual metabolites up or down regulated should be examined separately in order to further establish their role in the SSC response to the nacre topography. It is known that both creatine and carnitine promote osteogenic differentiation through inhibition of PI3K/Akt signalling pathway [333, 350, 351]. This could be studied further in SSCs cultured on nacre topography through observations of phosphorylation levels of PI3K protein and AKT, and comparing with unphosphorylated, which would give indication of activation in the pathway [333]. In order to understand the role of carnitine in topographically induced osteogenic differentiation on nacre topography, an inhibitor of carnitine synthesis could be used, and osteogenic differentiation studied in the presence of carnitine inhibitor through observations of expression of osteogenic markers. One such inhibitor is mildronate, an inhibitor of carnitine acetyl transferase, a key enzyme in carnitine synthesis [352, 353]. Treatment of SSC cultures with mildronate and, studying expression of osteogenic markers would strengthen understanding on carnitine in topographically induced osteogenic differentiation.

Although potential upregulation of osteogenic markers in SSCs cultured on nacre topographies have been identified, production of mineralised ECM was not assessed. This could be achieved through von Kossa or Alizarin Red staining of cultured of SSCs on nacre topographical surface [270, 354]. Following on from this, it is important that the next step in nacre topography research includes *in vivo* evaluation. This could be achieved through the use of nacre topography in a femur defect and use the “pull-out test” previously described by Hulshof *et al* [347], which would enable the surface to be tested for bone integration. Further to this, osteogenic differentiation on the topographical implants could be studied through removing cells from the surface through the use of a lysis buffer and studying expression of osteogenic markers using RT-q-PCR and using western blotting techniques to measure expression of osteogenic proteins. The nacre topography could, following extensive experiments, be taken to larger preclinical models (ovine) to model the surface of osteo-implants.

The experiments discussed in Chapter 3 originally aimed to study miRNA involved in topographically-induced differentiation on NSQ surfaces. Although this was not pursued due to the lack of osteogenic differentiation on NSQ, miRNAs involved in possible osteogenic differentiation of SSCs on nacre topography could be pursued in future. As well as identifying miRNAs dysregulated on the nacre surface and possible links to osteogenic differentiation, the use of miRNA inhibitors could help understand how essential the role of these potential miRNA involved could be in osteogenic differentiation.

The prism surface was not fully explored and metabolic activity suggested enhancement of stem cell associated metabolites. This could be expanded to study gene and protein

expression of markers of SSC including STRO-1 staining. It would be interesting to examine, through gene expression studies, whether or not SSCs had differentiated along known stromal terminal differentiation pathways including adipocytes, osteoblasts, and chondrocytes. If it was confirmed that prism topographical surface was maintaining SSC phenotype and therefore multipotency, this surface could be used to generate high numbers of SSCs required for research application in the long-term and indeed to supply multipotent SSCs for use in the clinic.

6.6. Conclusion

The work in this thesis has explored three main topographical surfaces with the aim of further understanding the role topography can have on SSC behaviour and differentiation. Previously studied NSQ topography was discovered, through microarray and gene expression experiments, to have minimal effect on SSC behaviour, in contrast to published studies. Next, cell bioimprint topographies were studied for their effect on SSCs and were discovered to have limited effect on SSC shape, behaviour and gene expression. There appeared to be a material effect on SSC behaviour, rather than a topographically-induced changes in SSC behaviour, as flat bioimprint appeared to be having a similar effect on SSCs as cell bioimprinted topography. Finally, the novel topography of *Pinctada maxima* inner shell surface, both nacre and prism areas, were studied, through the production of PCL replicas of the topography. SSCs were cultured on these surfaces and it was discovered that nacre topography could, in the absence of chemical signals, potentially induce osteogenic differentiation. This was observed though upregulation of osteogenic markers and metabolomic response to the topographical surface. The prism topography was thought to maintain stem cell phenotype, in investigations of metabolomic profile of SSCs cultured on the prism topography, which would prove very valuable in the clinic to maintain stem cell phenotype. Following on from these discoveries, further investigation of osteogenic response of SSCs on nacre topography should be studied, including analysing mineralisation and increasing patient data set. After the osteogenic potential has been confirmed, these experiments should be taken to *in vivo* animal studies where it could potentially progress to the clinic as a treatment for degenerative bone disease. Initial studies suggesting maintenance of SSC phenotype on prism surface should also further be studied by observations of SSC markers including STRO-1+ immunofluorescence staining, and identifying if SSCs are differentiating towards adipogenic and chondrogenic lineages.

In summary, the experiments described in this thesis have furthered our understanding of the effect of topography on primary SSCs behaviour. It has studied for the first time, the effect of

SSC bioimprinted surfaces on SSC behaviour and identified that the surface topography has limited effect, and suggested the material of the bioimprint has a stronger role in modifying behaviour. Further to this, in this thesis, the behaviour of primary SSC on nacre and prism surfaces was studied for the first time and identified through metabolic and gene expression studies, the potentially powerful role of the nacre topography at altering the behaviour of SSCs to an osteogenic fate.

Appendices

Appendix I: List of Materials

Company	Reagent	Product Code
ThermoFisher Scientific Ltd (Paisley UK)	Fetal Bovine Serum (FBS)	10270-098
	Bovine Serum Albumin (BSA)	BPE1600-100
	Ethylenediaminetetraacetic acid (EDTA)	BP2482-500
	Antibiotic-Antimycotic (100x) (ABAM)	15240-062
	Collagenase Type IV (Collagenase IV)	17104-019
	SuperScript® VILO™ cDNA Synthesis Kit and Master Mix	11754050
	TaqMan™ Reverse Transcription Reagents	N8080234
	TaqMan® microRNA assay	4427975
	TaqMan® Universal PCR Master Mix	4304437
	TaqMan® MicroRNA Reverse Transcription Kit	4366596
	SYBR® Green PCR Master Mix	4312704
	Quant-iT™ PicoGreen® dsDNA assay	P7589
	Gibco™ goat serum	1621006
	Alexa Fluor® 647 Phalloidin	A22287
	alamarBlue® Cell Viability Reagent	DAL1100
	DAPI (4',6-Diamidino-2-Phenylindole, Dihydrochloride)	D1306
Lonza Ltd, (Slough, UK)	Minimal Essential Media Alpha Eagle (α-MEM)	BE02-002F
	Phosphate Buffered Saline (PBS)	BE17-512F
	Penicillin-Streptomycin (P/S)	DE17-602E
	Trypsin Versene® (EDTA) mixture (10x) (Trypsin)	BE02-007E
Sigma-Aldrich Ltd (Dorset, UK)	1α,25-Dihydroxyvitamin D_3 (vitamin D_3)	D1530
	L-Ascorbic acid 2-phosphate sesquimagnesium salt hydrate (ascorbic acid)	A8960
	human serum	H4522
	quantitative real-time polymerase chain reaction (qRT-PCR) primers	Custom Product
	Napthol AS-MX phosphate	855
	Triton X-100	X100
	Tween® 20	P9416
	Igepal CA-630	I3021
	Fast Violet B Salt	F1631
	1.5 M alkaline buffer solution	A9226
	4-nitrophenol solution	N7660
	phosphate substrate	P4744
	Fluoromount™ Aqueous Mounting Medium	F4680
	Tris-EDTA buffer x100 (TE buffer)	T9285
	Tween® 20	P1379
Sigma-Aldrich Ltd (Auckland, New Zealand)	γ-butyrolactone (GBL)	20740
	polystyrene	331651
	sulphuric acid	35354

Qiagen Ltd (Manchester, UK)	RNeasy Plus micro kit	74106
	AllPrep DNA/RNA/miRNA universal kit	80224
	Reagent DX	19088
Promega Ltd (Southampton, UK)	Herring sperm DNA (10 mg, 10 μg/μl)	D1811
	GoTaq® qPCR Master mix	A6001
Miltenyi Biotech Ltd (Surrey, UK)	Anti-Mouse IgM MicroBeads	130-047-301
Dow Corning Ltd (Auckland, New Zealand)	SLYGARD® 184 silicone elastomer kit	
Alere Ltd (Stockport, UK)	Lymphoprep™	2224544
Merck Ltd (Abington, UK)	FAK100 Actin Cytoskeleton/Focal Adhesion Staining kit	FAK100

Table 5. Appendix I - Reagents used in methods detailed in this thesis as listed with company reagent was sourced from and product code.

All MACS (magnetic-activated cell sorting) related materials were obtained from Miltenyi Biotec (Surrey, UK). All cell culture plastic including plates and flasks were obtained from Greiner Bio-One (Stonehouse, UK).

Primary antibody	Dilution	Company	Secondary Antibody	Dilution	Company
Anti-Osteopontin mouse monocolonal IgG, (ab69498)	1:100	Abcam (Cambridge, UK)	Goat anti-Mouse IgG (H+L) Highly cross-adsorbed secondary antibody, Alexa Fluro 647 (A-21236)	1:100	ThermoFisher Scientific (Paisley, UK)
Anti-Collagen I rabbit polyclonal IgG, (ab34710)	1:100	Abcam (Cambridge, UK)	Goat anti-rabbit IgG (H+L) Highly cross-adsorbed secondary antibody, Alexa Fluro 647 (A-11034)	1:100	ThermoFisher Scientific (Paisley, UK)

Table 6. Appendix I - Primary and secondary antibody pairings for immunofluorescence. Dilution used and company antibody was obtained from is detailed.

Appendix II: Osteogenic potential of STRO-1+ SSC

Section 1 Molecular function of osteogenic markers

OCN

OCN, also known as bone gamma-carboxyglutamate (gla) protein, is a 49 a.a protein produced by osteoblasts and under the control of RUNX2 transcription factor [355]. OCN is produced as pro-osteocalcin, similar to many hormones, which is cleaved to OCN and modified by carboxylation of three glutamic acid residues to form γ-carboxyglutamic acid (GLA), before secretion from the osteoblast [13]. The addition of a second carboxyl group on glutamic acid could help it integrate with Ca^{2+} ions. Indeed, crystal structure of porcine OCN shed light on OCN binding to HA [356] and revealed a surface interaction between OCN and HA through Ca^{2+} coordination, making it an integral part of bone mineral matrix. *In vivo* experiments using *ocn*-null mice showed an increase in bone formation at 6 months [279]. These mice had a similar osteoblast surface area to wild type mice; implying increased bone formation is not due to increased osteoblast surface area. In addition, bone mineralisation as determined by Von Kossa staining, was similar in wild type and OCN-null mice. Therefore, OCN does not have an essential role in initiating bone mineralisation. A decrease in osteoclast surface area in OCN-null mice suggests OCN has a role in bone resorption though osteoclast regulation. OCN serum levels have been linked to an array of metabolic diseases including diabetes, obesity and cardiovascular disease [13], and is thought to impact glucose metabolism however contradictory studies suggest more investigation needs to be done [357, 358]. OCN could have role to play in feedback between bone and metabolic demands of the body [13].

RUNX2

One of a family of 3 RUNX genes (RUNX1, RUNX2 and RUNX3). All three members contain a DNA binding runt domain (homologous to drosophila runt domain). RUNX2 forms heterodimers with core binding factor β (CBF-β) and specifically recognises a consensus sequence. This binding to CBF-β is essential for RUNX2-dependent osteoblast differentiation [273]. Indeed, *runx2*-null mice show complete lack of endochondral ossification and intramembranous ossification, an example of the importance of RUNX2 in osteoblast differentiation [274]. RUNX2 directs MSCs down the osteoblast lineage to form preosteoblasts. After this stage, RUNX2 works with β-catenin and osterix to direct cells to continue to form osteoblasts [359]. RUNX2, as a transcription factor, induces expression of *OPN, COL1A1* and *OCN*, and RUNX2 binding site in their promoters have been identified [273, 355].

Overexpression of RUNX2 lead to a decrease in osteoblast maturation and transition to osteoclast [360]. Therefore, for correct osteoblast differentiation, RUNX is activated early and must be inhibited during late osteoblast maturation.

ALP

The enzyme alkaline phosphatase hydrolyses monophosphate esters in order to provide phosphates for HA. Because of this function, ALP has an essential role in bone mineralisation. It is modified post-translationally with the addition of a glycosylphosphatidylinositol anchor which allows for extracellular membrane insertion. Its expression is induced by RUNX2 [277] and this activation is essential for correct ALP activation.

OPN

Bone matricellular protein OPN is involved in a broad range of biological proteins?. OPN expression has been identified in skeletal tissue including chondrocytes and osteoblasts, however it has also been detected in brain, skeletal muscle, endothelial cells and kidney to name a few [284]. OPN is aspartic acid rich, giving it a high negative charge allowing it to bind to apatite crystals and inhibit bone mineralisation. Transcription of this protein is regulated by a combination of RUNX2, Vitamin D receptor and notch signalling [118]. *opn*-null mice displayed normal bone development and morphology formation [280]. However, mineral content was higher in bones of null mice, confirming OPNs role of inhibition of bone mineralisation [281]. Osteoclast formation was higher in $OPN^{-/-}$ bone marrow suggesting its role is with osteoclast differentiation [280]. OPN expression increased under mechanical stress, implying it could have a role in sensing mechanical stress and feedback to increase bone formation [282]. More recently, OPN has been found to have a role in inflammation [283, 284], and high serum levels have been observed in chronic inflammatory diseases including Crohn's disease and cancer, and appears to regulate innate immune cells and T cells [283].

Collagen Type 1

Collagens are complex extracellular molecules at high levels in connective tissue including bone. Collagens are synthesised in the endoplasmic reticulum, where three pro α-chains wind together in triple helix to form collagen fibrils [9]. Secretion vacuoles transport pro-collagen to the extracellular space where the prodomains are removed. Following this, collagen fibrils bundle to form collagen fibres, with covalent bonding [361]. Type 1 collagen is the most abundant collagen type and forms 90% of the organic mass in bone [361].

Section 2: Osteogenic differentiation of STRO-1+ SSCs

Aims

I. To investigate the osteogenic potential of STRO-1+ SSCs.

Specifically, this will be achieved through culturing the cells under osteogenic conditions and subsequent comparison to cells maintained in basal conditions using:

- Imaging of cell morphology
- Histological staining of ALP
- Biochemical analysis of protein activity
- Reverse transcriptase quantitative polymerase chain reaction (qRT-PCR) to quantify expression of osteogenic markers.

Methods

3.2.1. Patient samples

A total of three patients were used for each experiment. The samples utilised were from two female patients (57 and 66 years old) and one male patient (59 years old).

3.2.2. ALP Staining

To prepare for staining, cells were washed with PBS, fixed in 95% ethanol for 10 minutes, washed twice in PBS and left to dry for 10-30 minutes. To perform staining, 400 µL Naphthol AS-MX phosphate (Sigma-Aldrich) was added to 9.6 mL H_2O to achieve a 1:25 dilution of Naphthol AS-MX phosphate. To this, 2.4 mg Fast Violet B Salt (Sigma-Aldrich) was added to give a final concentration of 6.5 µM. A sufficient volume of the mixture was pipetted onto the cells to cover the bottom of the well (600 µL for 6 well plate). This was loosely covered with tin foil to prevent light interference and stored at 37°C for 30 – 60 minutes to allow the reaction to proceed. Wells were then washed with H_2O to stop the reaction and stored in PBS prior to imaging. Cells were imaged within 3 days of staining.

3.2.3 Specific ALP activity

Specific ALP activity was measured through normalising ALP activity to DNA concentration. ALP activity was measured with a metabolic activity based colorimetric assay and Quant-iT™ PicoGreen® dsDNA assay (Thermo Fisher Scientific, UK) to measure DNA concentration. To prepare lysate for assays, cells were washed twice in PBS and fixed in 95% ethanol for 10 minutes, washed twice in PBS and left to dry for 10-30 minutes. 0.05% Triton X in PBS was used to lysate the cells (200 µL for 24 well plate and 600 µL for 6 well plate) and cells scrapped from the well using a pipette tip. Repeated freeze/thaw cycles with cell scrapping after thawing ensured cell lysis, then samples were stored at -80°C. ALP assay measures a colorimetric

change in a sample as ALP presents in the lysate removes the phosphate from 4-nitrophenyl phosphate and converts it to 4-nitrophenol (Figure A2.1).

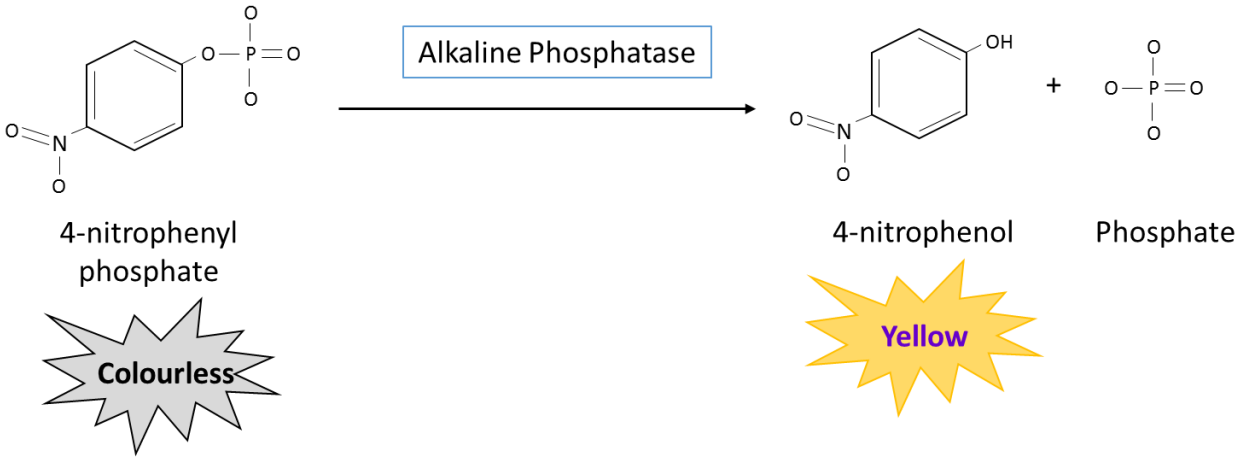

Figure A2.1. Conversion of 4-nitrophenyl phosphate to 4-nitrophenol and phosphate by the enzyme ALP. *The removal of the phosphate from 4-nitrophenyl phosphate by ALP causes a yellow colour change that can be measured using a spectrophotometer.*

The absorbance of the yellow colour of the 4–nitrophenol formed was read at 410 nm and compared to a standard curve of known 4–nitrophenol concentrations. To generate the standard curve, 4-nitrophenol (Sigma-Aldrich, UK) at 10 mM was diluted in a buffer consisting of: 10 mL distilled H_2O, 5 mL 1.5 M Alkaline Buffer Solution (Sigma-Aldrich, UK) and 30 µl Igepal CA-630. Standard curve was generated from concentrations 10, 50, 100 and 200 nM of 4-nitrophenol and a blank, and 100 µl of each standard added to one well of 96-well plate. For samples, 10 µl of cell lysate was added to 90 µl of substrate solution (10 mL 1.5 M alkaline buffer solution, 20 mL distilled H_2O and 40 mg phosphate substrate (Sigma-Aldrich, UK)) per well. Standards and samples were run in triplicates. The plate was incubated for 60 minutes or until samples have changed to slightly lighter than darkest standard. Colour change from colourless to yellow was measured in ELx800 absorbance reader (BioTek Instruments Inc., Swindon, UK). Using standard curve, ALP concentration was measured in nmol NNP $ml^{-1}hr^{-1}$.

Quant-iT™ PicoGreen® dsDNA assay utilises PicoGreen's unique property of fluorescing only when bound to double stranded DNA (dsDNA). To generate standards of known DNA concentration, herring sperm DNA (Promega, UK) at 10 µg/µl was diluted in 1x TE buffer (100x TE buffer concentrate diluted in distilled H_2O) (Sigma-Aldrich, UK) to 50, 100, 250, 500, 750 and 1000 ng/ml and 100 µl of each standard added to one well of 96-well plate. 10 µl of cell lysate was added to 90 µl 1x TE buffer. To this, 100 µl PicoGreen (diluted 1:200 in 1x TE buffer) was added. The plate was left to incubate at room temperature in the dark for 5 minutes. PicoGreen fluorescence was measured in FLx800 fluorescence reader (BioTek Instruments

Inc., Swindon, UK) with excitation at 480 nm and emission measured at 520 nm. Using standard curve, DNA concentration in each sample was calculated in ng/ml.

Specific ALP activity relative to DNA concentration was calculated using equation 3.

$$Specific\ ALP\ Activity = \frac{\text{ALP Activity (nmol pNPP /ml/hr)}}{\text{DNA (ng/ml)}}$$

Equation 3. Calculation of specific ALP activity in ALP activity assay.

Results

STRO-1+ SSCs in culture

STRO-1+ enriched SSCs were isolated as detailed in sections 2.1.3. and 2.1.4. Cells were cultured in T175 flasks and the media changed twice a week. When cells reached 60% confluence, cells were imaged using Zeiss Axiovert 200 (Figure A2.2). Passage 0 STRO-1+ enriched SSCs presented with a fibroblastic-like and elongated morphology. STRO-1+ enriched SSCs grew as large colonies upon isolation from bone marrow. Figures 2A show the centre of such colonies with cells at confluence and in alignment to each other. Near the edge of the colony, cells displayed a mixed orientation at mixed angles to each other (Figures A2.2B). High magnification images showed filopodia-like projections from the cells, as cells proliferated in culture (Figures A2.2C, white arrows).

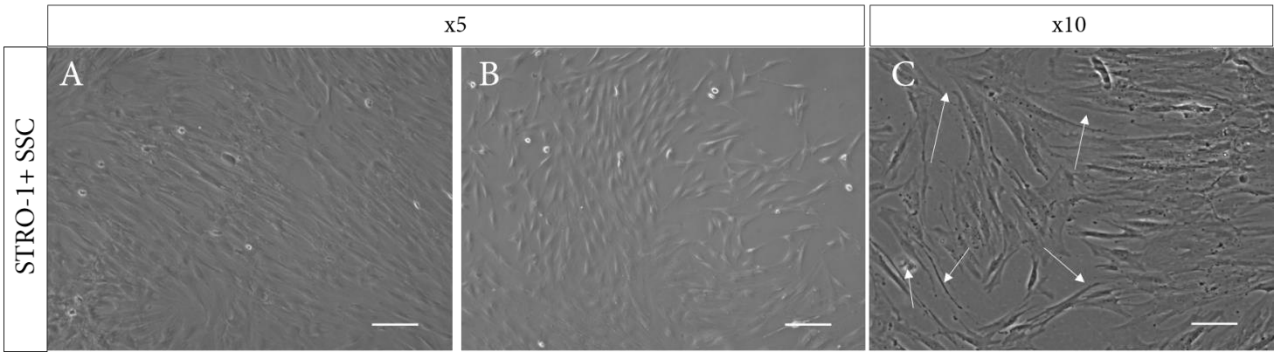

Figure A2.2. STRO-1 enriched SSCs. Brightfield images of STRO-1+ enriched SSCs (A, B, C). (A, B) x5 magnification (mag.) and scale bar 200 µm (C) x10 mag. and scale bar 100 µm. White arrows indicate filopodia-like projections.

3.3.2. STRO-1+ SSCs osteogenic differentiation

To investigate the osteogenic differentiation of STRO-1+ enriched SSCs, cells were transferred from T175 flasks to 6 well plates as detailed in section 2.1.5. Cells were plated at a concentration of 20,000 cells/well under both basal and osteogenic conditions (media content detailed in section 2.1.2.).

Brightfield images were taken of the cells on days 7, 14 and 21 and imaged using Zeiss Axiovert 200 (Figure A2.3). Cells at passage 1 under basal conditions displayed a similar morphology to cells at passage 0 (Figure A2.2). STRO-1 enriched SSCs exhibited clear differences following culture in basal and osteogenic media. Cells maintained under osteogenic conditions displayed increased discrete projections and a spindle-like morphology. This was most apparent at day 7 through to day 14, and by day 21, the cells were observed to be fully confluent. Even at this late stage morphological differences were observed, with cells under basal conditions displaying alignment, and a progression from the elongated morphology characteristic of day 7 cultures. In contrast, under osteogenic conditions, less alignment was observed, reflecting the spindle-like morphology observed at day 7 (Figure A2.3).

Following from these observations, passage 0 STRO-1+ enriched SSC were plated onto 24 well plates at a seeding density of 5,000 cells/well (described in section 2.1.5.) in order to investigate ALP protein levels. ALP activity was determined at days 7, 14 and 21 (section 3.2.2).

All cells, irrespective of culture in basal or osteogenic conditions, exhibited a low level of ALP staining on day 7 (Figure A2.4). Under osteogenic conditions, the number of ALP positive stained cells accumulated with time over 21 days. Thus by day 21, the majority of cells were observed to be positively stained for ALP. Interestingly, at day 21 under basal conditions, a select few cells exhibited strong ALP staining.

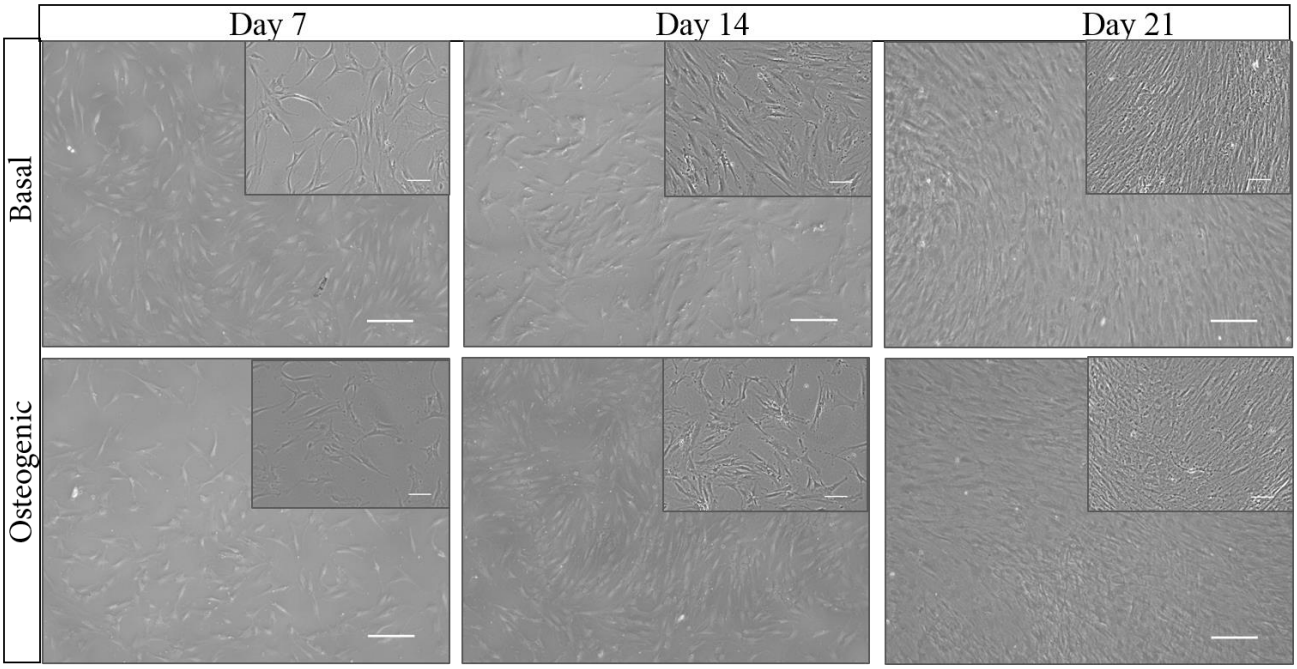

Figure A2.3. STRO-1+ SSCs cultured under basal and osteogenic conditions. *Brightfield images of STRO-1+ enriched SSCs grown under both basal and osteogenic conditions. In larger image, scale bar 200 µm and in smaller box, scale bar is 100 µm.* All images were captured using a *Zeiss Axiovert 200.*

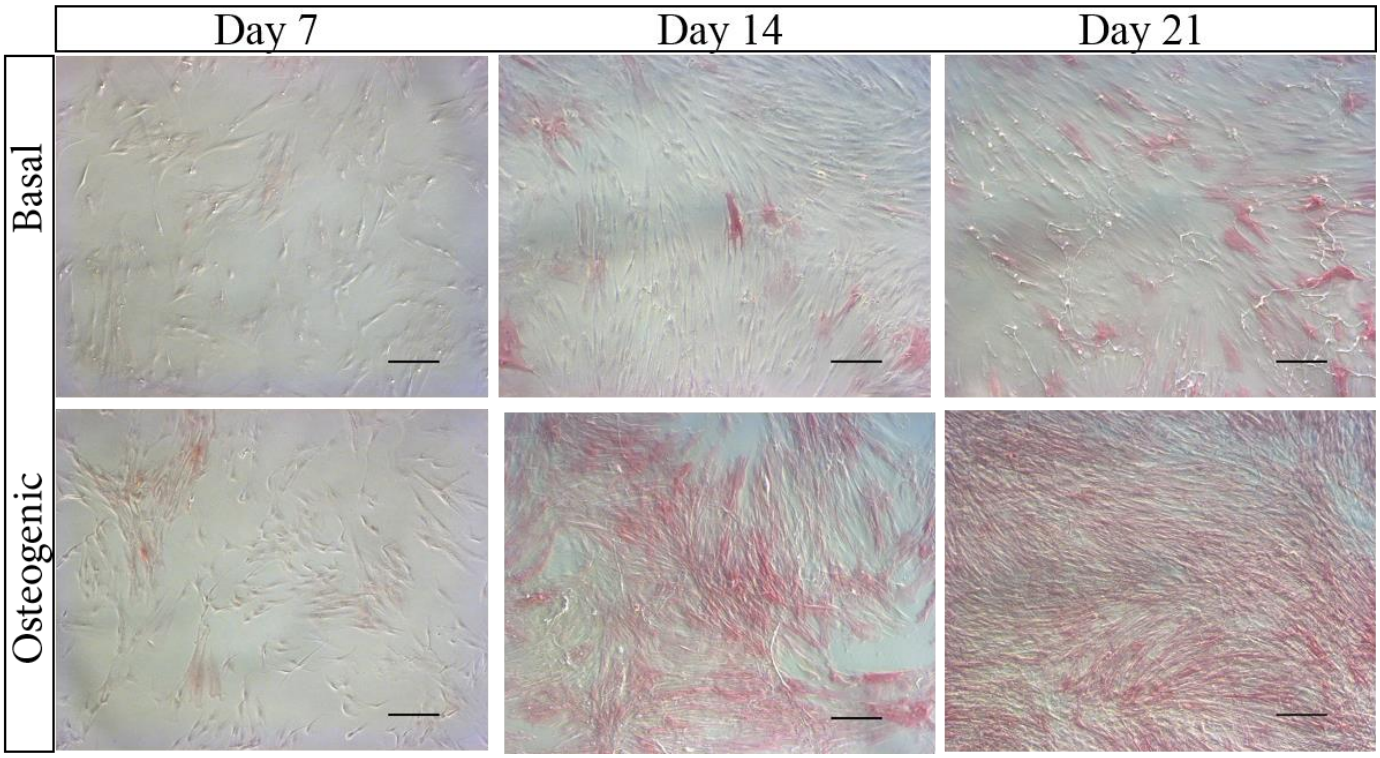

Figure A2.4. ALP staining of unselected STRO-1+ enriched SSCs under basal and osteogenic conditions. *STRO-1+ enriched SSCs were cultured for 21 days in either basal or osteogenic media and stained on days 7, 14 and 21 for ALP.* All images were captured using an *Zeiss Axiovert 200. Scale bar, n = 3 patients, representative images shown.*

Biochemical Analysis

Osteogenic differentiation was assessed by the production of bone-specific protein ALP using a colorimetric assay. Thus, STRO-1+ enriched SSCs were cultured under basal and osteogenic conditions and samples taken on day 7, 14 and 21, as detailed in section 3.2.3 to determine ALP specific activity.

All conditions examined showed low ALP levels on day 7 (STRO-1+ SSCs basal media 0.010 ± 0.0008, and STRO-1 + SSCs osteogenic media 0.065 ± 0.021) (Figure A2.5). In contrast, by day 14, ALP levels increased significantly from day 7 (e.g. STRO-1+ SSCs in basal media increased by 0.687 ± 0.10 and in osteogenic media by 2.355 ± 0.54) (Figure A2.5). At this time point, cells cultured with osteogenic media had higher ALP specific activity compared to basal media, with p≤0.0001 in STRO-1+ SSCs. From day 14 to 21, STRO-1+ SSCs also cultured under osteogenic conditions displayed no further changes in specific activity of ALP. Under basal conditions no significant change was observed.

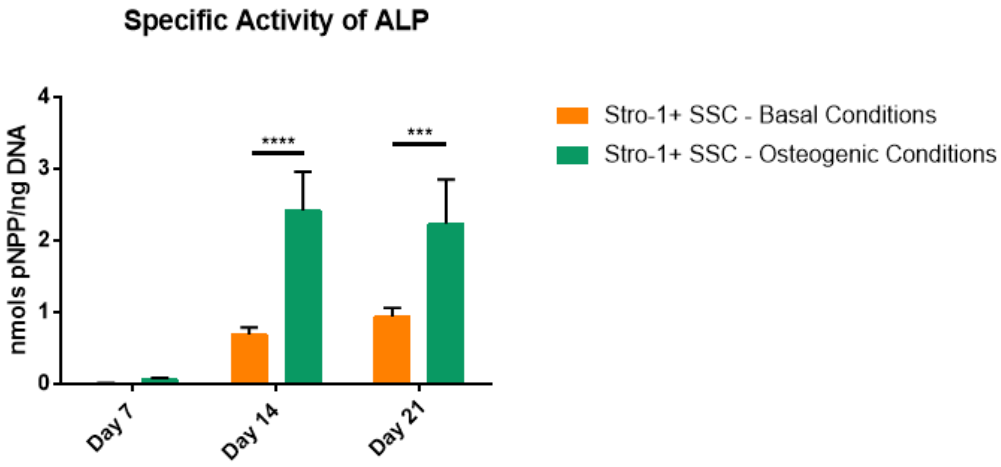

Figure A2.5. Specific activity of ALP Stro-1+ SSCs in basal and osteogenic conditions over 21 days. *pNPP – para-nitrophenylphosphate. Data presented as mean ± SD, Data represents 3 patients. 2-way ANOVA was performed on the data. * indicates p≤0.05, **** indicates p≤0.0001.*

Molecular Analysis

Expression of osteogenic markers was assessed using qRT-PCR to establish progression along the osteoblast lineage and to examine for differences, if any, in expression of osteogenic markers between STRO-1+ SSCs cultured under basal and osteogenic conditions. Both populations were cultured for 21 days and samples taken for qRT-PCR on days 7, 14 and 21 (Figure A2.6). Sample preparation, RNA extraction, cDNA synthesis and qRT-PCR were followed as detailed in sections 2.2.1., 2.2.2.1., 2.2.3., and 2.2.4.

RUNX2 expression remained constant in basal media over 21 days (Figure A2.6A), however expression under osteogenic conditions peaked on day 14. It was apparent that there was a large variation between patient samples observed. Expression of *ALP* increased over 21 days under both basal and osteogenic conditions. The increase in expression was greater in the presence of osteogenic media (Figures A2.6B). On day 7 *COL1A1* expression in STRO-1+ enriched SSCs on day 7 was comparable under both basal (3.57 ± 3.77) and osteogenic conditions (3.75 ± 3.43) (Figure A2.6C). On day 14 and day 21 however, *COL1A1* expression was greater on osteogenic conditions than basal.

OCN expression under osteogenic conditions was noted to increase modestly between days 7 and 14 in osteogenic conditions, followed by a large increase in expression between days 14 and 21 (Figure A2.6D). Substantial patient to patient variation was observed, precluding significance determination. *OCN* mRNA levels remained low under basal conditions. Expression of *OPN* under osteogenic conditions was low until day 21 when expression increased to 291.46 ± 360.83 (Figure A2.6D). Significant patient to patient variability was observed.

Each patient, illustrated by either a light, medium or dark shade throughout Figures A2.6 was colour coded to check if one patient was a consistent outlier. The medium colour patient was found to be highest expressing patient for *OCN* and *OPN* expression. However, it was the lightest patient for these markers who was the highest expressing *RUNX2* patient. This confirms the degree of patient variability both between patients and within patients.

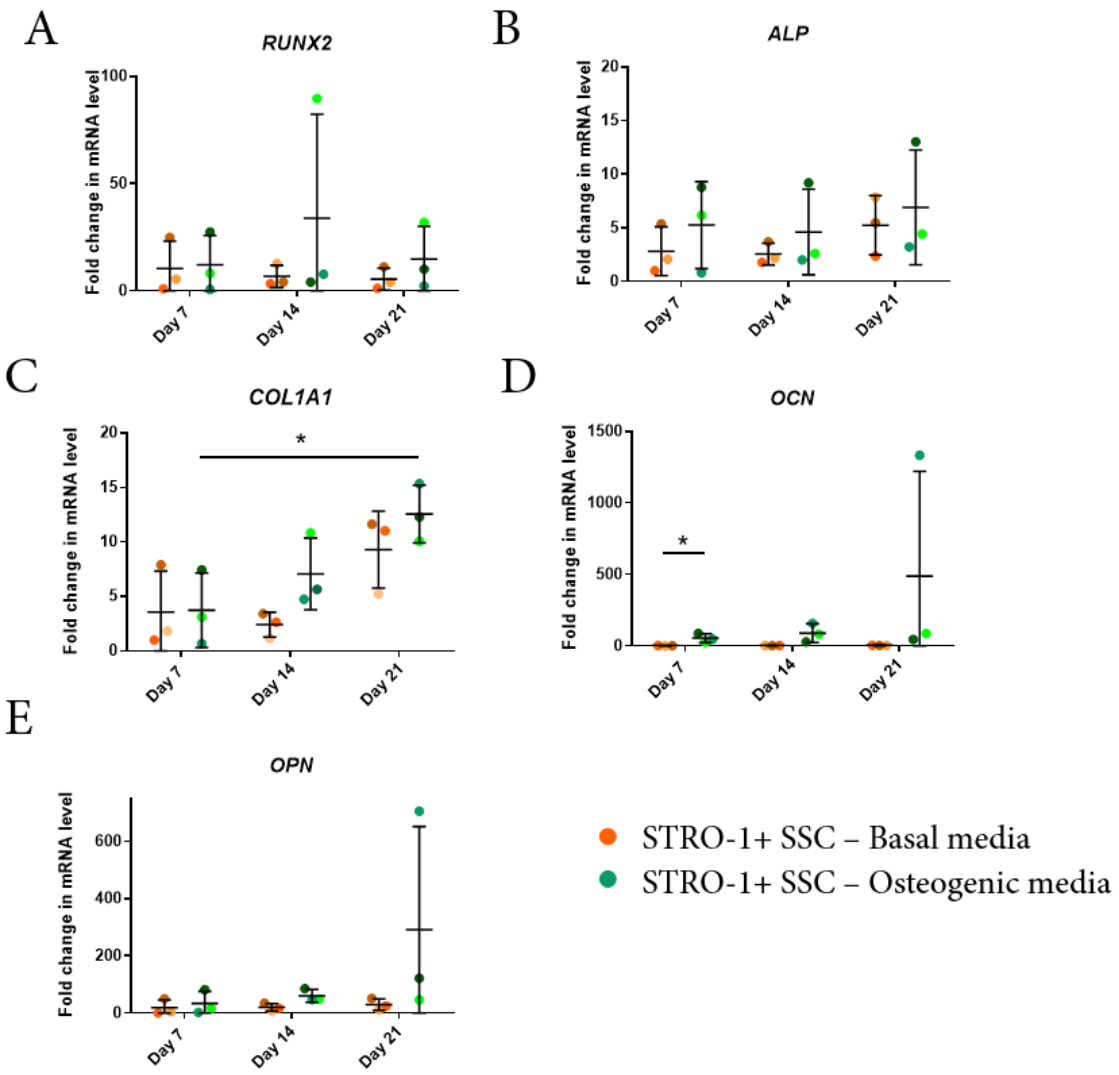

Figure A2.6. Expression of osteogenic markers in STRO-1+ SSCs under both basal and osteogenic conditions over 21 days. *Measured gene is at the top of each graph. Gene expression is calculated as fold change compared to basal expression on day 7. Figure legend below graphs. Mean for each sample is represented by middle horizontal line for each sample and standard deviation of the mean is shown as the vertical line. Each dot represents one patient sample. Patients are colour coded with lightest, medium and dark shades representing each of the three patients. N = 3.*

Summary

STRO-1+ SSCs have been shown previously to be capable of osteogenic differentiation (reference). The results shown in FiguresA2.1-6 indicate that the methods used in this thesis allows for selection of SSCs which are capable of osteogenic differentiation.

Appendix III: qPCR Evaluation

Section 1: Primer Sequences

All primers used in the RT-qPCR experiments detailed in this report were designed prior to use by Rahul Tare of Bone and Joint Research Group, University of Southampton. These primers have been used in published work [105] [362] and are detailed in Table A3.1

Gene	Forward	Reverse	Amplicon Size	Amplicon Sequence
ACTB	GGCATCCTCACCCTGAAGTA	AGGTGTGGTGCCAGATTTTC	82	**GGCATCCTCACCCTGAAGTA**CCCCATCGAGCACGGCATCGTCACCAACTGGGACGACATGGA**GAAAATCTGGCACCACACCT**
COL1A1	GAGTGCTGTCCCGTCTGC	TTTCTTGGTCGGTGGGTG	52	**GAGTGCTGTCCCGTCTGC**CCCGACGGCTCAGAGT**CACCCACCGACCAAGAAA**
ALP	GGAACTCCTGACCCTTGACC	GGAACTCCTGACCCTTGACC	86	**GGAACTCCTGACCCTTGACC**CCCACAATGTGGACTACCTATTGGGTCTCTTCGAGCCAGGGGCAT**GCAGTACGAGCTGAACAGGA**ACAACGT
RUNX2	GTAGATGGACCTCGGGAACC	GAGGCGGTCAGAGAACAAAC	78	**GTAGATGGACCTCGGGAACC**CAGAAGGCACAGACAGAAGCTTGATGACTCTAAACCTA**GTTTGTTCTCTGACCGCCTC**A
***OCN* – (October 2014 – June 2015)**	GGCAGCGAGGTAGTGAAGAG	CTCACACACCTCCCTCCT	102	G**GGCAGCGAGGTAGTGAAGAG**ACCCAGGCGCTACCTGTATCAATGGCTGGGAGCCCCAGTCCCCTACCCGGATCCCCTGGAGCCC**AGGAGGGAGGTGTGTGAG**
***OCN* – (June 2015 onwards)**	AAGAGACCCAGGCGCTACCT	AACTCGTCACAGTCCGGATTG	110	**AAGAGACCCAGGCGCTACCT**GTATCAATGGCTGGGAGCCCCAGTCCCCTACCCGGATCCCCTGGAGCCCAGGAGGGAGGTGTGTGAGCT**CAATCCGGACTGTGACGAGTT**
OPN	**GTTTCGCAGACCTGACATCC**	**CATTCAACTCCTCGCTTTCC**	80	**GTTTCGCAGACCTGACATCC**AGTACCCTGATGCTACAGACGAGGACATCACCTCACACAT**GGAAAGCGAGGAGTTGAATG**

Table A3.1. Forward and reverse primer sequences for osteogenic marker genes. CGTA refers to DNA bases. C- cytosine, G- guanine, T – thymine and A – adenine.

Section 2: Primer Efficiency

Primers were not designed during the course of these experiments. Primer efficiency testing was carried out to determine amplification efficiency of qPCR reaction. In order to do this, serial dilutions were performed on cDNA of STRO-1+ SSCs cultured in osteogenic media as detailed in Table A3.2 and RT-qPCR was carried out using the protocol detailed in section 2.3.4. The log(concentration of DNA) was plotted against C^t value and from the line of best fit, efficiency of primers was calculated using the equation in **Error! Reference source not found.** A3.1. The results (Figure A3.2) showed primer efficiency within the acceptable range of 90% to 110%. Efficiency of *ACTB* primer (Equation 4) is low, at 82.65 %.

Concentration of cDNA	Log (DNA Conc.)	Average C_t *ACTB*	Average C_t *ALP*	Average C_t *RUNX2*	Average C_t *OCN*	Average C_t *OPN*	Average C_t *COL1A1*
10	1	17.96	23.73	23.71	23.67	23.68	18.12
1	0	20.59	27.32	27.08	27.12	26.15	22.52
0.1	-1	26.18	32.34	31.25	31.91	30.39	25.89
0.01	-2	31.71	36.44	33.69	33.44	33.39	28.73
0.001	-3	35.31	36.03	35.70	35.92	35.89	31.87

Table A3.2. Calculated values used to measure primer efficiency. A sample of cDNA known to be producing each gene at a high level was selected for measuring efficiency.

$$\text{Efficiency} = \left[10^{\left(\frac{-1}{\text{slope}}\right)} - 1\right] \times 100\%$$

Equation 4. Equation used to calculate primer efficiency. Ct values of amplification over a range of known concentrations of cDNA was plotted (Figure A3.2) to give slope.

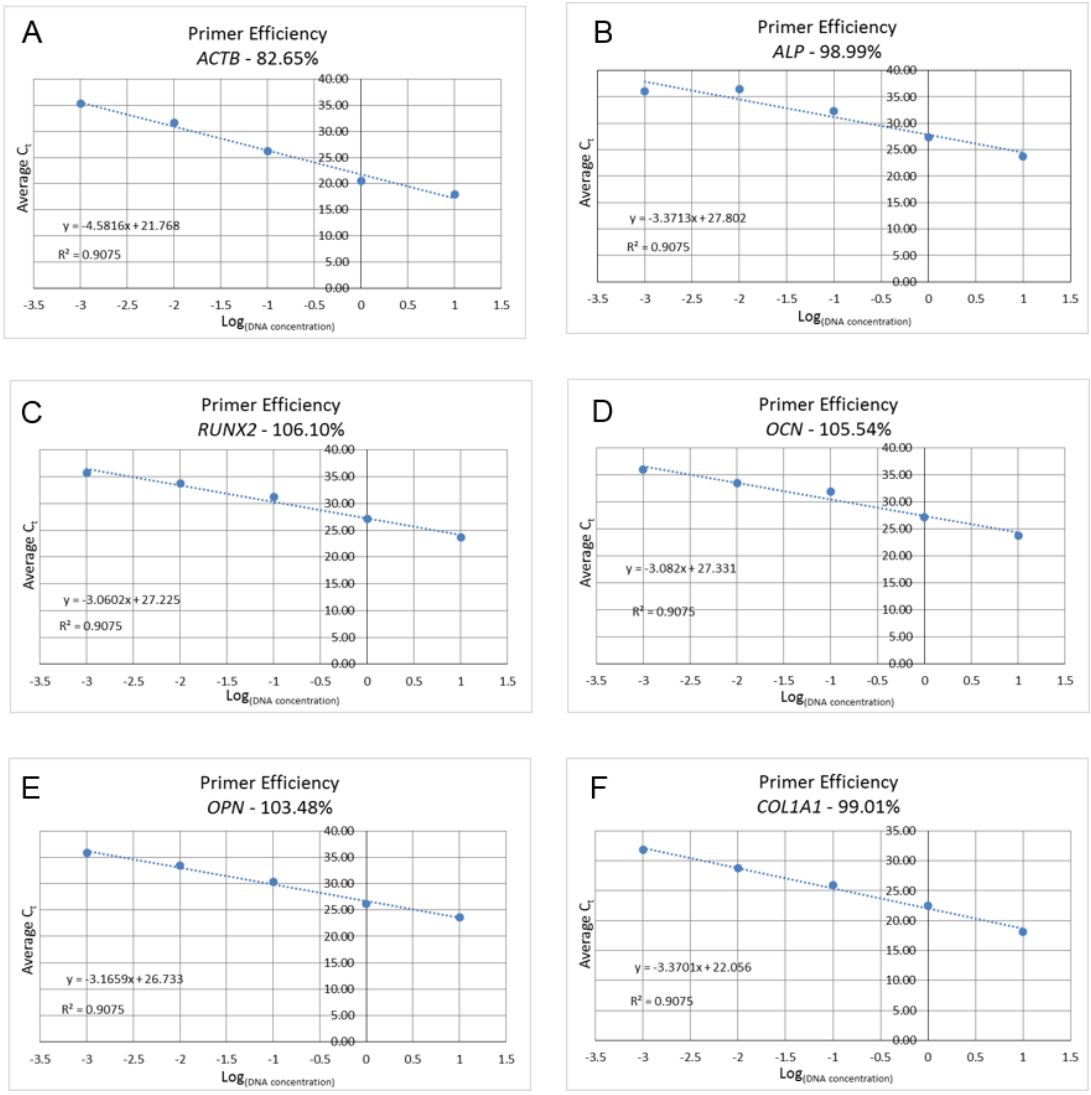

*Figure A3.2. Primer efficiency. Efficiency of primers to initiate DNA replication was calculated using C_t values at known DNA concentrations. Primer efficiency for each primer is displayed at the title of each graph. Amplification efficiency (E) =10^(-1/(slope)) and % amplification efficiency = (E-1)*100%.*

Section 3: Housekeeping Gene Selection

In order to determine ideal housekeeping gene for qPCR analysis, expression of *ALP* and *COL1A1* relative to housekeeping genes *ACTB* and *GAPDH* was calculated. Two patients SSCs samples, patient 1 (female 51) and patient 2 (female 63) were used and SSCs cultured on tissue culture plastic (TCP), flat PCL surface, nacre PCL topography and prism PCL topography.

Expression of *ALP* in patient 1 relative to housekeeping genes was similar for *ACTB* and *GAPDH* (Figure A3.3). On day 21, expression was measured to be higher with *GAPDH* housekeeping compared to *ACTB* (Figure A3.3). In patient 2 however, expression of *ALP* was found to be with a similar expression pattern on all surfaces, using either *GAPDH* (FigureA3.3D) or *ACTB* housekeeping genes (Figure A3.3C).

Measuring expression of *COL1A1* relative to both housekeeping genes *ACTB* and *GAPDH* allowed for further study into the effect of housekeeping gene selection on expression differences (Figure A3.4). The expression pattern is similar between both housekeeping genes however, the expression was higher when using *GAPDH*.

Because there were no differences in the pattern of expression between surfaces with using either of the two housekeeping genes selected, it was decided to pursue the use of *ACTB* as this was used in original studies by Dalby *et al* [250].

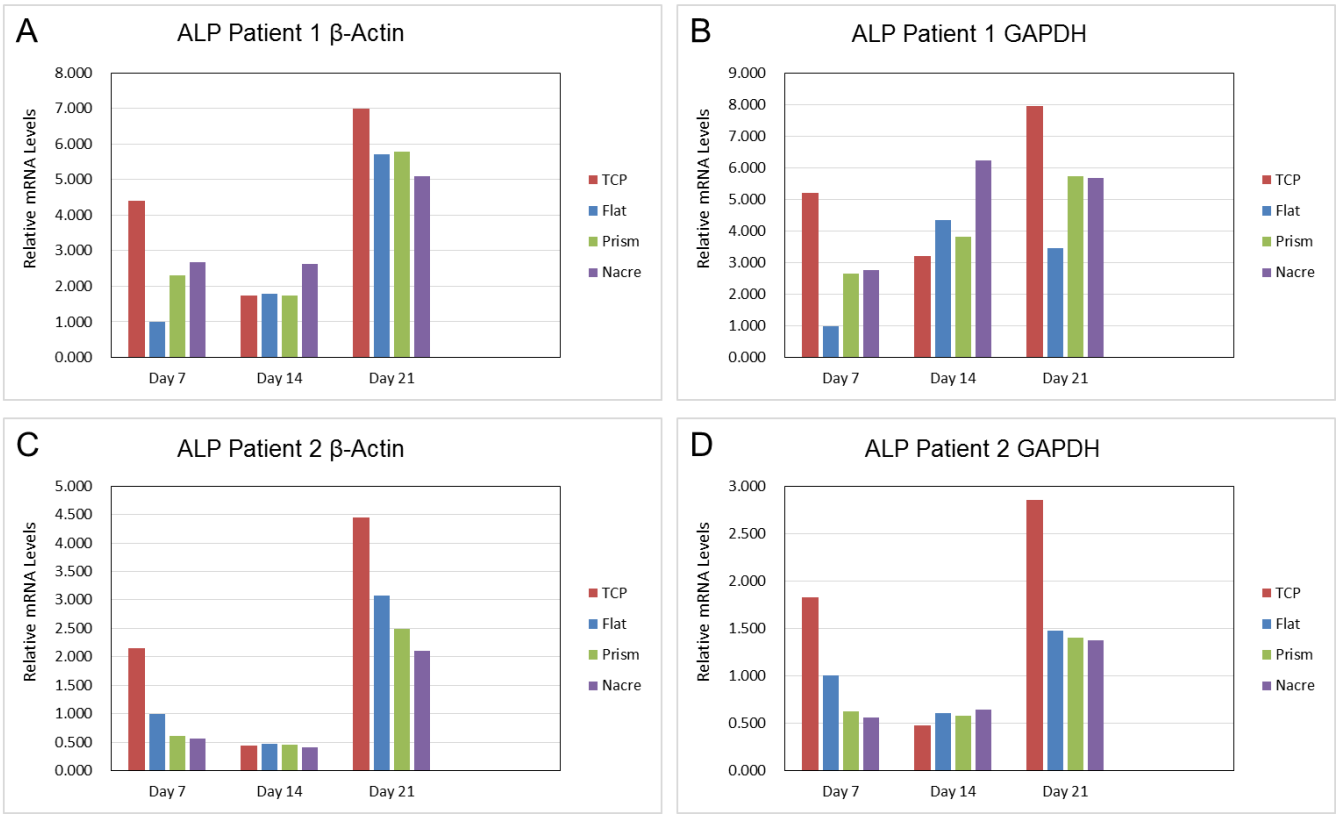

Figure A3.3. Evaluation housekeeping gene for qPCR measuring *ALP* expression. *Expression of ALP in SSCs cultured on tissue culture plastic (TCP), flat PCL surfaces, prism topographical surfaces and nacre topographical surfaces over 21 days. Expression is measured in patient 1 (A+B), and patient 2 (C+D), using housekeeping ACTB (A+C) and GAPDH (B+D).*

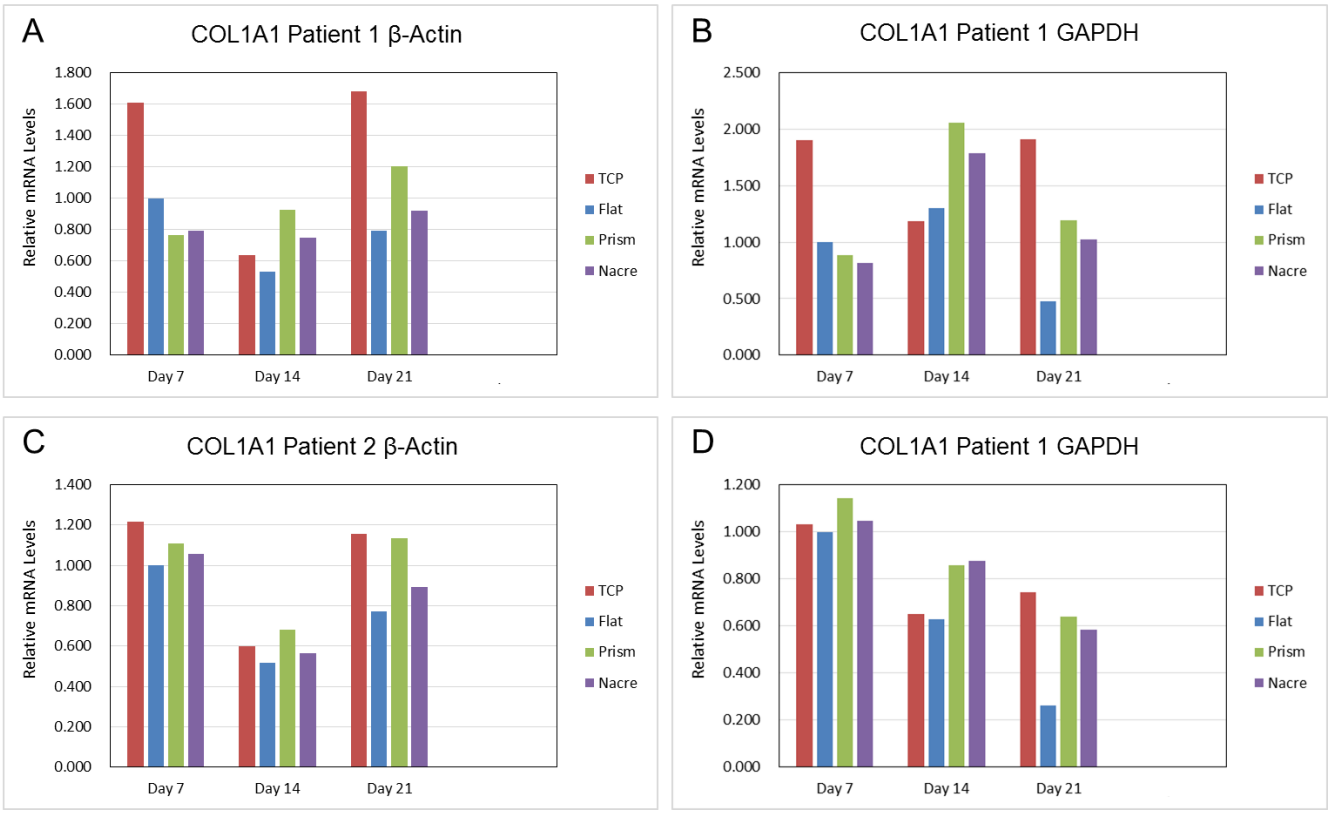

Figure A3.4. Evaluation housekeeping gene for qPCR measuring *COL1A1* expression. *Expression of ALP in SSCs cultured on tissue culture plastic (TCP), flat PCL surfaces, prism topographical surfaces and nacre topographical surfaces over 21 days. Expression is measured in patient 1 (A+B), and patient 2 (C+D), using housekeeping ACTB (A+C) and GAPDH (B+D).*

Appendix VI: Seeding Density Experiments for SSCs on Bioimprinted Surfaces

In order to determine ideal seeding density for SSCs cultured in bioimprinted surfaces detailed in Chapter 4, three seeding densities were studied, 1000 cells/well, 2000 cells/well and 4000 cells/well in 6-well plates. Expression of three osteogenic markers was studied in these seeding densities over 2 time points: day 7 and day 21 as described in section 2.3.4.

The results in Figure A4.1 show expression varied between the different seeding densities for the same gene and time point measured. For example, for *ALP* expression measured on day 7, expression was highest on blank bioimprint with 1000 cells/well, whereas on 2000 cells/well expression on late osteoblast bioimprint is higher. When seeding density was changed, the pattern of expression also changed. This could be expected as when seeding density is changed, the cell spreading has also altered (although this was not studied in these experiments). In general, expression of osteogenic markers was highest in 2000 cells/well and this was chosen for the experiments discussed in Chapter 4.

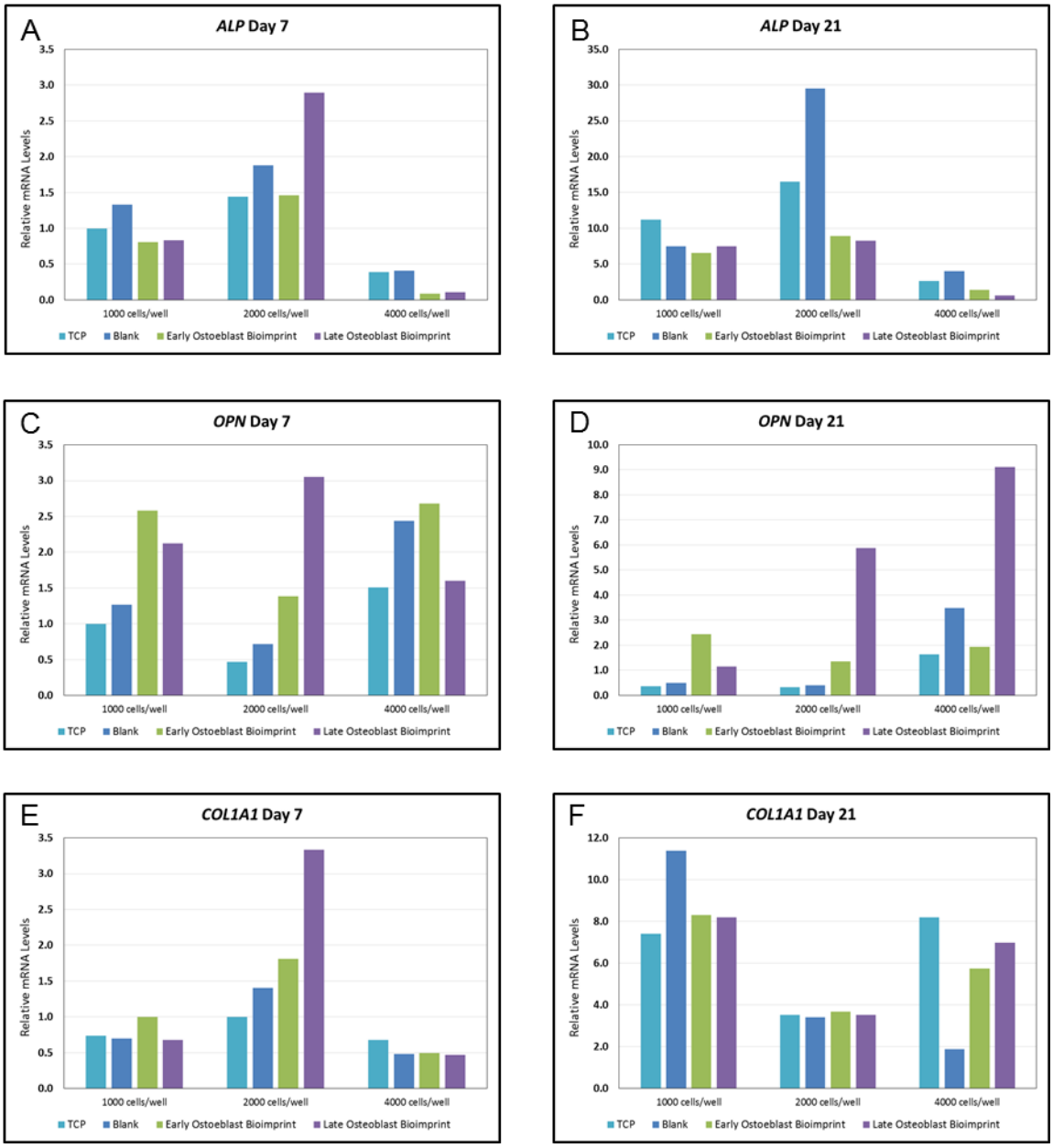

Figure A4.1. Expression of osteogenic markers in SSCs on bioimprinted surfaces with varying seeding densities. *Osteogenic markers ALP (A+B), OPN (C+D) and COL1A1 (E+F) measured on days 7 (A,C+E) and day 21 (B, D+F) on TCP (light blue), blank bioimprint (dark blue), early osteoblast (green) and late osteoblast (purple). Each sample was normalised to ACTB and relative to TCP on day 7. Name of gene expression measured is displayed at the top of each graph. n = 6 patients*

Appendix V: Papers published during this PhD

Curr Mol Bio Rep (2017) 3:263–275
https://doi.org/10.1007/s40610-017-0076-4

MOLECULAR BIOLOGY OF SKELETAL TISSUE ENGINEERING (D HUTMACHER, SECTION EDITOR)

The Potential of microRNAs for Stem Cell-based Therapy for Degenerative Skeletal Diseases

Emma Budd[1] · **Shona Waddell**[1] · **María C. de Andrés**[1] · **Richard O. C. Oreffo**[1]

Published online: 23 October 2017

Abstract
Purpose of Review Degenerative skeletal disorders including osteoarthritis (OA) and osteoporosis (OP) are the result of attenuation of tissue regeneration and lead to painful conditions with limited treatment options. Preventative measures to limit the onset of OA and OP remain a significant unmet clinical need. MicroRNAs (miRNAs) are known to be involved in the differentiation of stem cells, and in combination with stem cell therapy could induce skeletal regeneration and potentially prevent OA and OP onset.
Recent Findings The combination of stem cells and miRNA has been successful at regenerating the bone and cartilage in vivo. MiRNAs, including miR-146b known to be involved in chondrogenic differentiation, could provide innovative targets for stem cell-based therapy, for the repair of articular cartilage defects forestalling the onset of OA or in the generation of a stem cell-based therapy for OP.
Summary This review discusses the combination of skeletal stem cells (SSCs) and candidate miRNAs for application in a cell-based therapy approach for skeletal regenerative medicine.

Keywords miRNA · Skeletal stem cell · Cartilage · Bone · Osteoarthritis · Osteoporosis

Joint first authors are Emma Budd and Shona Waddell.

This article is part of the Topical Collection on *Molecular Biology of Skeletal Tissue Engineering*

✉ Richard O. C. Oreffo
roco@soton.ac.uk

[1] Bone & Joint Research Group, Centre for Human Development, Stem Cells and Regeneration, Faculty of Medicine, University of Southampton, Southampton SO16 6YD, UK

Introduction

Degenerative skeletal disorders are specific diseases associated with the ageing bone. These disorders can be divided into two main diseases: osteoarthritis (OA) and osteoporosis (OP). Given OA and OP are the result of the loss of the regenerative capacity of the skeletal tissues, skeletal stem cells (SSCs) have been investigated with the aim of harnessing their potential to improve the symptoms and treatment of these pathologies.

Ageing Cartilage and the Onset of OA

OA is a prevalent chronic disease and can be described as a heterogeneous condition, which results in joint signs and symptoms associated with defective integrity of the articular cartilage and changes to the bone at joint margins [1]. Articular cartilage is composed of non-migratory and non-proliferative resident chondrocytes embedded within an avascular, alymphatic and aneural specialised extracellular matrix (ECM), factors which following injury are likely to account for the limited capacity of articular cartilage to intrinsically repair [2]. Articular cartilage injury is likely to be causative to the onset of OA. Damage to the articular cartilage may appear asymptomatic but it is extremely likely that over time degenerative changes will result. Messner et al. demonstrated that athletes with isolated chondral lesions did not require treatment following initial injury. However, 14 years later, some of the athletes displayed with a reduction of the joint space, indicating that despite the initial chondral lesions having been asymptomatic, degradation of the articular cartilage supervened leading to permanent knee damage [3]. Cartilage damage is typically succeeded with long-term articular cartilage deterioration and OA.

Articular cartilage deterioration and onset of OA could potentially be prevented by repair of the initial articular cartilage

defect. A number of research groups have looked to identify the presence of chondroprogenitor cells within the articular cartilage and in tissues directly surrounding the articular cartilage, such as the synovium [4], the groove of Ranvier [5], the intrapatellar fat pad [6, 7] and the articular cartilage superficial zone [8, 9]. However, the source of progenitor populations for articular cartilage repair needs to be readily accessible and must not induce damage to the articular cartilage or tissues during isolation. Harnessing SSCs from bone marrow offers an option which does not involve further damage directly to articular cartilage or any surrounding tissue. The ability to direct bone marrow-derived SSCs to differentiate towards the chondrogenic lineage is a propitious option for articular cartilage regeneration. Thus, exploitation of mechanisms which govern chondrogenic differentiation of human SSCs could have significant implications for methods to induce novel articular cartilage formation and, potentially, help to prevent OA.

Loss of Regenerative Capacity of the Bone and Development of OP

The human skeleton reaches peak bone mass at around 30 years of age and, thereafter, bone mass is gradually lost. OP is a degenerative skeletal disorder, characterised by low bone mass and generalised disorder of the bone microarchitecture. OP is observed in men and women (in postmenopausal women, exacerbated by a fall in oestrogen production) and is a common cause of loss of bone mass and subsequent fracture [10]. It is estimated that 70% of inpatient fractures are a consequence of OP [11]. The regenerative capacity of the bone is reduced with age, leading to a decrease in bone mass [12–14]. Bone remodelling and therefore the regenerative potential of the bone is controlled by a careful balance between bone resorption, by osteoclasts, and bone deposition by osteoblasts. In OP, this process of bone remodelling is unbalanced with bone resorption exceeding bone formation resulting in the loss of bone mass observed in OP. The loss of regenerative capacity of the bone is multifactorial including (i) reduced stem cell potency/number, (ii) increased osteoclastic bone resorption, (iii) metabolic/factor imbalance and (iv) reduced osteoblast function [14, 15]. In addition, the increase in bone marrow adiposity is believed to play an important role in OP, with osteoporotic patients exhibiting a higher ratio of adipose tissue to total tissue volume in iliac crest bone biopsies compared to healthy controls [16, 17].

Currently, OP is treated with drugs which aim to increase bone density or inhibit bone resorption. Strategies include the use of bisphosphonates [18, 19], selective oestrogen receptor modulators [20], calcitonin [21, 22], sodium ranelate [23], RANK ligand inhibitors [24], the recombinant form of parathyroid hormone, teriparatide [25] and, more recently, the anti-sclerostin antibody, blosozumab [26, 27]. Although these drugs offer significant treatment options, development of efficacious anabolics for an increasing ageing population remains a goal.

Potential for Stem Cells and microRNAs for Treatment of Skeletal Disorders

Stem cells have been shown to be regulated in part by microRNAs (miRNAs), which regulate genes involved with differentiation post-transcriptionally. MiRNAs are processed from longer primary transcripts which undergo processing in the nucleus and the cytoplasm to form small non-coding RNA, which average 22 nucleotides in length [28]. Sequence complementarity between a miRNA and its target mRNA determines whether the miRNA induces post-transcriptional inhibition or degradation of the mRNA, which in turn prevents translation and protein synthesis [28]. This ability of miRNAs to regulate translation can allow for the potential exploitation of the function of miRNAs for use to control cellular processes including differentiation. Several miRNAs have been identified to play roles in chondrogenesis and osteogenesis [29–31]. MiRNAs found to be involved in these highly regulated processes, could therefore be exploited for their use to either induce stem cell chondrogenic differentiation for articular cartilage regeneration or osteogenic differentiation for bone regeneration. In essence, stem cells could be utilised for the regeneration of skeletal tissues in concert with miRNAs to enhance the differentiation of transplanted stem cells towards the chondrogenic or osteogenic lineages. Use of miRNAs could prime transplanted stem cells, directing them towards the desired cell fate. MiRNA modulation could serve as a tool to enhance stem cell differentiation, a novel approach to articular cartilage tissue reparation and bone regeneration. Not only could this novel concept induce the regeneration of skeletal tissues but, if applied early enough, could prevent the onset and progression of OA and OP. This review will examine the use of stem cells to regenerate skeletal tissue and the discovery of miRNAs which are involved in the chondrogenic and osteogenic differentiation of stem cells, including our own observations. Examples of studies which have demonstrated the use of miRNA modulated stem cell transplantation in vivo are discussed to reinforce the potential of miRNAs to direct stem cells to regenerate skeletal tissues.

The Use of Stem Cells for the Treatment of Degenerative Skeletal Disease

Properties of Skeletal Stem Cells

A stem cell is characterised by its ability to self-renew by means of asymmetrical cell division and its potential to differentiate into specialised types of cells, thereby retaining a pool

of stem cells and simultaneously producing transit amplifying cells [32]. Adult stem cells replace degenerating cells which facilitates tissue homeostasis. Adult stem cells can therefore be defined as the regenerators that follow the degeneration process which may occur due to trauma, age or pathogenic conditions [32].

The term skeletal stem cell (SSC), preferred by the authors and used in this review in reference to our own data defines, specifically, a self-renewing stem cell that resides in postnatal bone marrow and can differentiate into cartilage, the bone, haematopoiesis-supportive stroma and marrow adipocytes. It is the SSC of the bone marrow stroma that is responsible for the regenerative capacity inherent to the bone.

The heterogeneous population of cultured plastic adherent cells isolated from the bone marrow should be referred to as bone marrow stromal cells (BMSCs). However, it is acknowledged, the term mesenchymal stem cell (MSC), originally in reference to a hypothetical common progenitor of a wide range of "mesenchymal" (non-haematopoietic, non-epithelial, mesodermal) tissues, is commonly used and in this review will be retained where cited/used by others in the field.

Additional to their differentiation and proliferative properties, SSCs have been proposed to possess immunomodulatory properties which can regulate tumour evasion, autoimmunity and regulation of transplantation tolerance [33]. A combination of regulatory mechanisms exist within SSCs which act upon several immune cells including dendritic cells, T lymphocytes and natural killer (NK) cells [34]. Tse et al. observed that SSCs failed to stimulate allogeneic peripheral blood mononuclear cells and T cell proliferation and actively inhibited T cell proliferation [35]. Le Blanc et al. showed that alloreactive lymphocyte proliferative responses were not elicited in undifferentiated and also osteogenic and chondrogenic differentiated SSCs [36]. The immunosuppressive properties of SSCs, theoretically, limit any rejection of SSCs that could occur during therapeutic cell transplant. The concept that fibroblast-like cells migrate to distal sites of injury was fist hypothesised by the German pathologist Cohnheim [37]. Stem cells have the potential to home to sites of injury where they are likely to induce repair, through direct differentiation to replace damaged cells and/or secretion of mediators, which creates a reparative environment with immunoregulatory function and anti-apoptotic regulation [38].

Therapeutic Potential of SSCs in Degenerative Skeletal Disease

Osteoarthritis

Loss of chondrocytes and diminishment of the surrounding specialised ECM is as a result of the inability for cartilage to undergo spontaneous endogenous regeneration. The use of cell-based therapies to repair articular cartilage defects aims to produce a fully functional joint surface, capable of tolerating stress and strain.

Several studies have investigated the potential of SSCs in regenerating cartilage in animal models. For example, Im et al. induced osteochondral defects in to the patella grooves of rabbits, and autologous bone marrow-derived MSCs were applied to the defect sites. Histological and molecular analysis concluded that implantation of cultured MSCs could enhance cartilage repair [39]. In experimentally induced OA joint studies, non-operative administration of MSCs has also shown beneficial effects [40, 41]. A reduction in the degeneration of articular cartilage was observed following injection of autologous bone marrow-derived MSCs, in a hyaluronan solution, directly into OA-induced caprine knee joints [40].

A popular choice amongst research groups for investigating articular cartilage regeneration has been transplantation of SSCs combined with a scaffold. Previously, osteochondral progenitor cells expanded in vitro and dispersed into a type-1 collagen gel were transplanted into a full-thickness surgically induced articular cartilage defect in rabbits. At 24 weeks, the post-implantation subchondral bone was completely repaired with overlying articular cartilage [42]. Furthermore, Berninger et al. have suggested an experimental technique for combining MSCs in fibrin clots, followed by transplantation of pre-established fibrin-cell-clots into osteochondral defects in lapine knee joints. Preliminary experiments observed an intact and homogenous surface 12 weeks following implantation of the fibrin-MSC-clot into defect sites [43].

Previous clinical studies have reported the therapeutic effect of MSCs administration in patients [44–48]. Nejadnik et al. found that patients administered with bone marrow stem cells into chondral lesions demonstrated enhanced physical chondrocyte implantation [44]. Follow-up inspection found that transplantation of autologous expanded bone marrow-derived MSCs combined with platelet-rich fibrin glue, to full-thickness cartilage defects in five patients, resulted in improvement to symptoms in all patients. Complete defect filling and surface conformity with native cartilage was observed in three patients [45]. Kuroda et al. showed that administration of autologous bone marrow stromal cells to an articular cartilage defect in a young male athlete resulted in marked improved clinical outcomes. At 7 months post-surgery, arthroscopy revealed that the defect was completely covered with smooth tissues, and histologically the defect was filled with hyaline-like cartilage. Strikingly, 1 year post-surgery, the athlete returned to his previous activity level and experienced no pain with significant improvement in clinical symptoms [48].

Osteoporosis

Given OP is the result of altered bone remodelling, improving the efficiency or restoration of appropriate balance of this process would appear a natural strategy for the treatment of

OP. It is known that SSCs can be induced to form osteoblasts when cultured on tissue culture plastic [49]. However, translation to a cell-based treatment requires careful control of the differentiation of the stem cells. This could, potentially, be achieved through the use of miRNAs to control osteogenic differentiation. In addition, ensuring maximal osteogenic differentiation, with minimal differentiation to other lineages, remains a key challenge in translating skeletal stem and progenitor populations from the bench to clinical application. Various strategies have been proposed which would ensure maximal osteogenic lineage commitment. These approaches include selection of a specific stage of osteoprogenitor subsets [50, 51]. Other approaches to select for osteoprogenitor cells include the use of biomaterials to culture SSCs designed to enhance osteogenic differentiation. Examples of biomaterials include nanosurface geometries [52, 53] and osteoconductive scaffolds [54].

The use of bone tissue, autograft (patient derived) and allograft (donor), together with bone stem cells and progenitors has been examined. Marcacci et al., in a study of four patients with large bone defects, examined the potential of autologous culture-expanded SSCs onto a ceramic scaffold [55]. No major complications were reported after surgery and long-term follow-up of 6 to 7 years showed good integration of the scaffold [55]. Kim et al. studied the effect of osteoblast injection into long bone fractures to examine accelerated healing [56]. Autologous osteoblasts were expanded from patients with long bone fracture, and injected into the site of fracture, with the control group receiving no treatment [56]. The results demonstrated that osteoblast injection enhanced fracture healing with little complication [56]. The success of these important, albeit small, trials in humans emphasise the potential of SSC strategies for the treatment of bone fracture, bone defects and potentially degenerative bone diseases. In particular, culturing SSCs with a high osteogenic differentiation potential would prove important to generate the cell numbers required for cell-based therapy [57].

MiRNA Expression During Skeletal Differentiation of Stem Cells

In vitro models of stem cell differentiation have allowed for the analysis of miRNAs involved with post-transcriptional regulation of chondrocyte and cartilage development, as well as osteocyte and bone development. Such miRNAs are responsible for gene activation or suppression during the process of differentiation. A selection of miRNAs and their mRNA targets studied to date, known to be involved in stem cell differentiation, are listed in Table 1 (chondrogenic differentiation) and Table 2 (osteogenic differentiation) and further illustrated in Fig. 1. Comprehension of miRNA expression profiles and the role that miRNAs play in regulation of gene expression during differentiation of stem cells allows for a better understanding of molecular mechanisms which regulate stem cell differentiation. Critically, miRNAs which influence stem cell fate could be exploited to induce and enhance stem cells, providing a novel cell-based therapy approach. MiRNAs could induce and enhance transplanted stem cells at articular cartilage defect sites to regenerate articular cartilage. MiRNAs could induce and enhance stem cell osteogenic differentiation generating a cell-based therapy for OP treatment. Through the application of miRNA mimics or miRNA inhibitors, stem cell differentiation can be modulated to enhance direction towards the desired lineage. Tables 1 and 2 indicate potential miRNAs of which expression levels could be increased or decreased, using miRNA mimics and miRNA inhibitors, respectively, which could potentially enhance chondrogenic and osteogenic differentiation.

Therapeutic Potential of Modulating miRNAs for Skeletal Disorders

Given that miRNAs display the potential to regulate chondrogenic and osteogenic differentiation of stem cells, harnessing miRNAs offers an appealing strategy for skeletal tissue repair of cartilage or enhancement of differentiation of SSCs towards an osteogenic lineage for bone formation. The potential of miRNAs to augment articular cartilage regeneration has been demonstrated in a study conducted by Lolli and colleagues [79••]. MiR-221 has been identified as a negative regulator of chondrogenesis [77, 78]. Lolli et al. have previously shown that silencing miR-221 induced chondrogenic differentiation of hMSCs [78]. hMSCs transfected with an inhibitor of miR-221 were encapsulated in alginate. A cartilage defect in an osteochondral biopsy was then filled with the transfected and alginate encapsulated cells, followed by implantation of the biopsy into immunocompromised mice. Compared to control untreated hMSCs and alginate only controls, miR-221 silenced hMSCs enhanced cartilage repair in vivo and cartilaginous tissue was generated with no sign of hypertrophic associated type X collagen deposition [79]. This approach, combining hMSCs primed with miRNA inhibitor, in an in vivo cartilage defect model is the first of its kind and suggests a translational strategy to localise stem cells to defective cartilage sites and promote cartilage repair.

The potential of miRNAs to augment bone formation has been demonstrated in a number of murine studies. With both miR-138 and miR34a, a hydroxyapatite/tricalcium phosphate (HA/TCP) scaffold was utilised in order to localise stem cells subcutaneously. Chen et al. used a similar approach to study the role of miR-34a, which is a negative regulator of bone formation [83••]. hMSCs were transfected with pre-miR-34a, anti-miR-34a and control miR and loaded onto HA/TCP scaffolds and implanted subcutaneously into

Table 1 MiRNAs identified in chondrogenic differentiation of stem cells, target mRNA, effect of miRNA modulation on chondrogenesis and potential use of identified miRNAs to enhance chondrogenic differentiation

MiRNA	Expression during chondrogenesis	mRNA targets of miRNA and mRNA function in chondrogenesis	Reported effect of miRNA modulation on chondrogenesis	Potential use of miRNA in inducing chondrogenesis
miR-29a	miR-29a was reported to be down-regulated during chondrogenic differentiation of human MSCs (hMSCs) [58, 59].	miR-29a was demonstrated to directly target the 3′UTR of *FOXO3A*. Transcription factor *FOXO3A* was observed to be up-regulated during chondrogenesis, and modulation of *FOXO3A* expression was found to regulate *SOX9*, *AGCAN* and *COL2A1* expression, with FOXO3A binding sites also identified within the genomic sequences of these genes [59]. miR-29a is likely to be down-regulated during chondrogenesis enabling derepression of *FOX3A* expression.	The overexpression of miR-29a in hMSCs, using pre-miR-29a, resulted in inhibition of chondrocyte-specific markers and a suppressive effect on chondrogenic differentiation. [59].	Decrease endogenous miR-29a levels with a miR-29a inhibitor.
miR-140-3p	miR-140-3p was reported to be up-regulated during chondrogenic differentiation of hMSCs [60].	mRNA targets of miR-140-3p remain unknown [60].	–	Increase miR-140-3p levels with a miR-140-3p mimic.
miR-140-5p	miR-140-5p was reported to be up-regulated during chondrogenesis of hMSCs [60, 61] and equine cord blood mesenchymal stromal cells [62].	MiR-140-5p was demonstrated to directly target the 3′UTR of *RALA*. *RALA* encodes Ras-related protein Ral-A (RALA), a small GTPase which functions to bind and hydrolyse guanosine triphosphate. RALA has been shown to interact with the exocyst complex in mediating cytoskeletal and secretory pathways [63]. RALA has been shown to be involved in TGF-β signalling through internalisation of membrane receptor activin type II [64] and also may be involved with the trafficking and secretion of glycosaminoglycans [65].	Inhibition of endogenous miR-140-5p in differentiating hMSCs, using anti-miR-140-5p, resulted in impaired chondrogenesis with an observed down-regulation of SOX9 and aggrecan. Knockdown of RALA resulted in the up-regulation of SOX9 [60].	Increase miR-140-5p levels with a miR-140-5p mimic.
miR-145	miR-145 was reported to be down-regulated during chondrogenic differentiation of murine MSCs [66].	miR-145 was demonstrated to directly target the 3′UTR of *Sox9* [66]. SOX9 is required for aggrecan [67], Col2a1 [68], Col9a1 [69] and Col11a2 expression [70] and has been shown to bind to chondrocyte-specific enhancer elements in all of these genes. miR-145 is likely to be down-regulated during chondrogenesis enabling derepression of *Sox9* expression.	Overexpression of miR-145 in C3H10T1/2 cells, using pre-miR-146, resulted in the down-regulation of chondrogenic differentiation, evidenced by down-regulation of Sox9 protein and *Col2a1*, *Agcan*, *Col9a2*, *Col11a1* and *COMP* mRNA. Endogenous inhibition of miR-145, using anti-miR-145, resulted in enhancement of chondrogenic differentiation, evidenced by the up-regulation of Sox9 protein and *Col2a1*, *Agcan*,	Decrease endogenous miR-145 levels with a miR-145 inhibitor.

Table 1 (continued)

MiRNA	Expression during chondrogenesis	mRNA targets of miRNA and mRNA function in chondrogenesis	Reported effect of miRNA modulation on chondrogenesis	Potential use of miRNA in inducing chondrogenesis
			Col9a2, *Coll1a1* and *COMP* mRNA [66].	
miR-146a	miR-146a was reported to be down-regulated in chondrogenic epiphyseal cell populations isolated from the epiphyses of human foetal femora [71].	miR-146a was suggested to target positive mediators of chondrogenic signalling, *SMAD2* and *SMAD3* [71]. miR-146a is likely to be down-regulated during chondrogenesis enabling derepression of *SMAD2* and *SMAD3* expression.	Overexpression of miR-146a in cells derived from the epiphyses of human foetal femora, using miR-146a mimic, resulted in *SOX9* down-regulation, indicating the negative effect of miR-146a on chondrogenesis [71].	Decrease endogenous miR-146a levels with a miR-146a inhibitor.
miR-146b	miR-146b was reported to be down-regulated during chondrogenic differentiation of human SSCs [72•].	miR-146b was suggested to target early chondrogenic transcription factor *SOX5* [72•]. Early transcription factor SOX5 is co-expressed with SOX6 and SOX9 to enhance *Col2a1* expression [73] and to enable SOX9 binding to the *AGCAN* enhancer [67]. miR-146b is likely to be down-regulated during chondrogenesis, enabling derepression of *SOX5* expression.	Overexpression of miR-146b in human SSCs, using miR-146b mimic, resulted in down-regulation of SOX5 [72•].	Decrease endogenous miR-146b levels with a miR-146b inhibitor.
miR-193b	miR-193b was reported to be up-regulated during chondrogenic differentiation of human adipose-derived stem cells (hADSCs) [74, 75] and ATDC5 cells [74].	miR-193b was demonstrated to directly target the 3'UTRs of *Tgfb2* and *Tgfbr3* [74].	Overexpression of miR-193b in ATDC cells, using miR-193b mimic, resulted in the down-regulation of chondrogenic differentiation, evidenced by the down-regulation of early chondrogenic markers *col2a1*, *sox9* and *comp* as well as *Tgfb2* and *Tgfbr3*. Inhibition of endogenous miR-193b, using anti-miR-193b, resulted in the enhancement of chondrogenic differentiation, evidenced by the up-regulation of the early chondrogenic markers and *Tgfb2* and *Tgfbr3* [74].	Decrease endogenous miR-193b levels with a miR-193b inhibitor.
miR-194	miR-194 was reported to be down-regulated during chondrogenic differentiation of hADSCs [76].	miR-194 was demonstrated to directly target the 3'UTR of *SOX5* [76]. Early transcription factor SOX5 is co-expressed with SOX6 and SOX9 to enhance *Col2a1* expression [73] and to enable SOX9 binding to the *AGCAN* enhancer [67]. miR-194 is likely to be down-regulated during chondrogenic differentiation enabling derepression of *SOX5* expression.	Overexpression of miR-194 in hADSCs, using pre-miR-194, resulted in the down-regulation of chondrogenic differentiation, evidenced by the down-regulation of the chondrogenic markers *COL2A1*, *COL9A2*, *COL11A1*, *AGC1* and *COMP*. Inhibition of endogenous miR-194, using anti-miR-194, resulted in enhanced chondrogenesis evidenced by up-regulation of chondrogenic markers [76].	Decrease endogenous miR-194 levels with a miR-194 inhibitor.
miR-221	miR-221 was reported to be up-regulated during JNK inhibitor-induced chondrogenic differentiation inhibition in	miR-221 was demonstrated to directly target *MDM2* [77].	Silencing of miR-211 in hMSCs resulted in the up-regulation of chondrogenic markers such as *COL2A1* and *SOX9* [78]. In an in vivo cartilage defect model, miR-221 silenced and alginate encapsulated hMSCs, generated cartilaginous tissue with enhanced	Decrease endogenous miR-221 levels with a miR-221 inhibitor.

Table 1 (continued)

MiRNA	Expression during chondrogenesis	mRNA targets of miRNA and mRNA function in chondrogenesis	Reported effect of miRNA modulation on chondrogenesis	Potential use of miRNA in inducing chondrogenesis
	chick limb bud mesenchymal cells [77].		cartilage repair [79••].	
miR-495	miR-495 was reported to be down-regulated during chondrogenic differentiation of hMSCs [80•].	miR-495 was demonstrated to directly target the 3′UTR of *SOX9* [80•]. SOX9 is required for aggrecan [67], Col2a1 [68], Col9a1 [69] and Col11a2 expression [70] and binds to chondrocyte-specific enhancer elements in all of these genes. miR-495 is likely to be down-regulated during chondrogenesis enabling derepression of *SOX9* expression.	Overexpression of miR-495 in hMSCs during chondrogenic differentiation, using miR-495 mimic, resulted in the down-regulation chondrogenic differentiation, evidenced by down-regulation of *SOX9*, *COL2A1* and *AGCAN* mRNA. Inhibition of endogenous miR-495, using anti-miR-495, resulted in the enhancement of chondrogenic differentiation, evidenced by up-regulation of *SOX9*, *COL2A1* and *AGCAN* mRNA [80•].	Decrease endogenous miR-495 levels with a miR-495 inhibitor.

immunocompromised mice. Implantation of the scaffold with hMSCs transfected with anti-miR-34a resulted in a more than 3.5-fold increase in bone formation [83••]. Eskildsen et al. used lipofectamine to transfect pre-miR-138, anti-miR-138 and control miR into hMSCs [84]. The cells were loaded onto HA/TCP scaffold and implanted subcutaneously into immunocompromised mice. Implantation of the scaffold comprising hMSCs transfected with anti-miR-138 resulted in a 2.2-fold increase in bone formation. While, implantation of the scaffold comprising hMSCs transfected with miR-138 mimic resulted in a 6.7-fold decrease in bone formation, supporting the observation that miR-138 is a negative regulator of osteogenic differentiation and bone formation [84]. This approach, combining hMSC primed with miRNA inhibitor or mimic and a scaffold, suggests translational strategies to localise stem cells to the bone.

Li et al. used a miRNA intravenous therapy approach, without the use of the scaffold, to investigate the role of the positive regulator of osteogenic differentiation, miR-2861, on bone formation in mice [90]. When antagomiR miR-2861 was intravenously administered to induce miR-2861 silencing, a decrease in femur mineral density and trabecular thickness was observed. Following on from this work, Li et al. studied the role of miR-2681 in the development of OP in human patients with primary OP. The authors identified in a human sibling pair, both suffering from OP, an undetectable expression level of miR-2861 in their bone. A homozygous single nucleotide polymorphism (SNP) in pre-miR-2861 was identified and was suggested to be accountable for negligible miR-2861 expression levels and likely to be the confounding factor in the pathogenesis of primary OP. The authors suggest that dysregulation of miR-2861 is likely to induce defective osteoblast differentiation and subsequently contribute to OP. This mutation was found to be heterozygous in the parents of the sibling pair and these family members also suffered from OP. However, when extended to a larger cohort of 369 patients, the same SNP in pre-miR-2861 was not identified, indicating that the SNP was uncommon and not reflective of the general osteoporotic population. Nevertheless, the importance of miR-2861 in osteogenic differentiation and OP was highlighted, indicating its potential as a therapeutic approach.

For successful use of miRNA in stem cell therapeutics, it will be important to localise and minimise any miRNA off target effects. Qureshi et al. developed a technique for photoactivation of nanoparticle conjugated miR-148b [91•]; miR-148b has previously been reported to up-regulate osteogenic differentiation, increasing ALP activity in hMSCs [92]. The non-toxic conjugate remained inert until photoactivation by UV light, which was confirmed by an observed increase in *ALP* and *OCN* expression in photoactivated hADSCs compared to non-UV treated cells. In addition, the specific use of nanoparticle conjugated miR-148b resulted in delivery of miR-148b to the intracellular compartments of hADSCs,

Table 2 MiRNAs identified in osteogenic differentiation of stem cells, target mRNA, effect of miRNA modulation on osteogenesis and potential use of identified miRNAs to enhance osteogenic differentiation

MiRNA	Expression during osteogenesis	mRNA targets of miRNA and mRNA function in osteogenesis	Reported effect of miRNA modulation on osteogenesis	Potential use of miRNA in inducing osteogenesis
miR-23a	miR-23a was reported to be down-regulated during osteogenic differentiation of human BMSCs (hBMSCs) [81].	miR-23a was demonstrated to directly target the 3'UTR of *LRP5*; an essential component of the Wnt signalling pathway. miR-23a is likely to be down-regulated during osteogenesis, enabling derepression of *LRP5* expression, subsequently enabling Wnt signalling to direct osteogenesis [81].	Overexpression of miR-23a, using miR-23a mimic, resulted in the down-regulation of osteogenic differentiation, evidenced by the down-regulation of *ALP*, *OPN*, *RUNX2* and *IBSP* mRNA. Inhibition of endogenous miR-23a, using anti-miR-23a, resulted in enhancement of osteogenic differentiation, evidenced by the up-regulation of *ALP*, *OPN*, *RUNX2* and *IBSP* mRNA [81].	Decrease endogenous miR-23a levels with a miR-23a inhibitor.
miR-29a	miR-29a was reported to be up-regulated during the osteogenic differentiation of hFOB1.19 cells [82].	miR-29a was demonstrated to directly target the 3'UTRs of negative regulators of Wnt signalling: *Dkk1*, *Kremen2* and *sFRP2* [82]. miR-29a is likely to be up-regulated during osteogenesis to inhibit the negative regulators of Wnt signalling, indirectly promoting osteogenic differentiation.	Inhibition of endogenous miR-29a during osteogenic differentiation of hFOB1.19 cells, using miR-29a inhibitor, resulted in down-regulation of osteogenic differentiation, evidenced by down-regulation of *OCN* and *ALP* mRNA. Overexpression of miR-29a, using miR-29a mimic, resulted in the up-regulation of *OCN* mRNA [82].	Increase miR-29a levels with a miR-29a mimic.
miR-34a	miR-34a was reported to be up-regulated during osteogenic differentiation of hBMSC; however, miR-34a was found to negatively regulate differentiation [83••].	miR-34a was observed to target *JAG1* and cell cycle regulators *CDK4* and *CDK6* [83••].	Inhibition of endogenous miR-34a, using anti-miR-34a, was found to enhance osteogenic differentiation. hBMSCs transfected with anti-miR34a were subcutaneously implanted in mice, with the support of a scaffold. In this in vivo model of bone regeneration, an increase in bone formation was observed in mice which had received miR-34a silenced hBMSCs [83••].	Decrease endogenous miR-34a levels with a miR-34a inhibitor.
miR-138	miR-138 was reported to be down-regulated during osteogenic differentiation of human MSCs (hMSCs) [84].	miR-138 was demonstrated to directly target the 3'UTR of *PTK2*, which encodes focal adhesion kinase (FAK) [84]. During osteoblast differentiation is it thought that Grb2-Sos-Ras pathway is activated by FAK inducing ERK1/2, and subsequently downstream genes associated with osteogenesis [85].	Inhibition of endogenous miR-138 in hMSCs, using anti-miR-138, resulted in enhanced osteogenic differentiation as measured by an increase in *OCN* and *ALP* mRNA levels and matrix mineralisation. Overexpression of miR-138, using pre-miR-138, was found to reduce osteogenic differentiation. miR-138 silenced hMSCs loaded onto a scaffold and implanted subcutaneously in mice, resulted in an increase in bone formation and up-regulation *OCN* and *ALP* mRNA [84].	Decrease endogenous miR-138 levels with a miR-138 inhibitor.
miR-146a	miR-146a was reported to be up-regulated in osteogenic diaphyseal cell populations isolated from the diaphysis of human foetal femora [72•].	miR-146a targets positive regulators of chondrogenesis, *SMAD2* and *SMAD3*. Indirect promotion of osteogenic differentiation is suggested via miR-146a degradation of *SMAD2* and *SMAD3*, during endochondral foetal skeletogenesis [72•].	miR-146a overexpression, using miR-146a mimic, resulted in down-regulation of SMAD2 and SMAD3 and an increase in *RUNX2* mRNA, a marker of osteogenic differentiation [72•].	Increase miR-146a levels with a miR-146a mimic.
miR-218	miR-218 was reported to be up-regulated in MC3T3 cells [86] and hADSCs [87•] during osteogenic differentiation.	miR-218 was demonstrated to directly target the 3'UTR of negative regulators of Wnt signalling, *SFRP2* and *DKK1* [86].	Overexpression of miR-218 in murine BMSCs, using miR-210 lentivirus, resulted in enhanced osteogenic differentiation, evidenced by up-regulation of *Runx2*, *Alp* and *Ocn* mRNA [81].	Increase miR-218 levels with a miR-218 mimic.

Table 2 (continued)

MiRNA	Expression during osteogenesis	mRNA targets of miRNA and mRNA function in osteogenesis	Reported effect of miRNA modulation on osteogenesis	Potential use of miRNA in inducing osteogenesis
			Inhibition of miR-218 was found to reduce osteogenic differentiation of hADSCs [87•].	
miR-346	miR-346 was reported to be up-regulated during osteogenic differentiation of hBMSCs [88].	miR-346 was demonstrated to directly target the 3'UTR of *GSK-3β*, a negative regulator of Wnt signalling. An increase in nuclear accumulation of β-catenin was observed during miR-346 overexpression, indicating an enhancement of Wnt signalling. miR-346 was suggested to promote osteogenesis through activation of the Wnt signalling pathway [88]. miR-346 is likely to be up-regulated during osteogenesis to inhibit the negative regulators of Wnt signalling, indirectly promoting osteogenic differentiation.	Overexpression of miR-346 in hBMSCs, using miR-346 mimic, resulted in enhanced osteogenic differentiation, evidenced by up-regulation of *RUNX2*, *ALP* and *OPN* mRNA and increased matrix mineralisation and ALP activity. Inhibition of endogenous miR-346, using anti-miR-346, resulted in the down-regulation osteogenic differentiation, evidenced by down-regulation of osteogenic marker mRNA expression, ALP activity and matrix mineralisation [88].	Increase miR-346 levels with a miR-346 mimic.
miR-637	miR-637 was reported to be down-regulated during osteogenic differentiation of hMSCs [89].	miR-637 was demonstrated to directly target the 3'UTR of *OSX*, which encodes osterix, a key transcription factor of osteoblasts. Down-regulation of miR-637 during osteogenesis results in osterix derepression, promoting osteogenic differentiation [89].	Overexpression of miR-637 in hMSCs, using a lentiviral-pre-miR-673 vector, down-regulated osteogenic differentiation, evidenced by a decrease in ALP activity and down-regulation of *RUNX2* and *BMP2* mRNA. Inhibition of endogenous miR637, using a lentiviral short-hairpin of pre-miR-637 vector, enhanced osteogenic differentiation, evidenced by an increase in ALP activity and up-regulation of *RUNX2* and *BMP2* mRNA [89].	Decrease endogenous miR-637 levels with a miR-637 inhibitor.
miR-2861	miR-2861 was reported to be up-regulated in BMP2-induced osteogenesis of murine BMSCs [90].	miR-2861 was demonstrated to directly target an amino acid coding sequence in *Hdac4* mRNA [90]. miR-2861 is likely to be up-regulated during osteogenesis to suppress expression of the negative regulator of Runx2, *hdac4*.	Overexpression of miR-2861 in mice BMSCs, using pre-miR-2861, resulted in enhanced osteogenic differentiation, evidenced by increased ALP activity and osteocalcin secretion and up-regulation of Runx2. An in vivo model reported that injection of anti-miR-2861 in mice resulted in a reduction in femur bone mineral density and reduced osteoblast activity [90].	Increase miR-2861 levels with a miR-2861 mimic.

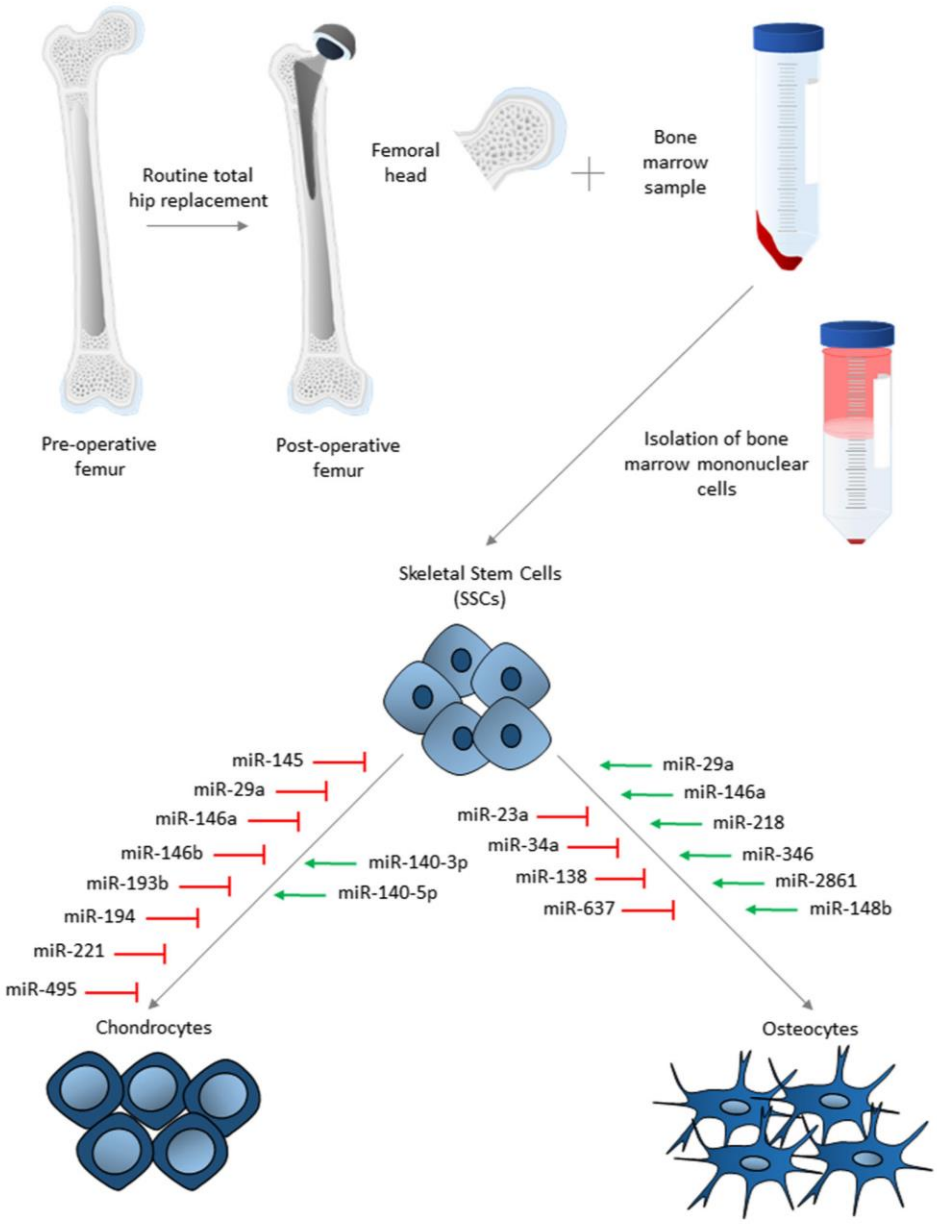

Fig. 1 miRNAs involved in osteogenic and chondrogenic differentiation of SSCs isolated from human bone marrow. Following routine total hip replacement, the femoral head is removed and bone marrow sample donated for isolation of SSCs. From the bone marrow sample, mononuclear cells are isolated by density centrifugation and the cell population enriched for SSCs by magnetic separation. MiRNAs involved in either chondrogenic or osteogenic differentiation are indicated by association with the relevant arrow. MiRNAs in red negatively regulate differentiation and in green positively regulate differentiation

without the need for additional, potentially damaging, chemical-based methods of transfecting stem cells.

Conclusion

The problems associated with degenerative skeletal disorders highlighted in this review indicate how miRNA could be used to treat these musculoskeletal conditions. The underlying aetiology of OA remains unknown which makes development of a treatment for this debilitating disease difficult. However, if initial chondral lesions can be targeted, the potential for a preventative approach in OA will become a clinical possibility. If the original chondral lesion can be repaired using stem cells enhanced to undergo chondrogenic differentiation efficiently with use of miRNAs modulation, inducing regeneration of the articular cartilage and reinstating integrity, then the degenerative changes, typical of OA could be reduced. Thus, an attractive approach, with knowledge of different miRNAs expression during chondrogenic differentiation, would be to administer specific miRNAs transfected stem cells to chondral defect sites to enhance articular cartilage regeneration capacity. The bone regeneration balance lost in osteoporosis can benefit from an SSC-based cell therapy which could

potentially restore bone microarchitecture and composition to a healthy state. The approach of priming these SSCs with miRNA could lead to enhanced direction of SSCs towards osteogenic differentiation. MiRNAs have been shown to enhance bone formation in murine trials, and known mutations in miRNAs have been identified in human osteoporotic patients. This cell-based approach could be advantageous when applied at early stages of the disease in order to prevent further bone loss and minimise any potential fracture risk that can occur with disease progression. While consideration of miRNAs in skeletal disease therapy is still in its infancy, with considerable research still to be undertaken, the potential for the use of miRNA in a therapeutic context offers an exciting treatment option for a growing ageing population.

Acknowledgements Work in the authors' laboratories was supported by grants from the BBSRC (BB/L021072/1 and BB/L00609X/1 and UK Regenerative Medicine Platform (MR/K026682/1) and University of Southampton to RO. The work presented here is based on many useful discussions with past and current members of the Bone and Joint Research Group in Southampton, UK.

Compliance with Ethical Standards

Conflict of Interest Emma Budd, Shona Waddell, María C. de Andrés, and Richard O. C. Oreffo declare that they have no conflicts of interest.

Human and Animal Rights and Informed Consent This article does not contain any studies with human or animal subjects performed by any of the authors.

References

Papers of particular interest, published recently, have been highlighted as:
- • Of importance
- •• Of major importance

1. Sarzi-Puttini P, Cimmino MA, Scarpa R, Caporali R, Parazzini F, Zaninelli A, et al. Osteoarthritis: an overview of the disease and its treatment strategies. Semin Arthritis Rheum. 2005;35(1 Suppl 1):1–10.
2. Sophia Fox AJ, Bedi A, Rodeo SA. The basic science of articular cartilage: structure, composition, and function. Sports Health. 2009;1(6):461–8.
3. Messner K, Maletius W. The long-term prognosis for severe damage to weight-bearing cartilage in the knee: a 14-year clinical and radiographic follow-up in 28 young athletes. Acta Orthop Scand. 1996;67(2):165–8.
4. De Bari C, Dell'Accio F, Tylzanowski P, Luyten FP. Multipotent mesenchymal stem cells from adult human synovial membrane. Arthritis Rheum. 2001;44(8):1928–42.
5. Karlsson C, Thornemo M, Henriksson HB, Lindahl A. Identification of a stem cell niche in the zone of Ranvier within the knee joint. J Anat. 2009;215(3):355–63.
6. Wickham MQ, Erickson GR, Gimble JM, Vail TP, Guilak F. Multipotent stromal cells derived from the infrapatellar fat pad of the knee. Clin Orthop Relat Res. 2003;412:196–212.
7. Candela ME, Yasuhara R, Iwamoto M, Enomoto-Iwamoto M. Resident mesenchymal progenitors of articular cartilage. Matrix Biol : J Int Soc Matrix Biol. 2014;39:44–9.
8. Dowthwaite GP, Bishop JC, Redman SN, Khan IM, Rooney P, Evans DJR, et al. The surface of articular cartilage contains a progenitor cell population. J Cell Sci. 2004;117(6):889–97.
9. Hattori S, Oxford C, Reddi AH. Identification of superficial zone articular chondrocyte stem/progenitor cells. Biochem Biophys Res Commun. 2007;358(1):99–103.
10. Szulc P, Delmas PD. Bone loss in elderly men: increased endosteal bone loss and stable periosteal apposition. The prospective MINOS study. Osteoporos Int. 2007;18(4):495–503.
11. Court-Brown CM, Caesar B. Epidemiology of adult fractures: a review. Injury. 2006;37(8):691–7.
12. Stenderup K, Justesen J, Clausen C, Kassem M. Aging is associated with decreased maximal life span and accelerated senescence of bone marrow stromal cells. Bone. 2003;33(6):919–26.
13. Nishida S, Endo N, Yamagiwa H, Tanizawa T, Takahashi HE. Number of osteoprogenitor cells in human bone marrow markedly decreases after skeletal maturation. J Bone Miner Metab. 1999;17(3):171–7.
14. Rodriguez JP, Garat S, Gajardo H, Pino AM, Seitz G. Abnormal osteogenesis in osteoporotic patients is reflected by altered mesenchymal stem cells dynamics. J Cell Biochem. 1999;75(3):414–23.
15. Caplan AI. Mesenchymal stem cells: cell-based reconstructive therapy in orthopedics. Tissue Eng. 2005;11(7–8):1198–211.
16. Justesen J, Stenderup K, Ebbesen EN, Mosekilde L, Steiniche T, Kassem M. Adipocyte tissue volume in bone marrow is increased with aging and in patients with osteoporosis. Biogerontology. 2001;2(3):165–71.
17. Verma S, Rajaratnam JH, Denton J, Hoyland JA, Byers RJ. Adipocytic proportion of bone marrow is inversely related to bone formation in osteoporosis. J Clin Pathol. 2002;55(9):693–8.
18. Drake MT, Clarke BL, Khosla S. Bisphosphonates: mechanism of action and role in clinical practice. Mayo Clin Proc. 2008;83(9):1032–45.
19. Brumsen C, Papapoulos SE, Lips P, Geelhoed-Duijvestijn P, Hamdy NAT, Landman JO, et al. Daily oral pamidronate in women and men with osteoporosis: a 3-year randomized placebo-controlled clinical trial with a 2-year open extension. J Bone Miner Res. 2002;17(6):1057–64.
20. Reginster JY, Ferrari S, Hadji P. Current challenges in the treatment of osteoporosis: an opportunity for bazedoxifene. Curr Med Res Opin. 2014;30(6):1165–76.
21. Binkley N, Bolognese M, Sidorowicz-Bialynicka A, Vally T, Trout R, Miller C, et al. A phase 3 trial of the efficacy and safety of oral recombinant calcitonin: the Oral Calcitonin in Postmenopausal Osteoporosis (ORACAL) trial. J Bone Miner Res. 2012;27(8):1821–9.
22. Rizzoli R, Sigaud A, Azria M, Herrmann FR. Nasal salmon calcitonin blunts bone microstructure alterations in healthy postmenopausal women. Osteoporos Int. 2015;26(1):383–93.
23. Reginster JY, Brandi ML, Cannata-Andia J, Cooper C, Cortet B, Feron JM, et al. The position of strontium ranelate in today's management of osteoporosis. Osteoporos Int. 2015;26(6):1667–71.

24. Sutton EE, Riche DM. Denosumab, a RANK ligand inhibitor, for postmenopausal women with osteoporosis. Ann Pharmacother. 2012;46(7–8):1000–9.
25. Lindsay R, Krege JH, Marin F, Jin L, Stepan JJ. Teriparatide for osteoporosis: importance of the full course. Osteoporosis. 2016;27(8):2395–410.
26. Clarke BL. Anti-sclerostin antibodies: utility in treatment of osteoporosis. Maturitas. 2014;78(3):199–204.
27. Recker RR, Benson CT, Matsumoto T, Bolognese MA, Robins DA, Alam J, et al. A randomized, double-blind phase 2 clinical trial of blosozumab, a sclerostin antibody, in postmenopausal women with low bone mineral density. J Bone Miner Res. 2015;30(2):216–24.
28. Pasquinelli AE, Hunter S, Bracht J. MicroRNAs: a developing story. Curr Opin Genet Dev. 2005;15(2):200–5.
29. Wu C, Tian B, Qu X, Liu F, Tang T, Qin A, et al. MicroRNAs play a role in chondrogenesis and osteoarthritis (review). Int J Mol Med. 2014;34(1):13–23.
30. Fang S, Deng Y, Gu P, Fan X. MicroRNAs regulate bone development and regeneration. Int J Mol Sci. 2015;16(4):8227–53.
31. Zhao X, Xu D, Li Y, Zhang J, Liu T, Ji Y, et al. MicroRNAs regulate bone metabolism. J Bone Miner Metab. 2014;32(3):221–31.
32. Weiner L. Definitions and criteria for stem cells. In: Weiner L, editor. Neural stem cells. Methods in molecular biology™, vol. 438. New York: Humana Press; 2008. p. 3–8.
33. Chen X, Armstrong MA, Li G. Mesenchymal stem cells in immunoregulation. Immunol Cell Biol. 2006;84(5):413–21.
34. Chen P-M, Yen M-L, Liu K-J, Sytwu H-K, Yen B-L. Immunomodulatory properties of human adult and fetal multipotent mesenchymal stem cells. J Biomed Sci. 2011;18(1):49.
35. Tse WT, Pendleton JD, Beyer WM, Egalka MC, Guinan EC. Suppression of allogeneic T-cell proliferation by human marrow stromal cells: implications in transplantation. Transplantation. 2003;75(3):389–97.
36. Le Blanc K, Tammik C, Rosendahl K, Zetterberg E, Ringden O. HLA expression and immunologic properties of differentiated and undifferentiated mesenchymal stem cells. Exp Hematol. 2003;31(10):890–6.
37. Cohnheim J. Ueber Entzündung und Eiterung. Archiv Pathol Anat Physiol Klin Med. 40(1):1–79.
38. Sordi V, Malosio ML, Marchesi F, Mercalli A, Melzi R, Giordano T, et al. Bone marrow mesenchymal stem cells express a restricted set of functionally active chemokine receptors capable of promoting migration to pancreatic islets. Blood. 2005;106(2):419–27.
39. Im GI, Kim DY, Shin JH, Hyun CW, Cho WH. Repair of cartilage defect in the rabbit with cultured mesenchymal stem cells from bone marrow. J Bone Joint Surg Br Vol. 2001;83(2):289–94.
40. Murphy JM, Fink DJ, Hunziker EB, Barry FP. Stem cell therapy in a caprine model of osteoarthritis. Arthritis Rheum. 2003;48(12):3464–74.
41. Al Faqeh H, Nor Hamdan BM, Chen HC, Aminuddin BS, Ruszymah BH. The potential of intra-articular injection of chondrogenic-induced bone marrow stem cells to retard the progression of osteoarthritis in a sheep model. Exp Gerontol. 2012;47(6):458–64.
42. Wakitani S, Goto T, Pineda SJ, Young RG, Mansour JM, Caplan AI, et al. Mesenchymal cell-based repair of large, full-thickness defects of articular cartilage. J Bone Joint Surg Am. 1994;76(4):579–92.
43. Berninger MT, Wexel G, Rummeny EJ, Imhoff AB, Anton M, Henning TD, et al. Treatment of osteochondral defects in the rabbit's knee joint by implantation of allogeneic mesenchymal stem cells in fibrin clots. J Vis Exp: JoVE. 2013(75):4423.
44. Nejadnik H, Hui JH, Feng Choong EP, Tai BC, Lee EH. Autologous bone marrow-derived mesenchymal stem cells versus autologous chondrocyte implantation: an observational cohort study. Am J Sports Med. 2010;38(6):1110–6.
45. Haleem AM, Singergy AAE, Sabry D, Atta HM, Rashed LA, Chu CR, et al. The clinical use of human culture–expanded autologous bone marrow mesenchymal stem cells transplanted on platelet-rich fibrin glue in the treatment of articular cartilage defects: a pilot study and preliminary results. Cartilage. 2010;1(4):253–61.
46. Kasemkijwattana C, Hongeng S, Kesprayura S, Rungsinaporn V, Chaipinyo K, Chansiri K. Autologous bone marrow mesenchymal stem cells implantation for cartilage defects: two cases report. J Med Assoc Thai = Chotmaihet Thangphaet. 2011;94(3):395–400.
47. Davatchi F, Abdollahi BS, Mohyeddin M, Shahram F, Nikbin B. Mesenchymal stem cell therapy for knee osteoarthritis. Preliminary report of four patients. Int J Rheum Dis. 2011;14(2):211–5.
48. Kuroda R, Ishida K, Matsumoto T, Akisue T, Fujioka H, Mizuno K, et al. Treatment of a full-thickness articular cartilage defect in the femoral condyle of an athlete with autologous bone-marrow stromal cells. Osteoarthr Cartil / OARS, Osteoar Res Soc. 2007;15(2):226–31.
49. Abdallah BM, Jafari A, Zaher W, Qiu W, Kassem M. Skeletal (stromal) stem cells: an update on intracellular signaling pathways controlling osteoblast differentiation. Bone. 2015;70:28–36.
50. Loebel C, Czekanska EM, Bruderer M, Salzmann G, Alini M, Stoddart MJ. In vitro osteogenic potential of human mesenchymal stem cells is predicted by Runx2/Sox9 ratio. Tissue Eng A. 2015;21(1–2):115–23.
51. Born AK, Lischer S, Maniura-Weber K. Watching osteogenesis: life monitoring of osteogenic differentiation using an osteocalcin reporter. J Cell Biochem. 2012;113(1):313–21.
52. Dalby MJ, Gadegaard N, Tare R, Andar A, Riehle MO, Herzyk P, et al. The control of human mesenchymal cell differentiation using nanoscale symmetry and disorder. Nat Mater. 2007;6(12):997–1003.
53. Kilian KA, Bugarija B, Lahn BT, Mrksich M. Geometric cues for directing the differentiation of mesenchymal stem cells. Proc Natl Acad Sci U S A. 2010;107(11):4872–7.
54. Thibault RA, Baggett LS, Mikos AG, Kasper FK. Osteogenic differentiation of mesenchymal stem cells on pregenerated extracellular matrix scaffolds in the absence of osteogenic cell culture supplements. Tissue Eng A. 2010;16(2):431–40.
55. Marcacci M, Kon E, Moukhachev V, Lavroukov A, Kutepov S, Quarto R, et al. Stem cells associated with macroporous bioceramics for long bone repair: 6- to 7-year outcome of a pilot clinical study. Tissue Eng. 2007;13(5):947–55.
56. Kim SJ, Shin YW, Yang KH, Kim SB, Yoo MJ, Han SK, et al. A multi-center, randomized, clinical study to compare the effect and safety of autologous cultured osteoblast (Ossron) injection to treat fractures. BMC Musculoskelet Disord. 2009;10:20.
57. Jones EA, Giannoudis PV, Kouroupis D. Bone repair with skeletal stem cells: rationale, progress to date and clinical application. Ther Adv Musculoskelet Dis. 2016;8(3):57–71.
58. Guérit D, Philipot D, Brondello J-M, Chuchana P, Jorgensen C, Noël D. Inhibitory effect of miR-29A on the chondrogenic differentiation of mesenchymal stem cells. Osteoarthr Cartil. 2012;20:S52.
59. Guerit D, Brondello JM, Chuchana P, Philipot D, Toupet K, Bony C, et al. FOXO3A regulation by miRNA-29a controls chondrogenic differentiation of mesenchymal stem cells and cartilage formation. Stem Cells Dev. 2014;23(11):1195–205.
60. Karlsen TA, Jakobsen RB, Mikkelsen TS, Brinchmann JE. microRNA-140 targets RALA and regulates chondrogenic differentiation of human mesenchymal stem cells by translational enhancement of SOX9 and ACAN. Stem Cells Dev. 2014;23(3):290–304.
61. Miyaki S, Nakasa T, Otsuki S, Grogan SP, Higashiyama R, Inoue A, et al. MicroRNA-140 is expressed in differentiated human articular chondrocytes and modulates interleukin-1 responses. Arthritis Rheum. 2009;60(9):2723–30.

62. Buechli ME, Lamarre J, Koch TG. MicroRNA-140 expression during chondrogenic differentiation of equine cord blood-derived mesenchymal stromal cells. Stem Cells Dev. 2013;22(8):1288–96.
63. Sugihara K, Asano S, Tanaka K, Iwamatsu A, Okawa K, Ohta Y. The exocyst complex binds the small GTPase RalA to mediate filopodia formation. Nat Cell Biol. 2002;4(1):73–8.
64. Matsuzaki T, Hanai S, Kishi H, Liu Z, Bao Y, Kikuchi A, et al. Regulation of endocytosis of activin type II receptors by a novel PDZ protein through Ral/Ral-binding protein 1-dependent pathway. J Biol Chem. 2002;277(21):19008–18.
65. Wang L, Li G, Sugita S. RalA-exocyst interaction mediates GTP-dependent exocytosis. J Biol Chem. 2004;279(19):19875–81.
66. Yang B, Guo H, Zhang Y, Chen L, Ying D, Dong S. MicroRNA-145 regulates chondrogenic differentiation of mesenchymal stem cells by targeting Sox9. PLoS One. 2011;6(7):e21679.
67. Han Y, Lefebvre V. L-Sox5 and Sox6 drive expression of the aggrecan gene in cartilage by securing binding of Sox9 to a far-upstream enhancer. Mol Cell Biol. 2008;28(16):4999–5013.
68. Bell DM, Leung KK, Wheatley SC, Ng LJ, Zhou S, Ling KW, et al. SOX9 directly regulates the type-II collagen gene. Nat Genet. 1997;16(2):174–8.
69. Zhang P, Jimenez SA, Stokes DG. Regulation of human COL9A1 gene expression. Activation of the proximal promoter region by SOX9. J Biol Chem. 2003;278(1):117–23.
70. Liu Y, Li H, Tanaka K, Tsumaki N, Yamada Y. Identification of an enhancer sequence within the first intron required for cartilage-specific transcription of the alpha2(XI) collagen gene. J Biol Chem. 2000;275(17):12712–8.
71. Cheung KS, Sposito N, Stumpf PS, Wilson DI, Sanchez-Elsner T, Oreffo RO. MicroRNA-146a regulates human foetal femur derived skeletal stem cell differentiation by down-regulating SMAD2 and SMAD3. PLoS One. 2014;9(6):e98063.
72.• Budd E, de Andres MC, Sanchez-Elsner T, Oreffo ROC. MiR-146b is down-regulated during the chondrogenic differentiation of human bone marrow derived skeletal stem cells and up-regulated in osteoarthritis. Sci Rep. 2017;7:11. **This study demonstrates dysregulation of miR-146b in osteoarthritic chondrocytes and thereby illustrating importance of controlling miRNA to treat OA.**
73. Lefebvre V, Li P, de Crombrugghe B. A new long form of Sox5 (L-Sox5), Sox6 and Sox9 are coexpressed in chondrogenesis and cooperatively activate the type II collagen gene. EMBO J. 1998;17(19):5718–33.
74. Hou C, Yang Z, Kang Y, Zhang Z, Fu M, He A, et al. MiR-193b regulates early chondrogenesis by inhibiting the TGF-beta2 signaling pathway. FEBS Lett. 2015;589(9):1040–7.
75. Zhang Z, Kang Y, Zhang Z, Zhang H, Duan X, Liu J, et al. Expression of microRNAs during chondrogenesis of human adipose-derived stem cells. Osteoarthr Cartil / OARS, Osteoarthr Res Soc. 2012;20(12):1638–46.
76. Xu J, Kang Y, Liao W-M, Yu L. MiR-194 regulates chondrogenic differentiation of human adipose-derived stem cells by targeting Sox5. PLoS One. 2012;7(3):e31861.
77. Kim D, Song J, Jin E-J. MicroRNA-221 regulates chondrogenic differentiation through promoting proteosomal degradation of slug by targeting Mdm2. J Biol Chem. 2010;285(35):26900–7.
78. Lolli A, Lambertini E, Penolazzi L, Angelozzi M, Morganti C, Franceschetti T, et al. Pro-chondrogenic effect of miR-221 and slug depletion in human MSCs. Stem Cell Rev. 2014;10(6):841–55.
79.•• Lolli A, Narcisi R, Lambertini E, Penolazzi L, Angelozzi M, Kops N, et al. Silencing of antichondrogenic microRNA-221 in human mesenchymal stem cells promotes cartilage repair in vivo. Stem Cells. 2016;34(7):1801–11. **This study demonstrates the first published use of miRNA silenced stem cells to successfully induce cartilage regeneration in vivo.**
80.• Lee S, Yoon DS, Paik S, Lee KM, Jang Y, Lee JW. microRNA-495 inhibits chondrogenic differentiation in human mesenchymal stem cells by targeting Sox9. Stem Cells Dev. 2014;23(15):1798–808. **This study demonstrates miRNA-459 altering chondrogenic differentation of hMSCs through the targeting of master regulator Sox9.**
81. Li T, Li HL, Wang YZ, Li TP, Fan JF, Xiao K, et al. microRNA-23a inhibits osteogenic differentiation of human bone marrow-derived mesenchymal stem cells by targeting LRP5. Int J Biochem Cell Biol. 2016;72:55–62.
82. Kapinas K, Kessler C, Ricks T, Gronowicz G, Delany AM. miR-29 modulates Wnt signaling in human osteoblasts through a positive feedback loop. J Biol Chem. 2010;285(33):25221–31.
83.•• Chen L, Holmstrom K, Qiu W, Ditzel N, Shi K, Hokland L, et al. MicroRNA-34a inhibits osteoblast differentiation and in vivo bone formation of human stromal stem cells. Stem Cells (Dayton, Ohio). 2014;32(4):902–12. **The authors used a murine preclinical model of heterotopic bone formation in which hMSCs transfected with anti-miR-34 in combination with a scaffold resulted in a positive effect in bone formation. This demonstrates potential use for miRNA/SSC in clinical therapeutics.**
84. Eskildsen T, Taipaleenmaki H, Stenvang J, Abdallah BM, Ditzel N, Nossent AY, et al. MicroRNA-138 regulates osteogenic differentiation of human stromal (mesenchymal) stem cells in vivo. Proc Natl Acad Sci U S A. 2011;108(15):6139–44.
85. Salasznyk RM, Klees RF, Williams WA, Boskey A, Plopper GE. Focal adhesion kinase signaling pathways regulate the osteogenic differentiation of human mesenchymal stem cells. Exp Cell Res. 2007;313(1):22–37.
86. Hassan MQ, Maeda Y, Taipaleenmaki H, Zhang W, Jafferji M, Gordon JA, et al. miR-218 directs a Wnt signaling circuit to promote differentiation of osteoblasts and osteomimicry of metastatic cancer cells. J Biol Chem. 2012;287(50):42084–92.
87.• Zhang WB, Zhong WJ, Wang L. A signal-amplification circuit between miR-218 and Wnt/beta-catenin signal promotes human adipose tissue-derived stem cells osteogenic differentiation. Bone. 2014;58:59–66. **This study demonstrates a relationship between the osteogenesis promoting miR-218, and the osteogenesis promoting Wnt/beta-catenin signalling network. Exploiting this relationship could have implications in miRNA therapies.**
88. Wang Q, Cai J, Cai X-H, Lei C. miR-346 regulates osteogenic differentiation of human bone marrow-derived mesenchymal stem cells by targeting the Wnt/B-catenin pathway. PLoS One. 2013;8(9):1–8.
89. Zhang JF, Fu WM, He ML, Wang H, Wang WM, Yu SC, et al. MiR-637 maintains the balance between adipocytes and osteoblasts by directly targeting Osterix. Mol Biol Cell. 2011;22(21):3955–61.
90. Li H, Xie H, Liu W, Hu R, Huang B, Tan YF, et al. A novel microRNA targeting HDAC5 regulates osteoblast differentiation in mice and contributes to primary osteoporosis in humans. J Clin Invest. 2009;119(12):3666–77.
91.• Qureshi AT, Monroe WT, Dasa V, Gimble JM, Hayes DJ. miR-148b-nanoparticle conjugates for light mediated osteogenesis of human adipose stromal/stem cells. Biomaterials. 2013;34(31):7799–810. **This study illustrates the technique of photoactivation to release miRNA, with potential clinical applications to control release of miRNA within skeletal tissues.**
92. Schoolmeesters A, Eklund T, Leake D, Vermeulen A, Smith Q, Force Aldred S, et al. Functional profiling reveals critical role for miRNA in differentiation of human mesenchymal stem cells. PLoS One. 2009;4(5):e5605.

Cell Engineering at the Micro/Nanoscale – dedicated to Prof Adam Curtis

Biomimetic oyster shell–replicated topography alters the behaviour of human skeletal stem cells

Journal of Tissue Engineering
Volume 9: 1–13

DOI: 10.1177/2041731418794007
journals.sagepub.com/home/tej
SAGE

Shona J Waddell[1], María C de Andrés[1], Penelope M Tsimbouri[2], Enateri V Alakpa[3], Maggie Cusack[4], Matthew J Dalby[2] and Richard OC Oreffo[1]

Abstract

The regenerative potential of skeletal stem cells provides an attractive prospect to generate bone tissue needed for musculoskeletal reparation. A central issue remains efficacious, controlled cell differentiation strategies to aid progression of cell therapies to the clinic. The nacre surface from *Pinctada maxima* shells is known to enhance bone formation. However, to date, there is a paucity of information on the role of the topography of *P. maxima* surfaces, nacre and prism. To investigate this, nacre and prism topographical features were replicated onto polycaprolactone and skeletal stem cell behaviour on the surfaces studied. Skeletal stem cells on nacre surfaces exhibited an increase in cell area, increase in expression of osteogenic markers *ALP* ($p < 0.05$) and *OCN* ($p < 0.01$) and increased metabolite intensity ($p < 0.05$), indicating a role of nacre surface to induce osteogenic differentiation, while on prism surfaces, skeletal stem cells did not show alterations in cell area or osteogenic marker expression and a decrease in metabolite intensity ($p < 0.05$), demonstrating a distinct role for the prism surface, with the potential to maintain the skeletal stem cell phenotype.

Keywords

Nacre, topography, skeletal stem cell, osteogenic differentiation, bone regeneration

Date received: 26 March 2018; accepted: 19 July 2018

Introduction

Currently in orthopaedic medicine, there is an unmet need for bone tissue to treat fractures and bone degeneration in an increasing ageing population[1–3]. Skeletal stem cells (SSCs) offer the potential to improve musculoskeletal repair given their capacity to differentiate into bone[4]. However, before SSCs can be used in the clinic, delineation of the developmental pathway and, critically, elucidation of the specific processes in SSC differentiation into osteoblasts are required.

A wealth of data have illustrated the role of topographical surface patterns, including patterns such as grooves, ridges, pits and pillars and their ability to act as cues to direct differentiation of stem cells[5–8]. The mechanism by which this occurs is yet to be fully understood. However, it is thought that integrins and cytoskeletal components together with intracellular signalling mechanisms play an important role[9]. In particular, integrin organisation and arrangement is of importance in transducing signal pathways to direct cell

[1]Centre for Human Development, Stem Cells and Regeneration, Institute of Developmental Sciences, Faculty of Medicine, University of Southampton, Southampton, UK
[2]Centre for Cell Engineering, Institute of Molecular, Cell and Systems Biology, CMVLS, University of Glasgow, Glasgow, UK
[3]Department of Integrative Medical Biology, Umeå University, Umeå, Sweden
[4]Division of Biological and Environmental Science, University of Stirling, Stirling, UK

Corresponding author:
Richard OC Oreffo, Centre for Human Development, Stem Cells and Regeneration, Institute of Developmental Sciences, Faculty of Medicine, University of Southampton, Southampton, SO16 6HW, UK.
Email: roco@soton.ac.uk

differentiation and function for enhancement of osteogenic differentiation[10]. Seminal studies over a decade ago have demonstrated that a regular nanotopographical arrangement with slight offset can increase focal adhesion formation and modulate osteogenic differentiation[9]. Interestingly, the majority of topographical designs studied to date have been machine generated. Application and lessons from nature in the use of a biomimetic approach could provide additional advantages over existing topographical designed approaches and bring unexplored surface patterns for which design may not readily replicate.

Background

The surface of the *Pinctada maxima* oyster shell, on initial observation, appears distinct from bone tissue and yet there are important similarities[11]. Nacre, the substance lining the inside of *P. maxima* and other bivalve mollusc shells, and bone are both composed of an inorganic, mineralised matrix and an organic fraction composed of proteins. The organic fraction provides a scaffold and biological signals which promote crystallisation. This allows for a substance which is strong and yet displays considerable flexibility. In bone, 70% of dry weight is composed of inorganic mineralised calcium phosphate in the form of hydroxyapatite[12]. Nacre, however, has a much greater proportion of inorganic mineralised matrix (97% of dry weight), which is mainly in the form of the calcium carbonate mineral, aragonite[13].

The potential for nacre and bone interactions was first noticed in 1931 when ancient Mayan skulls were discovered with dental implants composed of nacre[11]. This demonstrated the biocompatibility of nacre with bone. This phenomenon was studied further by Lopez and colleagues[14,15] many decades later in 1991, who showed that not only could human osteoblasts grow on nacre but, after prolonged culture, they also produced a mineralised tissue matrix between osteoblasts and nacre chips. Histological analysis of the composition of this tissue found that the tissue adjacent to the bone chips contained a hydroxyapatite-rich mineralised matrix. Interestingly, the mineralised tissue formed next to the nacre chips was composed of lamellar sheets which closely resembled those of nacreous shell. Raman spectroscopy allowed for confirmation of aragonite crystals present in the matrix[14]. Bone regeneration initiated by nacre was proven in experiments in ovine bone defects, rabbit defects and human maxillofacial defects, illustrating the powerful role of nacre in bone regeneration[16–19].

As nacre appeared to enhance bone regeneration in published in vivo studies, it could be hypothesised that nacre has the ability to drive SSC osteogenesis, leading to enhancement of bone regeneration. To date, only a limited number of studies have examined the role of nacre in directing osteogenesis from SSC populations. SSC population specifically refers to a self-renewing stem cell that resides in postnatal bone marrow stroma with the capacity to differentiate into cartilage, bone, haematopoiesis-supportive stroma and marrow adipocytes and, critically, responsible for the regenerative capacity inherent to bone. Bone marrow stromal cells (BMSCs) commonly refer to the heterogeneous population of cultured plastic adherent cells isolated from the bone marrow. The SSC, present within bone marrow stroma, is responsible for the regenerative capacity inherent to bone. The SSC population is a separate population to the typically stated mesenchymal stem cell (MSC). The term MSC was originally coined in reference to a hypothetical common progenitor of a wide range of 'mesenchymal' (non-hematopoietic, non-epithelial, mesodermal) tissues and it is widely accepted that MSCs exist in a broad range of postnatal tissues and organs, with a broad spectrum of lineage potentialities.

Nacre matrix was found to lead to an increase in expression of alkaline phosphatase (ALP) in rat BMSC[20]. Further to this, bone marrow–derived human SSCs cultured with nacre chips displayed an increase in ALP activity, indicating osteogenic differentiation[21]. Thus, it could be hypothesised that the nacre shell may provide SSCs with an ideal topography for SSC differentiation or/and provide a chemical environment to enhance differentiation. A previous study aimed to separate the topography from the chemistry by replicating nacre topographical features into polycaprolactone (PCL) and studied the behaviour of commercially available MSCs on the PCL replicas[22]. The authors studied the crystallinity of the mineralised matrix formed when MSCs were cultured on the PCL nacre replicas. The results detail that MSCs produced a mineralised matrix with higher crystallinity than chemically induced osteogenic differentiation, indicating a different pathway of differentiation[22].

In this study, a similar approach of using PCL replicas is taken to study the topographical effects of the nacre region of *P. maxima*, as well as the topography of the calcite prisms which form the outer layer of *P. maxima* shells (Figure 1). In addition, the current studies have used PCL replicas to examine the role of the topography from the prism region of *P. maxima*, which is also composed of calcium carbonate crystals and forms in the region where the two sections of the shell join together. Interestingly, the role of the topography from this part of the shell is less well-understood and this study has examined the role of this material and the topography of this material in modulation of SSC behaviour. The cell source used in the current studies was human primary bone marrow–derived SSCs from an aged population, clinically relevant for studying bone regeneration therapies. The effect of nacre and prism topography has not been studied on this SSC population and will inform translational and bone formation in human bone populations.

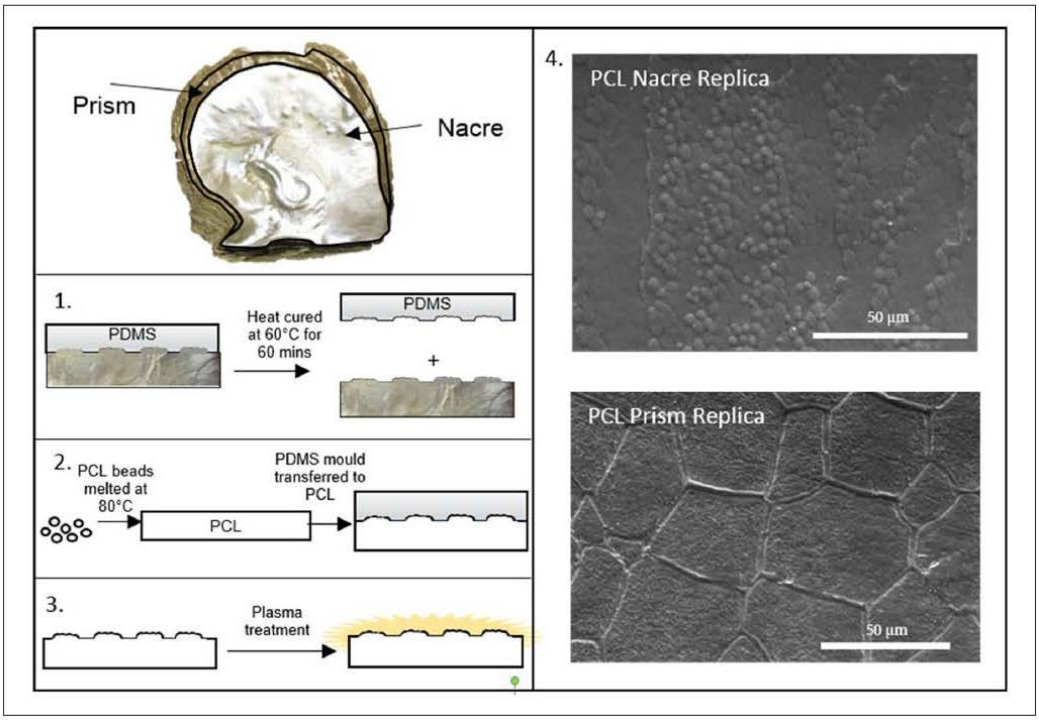

Figure 1. Schematic representation of biofabrication of PCL topographical surfaces. (1) Polydimethylsiloxane (PDMS) was poured on shell and heat cured at 60°C for 60 min. The mould was then removed from the shell. (2) Polycaprolactone (PCL) beads were washed in methanol and left to air dry. PCL beads were then melted at 80°C and PDMS mould transferred to molten PCL and features replicated using hot embossing. At this point, flat control PCL surfaces were generated using glass slides. When the PCL had cooled, the PDMS stamp was removed. (3) PCL topographical surfaces were prepared for cell culture with plasma treatment. (4) SEM images of PCL-replicated nacre and prism topographies. To prepare for SEM, surfaces were sputter coated with 7 nm platinum.

Aim

To date, the osteogenic effect of a solid two-dimensional (2D) nacre and prism surface on primary SSC behaviour and function remains unknown and this study sets out to delineate and examine this further. In order to distinguish the chemistry of nacre and prism substrate from topography, a soft lithography approach was used to develop cell culture surfaces with nacre and prism topographical features but without the surface chemistry of nacre or prism shell regions. As the *P. maxima* shell nacre topography is known to enhance osteogenic differentiation, potential for direction towards osteogenesis will be studied through observations of alterations in cell morphology, gene expression markers and metabolomics following SSC culture on the topographical surfaces. The topography of these bioimprinted surfaces could provide mechanical and topographical cues to alter SSC behaviour, potentially towards an osteogenic fate.

Methods

Surface generation

PCL prism and nacre topographical surfaces were fabricated as outlined in Figure 1 and the fabrication process detailed in Alakpa et al.[22] Prior to culturing, surfaces were sterilised under ultraviolet light for 30 min and washed twice with sterile phosphate-buffered saline (PBS).

SSC isolation

A total of four patient samples were used for this study (samples from females aged 51, 52, 56 and 71). Bone marrow from the four patients was utilised for isolation and culture of bone marrow SSCs. SSC isolation has been described previously.[23,24] Bone marrow was first washed and the solution was passed through a 70-µm cell strainer and subjected to density centrifugation using Lymphoprep™ (Lonza, Slough, UK). The buffy coat layer, containing bone marrow mononuclear cells, was incubated with blocking buffer (α-MEM (Lonza), 10% human serum (Sigma, Gillingham, UK), 5% foetal bovine serum (FBS) (Thermo Fisher Scientific, Basingstoke, UK) and 10 mg/mL bovine serum albumin (BSA) (Sigma)) followed by washing with magnetic-activated cell sorting (MACS) buffer (PBS with 0.5% BSA and 2 mM ethylenediaminetetraacetic acid (EDTA; Sigma)). Cell suspension was incubated with 1 mL STRO-1 antibody (generated in-house from hybridoma). Following washing with MACS buffer, cells were incubated in rat

anti-mouse IgM microbeads (Miltenyi Biotec Ltd, Woking, UK). After further washing with MACS buffer, target cell population was isolated by MACS and resuspended in basal media (α-MEM containing 10% FBS and 1% penicillin/streptomycin; Lonza) and plated into tissue culture flasks.

Cell culture

STRO-1+–enriched SSCs were maintained at 5% CO_2 at 37°C in culture flasks and used at passage 1. Cell culture media used was basal culture media unless otherwise stated. Osteogenic media was basal media supplemented with 10 nM vitamin D_3 (Sigma) and 100 μM ascorbic acid (Sigma). Prior to seeding, cells were treated with collagenase IV (Sigma) and released from the flask using 1× trypsin (Lonza). STRO-1+ SSC were seeded into 24-well plates at 1000 cells/cm^2. After 24 h of seeding, surfaces were transferred to new 24-well plate and media replaced. Media was subsequently changed every 3–4 days for the duration of the experiments.

Scanning electron microscopy

Surfaces were washed in sterile water and left to air dry. Surfaces were then sputter coated with 7 nm platinum using Q150T turbo-pumped sputter coater/carbon coater (Quorum Technologies Ltd, East Sussex, UK). In order to ensure charge distribution, Electrodag 1415 (AGG3648, Agar scientific, Essex, UK) was painted from the edge of surfaces to metal mounting stub. Samples were viewed using Quanta FEG 250 scanning electron microscope (SEM; FEI™, Eindhoven, The Netherlands). The SEM was controlled by xT microscope control software, which also allowed for image capturing.

CellTracker Green imaging

To visualise cells, 50 μg of CellTracker Green (CTG; Thermo Fisher) was dissolved in 10-μL sterile dimethyl sulfoxide. This was pipetted into a falcon tube containing 15 mL of α-MEM. Media was removed from wells, washed once with PBS and CTG/α-MEM mix was added to the well. Cells were then incubated in the dark at 37°C for 1 h. Cells were washed with PBS and the media replaced with basal media. Cells were imaged at the required time point. Sample images were captured using a Zeiss Axiovert 200 inverted microscope (Zeiss, Cambridge, UK) and Zeiss Axiovision software version 4.9. Fluorescent images were captured using Axiocam MR with the FITC filter.

Analysis of cell spreading

To quantify cell area in an unbiased fashion, CTG images were processed using image analysis software CellProfiler 2.2.0.[25,26] The image process pipeline is detailed in Table S1. For image analysis, a minimum of eight images per condition were used, and a minimum of 60 cells were used to generate average cell area. Each image was checked individually to ensure that CellProfiler recognised cell correctly and incorrect recognition was removed from analysis (Figure S1).

Quantitative reverse transcriptase-polymerase chain reaction

Prior to lysis, cells were washed twice with PBS. Lysis buffer buffer RLT (Qiagen, Manchester, UK) supplemented with 0.05% Reagent DX (Qiagen) was added to each well and cells lysed using pipette tip. RNA was extracted using AllPrep DNA/RNA/miRNA universal kit (Qiagen), following manufacturers' protocol. Equal amounts of RNA were used for complementary DNA (cDNA) synthesis using Taqman Reverse Transcription Reagents (Thermo Fisher Scientific) according to the manufacturers' protocol. Amplification by quantitative reverse transcriptase-polymerase chain reaction (qRT-PCR) was performed using human-specific primers (Sigma). Each 20-μL reaction contained 1 μL of diluted cDNA, 10 μL of GoTaq (Promega, Southampton, UK) and a final concentration of 1 μM forward and reverse primers. For the qRT-PCR run, Applied Biosystems (Thermo Fisher Scientific) Real-Time PCR system was set up to run first with two holding stages (2 min at 50°C, 10 min 95°C), followed by 40 cycles (15 s at 95°C, 1 min at 60°C) where fluorescence was measured and held at 4°C. Data were analysed using 7500 Software version 2.3 (Life Technologies, Basingstoke, UK). Threshold for calculating Ct (cycle threshold) value was set at 0.2 and all samples normalised to expression of *ACTB* as a housekeeping gene. The $2^{-\Delta\Delta Ct}$ method was used for relative quantification of gene expression.[27]

Immunofluorescent microscopy

Prior to staining, surfaces were washed twice with PBS and fixed in 4% paraformaldehyde (PFA; Sigma) for 30 min. Cells were blocked and permeabilised with blocking buffer composed of PBS, 0.3% Triton X-100 (Sigma-Aldrich) and 5% goat serum (Thermo Fisher Scientific) for 60 min at room temperature. Anti-osteopontin antibody (1:100 dilution; Abcam, UK) was added and incubated overnight at 4°C. After incubation, the surfaces were washed three times with PBS supplemented with 0.05% Tween 20 (Sigma-Aldrich). Following this, secondary antibody (goat anti-mouse; Abcam, Cambridge, UK) and TRITC-conjugated phalloidin (diluted at 1:500; Merck-Millipore, Watford, UK) were incubated with the cells for 1 h. Following this, cells were then incubated with DAPI (dilution 1:100 in PBS; Thermo Fisher Scientific) for 10 min. Cells were then washed three times with PBS/Tween. For storage before imaging, surfaces were mounted

with fluoromount™ (Sigma-Aldrich) and sealed with clear nail varnish. Surfaces were stored in the fridge, in the dark and imaged within 1 day. Cells were imaged as with imaging following CTG staining.

Cellular metabolomics

Female patient 56 was used for cellular metabolomics experiments. Metabolites were extracted on days 10 and 21 after seeding. Surfaces were washed twice with chilled PBS.Chilledextractionbuffer(chloroform:methanol:water, 1:3:1 (v/v)) was added to surfaces and agitated with shaking at 4°C. Samples were transferred to screw cap vials and centrifuged to pellet cell debris. Supernatant was then transferred to screw cap vials. A liquid chromatography–mass spectrometry (LC-MS) system was used for cellular metabolomics. Metabolomic analysis was performed at Glasgow Polyomics Centre (University of Glasgow) with 10 μL aliquot of supernatant. Hydrophilic interaction liquid chromatography (HILIC) was carried out on UltiMate 3000 RSLC system (Thermo Fisher Scientific) using ZIC-pHILIC 5 μm column (150 mm × 4.6 mm). The mobile phase was composed of 20 mM ammonium carbonate in either water or acetonitrile. A linear gradient was run for 24 min at 20% in water/80% acetonitrile, followed by change to 92%water/8% in acetronitrile for 8 min, before being brought down to 20% water/80% acetonitrile. Orbitrap QExactive (Thermo Fisher Scientific) was used for MS analysis in polarity switching mode, within the mass range *m/z* 70–1050. Metabolite identification used Glasgow Polyomics Centre in-house XCMS/MzMatch/IDEOM pipeline using a set of standards to define mass and chromatographic retention times.[28] Peak intensities were normalised to protein concentration using BSA assay (Thermo Fisher Scientific). Ratios for each metabolite were calculated using peak intensity, relative to flat control surfaces and these ratios were used for statistical analysis.

Statistical analysis

Cell area measurements were performed with patients 51, 52 and 56 and data represented as mean ± SD. Gene expression experiments were performed with patients 51, 52, 56 and 71 and data represented as mean ± SEM. Two-way analysis of variance (ANOVA) followed by Tukey's post hoc was performed on results of cell area measurements and gene expression analysis. Patient female 56 was used for metabolomics experiments and performed in triplicates, with data represented as mean ± SD. One-way ANOVA followed by Dunnett's post hoc was performed on metabolite intensity peak ratios. Principal component analysis (PCA) was carried out using MetaboAnalyst 4.0.[29] The p values less than 0.05 were considered significant.

Results

Morphological changes on shell topographies

STRO-1–enriched SSCs were cultured on nacre and prism replicated PCL topographies and control flat surfaces, cultured under basal conditions and the cell area measured at days 4 and 7, to ensure that cell density remained sufficiently low to allow for accurate single-cell measurements. As these PCL surfaces are opaque, cells were stained with CTG and imaged using fluorescence imaging (Figure 2(a)–(f)). On day 4, there were negligible differences in cell area between nacre, prism and control flat topography (Figure 2(g)). On day 7, as expected, there was a higher density of cells on the surfaces as the SSCs proliferate and an overall decrease in cell area was observed. From day 4 to day 7, average cell area decreased from 3250.9 ± 617.32 μm² to 2195.0 ± 359.0 μm² ($p < 0.001$). On day 7, an increase in cell area on nacre surfaces (2472.2 ± 447.8 μm²), compared to flat (2097.0 ± 220.1 μm²) and prism (2015.9 ± 298.0 μm²), was observed. However, due to patient variation between SSC samples, this did not reach statistical significance.

Enhancement of osteogenic markers on shell topographies

To investigate osteogenic differentiation on the PCL topographies, expression of a range of early to late osteogenic markers was examined over 28 days of culture and compared to SSC cultured on flat PCL surfaces under osteogenic conditions (flat OM) (Figure 3(a)–(e)). A 28-day culture was chosen as osteogenic differentiation can take up to 28 days to reach full maturation and full examination of any potential osteogenic differentiation. *RUNX2* expression did not vary between the topographical surfaces and flat control surfaces. A decrease in expression in *RUNX2* was identified on nacre topographies on day 28 (Figure 3(a)). It was apparent that expression of *RUNX2* was considerably higher in SSC cultured under osteogenic conditions. *ALP* expression on nacre topographies reached a maximum on day 14 ($p < 0.01$) (Figure 3(b)). This was observed to be nacre topography-specific and a similar result was not observed on prism topographies. Differences in expression between topographical surfaces at recorded time points were not observed for *COL1A1* expression. Interestingly, expression of *COL1A1* was found to be lower in the presence of OM compared to flat surfaces in the absence of OM.

On day 21, there was an increase in expression of *OCN* on SSCs cultured on both nacre (27.1 ± 15.2) and prism (21.8 ± 7.1) PCL topographies compared to the flat control (14.7 ± 3.7). On day 14, an increase in *OPN* expression was observed in nacre topographies (10.1 ± 7.4) compared to both prism (8.9 ± 5.4) and flat control (6.7 ± 3.7). It should be noted that there was a significant variation in

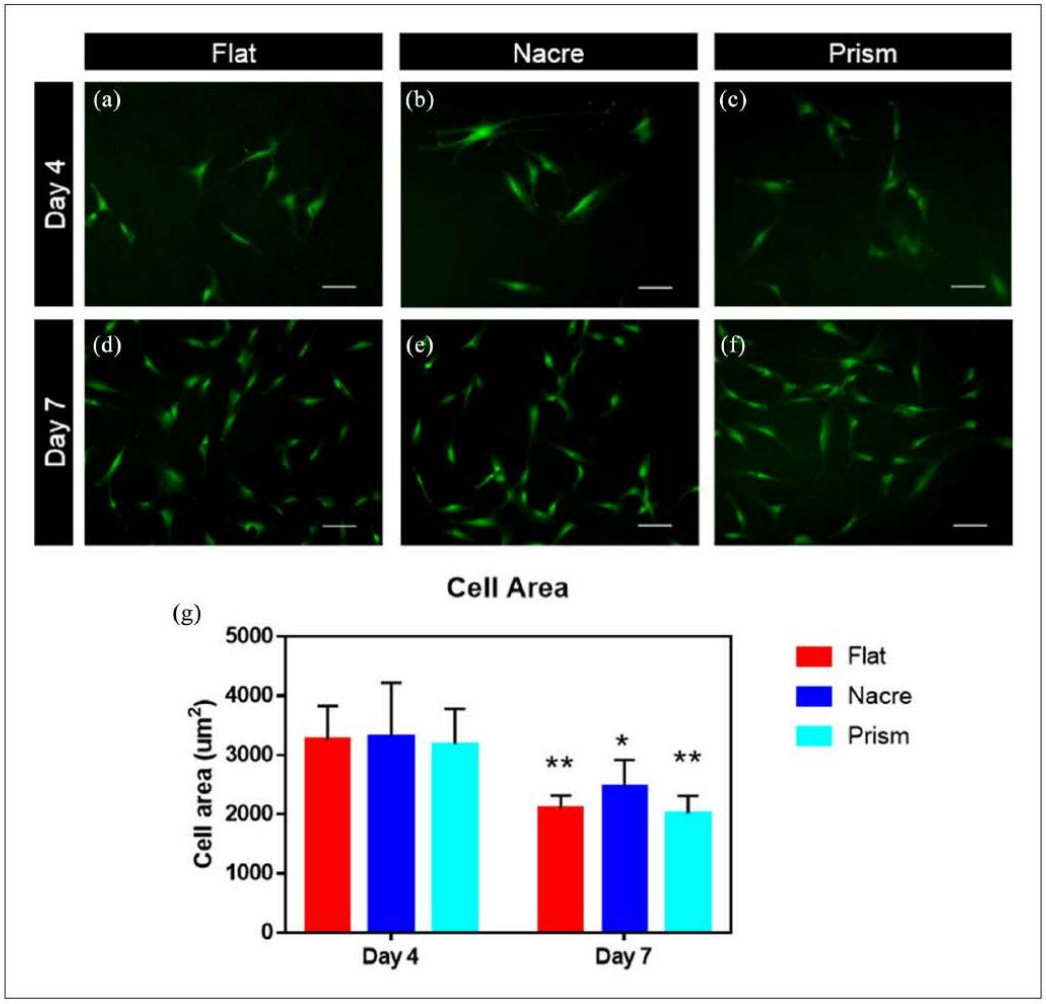

Figure 2. Morphology of SSCs cultured on nacre, prism and flat topographical surfaces. Cells were stained with CellTracker Green and imaged at (a–c) day 4 and (d–f) day 7. Mean cell area (μm^2) was calculated at day 4 and day 7 (g), ($n = 3$ patients – females aged 51, 52 and 56), *$p < 0.05$; **$p < 0.01$.

expression from different SSC patient donors. Further to this, there was also significantly higher expression of osteogenic markers when flat PCL surfaces were cultured in the presence of OM. Immunofluorescence staining of OPN confirmed gene expression data, indicating an increase in OPN levels on days 14 and 21 comparing nacre topographies to flat control (Figure 3(f)). Expression of miRNAs, known to be associated with osteogenesis, miR-138 and miR-218, showed no significant difference between flat and shell topographies (Figure S2).

Cellular metabolomic profile of SSCs on shell topographies

To determine how metabolic pathways within SSC populations responded to the nacre and prism topographies, we performed metabolomics analysis using LC-MS on SSCs cultured on the shell topographies. For this experiment, days 10 and 21 were chosen as during initial pilot studies, these time points displayed increased SSC metabolomic activity and therefore would reflect activity of metabolically active SSCs. We selected a 10-day time point for metabolomics to ensure that cell density was sufficiently low enough to avoid/minimise any cell interactions and ensure analysis was solely a reflection of the effect of the topography in the differentiation process of SSCs.

An overview of average metabolite intensity at day 10 detailed an increase in intensity on nacre topographies ($p < 0.05$) and a decrease in intensity on prism topographies ($p = 0.0455$) relative to flat control (Figure 4(a)–(c)). Interestingly, the metabolite intensity ratio was similar

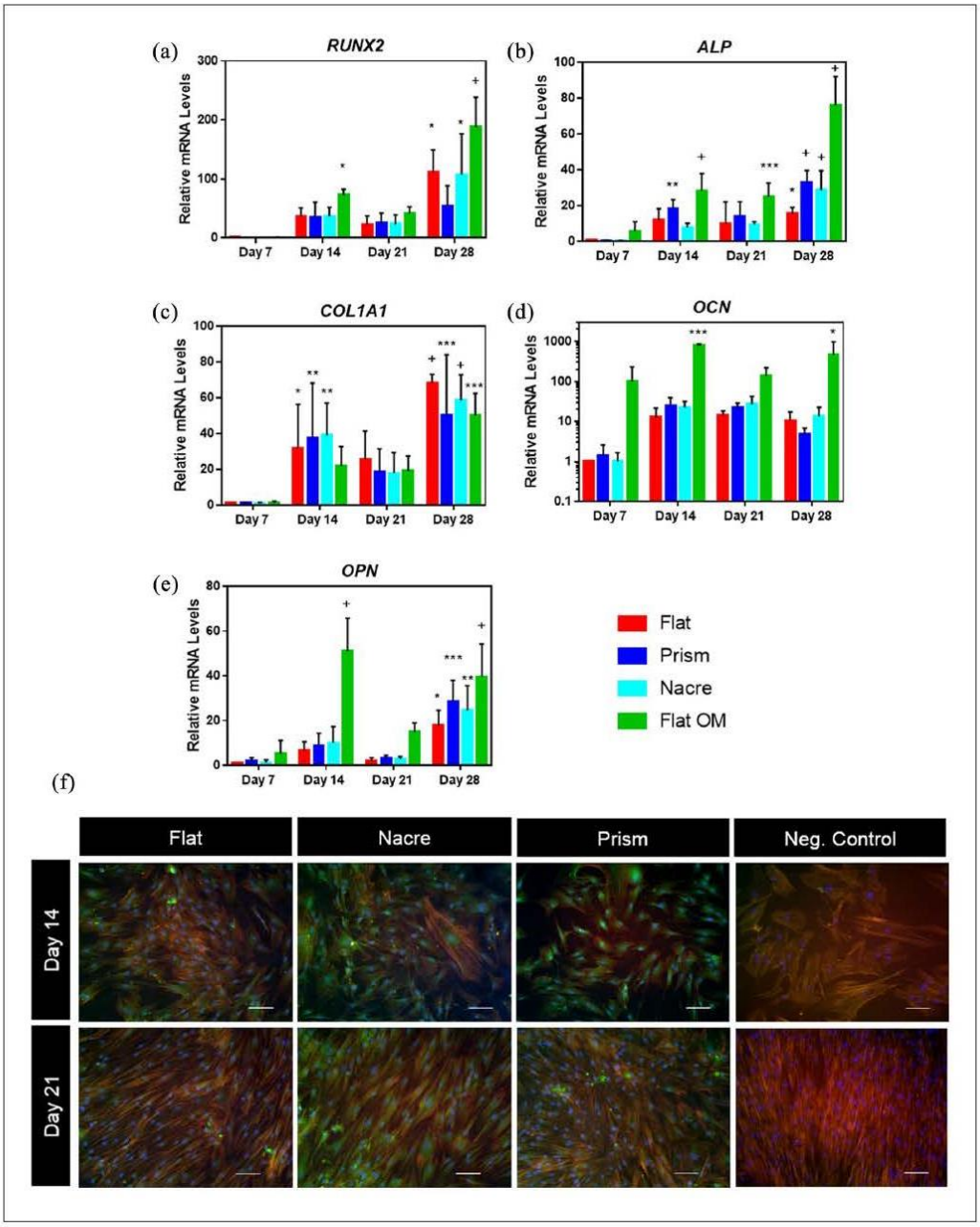

Figure 3. Changes in osteogenic mRNA and protein on shell topographies. (a–e) Expression of RUNX2, ALP, COL1A1, OCN and OPN mRNA in SSC cultured on nacre, prism and flat osteogenic media (flat OM) topographies over 28 days. $n = 3$ patient samples, $^{*}p < 0.05$; $^{**}p < 0.01$; $^{***}p < 0.001$; $^{+}p < 0.0001$. (f) Immunofluorescence of OPN on days 14 and 21 on flat, nacre and prism topographies. Negative control is SSCs stained in the absence of anti-OPN antibody, cultured on standard commercial tissue culture plastic. White arrows indicate area of OPN protein. Scale bar = 100 μm.

from nacre topography (2.32 ± 0.30) to flat control exposed to osteogenic media (flat OM) (2.35 ± 0.26) (Figure 4(a)) and this was also observed on a heat map displaying individual metabolites (Figure 4(h)). When this was analysed by carbohydrate- and lipid-associated metabolites, the similarity between nacre topography and flat OM remained (Figure 4(b) and (c)). At day 21, usually associated with differentiation towards a mature osteogenic phenotype, the

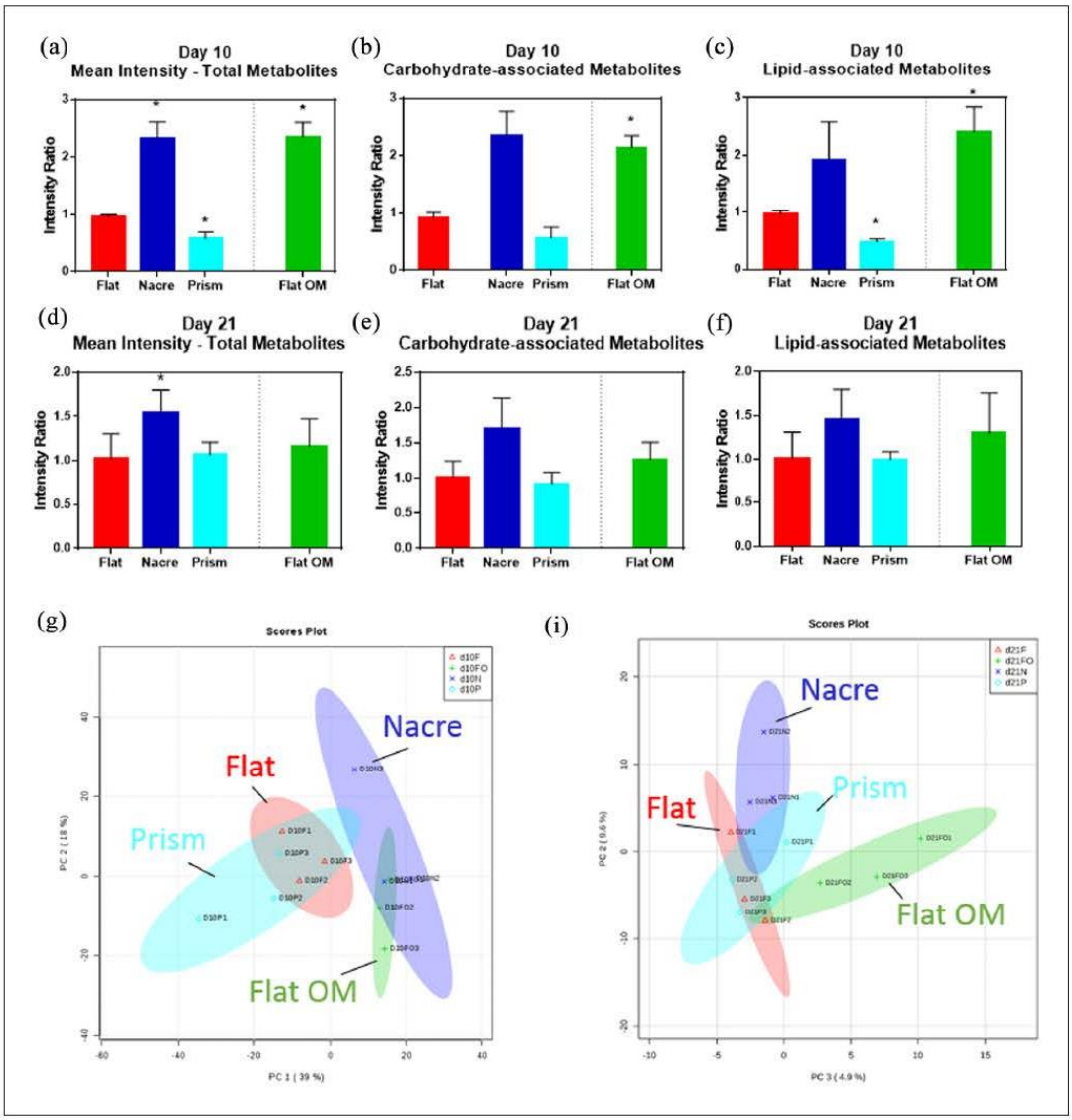

Figure 4. Metabolomic analysis of SSC culture on nacre and prism shell topographies. Intensity ratio, relative to flat control, of (a and d) total metabolites, (b and e) carbohydrate-associated metabolites, and (c and f) lipid-associated metabolites for (a–c) day 10 and (d–f) day 21. Flat OM represents flat surface cultured in osteogenic media. Peak intensity ratio normalised to flat control, $n = 3$ replicates. PCA plots for (g) day 10 and (h) day 21.

metabolite intensity was altered in comparison with the day 10 (Figure 4(d)–(f)). Metabolite intensity on flat control and flat OM was observed to be similar (1.02 ± 0.28 and 1.16 ± 0.31, respectively). Critically, an increase in metabolite intensity was only observed on nacre topographies (1.54 ± 0.6) (Figure 4(d)). This is reflected in the heat map of metabolites identified on day 10 (Figure S3) and day 21 (Figure S4). The heat map also showed differences between the triplicates. SSCs on prism surfaces appeared to be more metabolically active at this time point compared to day 10 (Figure 4(d)), as the intensity compared to flat control increased from 0.58 ± 0.1 to 1.07 ± 0.1. PCA plots show linkage between flat OM and nacre and flat and prism surfaces on day 10 (Figure 4(g)). However, this was lost by day 21 (Figure 4(h)). Individual metabolites L-creatine, L-glutamine, L-pyruvate and L-carnitine follow a similar result to the global trend (Figure S5).

Identified networks and canonical pathways associated with changes in metabolites

Through the use of Ingenuity Pathway Analysis (IPA) software (Qiagen), canonical pathways associated with nucleotide metabolism were analysed (Figure 5). IPA investigates

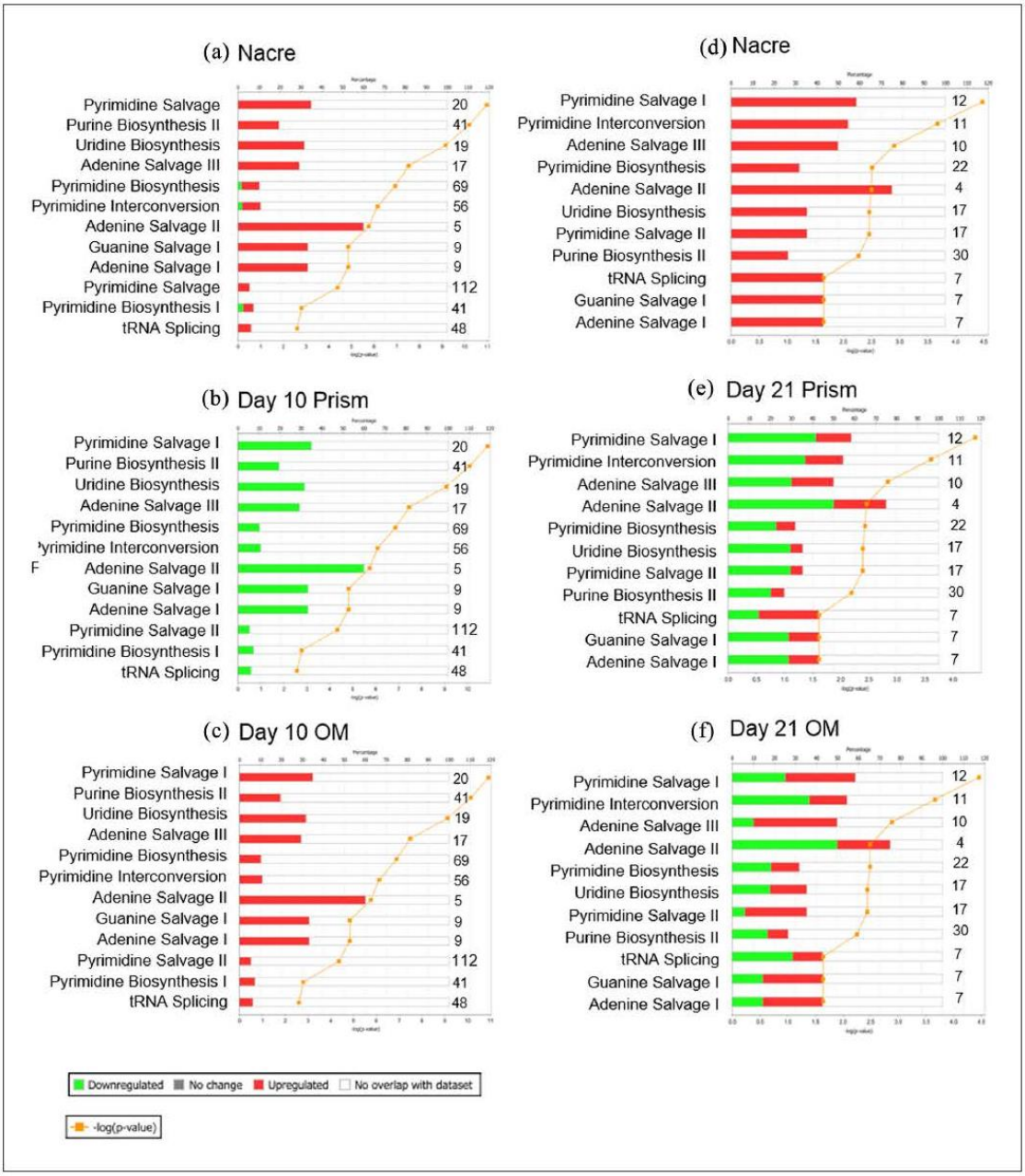

Figure 5. Nucleotide metabolism–associated canonical pathways for SSCs cultured on nacre, prism and control OM surfaces on days 10 and 21. IPA-generated canonical pathways associated with nucleotide metabolism for SSC on day 10 on (a) nacre topographies, (b) prism topographies and (c) flat osteogenic media control. Canonical pathways on day 21 on (d) nacre topographies, (e) prism topographies and (f) flat osteogenic media control. Shown in either red or green and on the numbers to the right of each bar was the number of metabolites identified in the sample out of all possible known associated metabolites. Threshold considered for the analysis was – log(*p* value) > 1.5. Legend on bottom left.

all known metabolites associated with these pathways and if they are up on nacre and prism topographies or flat OM. The majority of metabolites identified were upregulated on nacre topographies and flat OM on day 10 (Figure 5(a) and (c)). On prism topographies, metabolites associated with nucleotide metabolism were downregulated (Figure 5(b)). As identified on analysing peak intensity, on day 21, an increase in metabolite intensity on nacre topographies was observed compared to metabolites on flat OM surfaces (Figure 5(d) and (f)).

Application of IPA software (Qiagen) demonstrated networks of associated metabolites generated including

links to proteins known to be associated with metabolites from literature databases that predict the protein regulation/activation state. The network generated for nacre PCL topography and flat OM conditions were similar at day 10, indicating potential for a comparable cellular phenotype (Figure S6A and C). At day 21, the metabolomic networks generated for nacre topography showed enhanced activation in comparison with flat OM (Figure S7A and C). At day 10, on both nacre topographies and flat OM, key hubs associated with osteogenic differentiation were identified to be activated including ERK1/2, acetyl coA carboxylase (ACAC) and collagen 1α and increase in metabolites associated with the tricarboxylic acid (TCA) cycle. On prism topography, the opposite was observed and the network generated displayed different activation levels (Figure S6B). Here, at day 10, a predicted decrease in ERK1/2, ACAC and collagen 1α was discovered. Added to this, an activation of lactate dehydrogenase was observed in prism-associated networks. Due to difficulties in generating the high number of samples required for metabolomic analysis, one patient (female aged 56 years) was used for this experiment and examined in triplicates.

Discussion

This study has demonstrated the ability of SSCs to respond to shell topographical surfaces. The nacre surface induced osteogenic differentiation of human SSCs, with an increase in *OPN, OCN* and *ALP* expression, compared to flat control PCL surfaces. Furthermore, the similarities in metabolic profile between SSCs on nacre surfaces compared to SSCs cultured in osteogenic media strengthen the potential for the nacre surface to induce osteogenic differentiation. In contrast, primary SSCs cultured on the prism surface presented a distinct and, significantly, a different response. On prism surfaces, a mixed increase in expression of osteogenic markers was observed, with an increase in *OCN* but not *ALP* compared to flat control without OM. Through the use of IPA for metabolomics profiling, SSCs cultured on prism surfaces displayed considerably less activity compared to flat control.

Previous studies have suggested that an increase in cell area is observed during osteogenic differentiation[30]. In the current studies, a non-significant increase in cell area was observed on nacre surfaces and demonstrated the ability of SSCs to respond to nacre topographical surface features. Examination of the expression of master bone regulator *RUNX2* indicated no effect of topography on gene expression. *RUNX2* is known to be expressed early on during osteogenic differentiation and functions to enhance transcription of bone-associated proteins such as *ALP, OPN* and *OCN*[31–34]. Given that an increase in *ALP, OPN* and *OCN* was observed, it could be speculated that an increase in *RUNX2* expression occurs at a time point not investigated during this study. ALP, OCN and OPN are known to be indicators of osteogenic differentiation[35,36]. The increase in expression of these markers in the current studies supports the idea of potential osteogenic differentiation on the topographies. When comparing increases of observed expression to expression measured in flat OM surfaces, it is apparent that the expression observed on topographical surfaces is not as high as that identified during culture with OM. From this, we can tell that chemically induced osteogenic differentiation is more powerful than topographical-induced differentiation, though, nonetheless, topography has a moderate effect on gene expression.

When differentiating, SSCs form specialised, terminally differentiated cells and the environment within the cell changes, including the way in which cells process metabolites[37]. The metabolomic profile of SSCs is known to change during differentiation with more energy as a consequence of oxidative phosphorylation pathways in the mitochondria as differentiation progresses[37,38] and accompanying this is an increase in energy-related metabolite intensity[39]. In the current studies, this change in metabolite processing was illustrated by the comparison between SSCs on flat control to flat OM where we observed an increase in metabolite intensity and increase in oxidative phosphorylation–associated TCA cycle metabolites. The similarities between flat OM and nacre topographies in aspects studied including nucleotide processing canonical pathways and activation of network hubs support the hypothesis of osteogenic differentiation of SSCs on the nacre topographical surface. Networks generated suggested an increase in TCA cycle components on nacre surfaces and flat OM, an indication of increased levels of oxidative phosphorylation. An increase in individual metabolites (creatine, glutamine, pyruvate and carnitine) observed has been linked to osteogenic differentiation[40–42]. Coupled with this, a predicted activation of collagen α1 and ERK1/2 strengthens the case for osteogenic differentiation on the nacre topography[43,44]. ACAC catalyses the conversion of acetyl-CoA to malonyl-CoA and therefore enhances the level of malonyl-CoA available, an increase which has been previously linked to stem cells progressing from a quiescence to differentiated state[45]. An increase in activation observed in this study further details SSC differentiation on the nacre surfaces. Interestingly, at day 21, the metabolomic profile of SSCs on flat OM appears to be less active in comparison with the nacre topography. Since differentiation is promoted by two different mechanisms in these studies, either chemically or topographically, it is likely that the progression of differentiation is different on these surfaces which could explain the variation.

The nacre surface presents the cells with a nanodisordered feature arrangement, previously shown to be important for the induction of osteogenesis[8,9]. This type of surface is believed to induce integrin clustering resulting in altered phenotype. Nacre is a natural surface and therefore the topography is distinct to machine computer–designed and

generated topographies, which allows for further variation within the surface. It could be natural variation which allows nacre to provide the topographical cues necessary for osteogenic differentiation. In addition, when using the initial *P. maxima* shell as a mould, on the surface, there was not only the natural topography of the shell but also the proteins produced by the shell. The resulting PCL topographical mould is created via an intermediary polydimethylsiloxane (PDMS) mould and includes several washing steps. It is likely that during this time, the presence of these additions to the topography will have been removed, and only the shape of the proteins transferred during the soft lithography process, although it should be noted that this was not tested in the current studies, and the effect of the presence of these proteins remains currently unknown.

It has become apparent in recent studies that stem cells and wider bone regeneration processes benefit from a three-dimensional (3D) environment[46,47]. The use of a 2D topography, as in the current studies, could limit possible enhancement of osteogenesis observed in a 3D nacre topography environment. Future studies will evaluate the effect of a 3D nacre topographical environment on behaviour of SSCs.

To date, information on the role and function of the prism surfaces remains limited and the potential to modulate skeletal cell function and cell behaviour remains poorly understood. As this topography is vastly different to the nacre, it is not surprising that it has a different effect on the cell. Cell area of SSCs on prism surfaces was similar to flat control, indicating a lack of response to the surfaces, at least in terms of cell spreading. Analysis of gene expression demonstrated a significant increase in *OCN* expression. However, a similar result was not seen in other osteogenic markers tested including *ALP* and *OPN*, indicating lack of osteogenic response. Interestingly, there was an increase in *RUNX2* expression on day 28, however; since *RUNX2* expression is usually expected early on in osteogenic differentiation, this is unlikely to indicate potential osteogenic differentiation. Analysis of the metabolic profile of SSCs on prism surfaces demonstrated a decrease in metabolomic intensity. An increase in predicted activation of lactate dehydrogenase rather than those linked to TCA cycle indicated the potential for stem cell maintenance on this surface.[48] Further to this, a decrease in nucleotide biosynthesis and ACAC suggests a quiescent population. The role the prism surface remains to be fully elucidated; however, the current results suggest that the surface could provide topographical cues for maintenance of the stem cell phenotype.

In this study, SSCs were obtained from residual tissue samples of patients undergoing routine hip replacement and there are variations in sample retrieval area and health of bone marrow, both of which can result in differences in cell behaviour and their ability to respond to biomechanical factors. This patient sample variation has been observed previously[49] and has led to observed variation within the samples analysed in the authors' experiments. A similar variation has been observed in the current studies and most apparent in gene expression studies. While this can complicate results of an experiment, these variations reflect the natural variation when using primary human tissue and emphasise the importance of using a clinically relevant cell population. It should be noted here that during these initial studies, a small number of patient samples, a total of four, were examined. This could have led to the observed sample variation and further studies should add to the current studies by increasing the number of samples examined to reduce experimental variation as a consequence of patient variability. Although the results discussed in these current studies showed enhancement of expression of osteogenic markers on nacre topographies and an increase in metabolomic activity of SSC cultured on nacre topography, the results were not consistent for all messenger RNA (mRNA) investigated and, interestingly, for cell area. In addition, analysis for the presence of mineralised tissue in the current work was not performed and future planned studies will address this issue.

The enhancement of osteogenic differentiation of commercially available MSCs on nacre has previously been shown, and this was associated with mineral formation of a higher crystallinity compared to mineralised matrix produced from chemically stimulated MSCs[22]. This study details nacre and prism effect on primary SSCs from donors who were undergoing routine total hip replacement for bone degeneration. Evaluation of a clinically relevant population, as in the current studies, confirms that nacre topography could induce osteogenic differentiation in the clinic. In order to translate these findings to the clinic, future experiments using nacre PCL-replicated topography to investigate in vivo bone regeneration on 2D topography would be required.

Conclusion

This study demonstrates a role for nacre PCL topography from *P. maxima* oyster shells to induce osteogenic differentiation in human SSCs and progenitor populations. Increase in cell area; increase in *ALP, OCN* and *OPN* gene expressions; and increase in metabolites and close association with SSCs cultured in flat OM conditions illustrated the potential for the nacre surface to control osteogenic differentiation. Further to this, this study improves understanding of stem cell response to prism topography. While the gene expression studies produced mixed results, metabolomics network analysis from SSCs cultured on the prism surface indicates that there was a maintenance of the SSC phenotype on these surfaces. By studying cell behaviour using a clinically relevant population, we have shown the potential for nacre topography to be used for controlling osteogenic differentiation in patients with degenerative

bone disease and begun to understand the effects that the prism shell topography has on controlling SSC phenotype.

Acknowledgements

The authors gratefully acknowledge Carol-Anne Smith and Vineetha Jayawarna from University of Glasgow for preparation of topographical surfaces and Julia Wells from University of Southampton for technical support. This manuscript is dedicated to the memory of Professor Adam Curtis, who inspired, challenged and was unfailingly generous in his support of our work within the nanotopographical field over the last two decades.

Declaration of conflicting interests

The author(s) declared no potential conflicts of interest with respect to the research, authorship and/or publication of this article.

Ethical approval

Bone marrow samples were obtained from patients undergoing routine hip replacement. Surgery at University Hospital Southampton with full ethical consent and approval from the local hospital ethics committee (LREC 194/99/w, 27/10/10) and informed consent was obtained from all patients.

Funding

The author(s) disclosed receipt of the following financial support for the research, authorship, and/or publication of this article: The work in the authors' laboratories was supported by grants from the BBSRC (BB/L021072/1 and BB/L00609X/1 and UK Regenerative Medicine Platform (MR/K026682/1) and University of Southampton to R.O.C.O. M.J.D. and M.C. acknowledge MRC grant MR/K011278/1.

Supplemental Material

Supplemental material is available for this article online.

References

1. Dawson JI, Kanczler J, Tare R, et al. Concise review: bridging the gap: bone regeneration using skeletal stem cell-based strategies – where are we now? *Stem Cells* 2014; 32(1): 35–44.
2. Yamada Y, Nakamura S, Klein OD, et al. Current trends in stem cell therapy for improvement of bone quality. *Histol Histopathol* 2014; 29(6): 691–697.
3. Leal J, Gray AM, Prieto-Alhambra D, et al. Impact of hip fracture on hospital care costs: a population-based study. *Osteoporos Int* 2016; 27(2): 549–558.
4. Jones EA, Giannoudis PV and Kouroupis D. Bone repair with skeletal stem cells: rationale, progress to date and clinical application. *Ther Adv Musculoskelet Dis* 2016; 8(3): 57–71.
5. Kulangara K, Yang Y, Yang J, et al. Nanotopography as modulator of human mesenchymal stem cell function. *Biomaterials* 2012; 33(20): 4998–5003.
6. Abagnale G, Steger M, Nguyen VH, et al. Surface topography enhances differentiation of mesenchymal stem cells towards osteogenic and adipogenic lineages. *Biomaterials* 2015; 61: 316–326.
7. Brammer KS, Choi C, Frandsen CJ, et al. Hydrophobic nanopillars initiate mesenchymal stem cell aggregation and osteo-differentiation. *Acta Biomater* 2011; 7(2): 683–690.
8. Dalby MJ, Gadegaard N, Tare R, et al. The control of human mesenchymal cell differentiation using nanoscale symmetry and disorder. *Nat Mater* 2007; 6(12): 997–1003.
9. Dalby MJ, Gadegaard N and Oreffo ROC. Harnessing nanotopography and integrin-matrix interactions to influence stem cell fate. *Nat Mater* 2014; 13(6): 558–569.
10. Kilian KA, Bugarija B, Lahn BT, et al. Geometric cues for directing the differentiation of mesenchymal stem cells. *Proc Natl Acad Sci U S A* 2010; 107(11): 4872–4877.
11. Westbroek P and Marin F. A marriage of bone and nacre. *Nature* 1998; 392(6679): 861–862.
12. Clarke B. Normal bone anatomy and physiology. *Clin J Am Soc Nephrol* 2008; 3: S131–S139.
13. Zhang G, Brion A, Willemin AS, et al. Nacre, a natural, multi-use, and timely biomaterial for bone graft substitution. *J Biomed Mater Res A* 2017; 105(2): 662–671.
14. Silve C, Lopez E, Vidal B, et al. Nacre initiates biomineralization by human osteoblasts maintained in vitro. *Calcif Tissue Int* 1992; 51(5): 363–369.
15. Lopez E, Vidal B, Berland S, et al. Demonstration of the capacity of nacre to induce bone formation by human osteoblasts maintained in vitro. *Tissue Cell* 1992; 24(5): 667–679.
16. Atlan G, Balmain N, Berland S, et al. Reconstruction of human maxillary defects with nacre powder: histological evidence for bone regeneration. *Compt Rend Acad Sci* 1997; 320(3): 253–258.
17. Lamghari M, Berland S, Laurent A, et al. Bone reactions to nacre injected percutaneously into the vertebrae of sheep. *Biomaterials* 2001; 22(6): 555–562.
18. Duplat D, Chabadel A, Gallet M, et al. The in vitro osteoclastic degradation of nacre. *Biomaterials* 2007; 28(12): 2155–2162.
19. Shen Y, Yang S, Liu J, et al. Engineering scaffolds integrated with calcium sulfate and oyster shell for enhanced bone tissue regeneration. *ACS Appl Mater Interfaces* 2014; 6(15): 12177–12188.
20. Almeida MJ, Pereira L, Milet C, et al. Comparative effects of nacre water-soluble matrix and dexamethasone on the alkaline phosphatase activity of MRC-5 fibroblasts. *J Biomed Mater Res* 2001; 57(2): 306–312.
21. Green DW, Kwon HJ and Jung HS. Osteogenic potency of nacre on human mesenchymal stem cells. *Mol Cells* 2015; 38(3): 267–272.
22. Alakpa EV, Burgess KEV, Chung P, et al. Nacre topography produces higher crystallinity in bone than chemically induced osteogenesis. *ACS Nano* 2017; 11(7): 6717–6727.
23. Williams EL, White K and Oreffo RO. Isolation and enrichment of Stro-1 immunoselected mesenchymal stem cells from adult human bone marrow. *Methods Mol Biol* 2013; 1035: 67–73.
24. Gothard D, Greenhough J, Ralph E, et al. Prospective isolation of human bone marrow stromal cell subsets: a comparative study between Stro-1-, CD146- and CD105-enriched populations. *J Tissue Eng* 2014; 5: 1–17.

25. Carpenter AE, Jones TR, Lamprecht MR, et al. CellProfiler: image analysis software for identifying and quantifying cell phenotypes. *Genome Biol* 2006; 7(10): R100.
26. Kamentsky L, Jones TR, Fraser A, et al. Improved structure, function and compatibility for CellProfiler: modular high-throughput image analysis software. *Bioinformatics* 2011; 27(8): 1179–1180.
27. Schmittgen TD and Livak KJ. Analyzing real-time PCR data by the comparative C(T) method. *Nat Protoc* 2008; 3(6): 1101–1108.
28. Creek DJ, Jankevics A, Burgess KEV, et al. IDEOM: an Excel interface for analysis of LC-MS-based metabolomics data. *Bioinformatics* 2012; 28(7): 1048–1049.
29. Xia J, Sinelnikov IV, Han B, et al. MetaboAnalyst 3.0 – making metabolomics more meaningful. *Nucleic Acids Res* 2015; 43(W1): W251–W257.
30. Song W, Kawazoe N and Chen G. Dependence of spreading and differentiation of mesenchymal stem cells on micropatterned surface area. *J Nanomater* 2011; 2011: 265251.
31. Lian JB, Stein GS, Javed A, et al. Networks and hubs for the transcriptional control of osteoblastogenesis. *Rev Endocr Metab Disord* 2006; 7(1–2): 1–16.
32. Shen Q and Christakos S. The vitamin D receptor, Runx2, and the Notch signaling pathway cooperate in the transcriptional regulation of osteopontin. *J Biol Chem* 2005; 280(49): 40589–40598.
33. Weng JJ and Su Y. Nuclear matrix-targeting of the osteogenic factor Runx2 is essential for its recognition and activation of the alkaline phosphatase gene. *Biochim Biophys Acta* 2013; 1830(3): 2839–2852.
34. Zaidi SK, Javed A, Choi JY, et al. A specific targeting signal directs Runx2/Cbfa1 to subnuclear domains and contributes to transactivation of the osteocalcin gene. *J Cell Sci* 2001; 114(17): 3093–3102.
35. Kato RB, Roy B, De Oliveira FS, et al. Nanotopography directs mesenchymal stem cells to osteoblast lineage through regulation of microRNA-SMAD-BMP-2 circuit. *J Cell Physiol* 2014; 229(11): 1690–1696.
36. Yang W, Han W, He W, et al. Surface topography of hydroxyapatite promotes osteogenic differentiation of human bone marrow mesenchymal stem cells. *Mater Sci Eng C Mater Biol Appl* 2016; 60: 45–53.
37. Cliff TS and Dalton S. Metabolic switching and cell fate decisions: implications for pluripotency, reprogramming and development. *Curr Opin Genet Dev* 2017; 46: 44–49.
38. Chen CT, Shih YRV, Kuo TK, et al. Coordinated changes of mitochondrial biogenesis and antioxidant enzymes during osteogenic differentiation of human mesenchymal stem cells. *Stem Cells* 2008; 26(4): 960–968.
39. Tsimbouri PM, McMurray RJ, Burgess KV, et al. Using nanotopography and metabolomics to identify biochemical effectors of multipotency. *Acs Nano* 2012; 6(11): 10239–10249.
40. Lee N, Kim I, Park S, et al. Creatine inhibits adipogenesis by downregulating insulin-induced activation of the phosphatidylinositol 3-kinase signaling pathway. *Stem Cells Dev* 2015; 24(8): 983–994.
41. Karner CM, Esen E, Okunade AL, et al. Increased glutamine catabolism mediates bone anabolism in response to WNT signaling. *J Clin Invest* 2015; 125(2): 551–562.
42. Lu Q, Zhang Y and Elisseeff JH. Carnitine and acetylcarnitine modulate mesenchymal differentiation of adult stem cells. *J Tissue Eng Regen Med* 2015; 9(12): 1352–1362.
43. Kanno T, Takahashi T, Tsujisawa T, et al. Mechanical stress-mediated Runx2 activation is dependent on Ras/ERK1/2 MAPK signaling in osteoblasts. *J Cell Biochem* 2007; 101(5): 1266–1277.
44. Ge C, Xiao G, Jiang D, et al. Critical role of the extracellular signal-regulated kinase-MAPK pathway in osteoblast differentiation and skeletal development. *J Cell Biol* 2007; 176(5): 709–718.
45. Knobloch M, Pilz GA, Ghesquiere B, et al. A fatty acid oxidation-dependent metabolic shift regulates adult neural stem cell activity. *Cell Rep* 2017; 20(9): 2144–2155.
46. Ritz U, Gerke R, Gotz H, et al. A new bone substitute developed from 3D-prints of polylactide (PLA) loaded with collagen I: an in vitro study. *Int J Mol Sci* 2017; 18(12): E2569.
47. Shim KS, Kim SE, Yun YP, et al. Surface immobilization of biphasic calcium phosphate nanoparticles on 3D printed poly(caprolactone) scaffolds enhances osteogenesis and bone tissue regeneration. *J Ind Eng Chem* 2017; 55: 101–109.
48. Rogatzki MJ, Ferguson BS, Goodwin ML, et al. Lactate is always the end product of glycolysis. *Front Neurosci* 2015; 9: 22
49. Janeczek AA, Tare RS, Scarpa E, et al. Transient canonical Wnt stimulation enriches human bone marrow mononuclear cell isolates for osteoprogenitors. *Stem Cells* 2016; 34(2): 418–430.

References

References

1. Budd, E., et al., *The Potential of microRNAs for Stem Cell-based Therapy for Degenerative Skeletal Diseases.* Current Molecular Biology Reports, 2017. **3**(4): p. 263-275.
2. Gray, H., *Gray's Anatomy: The Anatomical Basis of Clinical Practice*. 40 ed. 2008, New York: Elsevier.
3. Clarke, B., *Normal Bone Anatomy and Physiology.* Clinical Journal of the American Society of Nephrology, 2008. **3**: p. S131-S139.
4. Allen, M.R., J.M. Hock, and D.B. Burr, *Periosteum: biology, regulation, and response to osteoporosis therapies.* Bone, 2004. **35**(5): p. 1003-12.
5. Colnot, C., X. Zhang, and M.L. Knothe Tate, *Current insights on the regenerative potential of the periosteum: molecular, cellular, and endogenous engineering approaches.* J Orthop Res, 2012. **30**(12): p. 1869-78.
6. Hernandez, C.J., R.J. Majeska, and M.B. Schaffler, *Osteocyte density in woven bone.* Bone, 2004. **35**(5): p. 1095-9.
7. Feng, X., *Chemical and Biochemical Basis of Cell-Bone Matrix Interaction in Health and Disease.* Curr Chem Biol, 2009. **3**(2): p. 189-196.
8. Garnero, P., *The Role of Collagen Organization on the Properties of Bone.* Calcified Tissue International, 2015. **97**(3): p. 229-240.
9. Lamande, S.R. and J.F. Bateman, *Procollagen folding and assembly: The role of endoplasmic reticulum enzymes and molecular chaperones.* Seminars in Cell & Developmental Biology, 1999. **10**(5): p. 455-464.
10. Viguet-Carrin, S., P. Garnero, and P.D. Delmas, *The role of collagen in bone strength.* Osteoporos Int, 2006. **17**(3): p. 319-36.
11. Alford, A.I. and K.D. Hankenson, *Matricellular proteins: Extracellular modulators of bone development, remodeling, and regeneration.* Bone, 2006. **38**(6): p. 749-57.
12. Morgan, S., A.A. Poundarik, and D. Vashishth, *Do Non-collagenous Proteins Affect Skeletal Mechanical Properties?* Calcif Tissue Int, 2015. **97**(3): p. 281-91.
13. Ferron, M. and J. Lacombe, *Regulation of energy metabolism by the skeleton: osteocalcin and beyond.* Arch Biochem Biophys, 2014. **561**: p. 137-46.
14. Chen, Q., et al., *An osteopontin-integrin interaction plays a critical role in directing adipogenesis and osteogenesis by mesenchymal stem cells.* Stem Cells, 2014. **32**(2): p. 327-37.
15. Gordon, J.A., et al., *Bone sialoprotein expression enhances osteoblast differentiation and matrix mineralization in vitro.* Bone, 2007. **41**(3): p. 462-73.
16. Baht, G.S., G.K. Hunter, and H.A. Goldberg, *Bone sialoprotein-collagen interaction promotes hydroxyapatite nucleation.* Matrix Biology, 2008. **27**(7): p. 600-608.
17. Sophia Fox, A.J., A. Bedi, and S.A. Rodeo, *The basic science of articular cartilage: structure, composition, and function.* Sports Health, 2009. **1**(6): p. 461-8.
18. Litwic, A., et al., *Epidemiology and burden of osteoarthritis.* Br Med Bull, 2013. **105**: p. 185-99.
19. Loeser, R.F., *Aging processes and the development of osteoarthritis.* Curr Opin Rheumatol, 2013. **25**(1): p. 108-13.
20. Mackie, E.J., et al., *Endochondral ossification: how cartilage is converted into bone in the developing skeleton.* Int J Biochem Cell Biol, 2008. **40**(1): p. 46-62.
21. Chan, C.K.F., et al., *Identification of the Human Skeletal Stem Cell.* Cell, 2018. **175**(1): p. 43-56 e21.
22. Mackie, E.J., L. Tatarczuch, and M. Mirams, *The skeleton: a multi-functional complex organ: the growth plate chondrocyte and endochondral ossification.* J Endocrinol, 2011. **211**(2): p. 109-21.

23. Crockett, J.C., et al., *Bone remodelling at a glance.* Journal of Cell Science, 2011. **124**(7): p. 991-998.
24. Bonewald, L.F., *The amazing osteocyte.* J Bone Miner Res, 2011. **26**(2): p. 229-38.
25. Bellido, T., *Osteocyte-driven bone remodeling.* Calcif Tissue Int, 2014. **94**(1): p. 25-34.
26. Jilka, R.L., B. Noble, and R.S. Weinstein, *Osteocyte apoptosis.* Bone, 2013. **54**(2): p. 264-71.
27. Henriksen, K., et al., *Local communication on and within bone controls bone remodeling.* Bone, 2009. **44**(6): p. 1026-33.
28. Bloemen, V., et al., *Intercellular adhesion molecule-1 clusters during osteoclastogenesis.* Biochem Biophys Res Commun, 2009. **385**(4): p. 640-5.
29. Everts, V. and P. Saftig, *Degradation of Bone and the Role of Osteoclasts, Bone Lining Cells and Osteocytes*, in *Extracellular Matrix Degradation*, W.C. Parks and R.P. Mecham, Editors. 2011, Springer: New York. p. 193-216.
30. Chambers, T.J. and K. Fuller, *Bone-cells predispose bone surfaces to resorption by exposure of mineral to osteclastic contact. .* Journal of Cell Science, 1985. **76**(JUN): p. 155-165.
31. Eck, S.M., et al., *Matrix metalloproteinase-1 promotes breast cancer angiogenesis and osteolysis in a novel in vivo model.* Breast Cancer Res Treat, 2009. **116**(1): p. 79-90.
32. Boyle, W.J., W.S. Simonet, and D.L. Lacey, *Osteoclast differentiation and activation.* Nature, 2003. **423**(6937): p. 337-342.
33. Rucci, N. and A. Teti, *The "love-hate" relationship between osteoclasts and bone matrix.* Matrix Biol, 2016. **52-54**: p. 176-190.
34. Florencio-Silva, R., et al., *Biology of Bone Tissue: Structure, Function, and Factors That Influence Bone Cells.* BioMed Research International, 2015. **2015**: p. 1-17.
35. Rousselle, A.V. and D. Heymann, *Osteoclastic acidification pathways during bone resorption.* Bone, 2002. **30**(4): p. 533-540.
36. Everts, V., et al., *The bone lining cell: Its role in cleaning Howship's lacunae and initiating bone formation.* Journal of Bone and Mineral Research, 2002. **17**(1): p. 77-90.
37. Golub, E.E. and K. Boesze-Battaglia, *The role of alkaline phosphatase in mineralization.* Current Opinion in Orthopaedics, 2007. **18**(5): p. 444-448 10.1097/BCO.0b013e3282630851.
38. Manolagas, S.C. and A.M. Parfitt, *What old means to bone.* Trends Endocrinol Metab, 2010. **21**(6): p. 369-74.
39. Schindeler, A., et al., *Bone remodeling during fracture repair: The cellular picture.* Semin Cell Dev Biol, 2008. **19**(5): p. 459-66.
40. Claes, L., S. Recknagel, and A. Ignatius, *Fracture healing under healthy and inflammatory conditions.* Nat Rev Rheumatol, 2012. **8**(3): p. 133-43.
41. Marsell, R. and T.A. Einhorn, *The biology of fracture healing.* Injury, 2011. **42**(6): p. 551-5.
42. Schmidt-Bleek, K., et al., *Boon and Bane of Inflammation in Bone Tissue Regeneration and Its Link with Angiogenesis.* Tissue Eng Part B Rev, 2015. **21**(4): p. 354-64.
43. Szulc, P. and P.D. Delmas, *Bone loss in elderly men: increased endosteal bone loss and stable periosteal apposition. The prospective MINOS study.* Osteoporos Int, 2007. **18**(4): p. 495-503.
44. Court-Brown, C.M. and B. Caesar, *Epidemiology of adult fractures: A review.* Injury, 2006. **37**(8): p. 691-7.
45. Stenderup, K., et al., *Aging is associated with decreased maximal life span and accelerated senescence of bone marrow stromal cells.* Bone, 2003. **33**(6): p. 919-926.
46. Nishida, S., et al., *Number of osteoprogenitor cells in human bone marrow markedly decreases after skeletal maturation.* Journal of Bone and Mineral Metabolism, 1999. **17**(3): p. 171-177.
47. Rodriguez, J.P., et al., *Abnormal osteogenesis in osteoporotic patients is reflected by altered mesenchymal stem cells dynamics.* Journal of Cellular Biochemistry, 1999. **75**(3): p. 414-423.

48. Caplan, A.I., *Mesenchymal stem cells: Cell-based reconstructive therapy in orthopedics.* Tissue Engineering, 2005. **11**(7-8): p. 1198-1211.
49. Justesen, J., et al., *Adipocyte tissue volume in bone marrow is increased with aging and in patients with osteoporosis.* Biogerontology, 2001. **2**(3): p. 165-171.
50. Verma, S., et al., *Adipocytic proportion of bone marrow is inversely related to bone formation in osteoporosis.* Journal of Clinical Pathology, 2002. **55**(9): p. 693-698.
51. Marie, P.J., *Bone cell senescence: mechanisms and perspectives.* J Bone Miner Res, 2014. **29**(6): p. 1311-21.
52. de Jesus, B.B., et al., *Telomerase gene therapy in adult and old mice delays aging and increases longevity without increasing cancer.* Embo Molecular Medicine, 2012. **4**(8): p. 691-704.
53. Fazeli, P.K., et al., *Marrow fat and bone--new perspectives.* J Clin Endocrinol Metab, 2013. **98**(3): p. 935-45.
54. Moerman, E.J., et al., *Aging activates adipogenic and suppresses osteogenic programs in mesenchymal marrow stroma/stem cells: the role of PPAR-gamma 2 transcription factor and TGF-beta/BMP signaling pathways.* Aging Cell, 2004. **3**(6): p. 379-389.
55. Chen, K., et al., *Decreased activity of osteocyte autophagy with aging may contribute to the bone loss in senile population.* Histochem Cell Biol, 2014. **142**(3): p. 285-95.
56. Rajawat, Y.S., Z. Hilioti, and I. Bossis, *Aging: central role for autophagy and the lysosomal degradative system.* Ageing Res Rev, 2009. **8**(3): p. 199-213.
57. Madeo, F., N. Tavernarakis, and G. Kroemer, *Can autophagy promote longevity?* Nat Cell Biol, 2010. **12**(9): p. 842-6.
58. Holroyd, C., C. Cooper, and E. Dennison, *Epidemiology of osteoporosis.* Best Pract Res Clin Endocrinol Metab, 2008. **22**(5): p. 671-85.
59. Drake, M.T., B.L. Clarke, and S. Khosla, *Bisphosphonates: Mechanism of action and role in clinical practice.* Mayo Clinic Proceedings, 2008. **83**(9): p. 1032-1045.
60. Brumsen, C., et al., *Daily oral pamidronate in women and men with osteoporosis: A 3-year randomized placebo-controlled clinical trial with a 2-year open extension.* Journal of Bone and Mineral Research, 2002. **17**(6): p. 1057-1064.
61. Clarke, B.L., *Anti-sclerostin antibodies: utility in treatment of osteoporosis.* Maturitas, 2014. **78**(3): p. 199-204.
62. Recker, R.R., et al., *A randomized, double-blind phase 2 clinical trial of blosozumab, a sclerostin antibody, in postmenopausal women with low bone mineral density.* J Bone Miner Res, 2015. **30**(2): p. 216-24.
63. Sarzi-Puttini, P., et al., *Osteoarthritis: an overview of the disease and its treatment strategies.* Semin Arthritis Rheum, 2005. **35**(1 Suppl 1): p. 1-10.
64. Johnson, V.L. and D.J. Hunter, *The epidemiology of osteoarthritis.* Best Pract Res Clin Rheumatol, 2014. **28**(1): p. 5-15.
65. Messner, K. and W. Maletius, *The long-term prognosis for severe damage to weight-bearing cartilage in the knee: a 14-year clinical and radiographic follow-up in 28 young athletes.* Acta Orthop Scand, 1996. **67**(2): p. 165-8.
66. Roach, H.I., et al., *Association between the abnormal expression of matrix-degrading enzymes by human osteoarthritic chondrocytes and demethylation of specific CpG sites in the promoter regions.* Arthritis Rheum, 2005. **52**(10): p. 3110-24.
67. Bui, C., et al., *cAMP response element-binding (CREB) recruitment following a specific CpG demethylation leads to the elevated expression of the matrix metalloproteinase 13 in human articular chondrocytes and osteoarthritis.* FASEB J, 2012. **26**(7): p. 3000-11.
68. Hashimoto, K., et al., *Regulated transcription of human matrix metalloproteinase 13 (MMP13) and interleukin-1beta (IL1B) genes in chondrocytes depends on methylation of specific proximal promoter CpG sites.* J Biol Chem, 2013. **288**(14): p. 10061-72.
69. Yamasaki, K., et al., *Expression of MicroRNA-146a in osteoarthritis cartilage.* Arthritis Rheum, 2009. **60**(4): p. 1035-41.

70. Miyaki, S., et al., *MicroRNA-140 plays dual roles in both cartilage development and homeostasis.* Genes & Development, 2010. **24**(11): p. 1173-1185.
71. Tsezou, A., *Osteoarthritis year in review 2014: genetics and genomics.* Osteoarthritis Cartilage, 2014. **22**(12): p. 2017-24.
72. Pereira, D., E. Ramos, and J. Branco, *Osteoarthritis.* Acta Medica Portuguesa, 2015. **28**(1): p. 99-106.
73. Wieland, H.A., et al., *Osteoarthritis - an untreatable disease?* Nat Rev Drug Discov, 2005. **4**(4): p. 331-44.
74. Culliford, D.J., et al., *The lifetime risk of total hip and knee arthroplasty: results from the UK general practice research database.* Osteoarthritis Cartilage, 2012. **20**(6): p. 519-24.
75. Dixon, T., et al., *Trends in hip and knee joint replacement: socioeconomic inequalities and projections of need.* Ann Rheum Dis, 2004. **63**(7): p. 825-30.
76. He, S., D. Nakada, and S.J. Morrison, *Mechanisms of stem cell self-renewal.* Annu Rev Cell Dev Biol, 2009. **25**: p. 377-406.
77. Ito, K. and T. Suda, *Metabolic requirements for the maintenance of self-renewing stem cells.* Nat Rev Mol Cell Biol, 2014. **15**(4): p. 243-56.
78. Tsai, C.C., et al., *Oct4 and Nanog directly regulate Dnmt1 to maintain self-renewal and undifferentiated state in mesenchymal stem cells.* Mol Cell, 2012. **47**(2): p. 169-82.
79. Yoon, D.S., et al., *SIRT1 directly regulates SOX2 to maintain self-renewal and multipotency in bone marrow-derived mesenchymal stem cells.* Stem Cells, 2014. **32**(12): p. 3219-31.
80. Chamberlain, G., et al., *Concise review: Mesenchymal stem cells: Their phenotype, differentiation capacity, immunological features, and potential for homing.* Stem Cells, 2007. **25**(11): p. 2739-2749.
81. Bianco, P. and P.G. Robey, *Skeletal stem cells.* Development, 2015. **142**(6): p. 1023-7.
82. Friedenstein, A.J., J.J. Piatetzky-Shapizo, and K.V. Petzakova, *Osteogenesis in transplants of bone marrow cells.* J Embryol Exp Morphol, 1966. **16**((3)): p. 381-390.
83. Friedens.Aj, Chailakh.Rk, and K.S. Lalykina, *DEVELOPMENT OF FIBROBLAST COLONIES IN MONOLAYER CULTURES OF GUINEA-PIG BONE MARROW AND SPLEEN CELLS.* Cell and Tissue Kinetics, 1970. **3**(4): p. 393-&.
84. Pittenger, M.F., et al., *Multilineage potential of adult human mesenchymal stem cells.* Science, 1999. **284**(5411): p. 143-147.
85. Bianco, P., et al., *The meaning, the sense and the significance: translating the science of mesenchymal stem cells into medicine.* Nat Med, 2013. **19**(1): p. 35-42.
86. Crisan, M., et al., *A Perivascular Origin for Mesenchymal Stem Cells in Multiple Human Organs.* Cell Stem Cell, 2008. **3**(3): p. 301-313.
87. Wada, N., S. Gronthos, and P.M. Bartold, *Immunomodulatory effects of stem cells.* Periodontology 2000, 2013. **63**(1): p. 198-216.
88. Sotiropoulou, P.A., et al., *Interactions between human mesenchymal stem cells and natural killer cells.* Stem Cells, 2006. **24**(1): p. 74-85.
89. Ren, H., et al., *Comparative Analysis of Human Mesenchymal Stem Cells from Umbilical Cord, Dental Pulp, and Menstrual Blood as Sources for Cell Therapy.* Stem Cells Int, 2016. **2016**: p. 3516574.
90. Konno, M., et al., *Adipose-derived mesenchymal stem cells and regenerative medicine.* Dev Growth Differ, 2013. **55**(3): p. 309-18.
91. Steigman, S.A., et al., *Sternal repair with bone grafts engineered from amniotic mesenchymal stem cells.* J Pediatr Surg, 2009. **44**(6): p. 1120-6; discussion 1126.
92. Robey, P.G., *Cell sources for bone regeneration: the good, the bad, and the ugly (but promising).* Tissue Eng Part B Rev, 2011. **17**(6): p. 423-30.
93. Takahashi, K., et al., *Induction of pluripotent stem cells from adult human fibroblasts by defined factors.* Cell, 2007. **131**(5): p. 861-72.
94. Okano, H., et al., *Steps toward safe cell therapy using induced pluripotent stem cells.* Circ Res, 2013. **112**(3): p. 523-33.

95. Janeczek, A.A., et al., *Transient Canonical Wnt Stimulation Enriches Human Bone Marrow Mononuclear Cell Isolates for Osteoprogenitors.* Stem Cells, 2016. **34**(2): p. 418-30.
96. Dominici, M., et al., *Minimal criteria for defining multipotent mesenchymal stromal cells. The International Society for Cellular Therapy position statement.* Cytotherapy, 2006. **8**(4): p. 315-7.
97. Stewart, K., et al., *Further characterization of cells expressing STRO-1 in cultures of adult human bone, marrow stromal cells.* Journal of Bone and Mineral Research, 1999. **14**(8): p. 1345-1356.
98. Gronthos, S., et al., *THE STRO-1(+) FRACTION OF ADULT HUMAN BONE-MARROW CONTAINS THE OSTEOGENIC PRECURSORS.* Blood, 1994. **84**(12): p. 4164-4173.
99. Peiffer, I., et al., *A sub-population of high proliferative potential-quiescent human mesenchymal stem cells is under the reversible control of interferon alpha/beta.* Leukemia, 2007. **21**(4): p. 714-24.
100. Fitter, S., et al., *The Mesenchymal Precursor Cell Marker Antibody STRO-1 Binds to Cell Surface Heat Shock Cognate 70.* Stem Cells, 2017. **35**(4): p. 940-951.
101. Dennis, J.E., et al., *The STRO-1+marrow cell population is multipotential.* Cells Tissues Organs, 2002. **170**(2-3): p. 73-82.
102. Gronthos, S., et al., *Molecular and cellular characterisation of highly purified stromal stem cells derived from human bone marrow.* J Cell Sci, 2003. **116**(Pt 9): p. 1827-35.
103. Nasef, A., et al., *Selected Stro-1-enriched bone marrow stromal cells display a major suppressive effect on lymphocyte proliferation.* Int J Lab Hematol, 2009. **31**(1): p. 9-19.
104. Gronthos, S., et al., *Differential cell surface expression of the STRO-1 and alkaline phosphatase antigens on discrete developmental stages in primary cultures of human bone cells.* Journal of Bone and Mineral Research, 1999. **14**(1): p. 47-56.
105. Gothard, D., et al., *Prospective isolation of human bone marrow stromal cell subsets: A comparative study between Stro-1-, CD146- and CD105-enriched populations.* J Tissue Eng, 2014. **5**: p. 2041731414551763.
106. MacArthur, B.D., et al., *A non-invasive method for in situ quantification of subpopulation behaviour in mixed cell culture.* J R Soc Interface, 2006. **3**(6): p. 63-9.
107. Gronthos, S., et al., *Molecular and cellular characterisation of highly purified stromal stem cells derived from human bone marrow.* Journal of Cell Science, 2003. **116**(9): p. 1827-1835.
108. Zannettino, A.C., et al., *Human mulipotential mesenchymal/stromal stem cells are derived from a discrete subpopulation of STRO-1bright/CD34 /CD45(-)/glycophorin-A-bone marrow cells.* Haematologica, 2007. **92**(12): p. 1707-8.
109. Simmons, P.J. and B. Torokstorb, *IDENTIFICATION OF STROMAL CELL PRECURSORS IN HUMAN BONE-MARROW BY A NOVEL MONOCLONAL-ANTIBODY, STRO-1.* Blood, 1991. **78**(1): p. 55-62.
110. Zannettino, A.C., et al., *Multipotential human adipose-derived stromal stem cells exhibit a perivascular phenotype in vitro and in vivo.* J Cell Physiol, 2008. **214**(2): p. 413-21.
111. Long, F., *Building strong bones: molecular regulation of the osteoblast lineage.* Nat Rev Mol Cell Biol, 2012. **13**(1): p. 27-38.
112. Deng, Z.L., et al., *Regulation of osteogenic differentiation during skeletal development.* Front Biosci, 2008. **13**: p. 2001-21.
113. Chen, G., C. Deng, and Y.P. Li, *TGF-beta and BMP signaling in osteoblast differentiation and bone formation.* Int J Biol Sci, 2012. **8**(2): p. 272-88.
114. Heldin, C.H., K. Miyazono, and P. tenDijke, *TGF-beta signalling from cell membrane to nucleus through SMAD proteins.* Nature, 1997. **390**(6659): p. 465-471.
115. Tsuji, K., et al., *BMP2 activity, although dispensable for bone formation, is required for the initiation of fracture healing.* Nat Genet, 2006. **38**(12): p. 1424-9.
116. Nelson, W.J. and R. Nusse, *Convergence of Wnt, beta-catenin, and cadherin pathways.* Science, 2004. **303**(5663): p. 1483-1487.

117. Gaur, T., et al., *Canonical WNT signaling promotes osteogenesis by directly stimulating Runx2 gene expression.* J Biol Chem, 2005. **280**(39): p. 33132-40.
118. Shen, Q. and S. Christakos, *The vitamin D receptor, Runx2, and the Notch signaling pathway cooperate in the transcriptional regulation of osteopontin.* J Biol Chem, 2005. **280**(49): p. 40589-98.
119. Fontaine, C., et al., *Hedgehog signaling alters adipocyte maturation of human mesenchymal stem cells.* Stem Cells, 2008. **26**(4): p. 1037-1046.
120. Nakamura, T., et al., *Induction of osteogenic differentiation by hedgehog proteins.* Biochemical and Biophysical Research Communications, 1997. **237**(2): p. 465-469.
121. Plaisant, M., et al., *Activation of hedgehog signaling inhibits osteoblast differentiation of human mesenchymal stem cells.* Stem Cells, 2009. **27**(3): p. 703-13.
122. Liu, Z.H., et al., *Coordination of chondrogenesis and osteogenesis by fibroblast growth factor 18.* Genes & Development, 2002. **16**(7): p. 859-869.
123. Rodda, S.J. and A.P. McMahon, *Distinct roles for Hedgehog and canonical Wnt signaling in specification, differentiation and maintenance of osteoblast progenitors.* Development, 2006. **133**(16): p. 3231-44.
124. Hu, H., et al., *Sequential roles of Hedgehog and Wnt signaling in osteoblast development.* Development, 2005. **132**(1): p. 49-60.
125. Zhang, R., et al., *Wnt/beta-catenin signaling activates bone morphogenetic protein 2 expression in osteoblasts.* Bone, 2013. **52**(1): p. 145-56.
126. Deng, Z.L., et al., *Regulation of osteogenic differentiation during skeletal development.* Frontiers in Bioscience-Landmark, 2008. **13**: p. 2001-2021.
127. Papachristou, D.J., et al., *Signaling networks and transcription factors regulating mechanotransduction in bone.* Bioessays, 2009. **31**(7): p. 794-804.
128. Dawson, J.I., et al., *Concise review: bridging the gap: bone regeneration using skeletal stem cell-based strategies - where are we now?* Stem Cells, 2014. **32**(1): p. 35-44.
129. Bajada, S., et al., *Updates on stem cells and their applications in regenerative medicine.* J Tissue Eng Regen Med, 2008. **2**(4): p. 169-83.
130. Loebel, C., et al., *In vitro osteogenic potential of human mesenchymal stem cells is predicted by Runx2/Sox9 ratio.* Tissue Eng Part A, 2015. **21**(1-2): p. 115-23.
131. Born, A.K., S. Lischer, and K. Maniura-Weber, *Watching osteogenesis: life monitoring of osteogenic differentiation using an osteocalcin reporter.* J Cell Biochem, 2012. **113**(1): p. 313-21.
132. Dalby, M.J., et al., *The control of human mesenchymal cell differentiation using nanoscale symmetry and disorder.* Nat Mater, 2007. **6**(12): p. 997-1003.
133. Kilian, K.A., et al., *Geometric cues for directing the differentiation of mesenchymal stem cells.* Proc Natl Acad Sci U S A, 2010. **107**(11): p. 4872-7.
134. Thibault, R.A., et al., *Osteogenic Differentiation of Mesenchymal Stem Cells on Pregenerated Extracellular Matrix Scaffolds in the Absence of Osteogenic Cell Culture Supplements.* Tissue Engineering Part A, 2010. **16**(2): p. 431-440.
135. Tilley, S., et al., *Taking tissue-engineering principles into theater: augmentation of impacted allograft with human bone marrow stromal cells.* Regenerative Medicine, 2006. **1**(5): p. 685-692.
136. Marcacci, M., et al., *Stem cells associated with macroporous bioceramics for long bone repair: 6- to 7-year outcome of a pilot clinical study.* Tissue Eng, 2007. **13**(5): p. 947-55.
137. Kim, S.J., et al., *A multi-center, randomized, clinical study to compare the effect and safety of autologous cultured osteoblast(Ossron) injection to treat fractures.* BMC Musculoskelet Disord, 2009. **10**: p. 20.
138. Jones, E.A., P.V. Giannoudis, and D. Kouroupis, *Bone repair with skeletal stem cells: rationale, progress to date and clinical application.* Ther Adv Musculoskelet Dis, 2016. **8**(3): p. 57-71.
139. Nagaraja, M.P. and D. Risin, *The current state of bone loss research: data from spaceflight and microgravity simulators.* J Cell Biochem, 2013. **114**(5): p. 1001-8.

140. Chen, J.H., et al., *Boning up on Wolff's Law: mechanical regulation of the cells that make and maintain bone.* J Biomech, 2010. **43**(1): p. 108-18.
141. Gharibi, B., et al., *Gene expression responses to mechanical stimulation of mesenchymal stem cells seeded on calcium phosphate cement.* Tissue Eng Part A, 2013. **19**(21-22): p. 2426-38.
142. Barczyk, M., S. Carracedo, and D. Gullberg, *Integrins.* Cell and Tissue Research, 2010. **339**(1): p. 269-280.
143. Dalby, M.J., N. Gadegaard, and R.O.C. Oreffo, *Harnessing nanotopography and integrin-matrix interactions to influence stem cell fate.* Nature Materials, 2014. **13**(6): p. 558-569.
144. Wang, N., J.P. Butler, and D.E. Ingber, *MECHANOTRANSDUCTION ACROSS THE CELL-SURFACE AND THROUGH THE CYTOSKELETON.* Science, 1993. **260**(5111): p. 1124-1127.
145. Hamidouche, Z., et al., *Priming integrin alpha5 promotes human mesenchymal stromal cell osteoblast differentiation and osteogenesis.* Proc Natl Acad Sci U S A, 2009. **106**(44): p. 18587-91.
146. Zou, C., et al., *Mesenchymal stem cells require integrin beta1 for directed migration induced by osteopontin in vitro.* In Vitro Cell Dev Biol Anim, 2011. **47**(3): p. 241-50.
147. Kanchanawong, P., et al., *Nanoscale architecture of integrin-based cell adhesions.* Nature, 2010. **468**(7323): p. 580-4.
148. Kanno, T., et al., *Mechanical stress-mediated Runx2 activation is dependent on Ras/ERK1/2 MAPK signaling in osteoblasts.* J Cell Biochem, 2007. **101**(5): p. 1266-77.
149. Jessop, H.L., et al., *Mechanical strain and fluid movement both activate extracellular regulated kinase (ERK) in osteoblast-like cells but via different signaling pathways.* Bone, 2002. **31**(1): p. 186-194.
150. Bakker, A.D., J. Klein-Nulend, and E.H. Burger, *Mechanotransduction in bone cells proceeds via activation of COX-2, but not COX-1.* Biochemical and Biophysical Research Communications, 2003. **305**(3): p. 677-683.
151. Wadhwa, S., et al., *Fluid flow induction of cyclo-oxygenase 2 gene expression in osteoblasts is dependent on an extracellular signal-regulated kinase signaling pathway.* Journal of Bone and Mineral Research, 2002. **17**(2): p. 266-274.
152. Lin, C., et al., *Sclerostin mediates bone response to mechanical unloading through antagonizing Wnt/beta-catenin signaling.* J Bone Miner Res, 2009. **24**(10): p. 1651-61.
153. Tu, X., et al., *Sost downregulation and local Wnt signaling are required for the osteogenic response to mechanical loading.* Bone, 2012. **50**(1): p. 209-17.
154. Dupont, S., et al., *Role of YAP/TAZ in mechanotransduction.* Nature, 2011. **474**(7350): p. 179-83.
155. Codelia, V.A., G. Sun, and K.D. Irvine, *Regulation of YAP by mechanical strain through Jnk and Hippo signaling.* Curr Biol, 2014. **24**(17): p. 2012-7.
156. Gumbiner, B.M. and N.G. Kim, *The Hippo-YAP signaling pathway and contact inhibition of growth.* J Cell Sci, 2014. **127**(Pt 4): p. 709-17.
157. Pan, H., et al., *YAP-mediated mechanotransduction regulates osteogenic and adipogenic differentiation of BMSCs on hierarchical structure.* Colloids Surf B Biointerfaces, 2017. **152**: p. 344-353.
158. Parsons, J.T., et al., *Focal Adhesion Kinase: a regulator of focal adhesion dynamics and cell movement.* Oncogene, 2000. **19**(49): p. 5606-5613.
159. Arnsdorf, E.J., et al., *Mechanically induced osteogenic differentiation--the role of RhoA, ROCKII and cytoskeletal dynamics.* J Cell Sci, 2009. **122**(Pt 4): p. 546-53.
160. Maniotis, A.J., C.S. Chen, and D.E. Ingber, *Demonstration of mechanical connections between integrins cytoskeletal filaments, and nucleoplasm that stabilize nuclear structure.* Proceedings of the National Academy of Sciences of the United States of America, 1997. **94**(3): p. 849-854.
161. Trappmann, B., et al., *Extracellular-matrix tethering regulates stem-cell fate.* Nat Mater, 2012. **11**(7): p. 642-9.

162. Curtis, A.S.G., et al., *ADHESION OF CELLS TO POLYSTYRENE SURFACES.* Journal of Cell Biology, 1983. **97**(5): p. 1500-1506.
163. Keselowsky, B.G., D.M. Collard, and A.J. Garcia, *Surface chemistry modulates focal adhesion composition and signaling through changes in integrin binding.* Biomaterials, 2004. **25**(28): p. 5947-5954.
164. Curran, J.M., R. Chen, and J.A. Hunt, *The guidance of human mesenchymal stem cell differentiation in vitro by controlled modifications to the cell substrate.* Biomaterials, 2006. **27**(27): p. 4783-4793.
165. Hynes, R.O., *The extracellular matrix: not just pretty fibrils.* Science, 2009. **326**(5957): p. 1216-9.
166. Ellis, S.J. and G. Tanentzapf, *Integrin-mediated adhesion and stem-cell-niche interactions.* Cell Tissue Res, 2010. **339**(1): p. 121-30.
167. Turner, L.-A. and M. J. Dalby, *Nanotopography – potential relevance in the stem cell niche.* Biomater. Sci., 2014. **2**(11): p. 1574-1594.
168. Swift, J., et al., *Nuclear lamin-A scales with tissue stiffness and enhances matrix-directed differentiation.* Science, 2013. **341**(6149): p. 1240104.
169. Wen, J.H., et al., *Interplay of matrix stiffness and protein tethering in stem cell differentiation.* Nat Mater, 2014. **13**(10): p. 979-87.
170. Tusan, C.G., et al., *Collective Cell Behavior in Mechanosensing of Substrate Thickness.* Biophys J, 2018. **114**(11): p. 2743-2755.
171. Sjostrom, T., et al., *Fabrication of pillar-like titania nanostructures on titanium and their interactions with human skeletal stem cells.* Acta Biomater, 2009. **5**(5): p. 1433-41.
172. Yim, E.K., et al., *Nanotopography-induced changes in focal adhesions, cytoskeletal organization, and mechanical properties of human mesenchymal stem cells.* Biomaterials, 2010. **31**(6): p. 1299-306.
173. Ahn, E.H., et al., *Spatial control of adult stem cell fate using nanotopographic cues.* Biomaterials, 2014. **35**(8): p. 2401-2410.
174. Oh, S., et al., *Stem cell fate dictated solely by altered nanotube dimension.* Proc Natl Acad Sci U S A, 2009. **106**(7): p. 2130-5.
175. McMurray, R.J., et al., *Nanoscale surfaces for the long-term maintenance of mesenchymal stem cell phenotype and multipotency.* Nat Mater, 2011. **10**(8): p. 637-44.
176. Li, Z., et al., *Differential regulation of stiffness, topography, and dimension of substrates in rat mesenchymal stem cells.* Biomaterials, 2013. **34**(31): p. 7616-25.
177. Tsimbouri, P., et al., *Nanotopographical effects on mesenchymal stem cell morphology and phenotype.* J Cell Biochem, 2014. **115**(2): p. 380-90.
178. Kim, J., et al., *Designing nanotopographical density of extracellular matrix for controlled morphology and function of human mesenchymal stem cells.* Sci Rep, 2013. **3**: p. 3552.
179. de Peppo, G.M., et al., *Osteogenic response of human mesenchymal stem cells to well-defined nanoscale topography in vitro.* Int J Nanomedicine, 2014. **9**: p. 2499-515.
180. McNamara, L.E., et al., *Skeletal stem cell physiology on functionally distinct titania nanotopographies.* Biomaterials, 2011. **32**(30): p. 7403-10.
181. Wang, K., et al., *Nanotopographical Modulation of Cell Function through Nuclear Deformation.* ACS Appl Mater Interfaces, 2016. **8**(8): p. 5082-92.
182. Liu, X., et al., *Subcellular cell geometry on micropillars regulates stem cell differentiation.* Biomaterials, 2016. **111**: p. 27-39.
183. Niinomi, M., *Mechanical biocompatibilities of titanium alloys for biomedical applications.* J Mech Behav Biomed Mater, 2008. **1**(1): p. 30-42.
184. Herath, H.M., L. Di Silvio, and J.R. Evans, *Osteoblast response to zirconia surfaces with different topographies.* Mater Sci Eng C Mater Biol Appl, 2015. **57**: p. 363-70.
185. Wang, X., et al., *Effect of RGD nanospacing on differentiation of stem cells.* Biomaterials, 2013. **34**(12): p. 2865-74.
186. Ye, K., et al., *Matrix Stiffness and Nanoscale Spatial Organization of Cell-Adhesive Ligands Direct Stem Cell Fate.* Nano Lett, 2015. **15**(7): p. 4720-9.

187. Teo, B.K., et al., *Nanotopography modulates mechanotransduction of stem cells and induces differentiation through focal adhesion kinase.* ACS Nano, 2013. **7**(6): p. 4785-98.
188. Lee, R.C., R.L. Feinbaum, and V. Ambros, *The C. elegans heterochronic gene lin-4 encodes small RNAs with antisense complementarity to lin-14.* Cell, 1993. **75**(5): p. 843-54.
189. Wightman, B., I. Ha, and G. Ruvkun, *Posttranscriptional regulation of the heterochronic gene lin-14 by lin-4 mediates temporal pattern formation in C. elegans.* Cell, 1993. **75**(5): p. 855-62.
190. Reinhart, B.J., et al., *The 21-nucleotide let-7 RNA regulates developmental timing in Caenorhabditis elegans.* Nature, 2000. **403**(6772): p. 901-906.
191. Chen, C., et al., *Real-time quantification of microRNAs by stem-loop RT-PCR.* Nucleic Acids Res, 2005. **33**(20): p. e179.
192. Lee, Y., et al., *MicroRNA genes are transcribed by RNA polymerase II.* Embo Journal, 2004. **23**(20): p. 4051-4060.
193. Cai, X., C.H. Hagedorn, and B.R. Cullen, *Human microRNAs are processed from capped, polyadenylated transcripts that can also function as mRNAs.* RNA, 2004. **10**(12): p. 1957-66.
194. Lee, Y., et al., *The nuclear RNase III Drosha initiates microRNA processing.* Nature, 2003. **425**(6956): p. 415-419.
195. Gregory, R.I., et al., *The Microprocessor complex mediates the genesis of microRNAs.* Nature, 2004. **432**(7014): p. 235-40.
196. Ameres, S.L. and P.D. Zamore, *Diversifying microRNA sequence and function.* Nat Rev Mol Cell Biol, 2013. **14**(8): p. 475-88.
197. Bohnsack, M.T., K. Czaplinski, and D. Gorlich, *Exportin 5 is a RanGTP-dependent dsRNA-binding protein that mediates nuclear export of pre-miRNAs.* Rna, 2004. **10**(2): p. 185-91.
198. Brennecke, J., et al., *Principles of microRNA-target recognition.* PLoS Biol, 2005. **3**(3): p. e85.
199. Brodersen, P. and O. Voinnet, *Revisiting the principles of microRNA target recognition and mode of action.* Nature Reviews Molecular Cell Biology, 2009. **10**(2): p. 141-148.
200. Wilczynska, A. and M. Bushell, *The complexity of miRNA-mediated repression.* Cell Death Differ, 2015. **22**(1): p. 22-33.
201. O'Carroll, D., et al., *A Slicer-independent role for Argonaute 2 in hematopoiesis and the microRNA pathway.* Genes Dev, 2007. **21**(16): p. 1999-2004.
202. Okamura, K., et al., *Distinct roles for Argonaute proteins in small RNA-directed RNA cleavage pathways.* Genes Dev, 2004. **18**(14): p. 1655-66.
203. Kapinas, K. and A.M. Delany, *MicroRNA biogenesis and regulation of bone remodeling.* Arthritis Research & Therapy, 2011. **13**(3).
204. Li, H., et al., *A novel microRNA targeting HDAC5 regulates osteoblast differentiation in mice and contributes to primary osteoporosis in humans.* Journal of Clinical Investigation, 2009. **119**(12): p. 3666-3677.
205. Hu, R., et al., *A Runx2/miR-3960/miR-2861 regulatory feedback loop during mouse osteoblast differentiation.* J Biol Chem, 2011. **286**(14): p. 12328-39.
206. Zhang, J.F., et al., *MiR-637 maintains the balance between adipocytes and osteoblasts by directly targeting Osterix.* Mol Biol Cell, 2011. **22**(21): p. 3955-61.
207. Nuttall, M.E. and J.M. Gimble, *Controlling the balance between osteoblastogenesis and adipogenesis and the consequent therapeutic implications.* Curr Opin Pharmacol, 2004. **4**(3): p. 290-4.
208. Hassan, M.Q., et al., *miR-218 directs a Wnt signaling circuit to promote differentiation of osteoblasts and osteomimicry of metastatic cancer cells.* J Biol Chem, 2012. **287**(50): p. 42084-92.
209. Zhang, W.B., W.J. Zhong, and L. Wang, *A signal-amplification circuit between miR-218 and Wnt/beta-catenin signal promotes human adipose tissue-derived stem cells osteogenic differentiation.* Bone, 2014. **58**: p. 59-66.

210. Chen, L., et al., *MicroRNA-34a inhibits osteoblast differentiation and in vivo bone formation of human stromal stem cells.* Stem Cells, 2014. **32**(4): p. 902-12.
211. Hwang, S., et al., *miR-140-5p suppresses BMP2-mediated osteogenesis in undifferentiated human mesenchymal stem cells.* FEBS Lett, 2014. **588**(17): p. 2957-63.
212. Gambardella, A., et al., *Glycogen synthase kinase-3alpha/beta inhibition promotes in vivo amplification of endogenous mesenchymal progenitors with osteogenic and adipogenic potential and their differentiation to the osteogenic lineage.* J Bone Miner Res, 2011. **26**(4): p. 811-21.
213. Wang, Q., Cai, J., Cai, X-H., and Lei, C., *miR-346 Regulates Osteogenic Differentation of Human Bone Marrrow-Dervied Mesenchymal Stem Celly by Targeting the Wnt/B-Catenin Pathway.* Plos One, 2013. **8**(9): p. 1-8.
214. Jing, D., et al., *The role of microRNAs in bone remodeling.* Int J Oral Sci, 2015. **7**: p. 131-43.
215. Vimalraj, S., N.C. Partridge, and N. Selvamurugan, *A positive role of microRNA-15b on regulation of osteoblast differentiation.* J Cell Physiol, 2014. **229**(9): p. 1236-44.
216. Tian, F., et al., *CXCL13 Promotes Osteogenic Differentiation of Mesenchymal Stem Cells by Inhibiting miR-23a Expression.* Stem Cells Int, 2015. **2015**: p. 632305.
217. Yang, J., et al., *Nanotopographical Induction of Osteogenesis through Adhesion, Bone Morphogenic Protein Cosignaling, and Regulation of MicroRNAs.* ACS Nano, 2014. **8**(10): p. 9941-53.
218. Wang, T. and Z. Xu, *miR-27 promotes osteoblast differentiation by modulating Wnt signaling.* Biochem Biophys Res Commun, 2010. **402**(2): p. 186-9.
219. Li, Z., et al., *Biological functions of miR-29b contribute to positive regulation of osteoblast differentiation.* J Biol Chem, 2009. **284**(23): p. 15676-84.
220. Eskildsen, T., et al., *MicroRNA-138 regulates osteogenic differentiation of human stromal (mesenchymal) stem cells in vivo.* Proc Natl Acad Sci U S A, 2011. **108**(15): p. 6139-44.
221. Li, J., et al., *MiR-154-5p regulates osteogenic differentiation of adipose-derived mesenchymal stem cells under tensile stress through the Wnt/PCP pathway by targeting Wnt11.* Bone, 2015. **78**: p. 130-141.
222. Kato, R.B., et al., *Nanotopography directs mesenchymal stem cells to osteoblast lineage through regulation of microRNA-SMAD-BMP-2 circuit.* J Cell Physiol, 2014. **229**(11): p. 1690-6.
223. Berg, J.M.T., J.L.; Stryker, L, *Biochemistry*. 5th ed. 2008, New York: W.H Freeman.
224. Korn, E.D., M.F. Carlier, and D. Pantaloni, *ACTIN POLYMERIZATION AND ATP HYDROLYSIS.* Science, 1987. **238**(4827): p. 638-644.
225. Glaister, M., *Multiple sprint work - Physiological responses, mechanisms of fatigue and the influence of aerobic fitness.* Sports Medicine, 2005. **35**(9): p. 757-777.
226. Heiden, M.G.V., L.C. Cantley, and C.B. Thompson, *Understanding the Warburg Effect: The Metabolic Requirements of Cell Proliferation.* Science, 2009. **324**(5930): p. 1029-1033.
227. Zheng, J., *Energy metabolism of cancer: Glycolysis versus oxidative phosphorylation (Review).* Oncology Letters, 2012. **4**(6): p. 1151-1157.
228. Liberti, M.V. and J.W. Locasale, *The Warburg Effect: How Does it Benefit Cancer Cells?* Trends Biochem Sci, 2016. **41**(3): p. 211-218.
229. Akram, M., *Citric acid cycle and role of its intermediates in metabolism.* Cell Biochem Biophys, 2014. **68**(3): p. 475-8.
230. MelendezHevia, E., T.G. Waddell, and M. Cascante, *The puzzle of the Krebs citric acid cycle: Assembling the pieces of chemically feasible reactions, and opportunism in the design of metabolic pathways during evolution.* Journal of Molecular Evolution, 1996. **43**(3): p. 293-303.
231. Cliff, T.S. and S. Dalton, *Metabolic switching and cell fate decisions: implications for pluripotency, reprogramming and development.* Curr Opin Genet Dev, 2017. **46**: p. 44-49.

232. Yanes, O., et al., *Metabolic oxidation regulates embryonic stem cell differentiation.* Nature Chemical Biology, 2010. **6**(6): p. 411-417.
233. Ryall, J.G., et al., *Metabolic Reprogramming of Stem Cell Epigenetics.* Cell Stem Cell, 2015. **17**(6): p. 651-662.
234. Peng, M., et al., *Aerobic glycolysis promotes T helper 1 cell differentiation through an epigenetic mechanism.* Science, 2016. **354**(6311): p. 481-484.
235. Cohn, D.V. and B.K. Forscher, *Aerobic metabolism of glucose by bone.* J Biol Chem, 1962. **237**: p. 615-8.
236. Esen, E. and F. Long, *Aerobic glycolysis in osteoblasts.* Curr Osteoporos Rep, 2014. **12**(4): p. 433-8.
237. Karner, C.M., et al., *Increased glutamine catabolism mediates bone anabolism in response to WNT signaling.* J Clin Invest, 2015. **125**(2): p. 551-62.
238. Karner, C.M. and F. Long, *Wnt signaling and cellular metabolism in osteoblasts.* Cell Mol Life Sci, 2017. **74**(9): p. 1649-1657.
239. DeBerardinis, R.J., et al., *Beyond aerobic glycolysis: transformed cells can engage in glutamine metabolism that exceeds the requirement for protein and nucleotide synthesis.* Proc Natl Acad Sci U S A, 2007. **104**(49): p. 19345-50.
240. Wu, Y., et al., *Lactate induces osteoblast differentiation by stabilization of HIF1 alpha.* Molecular and Cellular Endocrinology, 2017. **452**(C): p. 84-92.
241. Chen, C.T., et al., *Coordinated changes of mitochondrial biogenesis and antioxidant enzymes during osteogenic differentiation of human mesenchymal stem cells.* Stem Cells, 2008. **26**(4): p. 960-8.
242. Shum, L.C., et al., *Energy Metabolism in Mesenchymal Stem Cells During Osteogenic Differentiation.* Stem Cells and Development, 2016. **25**(2): p. 114-122.
243. Williams, E.L., K. White, and R.O. Oreffo, *Isolation and enrichment of Stro-1 immunoselected mesenchymal stem cells from adult human bone marrow.* Methods Mol Biol, 2013. **1035**: p. 67-73.
244. Olmer, R., et al., *Long term expansion of undifferentiated human iPS and ES cells in suspension culture using a defined medium.* Stem Cell Res, 2010. **5**(1): p. 51-64.
245. Tsimbouri, P.M., et al., *Using nanotopography and metabolomics to identify biochemical effectors of multipotency.* ACS Nano, 2012. **6**(11): p. 10239-49.
246. Schmittgen, T.D. and K.J. Livak, *Analyzing real-time PCR data by the comparative C-T method.* Nature Protocols, 2008. **3**(6): p. 1101-1108.
247. Candeias, L.P., et al., *The catalysed NADH reduction of resazurin to resorufin.* Journal of the Chemical Society-Perkin Transactions 2, 1998(11): p. 2333-2334.
248. Carpenter, A.E., et al., *CellProfiler: image analysis software for identifying and quantifying cell phenotypes.* Genome Biology, 2006. **7**(10).
249. Kamentsky, L., et al., *Improved structure, function and compatibility for CellProfiler: modular high-throughput image analysis software.* Bioinformatics, 2011. **27**(8): p. 1179-1180.
250. Dalby, M.J., et al., *The control of human mesenchymal cell differentiation using nanoscale symmetry and disorder.* Nature Materials, 2007. **6**(12): p. 997-1003.
251. Dalby, M.J., et al., *Osteoprogenitor response to semi-ordered and random nanotopographies.* Biomaterials, 2006. **27**(15): p. 2980-7.
252. Manfrinato, V.R., et al., *Resolution limits of electron-beam lithography toward the atomic scale.* Nano Lett, 2013. **13**(4): p. 1555-8.
253. Titushkin, I. and M. Cho, *Modulation of cellular mechanics during osteogenic differentiation of human mesenchymal stem cells.* Biophys J, 2007. **93**(10): p. 3693-702.
254. Chiquet, M., et al., *From mechanotransduction to extracellular matrix gene expression in fibroblasts.* Biochim Biophys Acta, 2009. **1793**(5): p. 911-20.
255. Crisp, M., et al., *Coupling of the nucleus and cytoplasm: role of the LINC complex.* J Cell Biol, 2006. **172**(1): p. 41-53.
256. Eshraghi, S. and S. Das, *Mechanical and microstructural properties of polycaprolactone scaffolds with one-dimensional, two-dimensional, and three-*

dimensional orthogonally oriented porous architectures produced by selective laser sintering. Acta Biomater, 2010. **6**(7): p. 2467-76.
257. Dalby, M.J., et al., *Investigating filopodia sensing using arrays of defined nano-pits down to 35 nm diameter in size.* Int J Biochem Cell Biol, 2004. **36**(10): p. 2005-15.
258. Zhang, Z.-j., et al., *miRNA expression profile during osteogenic differentiation of human adipose-derived stem cells.* Journal of Cellular Biochemistry, 2012. **113**(3): p. 888-898.
259. Hassan, M.Q., et al., *A network connecting Runx2, SATB2, and the miR-23a~27a~24-2 cluster regulates the osteoblast differentiation program.* Proc Natl Acad Sci U S A, 2010. **107**(46): p. 19879-84.
260. Zhang, Y., et al., *A program of microRNAs controls osteogenic lineage progression by targeting transcription factor Runx2.* Proc Natl Acad Sci U S A, 2011. **108**(24): p. 9863-8.
261. Wurdinger, T., et al., *miR-296 Regulates Growth Factor Receptor Overexpression in Angiogenic Endothelial Cells.* Cancer Cell, 2008. **14**(5): p. 382-393.
262. Egea, V., et al., *Tissue inhibitor of metalloproteinase-1 (TIMP-1) regulates mesenchymal stem cells through let-7f microRNA and Wnt/beta-catenin signaling.* Proc Natl Acad Sci U S A, 2012. **109**(6): p. E309-16.
263. Zhang, J.G., et al., *MiR-148b suppresses cell proliferation and invasion in hepatocellular carcinoma by targeting WNT1/beta-catenin pathway.* Sci Rep, 2015. **5**: p. 8087.
264. Schoolmeesters, A., et al., *Functional Profiling Reveals Critical Role for miRNA in Differentiation of Human Mesenchymal Stem Cells.* Plos One, 2009. **4**(5): p. 9.
265. Liao, Y.H., et al., *Osteogenic differentiation of adipose-derived stem cells and calvarial defect repair using baculovirus-mediated co-expression of BMP-2 and miR-148b.* Biomaterials, 2014. **35**(18): p. 4901-4910.
266. Kapinas, K., et al., *miR-29 modulates Wnt signaling in human osteoblasts through a positive feedback loop.* J Biol Chem, 2010. **285**(33): p. 25221-31.
267. Zhang, Z.J., et al., *miRNA expression profile during osteogenic differentiation of human adipose-derived stem cells.* Journal of Cellular Biochemistry, 2012. **113**(3): p. 888-898.
268. Kapinas, K., et al., *miR-29 Modulates Wnt Signaling in Human Osteoblasts through a Positive Feedback Loop.* Journal of Biological Chemistry, 2010. **285**(33): p. 25221-25231.
269. Hassan, M.Q., et al., *miR-218 Directs a Wnt Signaling Circuit to Promote Differentiation of Osteoblasts and Osteomimicry of Metastatic Cancer Cells.* Journal of Biological Chemistry, 2012. **287**(50): p. 42084-42092.
270. Wang, J.R., et al., *Nanotopology potentiates growth hormone signalling and osteogenesis of mesenchymal stem cells.* Growth Horm IGF Res, 2014. **24**(6): p. 245-50.
271. Gothard, D., J.I. Dawson, and R.O. Oreffo, *Assessing the potential of colony morphology for dissecting the CFU-F population from human bone marrow stromal cells.* Cell Tissue Res, 2013. **352**(2): p. 237-47.
272. McNamara, L.E., et al., *Nanotopographical control of stem cell differentiation.* J Tissue Eng, 2010. **2010**: p. 120623.
273. Komori, T., *Regulation of skeletal development by the Runx family of transcription factors.* J Cell Biochem, 2005. **95**(3): p. 445-53.
274. Komori, T., et al., *Targeted disruption of Cbfa1 results in a complete lack of bone formation owing to maturational arrest of osteoblasts.* Cell, 1997. **89**(5): p. 755-764.
275. Ducy, P., et al., *Osf2/Cbfa1: A transcriptional activator of osteoblast differentiation.* Cell, 1997. **89**(5): p. 747-754.
276. Komori, T., *Runx2, a multifunctional transcription factor in skeletal development.* J Cell Biochem, 2002. **87**(1): p. 1-8.

277. Weng, J.J. and Y. Su, *Nuclear matrix-targeting of the osteogenic factor Runx2 is essential for its recognition and activation of the alkaline phosphatase gene.* Biochim Biophys Acta, 2013. **1830**(3): p. 2839-52.
278. Javed, A., et al., *Multiple Cbfa/AML sites in the rat osteocalcin promoter are required for basal and vitamin D-responsive transcription and contribute to chromatin organization.* Molecular and Cellular Biology, 1999. **19**(11): p. 7491-7500.
279. Ducy, P., et al., *Increased bone formation in osteocalcin-deficient mice.* Nature, 1996. **382**(6590): p. 448-452.
280. Rittling, S.R., et al., *Mice lacking osteopontin show normal development and bone structure but display altered osteoclast formation in vitro.* Journal of Bone and Mineral Research, 1998. **13**(7): p. 1101-1111.
281. Boskey, A.L., et al., *Osteopontin Deficiency Increases Mineral Content and Mineral Crystallinity in Mouse Bone.* Calcified Tissue International, 2002. **71**(2): p. 145-154.
282. Morinobu, M., et al., *Osteopontin expression in osteoblasts and osteocytes during bone formation under mechanical stress in the calvarial suture in vivo.* Journal of Bone and Mineral Research, 2003. **18**(9): p. 1706-1715.
283. Lund, S.A., C.M. Giachelli, and M. Scatena, *The role of osteopontin in inflammatory processes.* J Cell Commun Signal, 2009. **3**(3-4): p. 311-22.
284. Kahles, F., H.M. Findeisen, and D. Bruemmer, *Osteopontin: A novel regulator at the cross roads of inflammation, obesity and diabetes.* Mol Metab, 2014. **3**(4): p. 384-93.
285. Nakamura, A., et al., *Osteocalcin secretion as an early marker of in vitro osteogenic differentiation of rat mesenchymal stem cells.* Tissue Eng Part C Methods, 2009. **15**(2): p. 169-80.
286. Kollmer, M., et al., *Markers Are Shared Between Adipogenic and Osteogenic Differentiated Mesenchymal Stem Cells.* J Dev Biol Tissue Eng, 2013. **5**(2): p. 18-25.
287. Maroney, P.A., et al., *Evidence that microRNAs are associated with translating messenger RNAs in human cells.* Nat Struct Mol Biol, 2006. **13**(12): p. 1102-7.
288. Zhang, Y., et al., *A program of microRNAs controls osteogenic lineage progression by targeting transcription factor Runx2.* Proceedings of the National Academy of Sciences of the United States of America, 2011. **108**(24): p. 9863-9868.
289. Egea, V., et al., *Tissue inhibitor of metalloproteinase-1 (TIMP-1) regulates mesenchymal stem cells through let-7f microRNA and Wnt/beta-catenin signaling.* Proceedings of the National Academy of Sciences of the United States of America, 2012. **109**(6): p. E309-E316.
290. Schoolmeesters, A., et al., *Functional Profiling Reveals Critical Role for miRNA in Differentiation of Human Mesenchymal Stem Cells.* Plos One, 2009. **4**(5).
291. Guilak, F., et al., *Control of stem cell fate by physical interactions with the extracellular matrix.* Cell Stem Cell, 2009. **5**(1): p. 17-26.
292. Brammer, K.S., et al., *Hydrophobic nanopillars initiate mesenchymal stem cell aggregation and osteo-differentiation.* Acta Biomater, 2011. **7**(2): p. 683-90.
293. Abagnale, G., et al., *Surface topography enhances differentiation of mesenchymal stem cells towards osteogenic and adipogenic lineages.* Biomaterials, 2015. **61**: p. 316-326.
294. von Erlach, T.C., et al., *Cell-geometry-dependent changes in plasma membrane order direct stem cell signalling and fate.* Nat Mater, 2018. **17**(3): p. 237-242.
295. Green, D., et al., *The potential of biomimesis in bone tissue engineering: Lessons from the design and synthesis of invertebrate skeletons.* Bone, 2002. **30**(6): p. 810-815.
296. Muys, J.J., M.M. Alkaisi, and J.J. Evans, *Bioimprint: Nanoscale Analysis by Replication of Cellular Topography Using Soft Lithography.* Journal of Biomedical Nanotechnology, 2006. **2**(1): p. 11-15.
297. Samsuri, F., et al., *Detection of changes in cell membrane structures using the Bioimprint technique.* Microelectronic Engineering, 2011. **88**(8): p. 1871-1874.
298. DePorter, S.M., I. Lui, and B.R. McNaughton, *Programmed cell adhesion and growth on cell-imprinted polyacrylamide hydrogels.* Soft Matter, 2012. **8**(40): p. 10403.

299. Murray, L.M., et al., *Fabrication of polymeric substrates with micro- and nanoscale topography bioimprinted at progressive cell morphologies.* Journal of Vacuum Science & Technology B: Microelectronics and Nanometer Structures, 2012. **30**(6): p. 06F902.
300. Murray, L.M., et al., *Bioimprinted polymer platforms for cell culture using soft lithography.* J Nanobiotechnology, 2014. **12**: p. 60.
301. Mutreja, I., et al., *Positive and negative bioimprinted polymeric substrates: new platforms for cell culture.* Biofabrication, 2015. **7**(2): p. 025002.
302. Song, W., N. Kawazoe, and G. Chen, *Dependence of Spreading and Differentiation of Mesenchymal Stem Cells on Micropatterned Surface Area.* Journal of Nanomaterials, 2011. **2011**: p. 1-9.
303. Li, Z., et al., *Differential regulation of stiffness, topography, and dimension of substrates in rat mesenchymal stem cells.* Biomaterials, 2013. **34**(31): p. 7616-7625.
304. Wu, Y.N., et al., *The Combined Effect of Substrate Stiffness and Surface Topography on Chondrogenic Differentiation of Mesenchymal Stem Cells.* Tissue Engineering Part A, 2017. **23**(1-2): p. 43-54.
305. Nock, V., et al., *Microfluidic arrays for bioimprint of cancer cells.* Microelectronic Engineering, 2011. **88**(8): p. 1828-1831.
306. Jeon, H. and G. Kim, *Effects of a cell-imprinted poly(dimethylsiloxane) surface on the cellular activities of MG63 osteoblast-like cells: preparation of a patterned surface, surface characterization, and bone mineralization.* Langmuir, 2012. **28**(37): p. 13423-30.
307. Kowalczynska, H.M., et al., *Albumin adsorption on unmodified and sulfonated polystyrene surfaces, in relation to cell-substratum adhesion.* Colloids Surf B Biointerfaces, 2011. **84**(2): p. 536-44.
308. Waddell, S.J., et al., *Biomimetic oyster shell–replicated topography alters the behaviour of human skeletal stem cells.* Journal of Tissue Engineering, 2018. **9**: p. 2041731418794007.
309. Dawson, J.I., et al., *Concise Review: Bridging the Gap: Bone Regeneration Using Skeletal Stem Cell-Based Strategies-Where Are We Now?* Stem Cells, 2014. **32**(1): p. 35-44.
310. Yamada, Y., et al., *Current trends in stem cell therapy for improvement of bone quality.* Histology and Histopathology, 2014. **29**(6): p. 691-697.
311. Leal, J., et al., *Impact of hip fracture on hospital care costs: a population-based study.* Osteoporos Int, 2016. **27**(2): p. 549-58.
312. Jones, E.A., P.V. Giannoudis, and D. Kouroupis, *Bone repair with skeletal stem cells: rationale, progress to date and clinical application.* Therapeutic Advances in Musculoskeletal Disease, 2016. **8**(3): p. 57-71.
313. Kulangara, K., et al., *Nanotopography as modulator of human mesenchymal stem cell function.* Biomaterials, 2012. **33**(20): p. 4998-5003.
314. Kilian, K.A., et al., *Geometric cues for directing the differentiation of mesenchymal stem cells.* Proceedings of the National Academy of Sciences of the United States of America, 2010. **107**(11): p. 4872-4877.
315. Westbroek, P. and F. Marin, *A marriage of bone and nacre.* Nature, 1998. **392**(6679): p. 861-862.
316. Zhang, G., et al., *Nacre, a natural, multi-use, and timely biomaterial for bone graft substitution.* J Biomed Mater Res A, 2017. **105**(2): p. 662-671.
317. Silve, C., et al., *Nacre initiates biomineralization by human osteoblasts maintained in vitro.* Calcif Tissue Int, 1992. **51**(5): p. 363-9.
318. Lopez, E., et al., *DEMONSTRATION OF THE CAPACITY OF NACRE TO INDUCE BONE-FORMATION BY HUMAN OSTEOBLASTS MAINTAINED INVITRO.* Tissue & Cell, 1992. **24**(5): p. 667-679.
319. Atlan, G., et al., *Reconstruction of human maxillary defects with nacre powder: histological evidence for bone regeneration.* Comptes Rendus De L Academie Des Sciences Serie Iii-Sciences De La Vie-Life Sciences, 1997. **320**(3): p. 253-258.

320. Lamghari, M., et al., *Bone reactions to nacre injected percutaneously into the vertebrae of sheep.* Biomaterials, 2001. **22**(6): p. 555-562.
321. Duplat, D., et al., *The in vitro osteoclastic degradation of nacre.* Biomaterials, 2007. **28**(12): p. 2155-62.
322. Shen, Y., et al., *Engineering scaffolds integrated with calcium sulfate and oyster shell for enhanced bone tissue regeneration.* ACS Appl Mater Interfaces, 2014. **6**(15): p. 12177-88.
323. Almeida, M.J., et al., *Comparative effects of nacre water-soluble matrix and dexamethasone on the alkaline phosphatase activity of MRC-5 fibroblasts.* Journal of Biomedical Materials Research, 2001. **57**(2): p. 306-312.
324. Green, D.W., H.J. Kwon, and H.S. Jung, *Osteogenic potency of nacre on human mesenchymal stem cells.* Mol Cells, 2015. **38**(3): p. 267-72.
325. Alakpa, E.V., et al., *Nacre Topography Produces Higher Crystallinity in Bone than Chemically Induced Osteogenesis.* ACS Nano, 2017. **11**(7): p. 6717-6727.
326. Creek, D.J., et al., *IDEOM: an Excel interface for analysis of LC-MS-based metabolomics data.* Bioinformatics, 2012. **28**(7): p. 1048-1049.
327. Xia, J., et al., *MetaboAnalyst 3.0--making metabolomics more meaningful.* Nucleic Acids Res, 2015. **43**(W1): p. W251-7.
328. Lian, J.B., et al., *Networks and hubs for the transcriptional control of osteoblastogenesis.* Rev Endocr Metab Disord, 2006. **7**(1-2): p. 1-16.
329. Zaidi, S.K., et al., *A specific targeting signal directs Runx2/Cbfa1 to subnuclear domains and contributes to transactivation of the osteocalcin gene.* Journal of Cell Science, 2001. **114**(17): p. 3093-3102.
330. Yang, W., et al., *Surface topography of hydroxyapatite promotes osteogenic differentiation of human bone marrow mesenchymal stem cells.* Mater Sci Eng C Mater Biol Appl, 2016. **60**: p. 45-53.
331. Chen, C.T., et al., *Coordinated changes of mitochondrial biogenesis and antioxidant enzymes during osteogenic differentiation of human mesenchymal stem cells.* Stem Cells, 2008. **26**(4): p. 960-968.
332. Tsimbouri, P.M., et al., *Using Nanotopography and Metabolomics to Identify Biochemical Effectors of Multipotency.* Acs Nano, 2012. **6**(11): p. 10239-10249.
333. Lee, N., et al., *Creatine inhibits adipogenesis by downregulating insulin-induced activation of the phosphatidylinositol 3-kinase signaling pathway.* Stem Cells Dev, 2015. **24**(8): p. 983-94.
334. Lu, Q., Y. Zhang, and J.H. Elisseeff, *Carnitine and acetylcarnitine modulate mesenchymal differentiation of adult stem cells.* J Tissue Eng Regen Med, 2015. **9**(12): p. 1352-62.
335. Ge, C., et al., *Critical role of the extracellular signal-regulated kinase-MAPK pathway in osteoblast differentiation and skeletal development.* J Cell Biol, 2007. **176**(5): p. 709-18.
336. Knobloch, M., et al., *A Fatty Acid Oxidation-Dependent Metabolic Shift Regulates Adult Neural Stem Cell Activity.* Cell Rep, 2017. **20**(9): p. 2144-2155.
337. Ritz, U., et al., *A New Bone Substitute Developed from 3D-Prints of Polylactide (PLA) Loaded with Collagen I: An In Vitro Study.* International Journal of Molecular Sciences, 2017. **18**(12): p. 14.
338. Shim, K.S., et al., *Surface immobilization of biphasic calcium phosphate nanoparticles on 3D printed poly(caprolactone) scaffolds enhances osteogenesis and bone tissue regeneration.* Journal of Industrial and Engineering Chemistry, 2017. **55**: p. 101-109.
339. Rogatzki, M.J., et al., *Lactate is always the end product of glycolysis.* Front Neurosci, 2015. **9**: p. 22.
340. Yang, J.L., et al., *Nanotopographical Induction of Osteogenesis through Adhesion, Bone Morphogenic Protein Cosignaling, and Regulation of MicroRNAs.* Acs Nano, 2014. **8**(10): p. 9941-9953.

341. Langenbach, F. and J. Handschel, *Effects of dexamethasone, ascorbic acid and beta-glycerophosphate on the osteogenic differentiation of stem cells in vitro.* Stem Cell Research & Therapy, 2013. **4**.
342. Song, S., et al., *The synergistic effect of micro-topography and biochemical culture environment to promote angiogenesis and osteogenic differentiation of human mesenchymal stem cells.* Acta Biomater, 2015. **18**: p. 100-11.
343. Costa-Rodrigues, J., et al., *Osteoclastogenic differentiation of human precursor cells over micro- and nanostructured hydroxyapatite topography.* Biochim Biophys Acta, 2016. **1860**(4): p. 825-35.
344. Dulgar-Tulloch, A.J., R. Bizios, and R.W. Siegel, *Differentiation of human mesenchymal stem cells on nano- and micro-grain size titania.* Materials Science and Engineering: C, 2011. **31**(2): p. 357-362.
345. Skoog, S.A., et al., *Biological responses to immobilized microscale and nanoscale surface topographies.* Pharmacol Ther, 2018. **182**: p. 33-55.
346. Zouani, O.F., et al., *Altered nanofeature size dictates stem cell differentiation.* J Cell Sci, 2012. **125**(Pt 5): p. 1217-24.
347. Hulshof, F.F.B., et al., *Mining for osteogenic surface topographies: In silico design to in vivo osseo-integration.* Biomaterials, 2017. **137**: p. 49-60.
348. Zipori, D., *The stem state: plasticity is essential, whereas self-renewal and hierarchy are optional.* Stem Cells, 2005. **23**(6): p. 719-26.
349. English, A., et al., *Substrate topography: A valuable in vitro tool, but a clinical red herring for in vivo tenogenesis.* Acta Biomater, 2015. **27**: p. 3-12.
350. Ge, P., et al., *L-carnitine affects osteoblast differentiation in NIH3T3 fibroblasts by the IGF-1/PI3K/Akt signalling pathway.* Biosci Trends, 2015. **9**(1): p. 42-8.
351. Lu, Q.Z., Y.F. Zhang, and J.H. Elisseeff, *Carnitine and acetylcarnitine modulate mesenchymal differentiation of adult stem cells.* Journal of Tissue Engineering and Regenerative Medicine, 2015. **9**(12): p. 1352-1362.
352. Jaudzems, K., et al., *Inhibition of carnitine acetyltransferase by mildronate, a regulator of energy metabolism.* J Enzyme Inhib Med Chem, 2009. **24**(6): p. 1269-75.
353. Liepinsh, E., et al., *Mildronate, an inhibitor of carnitine biosynthesis, induces an increase in gamma-butyrobetaine contents and cardioprotection in isolated rat heart infarction.* Journal of Cardiovascular Pharmacology, 2006. **48**(6): p. 314-319.
354. Twine, N.A., et al., *Identification of differentiation-stage specific markers that define the ex vivo osteoblastic phenotype.* Bone, 2014. **67**: p. 23-32.
355. Jang, W.G., et al., *BMP2 protein regulates osteocalcin expression via Runx2-mediated Atf6 gene transcription.* J Biol Chem, 2012. **287**(2): p. 905-15.
356. Hoang, Q.Q., et al., *Bone recognition mechanism of porcine osteocalcin from crystal structure.* Nature, 2003. **425**(6961): p. 977-980.
357. Hong, S.H., et al., *Changes in Serum Osteocalcin are Not Associated with Changes in Glucose or Insulin for Osteoporotic Patients Treated with Bisphosphonate.* J Bone Metab, 2013. **20**(1): p. 37-41.
358. Schafer, A.L., et al., *Change in undercarboxylated osteocalcin is associated with changes in body weight, fat mass, and adiponectin: parathyroid hormone (1-84) or alendronate therapy in postmenopausal women with osteoporosis (the PaTH study).* J Clin Endocrinol Metab, 2011. **96**(12): p. E1982-9.
359. Komori, T., *Regulation of osteoblast differentiation by transcription factors.* J Cell Biochem, 2006. **99**(5): p. 1233-9.
360. Liu, W., et al., *Overexpression of Cbfa1 in osteoblasts inhibits osteoblast maturation and causes osteopenia with multiple fractures.* J Cell Biol, 2001. **155**(1): p. 157-66.
361. Gelse, K., *Collagens—structure, function, and biosynthesis.* Advanced Drug Delivery Reviews, 2003. **55**(12): p. 1531-1546.
362. Tare, R.S., et al., *A microarray approach to the identification of polyurethanes for the isolation of human skeletal progenitor cells and augmentation of skeletal cell growth.* Biomaterials, 2009. **30**(6): p. 1045-55.